

Design, construction and commissioning of a gas-mixing-system for gaseous particle detectors

Von der Fakultät für Mathematik, Informatik und Naturwissenschaften der
RWTH Aachen University zur Erlangung des akademischen Grades
eines Doktors der Naturwissenschaften genehmigte Dissertation

vorgelegt von

Diplom-Physiker Jochen Steinmann

aus Unna (Nordrhein-Westfalen)

Berichter: Priv. Doz. Stefan Roth
Prof. Dr. Lutz Feld

Tag der mündlichen Prüfung: 09.12.2014

Diese Dissertation ist auf den Internetseiten der Hochschulbibliothek online verfügbar.

Abstract

The success of gaseous particle detectors started around 1900, when first attempts were made by Curie, Townsend and Geiger [28]. After the development of the Geiger-Müller counter, gaseous detectors have been used in many particle physics experiments and they were involved in many particle discoveries.

Today gaseous particle detectors are part of the majority of particle physics experiments. A large variety of detector types has been developed until now ranging from drift tube systems for muon detectors over large volume time projection chambers to micro pattern gas detectors. For their operation gaseous detectors need gas systems, which supply the gas mixture at the needed flow and pressure.

The gas system presented in this thesis can be used for research and development of gas ionisation particle detectors. During the commissioning phase and beyond, this system was used to do systematic measurements of various gas parameters. These studies help understanding gas properties and can improve detector simulations.

Commissioning tests were done using one monitoring chamber, which is the same that are used for the Time Projection Chamber inside the ND280 detector of the T2K-experiment. Due to the high precision of the gas mixture, the system helps understanding the systematic effects of the monitoring chambers. At the same time possible alternative gas mixtures for the Time Projection Chamber (TPC) operation were investigated. Also a sensitivity study of the drift velocity regarding the gas composition has been done.

Furthermore also other mixtures have been mixed and have been tested for future use in particle detectors. All the tests done with this system may assist the selection of the gas mixture.

In this thesis, the general concept and the physical results achieved during commissioning and fine tuning are presented. A more detailed look at the mechanical and electrical design and dimensioning is described in [37]. In this technical documentation, also the calculations regarding safety issues are shown.

Kurzfassung

Der Erfolg von gasbasierten Teilchendetektoren begann ungefähr im Jahr 1900, als die ersten Versuche mit diesem Detektortyp von Curie, Townsend und Geiger durchgeführt wurden [28]. Nachdem das Geiger-Müller-Zählrohr entwickelt worden war, wurden gasbasierte Detektoren in vielen Experimenten der Teilchenphysik benutzt. Dadurch waren diese Detektoren auch an vielen Entdeckungen von neuen Teilchen beteiligt.

Heute sind gasbasierte Detektoren immer noch Teil der meisten Experimente in der Teilchenphysik. In der Vergangenheit wurden eine Vielzahl von Varianten und Typen entwickelt. Diese Vielzahl reicht von kleinen Driftröhrchen für Myon-Detektoren über großvolumige Detektoren, wie Zeitprojektionskammern, bis hin zu feinen Mikrostrukturen. Damit diese Detektoren betrieben werden können, wird immer auch ein Gassystem benötigt, welches dem Detektor das vorgesehene Gas mit dem notwendigen Fluss und Druck zur Verfügung stellt.

Das in dieser Arbeit vorgestellte Gassystem kann vor allem für die Forschung und Entwicklung von gasbasierten Teilchendetektoren genutzt werden. Während und nach der Inbetriebnahme wurde dieses System bereits für die Messung verschiedener Parameter der gemischten Gase eingesetzt. Diese Studien helfen Eigenschaften der Gasmischungen zu verstehen und die Simulationen von gasbasierten Detektoren zu verbessern.

Die Tests und Messungen während der Inbetriebnahme wurden mit einer Gas-Monitor-Kammer durchgeführt. Diese Kammer entstammt der gleichen Baureihe wie die beiden, die zur Überwachung des Gases in den TPCs des ND280-Detektors benutzt werden. Der ND280-Detektor ist Teil des T2K-Experiments. Durch die hohe Präzision der Gasmischungen, hat das System auch dazu beigetragen, die Systematiken dieser Kammern besser zu verstehen. Gleichzeitig wurden Studien für eine mögliche Alternative für das bisher verwendete Driftgas durchgeführt. Diese Studie beinhaltet auch eine Untersuchung der Sensitivität der Driftgeschwindigkeit auf Abweichungen in der bisherigen Gasmischung.

Weiterhin wurden andere Gasmischungen erzeugt und für einen eventuellen Einsatz in zukünftigen Teilchendetektoren getestet. Alle bisherigen Studien können bei der Selektion der Gasmischung helfen.

In dieser Arbeit wird das grundlegende Konzept, die physikalischen Ergebnisse während der Inbetriebnahme und die Feinabstimmung beschrieben. Eine tiefgründige Betrachtung des mechanischen und elektrischen Designs und dessen Auslegung ist in [37] beschrieben. Gleichzeitig finden sich in [37] auch die Berechnungen bezüglich Sicherheit des gesamten Systems.

Contents

1	Motivation for a Universal Gas Mixing Apparatus	11
2	Introduction	13
2.1	Gaseous detectors	13
2.1.1	Ionisation chamber	13
2.1.2	Wire chamber	14
2.1.3	Time-Projection-Chamber	15
2.2	Gas mixtures and properties of gases	17
2.2.1	Properties of gases	18
2.3	Selection of the drift gas	27
2.4	Density effects inside the detectors	28
2.4.1	Primary ionisation	28
2.4.2	Drift velocity	29
2.4.3	Amplification	29
2.4.4	Applying the corrections to data	31
3	Requirements	37
3.1	Flow and pressure inside the connected detector	37
3.2	Mixing	38
3.2.1	Calculation	38
3.2.2	Mixing methods	40
3.3	Mechanical constraints	42
3.4	Electrical requirements	42
3.5	Usability	43
3.5.1	Connections	43
4	Mechanics	45
4.1	Concept	45
4.1.1	Valve concept	46
4.1.2	Piping concept	47
4.2	System Overview	49
4.2.1	Mixer	50
4.2.2	Analysis Loop	52
4.2.3	Buffer	52
4.2.4	Purifier	53
4.2.5	Chamber	54
4.3	Explosion Safety	56

5	Electronics	59
5.1	System overview	59
5.2	Communication	60
5.3	Analogue inputs	61
5.4	Sensors	61
5.4.1	Pressure sensors	61
5.4.2	Temperature sensors	62
5.5	Digital inputs and outputs	62
5.6	Valve-driver	62
5.7	Power distribution	63
5.8	Valve island	65
6	Software	67
6.1	Frameworks	69
6.1.1	SubSystem	69
6.1.2	LibLab	70
6.2	Software concept	70
6.3	Data flow inside UGMA	71
6.4	Programs	73
7	Mixing gas	77
7.1	Parallel flow mixing	77
7.1.1	Function of a Mass Flow Controller	77
7.1.2	Uncertainty of the mixture	78
7.1.3	Conversion factor used inside a Mass Flow Controller	81
7.2	Partial pressure mixing	85
7.2.1	Using ideal gas	86
7.2.2	Using Redlich-Kwong equation	87
7.2.3	Contamination caused by old mixtures	89
7.2.4	Time needed to create a gas mixture	90
8	Analysis of mixed gas	91
8.1	Water-sensor	91
8.1.1	Operation principle	91
8.1.2	Integration into the UGMA	92
8.2	Oxygen-sensor	96
8.2.1	Principle of operation	96
8.2.2	Pressure dependence	96
8.2.3	Error of measurement	97
8.3	Gas chromatograph	97
8.3.1	Analysis	102
8.3.2	Off-line analysis	102
8.3.3	Resolution	102
8.4	Cavity Enhanced Differential Optical Absorption Spectroscopy	104
8.5	Gas Monitoring Chambers	105
8.5.1	ND280 TPC Gas Monitoring Chambers	105
8.5.2	L3 TEC Velocity Drift Chamber	107

9	Commissioning of assembly groups	111
9.1	Power supply	111
9.2	PowerBar	111
9.3	Valve-driver	113
9.4	Tightness & leakage	114
9.4.1	Determination of vacuum-leakage-rate in the buffer & purifier	114
9.5	Analysis-loop	116
9.6	Vacuum	117
9.6.1	Minimal pressure	117
9.6.2	Effective throughput	118
9.7	Mixing	118
9.8	Pressure drop	124
9.8.1	Characteristic curve of the analysis loop	124
10	Systematic studies	127
10.1	Sensors	127
10.1.1	Temperature sensors	127
10.1.2	Pressure sensors	129
10.2	Purifier	130
10.2.1	Heater	130
10.2.2	Regeneration	131
10.3	Buffer	132
10.3.1	Volume	132
10.3.2	Evacuation-time	134
10.3.3	Maximal blow-off rate	134
10.3.4	Maximum filling rate	135
11	Drift velocity	137
11.1	Systematic studies	137
11.1.1	Argon-Methane-Carbondioxide	139
11.1.2	Argon-Methane-Isobutane	139
11.1.3	Argon-Methane-Hydrogen	140
11.1.4	Argon-Isobutane-Tetrafluoromethane	140
11.1.5	Argon-Propane-Tetrafluoromethane	142
11.1.6	Conclusion	142
11.2	Fitting of the mixture	144
11.2.1	Binary mixtures	146
12	Conclusion	151
A	Convention	153
A.1	Naming	153
A.2	Units	154
A.2.1	Pressure	154
A.2.2	Volume	154
A.2.3	Volume-flow	154
A.3	Commonly used gas mixtures	155

A.4 Norms, law and provisions	155
List of abbreviations	157
Bibliography	163

1. Motivation for a Universal Gas Mixing Apparatus

If a new type of gas-filled detector has been developed and is going to be tested inside the laboratory, it needs to be supplied with the proper gas. If no further requirements regarding the supply exist, a very simple approach can be used. This consists of a needle-valve and a variable area flowmeter, also called rotameter. If the needle-valve is located in front of the detector, the flow can be regulated. But this solution only works for a very simple setup, because the flow through the valve depends on the pressure difference across the valve. Hence, the flow depends on the pressure difference between the detector and the supply line. For a simple test setup, the detector follows ambient pressure. If the pressure in the supply line can be assumed to be constant, the flow through the detector varies. To perform precise measurements, stable conditions are needed. This implies a regulation in pressure and flow. To get stable conditions, the simple setup should be extended with a pressure regulation behind the chamber.

During detector R & D one would like to change the gas composition to measure the response of the detector. Mixtures used in high energy physics are mostly not compatible with the mixtures used in industrial applications. One exception are the barrel muon-chambers of the Compact Muon Solenoid (CMS) detector. They are fed with a mixture of 82 % Argon and 18 % carbon-dioxide [47, p. 53]. This mixture is commonly used in industrial metal active gas (MAG) welding. The premixed gas is either called *Sagox18*, *Corgon18* or *Tycon18* depending on the supplier. This gas can be delivered from stock with small delivery delays if no extra high purity is needed.

If the gas is not commercially available it can be created by the gas companies, but due to the customisation, it takes very long for the delivery. Also the costs for this process are high.

In the following part, a scenario is discussed, where the variation of a mixture based on three gases should be measured. Two components should be varied in steps of 1 vol.-%. The third component is balance.

If the effect of the admixtures should be measured within a range of 1 vol.-% around the normal content for each admixture, nine different mixtures are needed. Under the assumption, that it takes 24 hours to measure one mixture with the required precision and the flow through the detector is $10 \ell_n/h$, 240 ℓ gas is needed per measurement cycle. Among the delivery time, also the logistical effort forms an obstacle.

If it happens, that the mixture is usable for detection, further studies needs to be performed with this special mixture. They can last several days, evens weeks. But at the same time, this means, that more gas is needed. This needs a lot of scheduling well in advance. When

the order has been placed, changes in the measurement timetable are not possible. These obstacles are one of the reasons for the development of the Universal Gas Mixing Apparatus (UGMA) described in the following.

For the gas-supply of a large detector system at modern particle physics experiments special dedicated systems are set up that only serve the gas for this special detector. Those systems are specialised to supply one mixture at a high flow rate, which is needed to supply the detectors mounted inside a running experiment. Due to their concept, they cannot supply smaller amounts of gas. Hence they cannot be used for smaller prototypes. At the same time, this means, that during the development phase of the detector, a lot of work must be spent on the gas infrastructure as well. If it is planned to reuse a system from an earlier experimental setup, most of the parameters need to be changed and in the worst case some hardware parts also need to be changed due to the new mixture. On the other hand, it is not easy to scale a small system up for usage in a larger detector.

Hence the idea was born to save work for the gas infrastructure and develop one system, which can be used for typical R & D detectors and mixtures.

2. Introduction

Even if the field of gaseous particle detectors has a quite long history, there is still research and development to improve detectors and gases.

At the Large Electron-Positron Collider and also later at the Large Hadron Collider each of the experiments used and uses gaseous detectors. Some of them were a Time Projection Chamber, others drift tubes or straw tubes. Also elsewhere in almost every large particle physics experiment gaseous detectors are used. Always, when a large volume has to be instrumented with high precision and a low channel number, gaseous detectors are chosen. The success of gaseous detectors continues, since future experiments and their detectors plan to use gaseous detectors.

Today a combination of silicon readout chips with gaseous detectors is investigated [10]. This kind of detectors combine the advantages of the small structures with integrated readout from the silicon detectors with the low radiation length and large volume from gaseous detectors. For future large detectors like the International Large Detector at the International Linear Collider this combination might be an alternative to classical gaseous detectors and currently under investigation.

2.1. Gaseous detectors

Gases play a decisive role in high energy physics. They are used for various purposes but mostly as a medium where high energy particles produce ionisation which is detected. One of the most famous gaseous detectors is the Geiger-Counter, which was invented in 1908 by Hans Geiger [34] in liaison with Ernest Rutherford for detection of α -particles. In 1928 the detection principle has been improved and from then on, it was possible to detect very small activities of radiation [17]. From this time on the developments and their success started. They are still foreseen for future experiments. Using gaseous detectors the instrumentation of large detection volumes with a relatively small number of channels is possible.

2.1.1. Ionisation chamber

One very basic particle detector is the ionisation chamber. It consists of two plates, which are situated inside a gas volume. The voltage applied between both plates is high enough to prevent recombination of ionised molecules. Depending on the geometry of the chamber, this can be done by applying a few volts. The voltage is too low to start gas amplification. Due to the small primary charge, it is not possible to get a sufficient electrical signal from a single particle crossing. Mostly these chambers are used for dosimetry. For this purpose, they are operated in current mode and the electrical current through the chamber is measured. The

current is proportional to the number of electron ion pairs created in the gas volume. Due to their different specific ionisation α and β particles create a different current.

2.1.2. Wire chamber

For detection of single tracks, gas amplification is needed to create of a sufficient large electrical signal. This can be achieved using high electrical fields which enable gas amplification. This way the signal is amplified and one can measure single hits. On the other hand, it is important, that the amplified signal is proportional to the incoming electrons. Hence, the electrical field should not be too high, otherwise the signal is no longer proportional and additionally continuous discharges might happen.

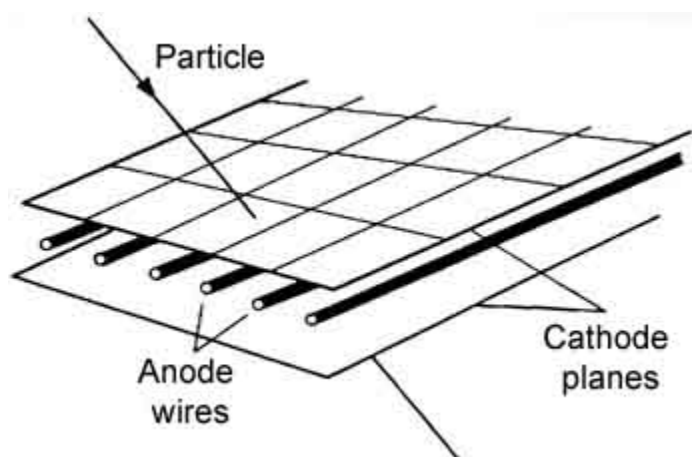


Figure 2.1.: The drawing shows the principle of how a MWPC functions. Several anode wires are attached between two cathode planes. This figure shows an example of a plane wire chamber, but other geometric solutions exist as well. [22]

As pointed out by the name, wires are strained between parallel plates. A schematic view of a wire chamber is shown in figure 2.1. Both plates are at the same potential. Also cylindrical wire chambers have been used in the past. If they are located around a beam pipe, they consist of an inner and outer cylinder where the wires are in between. For safety reasons mostly ground potential is chosen as the potential of the outer structure. To produce the electrical field, the wires are supplied with a high positive voltage. The field increases next to the wire and gas amplification starts. The signal from the wire is amplified in an external second stage. The electrical amplifiers are connected using decoupling capacitors. Using capacitors, the inputs of the amplifiers can be designed with respect to ground and have no contact with the high voltage applied on the wire. This simplifies the design of the amplification stage.

The resolution of a wire chamber is dominated by the spacing of the wires. Another important point for limited spatial resolution is diffusion. This gas parameter describes the spreading of the electron cloud during drift.

2.1.3. Time-Projection-Chamber

The Time Projection Chamber has been invented by David R. Nygren in the late 1970s. A TPC consists of a gas filled detection volume, which is located inside an electrical field. The typical TPC has a cylindrical shape and is equipped with Multi-Wire-Proportional-Chamber (MWPC)s as endplates. This geometry allows the TPC to be positioned around the beam pipe. But for fixed target experiments also other geometries are used.

Often a magnetic field is applied in parallel to the electrical field in order to minimize the diffusion of the electrons created in primary ionisations. At the same time the magnetic field can be used for reconstruction of the particle momentum. The x and y or r and ϕ coordinates of the particle track can be readout from the pad plane while z -coordinate can be reconstructed using the drift time. A basic sketch showing the working principle of a TPC is shown in figure 2.2.

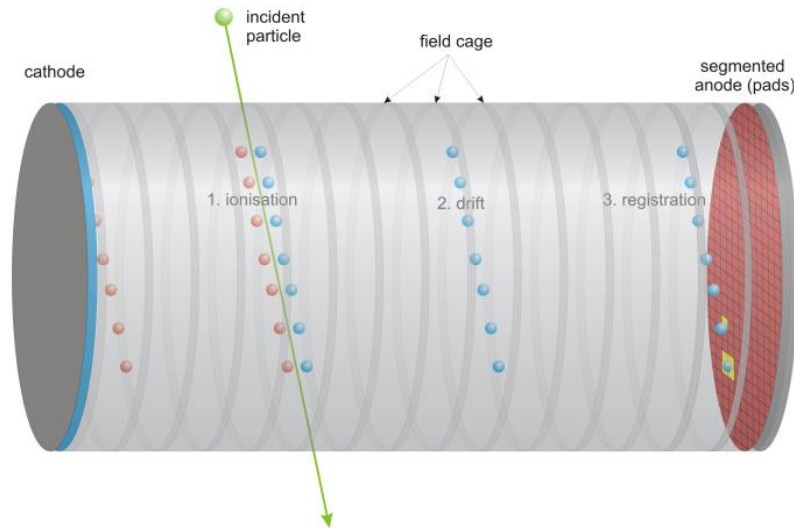


Figure 2.2.: Working principle of a TPC [14]

TPCs allow observation of a large volume with few channels compared to silicon trackers. A great benefit is the very low material budget of TPCs along the particle flow. The main material budget is caused by the containment and the electrodes. Compared to copper ($X_0 = 1.43$ cm [42]) the radiation length of gaseous Argon ($X_0 = 117.63$ m [42]) is about 8000 times larger. At the end of the TPC, where the material budget is irrelevant, the readout plane is located. Although there is less material inside the area of interest TPCs can achieve a resolution of few hundred microns, even if pileup happens. This is why they are very interesting for future experiments.

For experiments at low collision rates, TPCs are well suited. But if the collision rate increase, their performance start to suffer. On the one hand different tracks become indistinguishable because they got smeared by diffusion effects. On the other hand if there are lot of primary tracks inside the TPC, shielding of the electrical field and recombination increases, because of the number of created ions. When talking about ions, one effect called „ion backdrift“ should also be mentioned. This effect names the drift of ions from the gas amplification

region to the drift volume. By optimising the gas amplification process, the amount of back drifting ions can be minimized.

ND280 detector for the T2K experiment

One of largest volume read out with Micro-Mesh-Gaseous-Structure (MicroMegas) are the three TPCs located at the ND280 detector. Here a total area of 9 m^2 are readout with 72 Modules. Each module is divided into 1726 Pads of $6.85 \times 9.65\text{ mm}^2$ size. The results of the first years of operation have shown, that the specifications can be met [23]. All three TPCs are operated in a magnetic field of 0.2 T to allow measurements of the particle momentum.

For monitoring the gas quality, two gas monitoring chambers are located at the surface inside the gas mixing hut. For a detailed description see section 8.5.1. One is connected to the supply line of the TPCs and the other one to the return line. Using the measurements of both chambers, the conditions inside the large TPCs can be interpolated. The chamber connected to the supply line can act as a mixing interlock. In case of an accidental creation of a wrong mixture, the supply chamber allows preserving the rest of the system to be supplied with this wrong mixture. One incident from the past has shown, that the monitoring system in combination with the interlock system successfully reacted in the safe way.

The gas mixture used for the TPCs consists of 95 vol.-% Argon, 3 vol.-% Tetrafluoromethane and 2 vol.-% Isobutane.

Each monitoring chamber is supplied with $6\text{ }\ell_{\text{n}}/\text{h}$, which results in about five volume changes per hour.

Performance of the TPC inside ALICE at LHC

A Large Ion Collider Experiment (ALICE) is one of the four large experiments at the Large Hadron Collider (LHC). It is located at Interaction Point (IP) two. This IP is optimised for interactions of heavy ions. Parts of the detector are installed inside the old octagonal L3 magnet, which remained inside the cavern and is now reused. The magnetic field is about 0.5 T. [13]

Inside the L3 magnet one of the largest, currently operating TPC can be found. This TPC has a cylindrical shape with an inner radius of about 80 cm and an outer radius of 280 cm. Within the inner volume the Inner Tracking System (ITS) is installed to improve the vertex reconstruction resolution. The whole TPC has an overall length of 500 cm in the beam direction. This length is divided by a central cathode into two drift volumes, which are both equipped with a potential degrader to create a uniform drift field.

Each drift volume is read out by conventional multi-wire proportional counters with cathode pad readout. These are made of standard wire planes above the readout plane and a gating wire plane facing the drift volume.

Due to the radial dependence of the track density, two different types of readout chambers and segmentations are used. In total the active area is about 32.5 m^2 . The readout chambers can identify the track in the polar coordinates r and ϕ . The z -component can be reconstructed

from timing information and known drift velocity. The whole TPC is capable of a central collision rate of 200 Hz.

The ALICE TPC is operated with a gas mixture consisting out of 90 vol.-% Neon and 10 vol.-% carbon dioxide.

Current Developments

To reach unprecedented center of mass energies in $e^+ e^-$ collisions a linear collider is planned. Due to synchrotron radiation losses, it is not feasible to build a storage ring for high energy electrons. This new accelerator is called International Linear Collider (ILC). It is not yet clear when and where it will be build. One plan is a linear accelerator with two detectors. Each detector is moveable and can be moved into the interaction point. One of these detectors is called International Large Detector (ILD).

Inside the calorimeter system of ILD a high-precision tracking system will be installed. To enable good momentum resolution, it will be placed inside a solenoid, which will produce the high magnetic field of 4 T. A TPC is planned according to the ILC Reference Design Report [3] with a momentum resolution of

$$\sigma(1/p_t) \approx 5 \cdot 10^{-5} \text{ GeV}^{-1} \quad (2.1)$$

The final chamber will have a size of 3 - 4.6 m in length and a diameter of 2.8 - 4 m. Along the particle track a spatial resolution of 100 μm per row or better should be achieved.

For studying various readout-techniques the Large Prototype TPC (LPTPC) has been built. This TPC has a diameter of 750 mm and a length of about 600 mm [43]. Since end of 2008, the LPTPC is inserted into a 1.25 T magnet located in one of the test beam areas of Deutsches Elektronen-Synchrotron (DESY).

At present, various tests and measurements are done by using this prototype. The current end flange can be equipped with seven different readout modules, equipped with Micro-Mesh-Gaseous-Structure or Gas Electron Multiplier detectors. Measurements using GridPix readouts are possible as well. These tests help to decide, which readout-technique will be used in the final design. For a more detailed explanation of the gas amplification methods have a look at section 2.2.1.

2.2. Gas mixtures and properties of gases

Applications in high energy physics require specific properties of the gas mixtures in use. Each mixture is optimised to its application.

For numerical simulations, there are frameworks and programs like `Magboltz` [99], `Garfield` [106] and the rewrite `Garfield++` [107]. With the results obtained from the simulations, it can be checked, whether the mixture meets all the physical requirements. Limits given by safety rules or other mechanical properties should be manually checked, because often, they are much more complex to meet.

If a new gas mixture has been chosen, further tests need to be done. On the one hand, all parameters from the simulation should be checked, if they can be measured with a real detector. For this purpose small test detectors are used. On the other hand, one has to check, how small variations in the gas composition change the properties of the gas and through this the detection results. The physical parameters should change only little, when small changes to the composition are applied. These small changes might happen due to uncertainties in the mixing process. In the past many of these tests were based on simulations only [20,40].

2.2.1. Properties of gases

For use in particle physics detectors some gas properties are important. Those are described in the following section.

Mean energy to create one free electron

Only a small fraction of the energy loss of a charged particle in a gas is ionising directly. Additional processes can create electrons or result in energy loss. Hence the average energy needed for one free electron W is defined according to [5, p. 4] as:

$$W \langle N_I \rangle = L \left\langle \frac{dE}{dx} \right\rangle \quad (2.2)$$

where $\langle N_I \rangle$ represents the average number of ionised electrons, which are created along a trajectory of length L . $\langle dE/dx \rangle$ stands for the mean energy loss per unit of length of the charged particle. Due to different cross sections of electrons and α particles two values (W_β and W_α) are given in literature.

To calculate the value for a gas mixture, a simple composition law can be used for an estimation of the value of W_{Mix} : [35, p. 9]

$$W_{\text{Mix}} = \sum_i \eta_i W_i \quad (2.3)$$

In the equation above η_i represents the volume fraction of gas i in the mixture. One major disadvantage of equation 2.3 is the missing consideration of the reactions between the gases, which can also cause free electrons.

To assist the user in his decision towards selecting the right gas also the W-value of the selected gas mixture is shown on the user interface. The displayed values are received from a numerical simulation with `Garfield++`. This was done by tracking 2000 electrons with an energy equal to the decay energy of Sr^{90} 0.546 MeV respectively Y^{90} 2.283 MeV. The results of both energies are compatible with respect to their statistical uncertainties. Therefore in the following only the results created by the electrons with the decay energy of Y^{90} are shown. In this simulation, the mean energy necessary for one free electron can be calculated from the sum of all energy losses during the ionisation process of the incoming particle. Per event, i.e. per one incoming particle, many clusters are generated. Each cluster can be

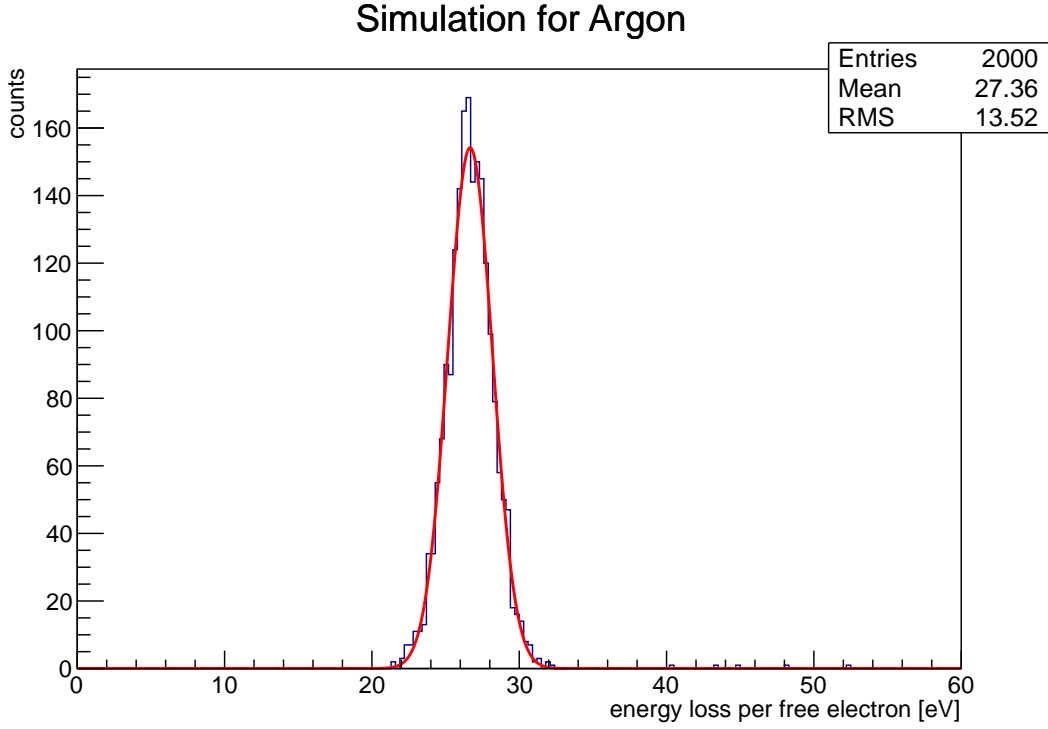


Figure 2.3.: Simulation result of energy loss of 2000 electrons in argon. The energy of the electrons is $E = 2.283$ MeV.

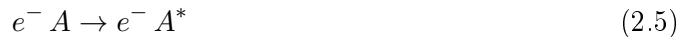
specified by the energy loss ΔE_C and the number of electrons per collision N_C . The mean energy for one free electron therefore is given by

$$W = \frac{\sum \Delta E_C}{\sum N_C} \quad (2.4)$$

Using this calculation, the computation of W is independent of the length the electrons travel through the selected gas. If their way through the gas is longer, they create more clusters and hence they lose more energy. **Garfield++** also does an internal calculation of the W -value. This value can be read out accessing the internal variable **HeedTrack**. The calculation is hidden in the library and it is not clear whether **Garfield++** uses the value for electrons or α -particles.

All three values (basic calculation, **HeedTrack** and full simulation), are displayed to the user. These values are used only to assist the user with the decision, which gas will fit the detectors requirements. The decision, which value to trust is transferred to the user.

Penning effect If one electron does not transfer enough energy for ionisation, the molecule A only gets excited.



If this molecule collides with another one, whose ionisation level is lower than the excitation energy of A , B gets ionised due to the collision.



By this reaction a free electron is produced. If the excitation of the molecule is caused by an electron this effect is called Penning-effect. The resulting electrons are called Penning-electrons.

The same process can also be triggered by photons, which are absorbed by a molecule and exciting it. This process is called Jesse-effect. The resulting electrons are named Jesse-electrons. [5, p. 4]

If these effects are to be taken into account, one has to do a proper simulation to derive W . This can either be done by `Garfield` [106], its rewrite `Garfield++` [107], `MIPS` [98] or `Heed` [103]. The Penning- and Jesse-effect are implemented in all simulation programs by assuming a certain probability for the creation of a free electron at a collision. One usual approach to match the simulation to the measured values is tuning these probabilities. They depend on the concrete composition of the mixture and hence the probability has to be determined for each mixture separately.

It is not possible to distinguish between the Jesse- and Penning-effect at the signal side. Hence the probabilities for Jesse- and Penning-electrons are merged into one probability, which is called at least in `Garfield++` Penning-probability.

In table 2.1 a comparison between different calculations is shown. The simulation was done by using a small program using `Garfield++` simulating the ionisation of 2.28 MeV electrons inside the specified gas mixture. At the same time a value from `Heed`, which is also part of `Garfield++`, is derived. The calculation is based on equation 2.3 in combination with values from literature.

Table 2.1.: Comparison of different values of W_β from different references and simulations.

Gas	literature [5]		Heed	simulation	calculation
	W_α	W_β	W	W_β	$W_{\alpha,\beta}$
Ar(97 %) CH ₄ (3 %)	26,0 eV	-	26,41 eV	26,67 ± 1,48 eV	26,48 eV
Ar	26,4 eV	26,3 eV	26,40 eV	26,69 ± 1,57 eV	-
CH ₄	29,1 eV	27,1 eV	27,30 eV	22,34 ± 2,04 eV	-

Approach for binary mixtures For binary mixtures another approach for the calculation of W is described in [6]:

$$\frac{1}{W_{\text{Mix}}} = \left(\frac{1}{W_1} - \frac{1}{W_2} \right) \cdot \frac{P_1}{P_1 + aP_2} + \frac{1}{W_2} \quad (2.7)$$

In this equation P represents the partial pressure of each gas. Within this approach, the parameter a takes into account, that there is a reaction between both gases. For some mixture a is equal to the molecular stopping power S . But on the other hand reference [6, Table III] shows that this is only the case for very few mixtures. Many others have significant differences. There is no calculation for a , so this parameter must be measured for each gas combination. The concentration is not important for these measurements, only the type of gas. A summary for some values is also shown in [6].

In practise for many cases it is sufficient to use the simplified approach from equation 2.3.

Gas amplification

When a gas based particle detector is operated without an electric field, the primary electrons and ions recombine, because there is no force to separate them (Fig. 2.4, 1). Increasing the field reduces recombination and causes the electrons to drift towards the anode. At low fields, the charge collected at the readout plane is equal to the primary one (Fig. 2.4, 2). If the field applied inside a detector rises, the primary electrons gain more and more energy and their energy becomes large enough to ionise further gas molecules (Fig. 2.4, 3). Over a wide range of field strengths the amplified charge is proportional to the primary charge. If the field increases further, the proportionality is lost (Fig. 2.4, 4) and the amplified signal gets independent from the primary charge (Fig. 2.4, 5). At this point a Geiger-Müller-Counter operates. At even higher fields continuous discharge sets in (Fig. 2.4, 6).

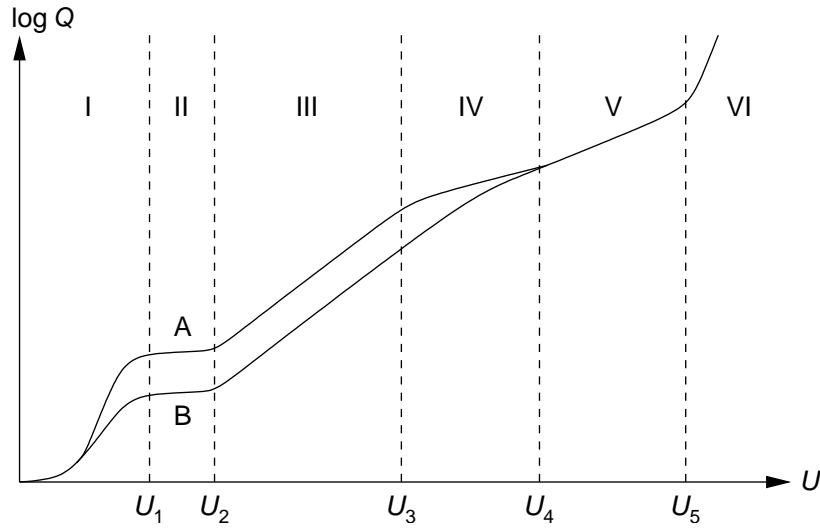


Figure 2.4.: Detected charge in dependency of the operation voltage. Plot taken from [46]

To enable particle identification, the specific energy loss is measured. Each particle has its specific energy loss at a certain momentum. This is the reason, why particle detectors are usually operated in the proportional region. After calibration, the output signal can be converted into the energy loss of the observed particle. Together with the particle momentum, this allows particle identification.

Amplification by the gas is used for detection of the small primary charge. Without amplification, the signal of the primary charge is too low for direct electronic processing. As an example the number of electrons generated by an Fe^{55} photon of the energy $E_\gamma = 5.899 \text{ keV}$ in Argon (see table 2.1) can be calculated to

$$N_{e^-} = \frac{E_\gamma}{W_\beta} = \frac{5.9 \text{ keV}}{26 \text{ eV}} = 227 \quad (2.8)$$

The primary charge follows by multiplication of this value with the elementary charge

$$Q_{e^-} = N_{e^-} \cdot Q_e = 227 \cdot 1.6021 \cdot 10^{-19} \text{ C} = 3.6 \cdot 10^{-17} \text{ C} \quad (2.9)$$

This charge is neither suitable to be fed into electronic amplifiers nor to be acquired by digitisers. Hence it needs to be amplified inside the gas volume. This can be done by using gas amplification. Typical values of gas amplification gain are about $N/N_0 = 1000$. With this the charge on the readout plane is increased to

$$Q'_{e^-} = Q_{e^-} \cdot \frac{N}{N_0} \approx 36 \text{ fC} \quad (2.10)$$

This charge is large enough for further electronic amplification. The gas amplification strongly depends on the electrical field inside the detector, which is given by the applied voltage and geometry. The parameter describing the influence of the gas is called Townsend coefficient. This parameter describes the number of secondary electrons created along a path at a given electrical field. If there is gas amplification, the number of additional electrons is given by [5, 4.1]

$$dN = N \alpha(E) ds \quad (2.11)$$

The Townsend coefficient α mainly depends on the cross section for excitation and ionisation. It is based on various transport mechanisms and therefore only a numerical simulation can be done. The framework **Garfield++** gives the opportunity to simulate the Townsend coefficient for different electrical fields. To get the gas amplification factor, equation 2.11 needs to be integrated over the path s of the primary electron. It can be assumed, that the path of the electron is given by the electrical field lines. Using this, the integration can be converted into an integration along the electrical field lines.

$$\frac{N}{N_0} = \exp \int \alpha(s) ds = \exp \int \frac{\alpha(E)}{dE/ds} dE \quad (2.12)$$

Earlier simulations have shown, that this simplification is not valid in every detector. Instead integrating along the electric field, the integration should be done along the particle trajectory. Hence, it is not possible to perform this calculation analytically. Only a complete simulation can point out the correct results for gas amplification in complex detectors. Such simulations can be done using **Garfield++**. In the past various approaches failed because not all effects of the gas could be represented in the simulation [26].

Up to now, the simulation assumes a constant probability to take Penning- and Jesse-effects into account. This probability is tuned to match the measured values or it is guessed from earlier experience. If the simulation uses enough Monte-Carlo events, the effect of the probability on the mean Townsend-coefficient $\langle \alpha \rangle$ can be expressed by

$$\langle \alpha^* \rangle = (1 + P_{\text{Jesse}}) \cdot (1 + P_{\text{Penning}}) \cdot \langle \alpha \rangle \quad (2.13)$$

Approaches to measure α directly are described in [26]. But these measurements have shown, that there is a strong dependence on the precision of the whole experiment.

Methods used for gas amplification For two-dimensional pixel-readout-planes homogeneous gas amplification along the plane is needed. This cannot be reached with wires, therefore other techniques are used.

Micro-Mesh-Gaseous-Structure To get a higher and more homogeneous gas amplification MicroMegas were developed in 1996 by Y. Giomataris et al. [18]. By using a woven mesh which is located about $100\ \mu\text{m}$ above the readout plane, high gains can be obtained. The voltage applied to the mesh is of the order of 350-500 V depending on the Townsend coefficient of the gas. This voltage creates an electrical field in the order of 10 kV/cm sufficient for gas amplification. The ions created inside the amplification gap do not reach the drift volume, because the field lines end on the wires of the mesh. This feature is a great benefit, because the electric field inside the drift volume is not distorted by ion feedback.

Developments were started in the past, which do research on combination of MicroMegas and silicon detectors, which are used as readout. This combination is called GridPix [8]. This detector is equipped with 256×256 Pixels, each with a size of $55 \times 55\ \mu\text{m}^2$. This allows an excellent resolution in space. Although the chip originally was designed for other purposes, the timing information is usable. Further development focusing on more precise timing information is done as well.

Gas Electron Multiplier In 1997 a new detector technology was developed by F. Sauli et. al. called Gas Electron Multiplier (GEM) [36]. In this mechanism, the amplification is done in a very small region. A typical GEM is constructed using a thin insulating polymer foil, which

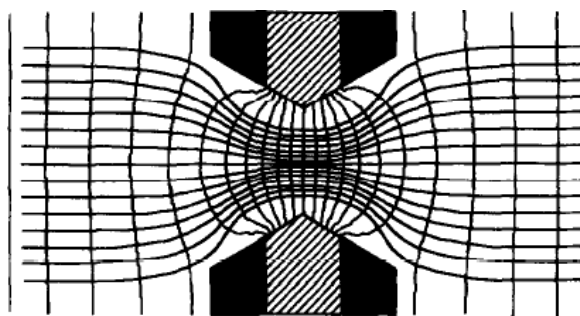


Figure 2.5.: Computed electric field in one multiplying channel of a GEM. Only the central field lines have been plotted. (taken from [36])

is copper plated on both sides. Inside this sandwich holes are etched. Due to the process itself, the holes are conical. When the difference of potential between both electrodes is high enough a high field inside the GEM holes, as shown in figure 2.5, is created. With about 200 V applied, the field strength along the central lines reaches up to 40 kV/cm, which is high enough for gas amplification. [36]

It has been shown, that single GEMs can be operated stably up to gains of $5 \cdot 10^2$. For better performance and reduction of ion back drift GEMs can be stacked upon each other and thus reach higher gain of about 10^5 . Each single stage is operating at a limited gain, but together a high gain (shown in figure 2.6) can be reached [24].

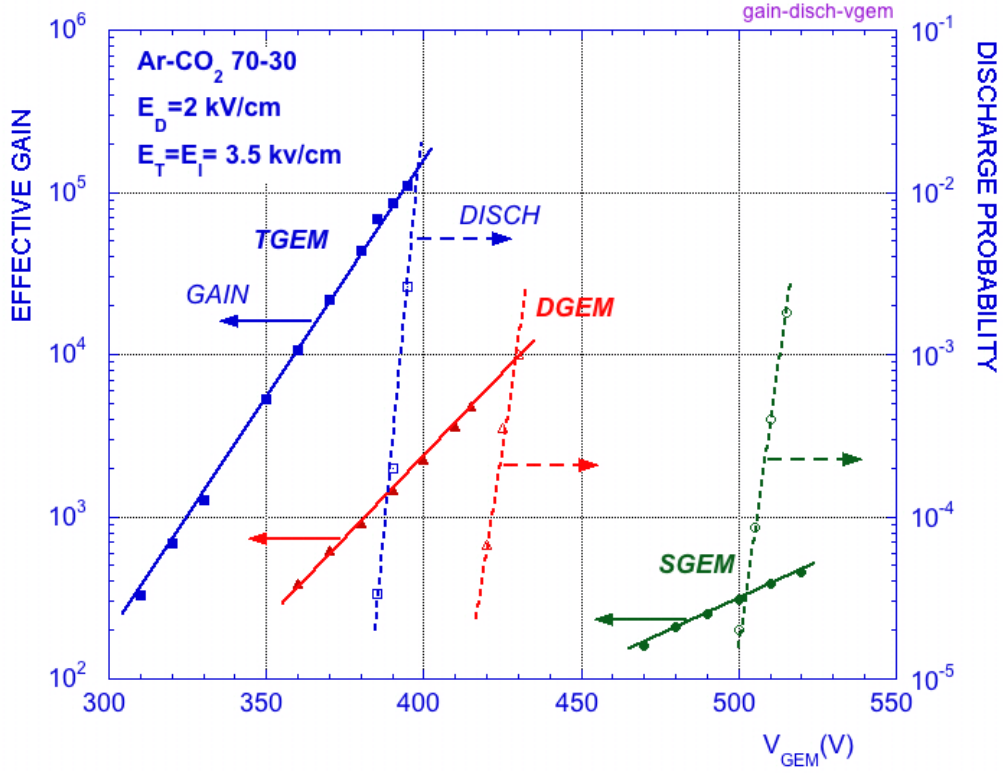


Figure 2.6.: Gain and discharge probability on irradiation with alpha particles for the single, double and triple GEM (from CERN gas detector group [44])

Drift velocity

Motion in vacuum In vacuum the motion of a charge q with mass m inside an electric and magnetic field is driven by the Lorentz-force

$$m\dot{\vec{v}} = q(\vec{E} + \vec{v} \times \vec{B}) \quad (2.14)$$

Typically this results in helical trajectories.

Motion in gas When low energy drifting electrons inside a gas are exposed to a uniform E and B field, they do not follow this spiral motion at least not on a scale larger than the mean free path. The mean free path at standard pressure and temperature inside a typical detector gas is only a few microns. Rather they move on straight lines. This is caused by the collisions of the electrons and the gas molecules. Hence the electron velocity gets randomised in all directions.

The steady-state drift velocity v_D follows equation

$$\vec{v}_D = \frac{q\tau}{m}(\vec{E} + \vec{v}_D \times \vec{B}) \quad (2.15)$$

In this equation τ represents the transition time to reach the steady-state drift velocity. This equation can be derived from equation 2.14 when one substitutes $\dot{v} = v_D/\tau$. The value $\mu = q\tau/m$ is called mobility and depends on the electric and magnetic field. The Langevin equation presents a solution of equation 2.15.

$$\vec{v}_D = \frac{\mu}{1 + \mu^2 B^2} \left(\vec{E} + \mu \vec{E} \times \vec{B} + \mu^2 \vec{B} \left(\vec{E} \cdot \vec{B} \right) \right) \quad (2.16)$$

The mobility depends on the electric and magnetic field.

$$\mu(E, B) = \frac{q}{m} \tau(E, B) \quad (2.17)$$

All tests presented in this thesis were done without a magnetic field $B = 0$. Hence equation 2.16 simplifies to

$$v_D = \mu(E) \cdot E \quad (2.18)$$

If the temperature and pressure of the gas are not standard conditions, further dependencies are introduced.

$$v_D = \mu \cdot \frac{E}{n} = \mu \cdot \frac{ET}{p} \quad (2.19)$$

where the mobility μ depends on the reduced electrical field $E/n = ET/p$. Furthermore μ depends on the cross section of electron and gas molecule and the mean electron energy.

Diffusion

Since the electrons are scattered on the gas molecules, their drift velocity deviates from the average owing to the random nature of the collisions. Assuming a simple case, with the same diffusion in all directions, a point-like cloud of electrons starting to drift at time $t = 0$ from the origin in z direction will, after some time t , take over the following Gaussian density distribution. [5, p. 67]

$$n = \left(\frac{1}{\sqrt{4\pi Dt}} \right)^3 \exp \left(\frac{-r^2}{4Dt} \right) \quad (2.20)$$

where $r^2 = x^2 + y^2 + (z - v_D t)^2$ and D is the diffusion constant. The electrical field determines the diffusion width σ_x of an electron cloud which, after starting point-like, has travelled over a distance L [5, p. 69]

$$\sigma_x^2 = 2Dt = \frac{2DL}{\mu E} \quad (2.21)$$

In particle detectors the diffusion is separated into transversal (perpendicular to the drift velocity) and longitudinal (parallel to the drift velocity) diffusion.

The longitudinal diffusion limits the potential of separating two tracks drifting behind each other. If the diffusion is too large, the electron clouds merge and the readout plane only sees a large electron cloud. This cloud gets interpreted as one large track with the combined primary charge.

The transversal diffusion limits the resolution in x and y direction. If two tracks are close to each other, they cannot be distinguished. The transverse diffusion can be reduced by applying a magnetic field in parallel to the electrical field.

Diffusion strongly depends on the gas composition. Some gases exist, which are recommended for use in a TPC where low diffusion is requested. On the other hand the diffusion has to match the readout chain. It is not feasible to use a low diffusion gas when the readout chain does not support this low diffusion, e.g. the pad size is much larger than the estimated width of the electron cloud. If this is the case no charge division can happen, and the resolution cannot benefit from the diffuse electron cloud. It might also be possible, that the resolution using this readout can be increased by a gas with a slightly higher diffusion.

Ageing

If a gas is exposed to ionising radiation, an effect called „ageing“ appears. If Hydrocarbons are present in the detector gas, they can be transformed into polymers by exposition to ionising radiation. The hydrocarbons are cracked by the radiation and attracted by the anodes and cathodes. At high field, they stick together and an isolating barrier of polymers is created. Hence, the sensitivity of the detector is weakened. Sometimes parts of the detector become even unusable [9]. This may be caused by shortening small distances between different potentials by polymer bridges. On the other hand, the polymers may form small needles, which can be a source of sparks.

This effect strongly depends on the electrical field and due to this on the geometry and voltage used inside the detector. Another parameter is the exposed radiation dose. Up to now it is not possible to simulate this effect. Hence measurements in a test beam or special irradiation facilities are necessary. With these measurements the accumulated radiation dose expected during the lifetime of the detector can be applied in a reasonable time. After measurements are done, usually a study of the deposits created by polymers inside the detector is done. A detailed study of the deposits help understanding which materials caused their creation. During construction of a new detector sometimes materials like glue and grease is used, which gas out and hence contaminate the gas. Often these contaminations cause ageing.

By selecting the right mixture, ageing can be reduced to a minimal acceptable level. On the other hand, there are detector types, which also reduce the possibility of ageing. These types are mainly GEMs and MicroMegs, because their electrical field in the gas amplification region is much lower, than the field for a single wire.

Quenching

If excited Ar-Atoms return to their base state, they can send out a photon. This photon has enough energy to release electrons from the wall or the cathode of the detector. This effect disturbs the measurement and hence it should be suppressed. Suppression of this effect can be done by adding large molecules, which get excited by the photons. Large molecules have a lot of different excitation modes, like oscillation, rotation, etc. If they absorb one photon the energy of the photon gets transferred into mechanical energy. This effect is called „quenching“ and the large molecular admixtures are often called „quencher“.

2.3. Selection of the drift gas

The gas mixtures of detectors are usually chosen in order to optimise the performance of the detector and to meet the constraints from outside. Some of these are the regulations of the experimental area, some are given by the detector itself. For most underground experiments flammable gases are not allowed.

One of the most important constraints, which should be met are diffusion and drift velocity. By choosing a gas with a low transversal diffusion, the spatial resolution can be increased. But on the other hand, if the diffusion is too small, all charge is accumulated on one pad and thus the resolution suffers. If the charge is spread over multiple pads, the position of the primary track can be calculated using a weighted mean.

Hence, the diffusion should be as small as possible but still large enough, that charge division between pads takes place. The drift velocity limits the speed of the digitisers and the occupancy when multiple events happen during one readout cycle. By choosing a high drift velocity, all tracks move to the readout plane rapidly and the volume gets ready for the next event. To clear the volume, also the ion drift velocity is important. For an ideal performance the ions should be removed from the detection volume before the next tracks cross this volume again.

Another very important constraint for selecting a gas is the chemical resistance of the chamber materials against the gas itself. Incompatibilities must be avoided, because otherwise the performance and the durability of the detector can suffer.

One very special admixture is carbon tetrafluoride CF_4 , which is also known as Tetrafluoromethane. This admixture has shown, that it can prevent or even remove deposits. But on the other hand CF_4 releases very aggressive Fluorine ions and radicals. In presence of water they can form HF , which is one of the most powerful acids and can attack even glass and epoxies, for example. One possible reaction might be



But CF_4 is very interesting for use in particle detectors, because of the following reasons.

- Non-flammable. This is important for usage in underground areas.
- Hydrogen-free. The cross-sections for scattering and absorption of neutrons are quite high for hydrogen. If neutron background is an issue, the amount of hydrogen present should be as low as possible.
- Fast drift velocity. By adding small amounts of CF_4 , the drift velocity can be increased to values larger than $100 \mu\text{m}/\text{ns}$.
- Very small diffusion. The diffusion of gas mixtures containing CF_4 is only one third compared to P10 (ArCH_4 90:10) at a magnetic field of 0 T.
- Silicon etching is the original purpose of this gas, when it is not used in particle detectors. By controlled adding of a small fraction of water to the gas in the order of 100 vol.-ppm, the „ageing“ process can be stopped or even removed [12].

2.4. Density effects inside the detectors

Since the detectors, connected to the UGMA, are operated with gas, small changes in temperature and pressure reflect in changes in density. Starting with an ideal gas, the density is given by

$$\rho \propto n \propto \frac{p}{T} \quad (2.23)$$

Unless it is possible to operate the detector at stable temperature and pressure, all effects can only be corrected offline. Starting from the ionisation of the primary track, continuing the drift inside the gas and at a last point the amplification inside a Micro Pattern Gas Detector (MPGD) all steps depend on the gas density.

The simplifications and assumptions done below, are only feasible, if the Penning- and Jesse-effect can be neglected. There is no possibility to measure this effect directly. The probabilities for both effects to create one additional electron have to be derived from the comparison of simulation and measurement. In the following part, both probabilities have been set to zero.

2.4.1. Primary ionisation

If a high energetic particle passes through a layer of gas, it loses energy. This effect can be expressed by the Bethe-formula [5, p. 29].

$$\frac{dE}{dx} = \frac{4\pi N_e e^4}{mc^2 \beta^2} z^2 \left(\ln \frac{2mc^2 \beta^2 \gamma^2}{I} - \beta^2 \right) \quad (2.24)$$

For the density effects, the important variable in the formula above is the electron density N_e . This can be expressed through the Avogadro's number N_A , the gas density ρ and the ratio of atomic number Z and atomic weight A of the medium.

$$N_e = \rho \frac{Z}{A} N_A \quad (2.25)$$

If this is combined with the Bethe-formula, the density dependency of the loss of energy can be written as

$$\frac{dE}{dx} \propto \rho \propto n \quad (2.26)$$

The mean energy to create one free electron W does not depend on the density, except, the probability for Penning- or Jesse-transfer changes with density. One hint, that both changes with density, is the reduced free path with increasing density. Hence the probability that two molecules hit each other and transfer energy increases. But until now, there are no experimental results focussing on this dependency.

Correction

If measurements taken at different conditions should be compared, the measured energy loss should be corrected for standard conditions. This can be done by a simple multiplicative

approach. n_{TPC} is the gas density inside the TPC and n_{STP} is the gas density at standard or reference conditions.

$$\left(\frac{dE}{dx}\right)_{\text{STP}} \cdot n_{\text{TPC}} = \left(\frac{dE}{dx}\right)_{\text{TPC}} \cdot n_{\text{STP}} \quad (2.27)$$

2.4.2. Drift velocity

The drift velocity depends on the energy and the mean free path of the drift electrons. If the density changes, the free path changes accordingly. Hence, the collision frequency of the electrons and their energy varies. Varying energy results in changes of the cross section of the gas mixture. At the end, this changes the drift velocity. But this effect can not be corrected as simple as shown in equation 2.27.

To correct for the density effects in the drift velocity, the drift velocity must be measured over a wide range of ET/p . When this is done, the result can be parametrised. With this the density effects can be corrected. Usually, the detector is operated at the maximal drift velocity. At this point, the dependency from density changes is minimal. Hence most of the detectors do not need a special correction.

If large variations in density are expected, either the gas should be chosen in a way, that the plateau of stable drift velocity is large enough, or the operation point is moved into the region of maximal dependency on density effects. The advantage of moving the operation point into maximal dependency is an almost linear relation between ET/p and the drift velocity.

2.4.3. Amplification

If we assume that the gas amplification is done inside a MicroMegas, we can assume a homogeneous field between mesh and readout planes. Both are separated by the distance d . For a homogeneous field E , the amplification described in equation 2.12 is simplified.

$$G = \frac{N}{N_0} = \exp(\alpha(E) \cdot d) \quad (2.28)$$

where α is the Townsend coefficient at the given electrical field E and d is the distance between mesh and readout plane. For sufficient high fields, the Townsend coefficient α can be expressed by a linear relation [5, p. 132] depending on the density ρ .

$$\alpha = \alpha\left(\frac{E}{\rho}, \rho\right) = f\left(\frac{E}{\rho}\right) \rho \quad (2.29)$$

In the following part, the density ρ is replaced by the gas density n . For high electric fields the function f can be approximated by

$$f\left(\frac{E}{n}\right) = a + b\frac{E}{n} \quad (2.30)$$

In combination with equation 2.28, we get

$$G = \exp \left(\left(a + b \frac{E}{n} \right) \cdot n \cdot d \right) = \exp (and + bEd) \quad (2.31)$$

The density dependence of the gain of a proportional wire chamber is described in [5, p. 136].

$$\frac{dG}{G} = - \frac{\lambda \ln 2}{\Delta V 2\pi\epsilon_0} \frac{d\rho}{\rho} \quad (2.32)$$

Here ΔV is derived from the average energy to produce one more electron $E_e = e\Delta V$. The second parameter λ is the linear charge density, which depends on the potentials and geometry of the wire chamber. Using the electric field the charge per unit length is given by [5, 4.4]

$$E(r) = \frac{\lambda}{2\pi\epsilon_0 r} \quad (2.33)$$

If the used gas amplification method is different from a proportional wire only the principle from equation 2.32 can be used. To derive this equation, many assumptions have been made, which cannot be made in other detectors. Continuing the approach with a homogeneous field MicroMegas, we take a look at the quotient of the gain at standard temperature and pressure (STP) and the current measured gain at the same electric field E .

$$\frac{G}{G_{\text{STP}}} = \frac{\exp (and + bEd)}{\exp (an_{\text{STP}}d + bEd)} = \frac{\exp (and)}{\exp (an_{\text{STP}}d)} = \exp (and - an_{\text{STP}}d) \quad (2.34)$$

By introducing a new constant Ξ , this equation can be simplified

$$\frac{G}{G_{\text{STP}}} = \Xi^{n/n_{\text{STP}}-1} \quad (2.35)$$

With $\Xi = \exp (adn_{\text{STP}})$. For small changes in $\Delta n = n - n_{\text{STP}}$ this formula can be approximated by a linear approach similar to equation 2.32.

$$\frac{\Delta G}{G} \approx m \cdot \frac{\Delta n}{n} \quad (2.36)$$

$$\frac{G_{\text{STP}}}{G} - 1 \approx m \cdot \left(\frac{n_{\text{STP}}}{n} - 1 \right) \quad (2.37)$$

The new variable m is the slope of the linear approximation. By applying this correction, it is possible to calculate G_{STP} from the measured gain. This way is used for the Gas Monitoring Chamber (GMC) of the ND280 detector. For the TPC, the correction is applied the other way around because here the current gain is needed.

$$G_{\text{TPC}} = \frac{G_{\text{STP}}}{1 + m \cdot \left(\frac{n_{\text{STP}}}{n_{\text{TPC}}} - 1 \right)} \quad (2.38)$$

Due to production of a detector with a pad readout plane, small differences in gain between multiple pad and also between multiple detectors might be observable. One possibility to remove these differences is to measure the gain of every pad. With these values a gain map can be created. In many cases the ambient conditions of the test bench do not match the norm

Table 2.2.: Run periods of the ND280 experiment.

run period	start	end
RUN1	2010-03-19	2010-06-26
RUN2	2010-11-18	2011-03-11
RUN3	2012-02-27	2012-06-09
RUN4	2012-10-19	2013-05-08

conditions. Hence in a first step, these measured gain values need to be converted to norm conditions. In a second step, these nominal gain values are starting point for calculation of the gain inside the TPC (see equation 2.38). Using the calculated current gain, the primary charge, and thus the energy loss can be calculated. The method described above is used at the TPCs of the ND280 detector.

2.4.4. Applying the corrections to data measured with the gas monitoring chambers at the ND280 detector

As an example, the corrections, which are described above, are applied to the measured data of the gas monitoring chambers. These chambers observe the supply and return gas flow of the TPC inside the ND280-detector. The operation principle of the monitoring chambers is described in 8.5.1.

All corrections are applied to the four different run periods, which were done since successful commissioning of the ND280 detector. The run periods are listed in table 2.2.

Density correction of the drift velocity

Due to the fact that the TPC is operated at the maximum of the drift velocity, the dependence on density effects is quite small. The measurements, which are shown in figure 2.7, result in a negligible dependence on the density. The shown monitoring chamber is connected to the return gas from the TPC. Hence, there are impurities inside the gas causing the drift velocity to be lower than the shown simulation. The impurities are mainly H_2O , O_2 and CO_2 , due to the location of the sensitive volume inside a CO_2 filled isolation volume. The exact amount of contaminations is not known, and thus the matching to the simulation suffers.

Inside the ND280 offline software, changes in the drift velocity caused by the gas are corrected by a reference table. This table is filled with the average of the measurements of a period of 10 hours. The reconstruction software uses the last entry before the recorded event for reconstructing the third dimension.

Density correction of the gas amplification

Without density correction, the ratio of the measured gain values and the average gain is plotted against the relative density, which is defined as the ratio of the current density and

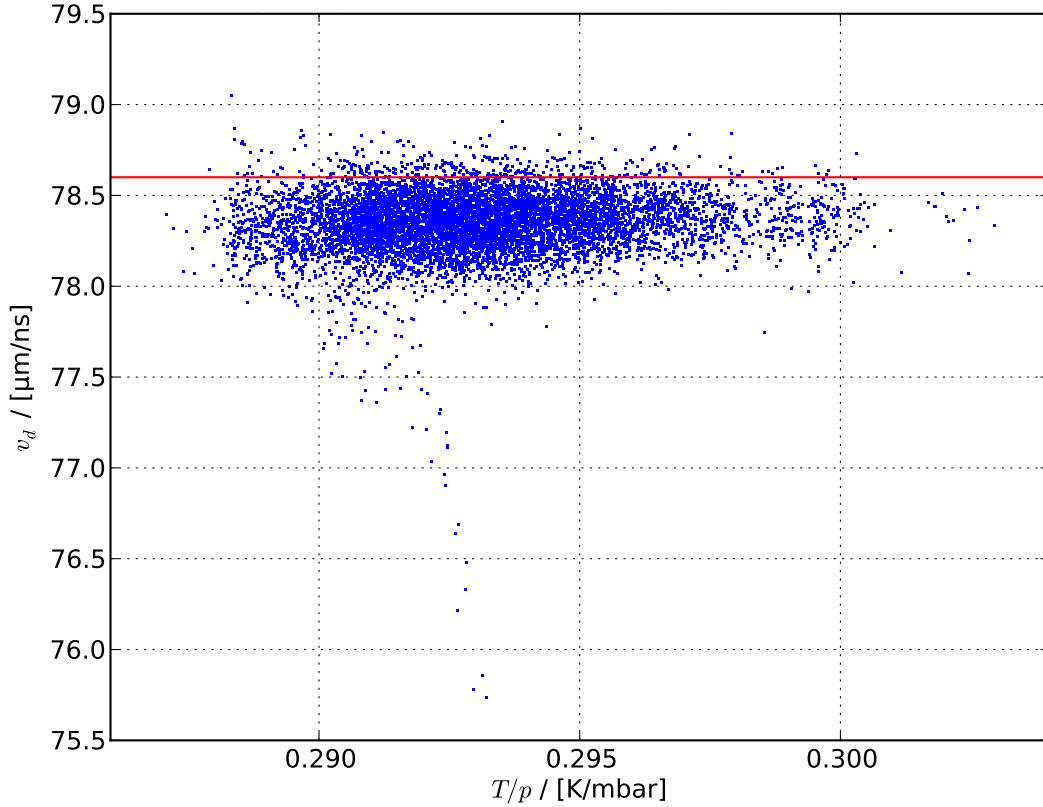


Figure 2.7.: All v_d measurements of GMC A during RUN3. Outliers are caused by impurities in the gas at the beginning of the run, before official data taking. The red line shows the simulated drift velocity of T2K-gas at 293.15 K and 1013.25 mbar. [27]

the density at Standard temperature and pressure (STP) conditions. The result for RUN4 is shown in figure 2.8.

The gain measurement is done by measuring the electrons created by X-ray ionisation, the photon is totally absorbed and density effects on the specific energy loss are irrelevant. Only changes in the Penning-probability may cause differences in the primary ionisation. Hence only the gain corrections can be applied to the data.

For the gain-correction the variable m can be derived directly from the data. m is derived by minimisation of the resulting width of the gain measurements. The minimisation is done by a χ^2 optimisation of the standard deviation σ of the corrected data.

An example for this minimisation is shown in 2.9(b). The corresponding histogram, with the best correction applied is shown in 2.9(a). We expect a small width, caused from the primary ionisation. Since the photon deposits its full energy in the gas volume, the number of primary electrons should be constant. The resulting width is caused by electronic noise and differences in the primary ionisation, which may be caused by Penning- and Jesse effects. Additionally the resulting width gets broadened by statistical fluctuations caused by the gas amplification.

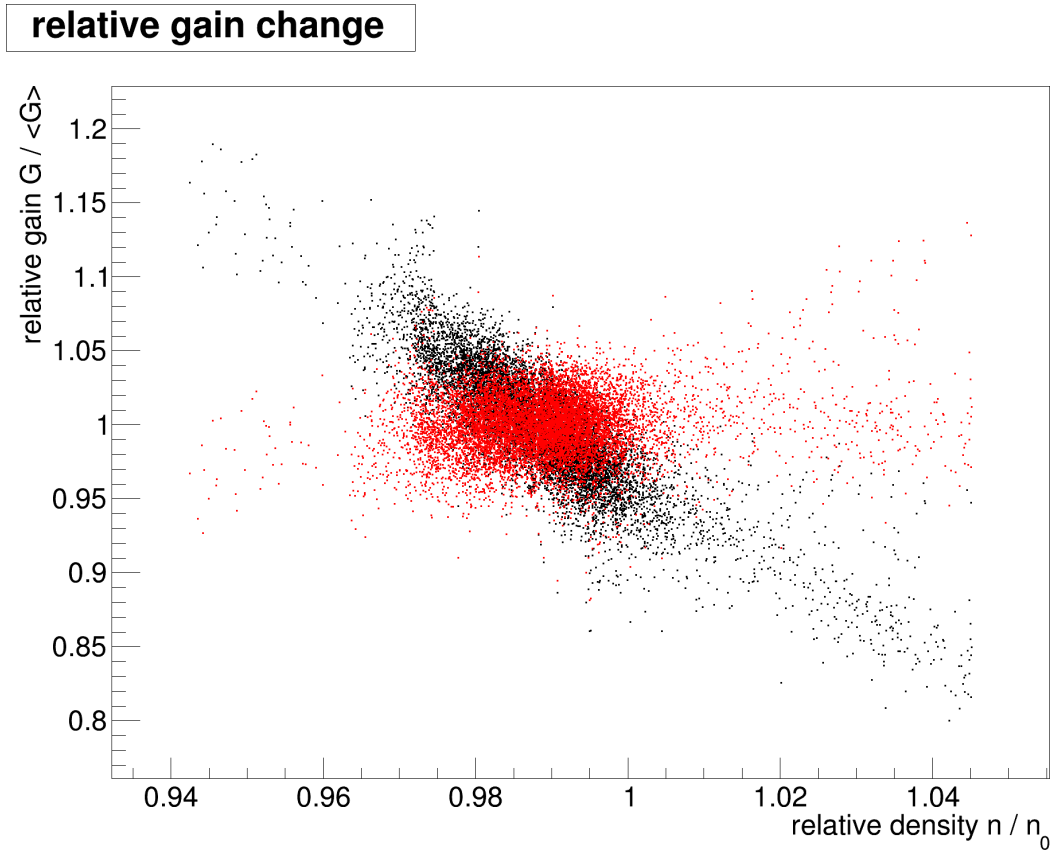


Figure 2.8.: Relative gain versus relative density change. The data shown in this plot were taken during RUN4. One can clearly see about 3% change in gain per percent density change in the uncorrected data points (black). After applying the correction (red) no dependency on the density can be observed.

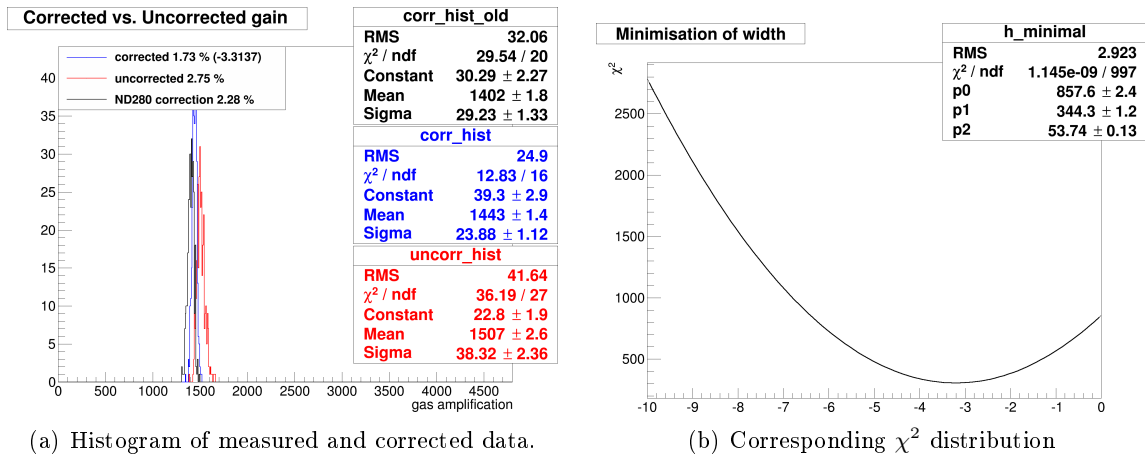


Figure 2.9.: Correction of the data sample containing the first week of RUN4.

The measured data is separated into intervals of one week. In this time span enough data points have been measured to allow a proper determination of m . As it can be seen in figure

2.10, it is sufficient to choose one slope m per run period. The changes of the derived slopes in one run period is compatible with the expected statistical fluctuations. After applying

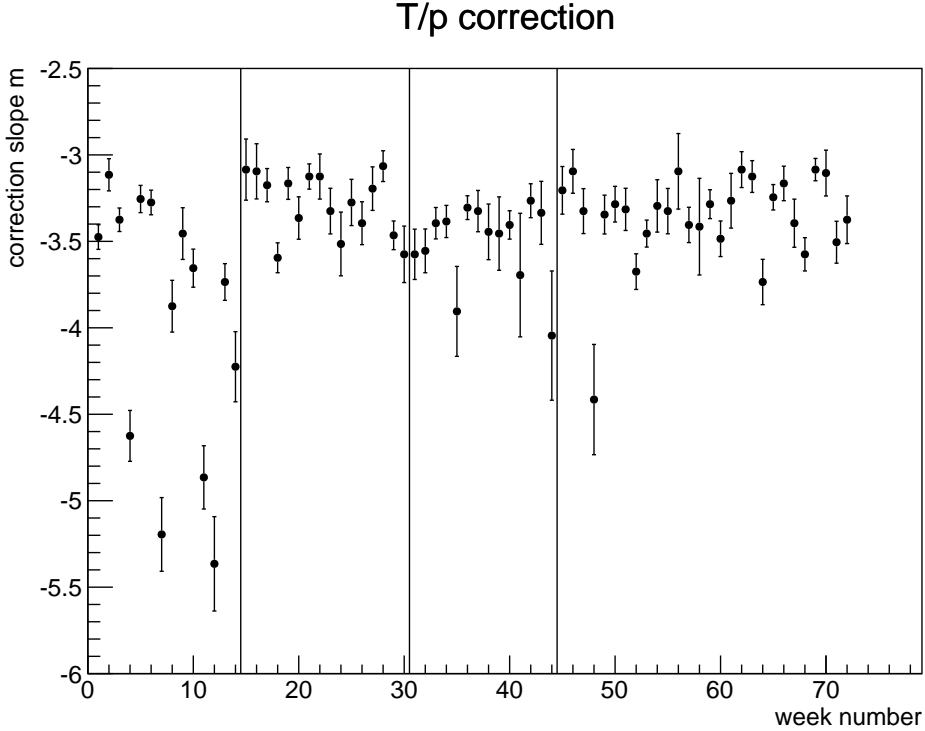


Figure 2.10.: Determined slope of one week data. For better comparison, the week number is assigned to each data sample. The vertical lines mark the different runs of the ND280 experiment.

this correction, the effect of density changes should be corrected. The resulting points are shown in figure 2.11. The fluctuations, which are still observable, result from changes in the gas amplification itself, which are caused by the gas. If the composition of the gas changes, also the value of the Townsend-coefficient changes. This results in a change of the gain, if the mesh voltage is kept constant.

To take changes of the gas into account, which change the amplification itself the ratio Λ of the corrected gain G_{STP} and a proper defined value G_{00} is needed.

$$\Lambda = \frac{G_{\text{GMC},00}}{G_{\text{GMC},\text{STP}}} = \frac{G_{\text{TPC},00}}{G_{\text{GMC},\text{STP}}} \quad (2.39)$$

Due to changes in the acquisition chain, the reference gain has to be defined for the first run and all other runs separately. The result of Λ is shown in figure 2.12(a). In figure 2.12(b) the ratio of the Root Mean Square (RMS) of the current correction and the new correction described above is shown. A smaller RMS results in a better energy resolution in the TPCs.

The changes caused by Λ are only about 1%. Before implementing this method, one has to measure $G_{\text{TPC},00}$ for the three TPCs. This is more difficult than for a GMC, because the

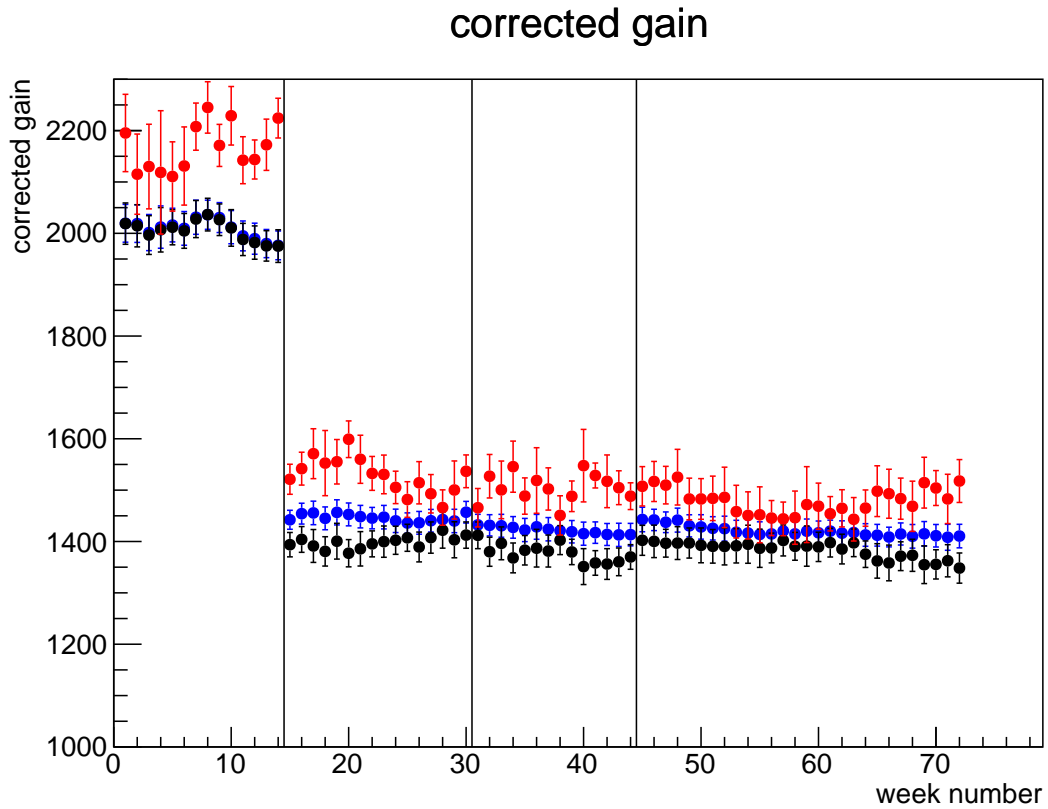
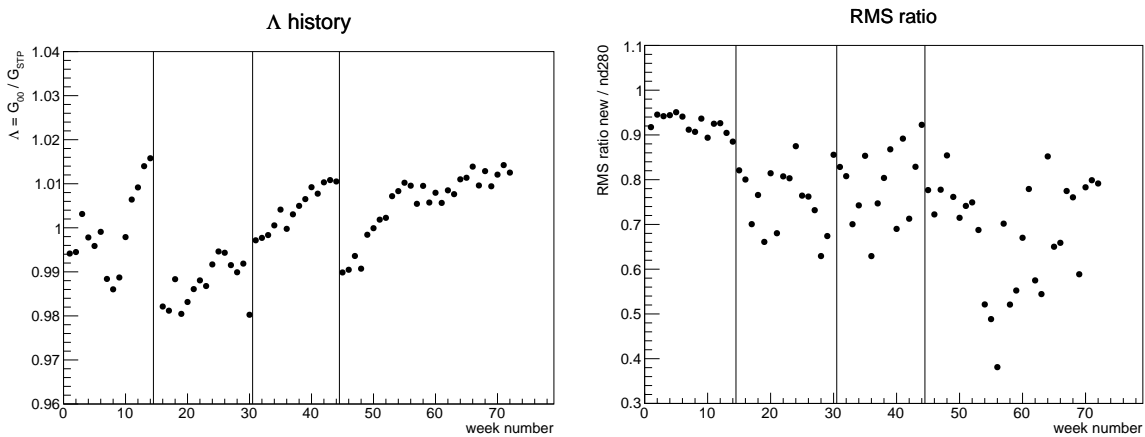


Figure 2.11.: Average gain over one week data. In red, the uncorrected raw data points are shown. In black, the existing correction is shown, and in blue, the correction described above is shown.



(a) Fraction of measured gain and reference gain against week number of run time.

(b) Ratio of the standard deviation of the histogram derived using the already implemented correction and the method described above.

Figure 2.12.: Overview of the improvement gained by the new correction and the change of the gas amplification with corrected density effects.

2. Introduction

primary charge is created by several particles, each having a different momentum and thus a different energy loss. Up to now, the value has not yet been defined. Unless $G_{\text{TPC},00}$ is defined, this correction should be disabled. This can be done via setting $\Lambda = 1$.

3. Requirements

All requirements to the Universal Gas Mixing Apparatus, preferentially designed for testing detectors, were developed during measurements in the laboratory. Most of the ideas and problems to be solved have their origin in testing and commissioning of the GMC for the ND280 detector. These chambers are described in detail in section 8.5.1. Some parameters and features are a tailor-made solution for these chambers. But due to the flexibility, they can also be used in a different setup. Nevertheless the main focus was put on generalisation. Thus many different chambers can be connected and used in combination with the UGMA.

3.1. Flow and pressure inside the connected detector

Only few requirements of the UGMA can be obtained from the connected detectors. The two main parameters are pressure and flow of the chambers connected.

Gas based particle detectors are mostly operated using a continuous flow through the detector to keep possible contaminations at an acceptable level. If the detector is not absolutely tight, air can diffuse in and contaminate the gas. Furthermore, many materials are porous for gases which causes diffusion of gas in both directions. Hence, some components diffuse to the ambient and air diffuses in. Another important reason for exchanging the gas is the demand for a constant composition of the gas mixture. Due to absorption or chemical reactions, the composition of the gas might change. Also radiation can damage the gas and split molecules into radicals, which can form new molecules. Those can reduce the performance of the detector.

The rate of gas exchange depends on the tightness of detector and piping and the amount of tolerable contaminations. On the other hand, the higher the rate of gas changes the higher the operational costs. Very rare gases should be recycled to reduce their loss. If the detector is operated using the half-open mode of the UGMA, possible contaminations can be filtered using purification materials. For setups in laboratories a typical rate of recirculation is about one to five volume changes per hour. This value originates from practical experience and should keep the contaminations at a tolerable level. But on the other hand, in the past it has been shown that it is possible to operate a detector with much lower gas flow. The ALICE TPC needs about five hours for one volume exchange. [13, p. 35].

Detectors, which might be connected to the system can have volumes between about 1ℓ to about 1000ℓ . Because this gas system is designed to be used with detectors at the development stage, most of them have a rather small volume. If large volume detectors are connected to the system, one has to cope with a lower volume exchange rate.

3. Requirements

Because of availability of flow controllers the maximal flow, which can be handled by the system is limited to $100 \ell_n/h$.

Many gas-filled detectors have a thin housing. This has the advantage, that the incoming particles interact only little with the wall. On the other hand, it causes the chamber not to resist high differential pressure between inside and outside. But there are also chambers which are operated at a quite high pressure. One example are the Muon Drift Tubes (MDT), which are used in the ATLAS detector [2]. These tubes are operated at 3 bara [1]. Hence, our system should be able to operate test chambers at over pressure.

One very important point is the regulation of the chamber pressure independent from the ambient pressure. This behaviour is useful for studies regarding pressure dependence of quantities to be measured. Without pressure regulation all measurements depend on the variations in ambient pressure.

Pressure regulation below ambient pressure is quite useful, too. This allows measurements in the whole pressure range of 0-4 bara. For the pressure regulation, the time constant needed to reach the setpoint depends on the volume. Due to the very different volumes, this time constant varies a lot, depending on the detector connected. To handle the return flow, the system is equipped with a flow sensor. Thus the pressure ramp can be adjusted such that the return flow does not exceed $100 \ell_n/h$.

3.2. Mixing

Mixing the gas can be realised via three different methods selected by the user.

1. partial pressure method
2. volume method
3. parallel flow mixing

3.2.1. Calculation

Three input lines are designed for the UGMA. Thus three gases can be mixed. The calculation how the final mixture can be composed from the three input lines is the same for all mixing methods. The fraction η of a given gas component of the mixture is always given as volume percentage. The sum of all fractions must follow

$$\sum \eta_i = 100 \text{ vol.-%} \quad (3.1)$$

In the following, η_{gas} represents the fraction of one gas component of the mixture. Here, it is important to realise, that one gas component can consist of multiple pure gases. For pure gases the calculation of η_{gas} is trivial. But if an existing mixture should be varied by admixture of small amounts of pure gases, a linear system of equations has to be solved.

$$\mathbf{M} \cdot \vec{\eta}_{\text{gas}} = \vec{\eta}_{\text{set}} \quad (3.2)$$

The matrix \mathbf{M} is a $m \times 3$ dimensional matrix. The number of rows m is given by the number of pure gases, which can be found in the connected gas bottles. The number of columns is

fixed by the number of input lines. If only two input lines are used the number of columns can be reduced.

To get the setpoint for each gas line, the equation must be solved for $\vec{\eta}_{\text{gas}}$.

$$\vec{\eta}_{\text{gas}} = \mathbf{M}^{-1} \cdot \vec{\eta}_{\text{set}} \quad (3.3)$$

Example: Modification of premixed T2K-gas

As an example, the modification of premixed T2K-gas is shown. T2K-gas is the gas mixture used inside the TPCs of the ND280-detector within the T2K-experiment. This mixture consist of

- 95 vol.-% Argon,
- 3 vol.-% Tetrafluoromethane (CF_4) and
- 2 vol.-% Isobutane (iC_4H_{10}).

If we assume that the modification should increase the CF_4 component by 0.1 vol.-% and decrease Isobutane by 0.1 vol.-%. The result should be achieved using T2K-gas, Argon and Tetrafluoromethane. The equation which has to be solved can then be written as:

$$\begin{pmatrix} 95 & 100 & 0 \\ 3 & 0 & 100 \\ 2 & 0 & 0 \end{pmatrix} \cdot \vec{\eta}_{\text{gas}} = \vec{\eta}_{\text{set}} = \begin{pmatrix} 95 \\ 3.1 \\ 1.9 \end{pmatrix} \quad (3.4)$$

It can be solved by matrix inversion. In this example the inverted matrix is given by

$$\mathbf{M}^{-1} = \begin{pmatrix} 0 & 0 & \frac{1}{2} \\ \frac{1}{100} & 0 & -\frac{19}{40} \\ 0 & \frac{1}{100} & -\frac{3}{200} \end{pmatrix} \quad (3.5)$$

Multiplied with the requested composition, the setpoint for each line can be derived

$$\vec{\eta}_{\text{gas}} = \mathbf{M}^{-1} \cdot \vec{\eta}_{\text{set}} = \begin{pmatrix} 0 & 0 & \frac{1}{2} \\ \frac{1}{100} & 0 & -\frac{19}{40} \\ 0 & \frac{1}{100} & -\frac{3}{200} \end{pmatrix} \cdot \begin{pmatrix} 95 \\ 3.1 \\ 1.9 \end{pmatrix} = \begin{pmatrix} 95 \\ 4.75 \\ 0.25 \end{pmatrix} \quad (3.6)$$

Assuming that flow mixing is used, this means, that the flow of each gas line has to be set according to η_{gas} . To achieve the requested flow \dot{V}_{req} the setpoints of all three gas lines are given by:

$$\dot{V}_{\text{T2K}} = 95 \% \cdot \dot{V}_{\text{req}} \quad (3.7)$$

$$\dot{V}_{\text{Ar}} = 4.75 \% \cdot \dot{V}_{\text{req}} \quad (3.8)$$

$$\dot{V}_{\text{CF}_4} = 0.25 \% \cdot \dot{V}_{\text{req}} \quad (3.9)$$

This calculation method is the basis for every mixing algorithm used in the system.

3.2.2. Mixing methods

Gas mixtures can be created by various methods. Those which are going to be realised are described in the following part. The performance of the tested mixing methods is shown in section 11.2.

Partial-pressure-method

In order to create precise gas mixtures, the partial pressure methods can be used. This method needs a buffer volume, which is filled with the partial pressures of the input gases to match the requested mixture. The process itself depends on the pressure only and is independent of any volume.

In first order, this method is based on the assumption, that the volume ratios are proportional to the partial pressure ratios. This is valid for ideal gases.

The partial pressure p_i , which needs to be filled into the buffer is given by

$$p_i = \eta_i \cdot p_{\max} \quad (3.10)$$

If a large volume flow through the chamber is requested, the filled buffer has to last until the next mixture is created. Because using only the Mass Flow Controller (MFC) of the mixing module (see section 4.2.1) needs too much time to create the mixture, a bypass valve is build in. This bypass valve connects the mixer output to the input of the selected gas line. Hence the volume flow is much larger than through the MFC. By just using the MFC with a maximal flow rate of $100 \ell_n/h$ filling one buffer with a volume of 50ℓ up to 3 barg takes about

$$T \approx \frac{50 \ell \cdot 3 \text{ barg}}{100 \ell_n/h} = 1.5 \text{ h} \quad (3.11)$$

This time can be reduced using the bypass valve to less than 15 min (see section 10.3.4).

On the other hand, using the bypass valve, the flow is only limited by the flow resistance caused by the piping and valves. These valves must not be used in combination with flammable gases. Hence flammable gases have to be filled through the MFCs. Otherwise due to the very high flow, safety cannot be guaranteed.

The mixing result itself is independent of the way the gas is filled into the buffer. Only the time needed for mixing of the buffer strongly depends whether a bypass valve can be used or not.

Volume-method

The MFC have a feature called „batch-mode“. In this mode, they can be programmed that they close their valve when reaching an amount of gas flown through them. This is done by using the internal counter and alarm mechanism. They internally integrate the flow measured and trigger an alarm. When the alarm is triggered, the MFC can be configured to close its valve.

This mode can be used to test the response of a detector to contaminations with other gases, like O₂. For this test a very small amount of an admixture has to be added to an existing mixture. Due to the fact, that the MFC can only fill a volume at norm conditions, first the filled norm volume of the buffer has to be calculated. This can be done using the buffer volume V_{buffer} and the ratio of the fill pressure p and the norm pressure $p_0 = 1023.15 \text{ mbar}$. Using the ideal gas law leads to

$$V_{\text{buffer, filled}} = V_{\text{buffer}} \cdot \frac{p}{p_0} \quad (3.12)$$

If a small volume V_i is added to the already filled volume $V_{\text{buffer, filled}}$, the fraction η_i can be calculated. With this, the volume, which should be added can be calculated.

$$\eta_i = \frac{V_i}{(V_{\text{buffer, filled}} + V_i)} \quad (3.13)$$

To use this method the fraction of the gas will be given and hence equation 3.13 has to be solved for V_i . The shown calculation is only valid for a single admixture.

The minimal concentration, which can be added, is given by the minimal volume, which can be set inside the MFC. The smallest MFC of one line has a maximal flow of $1 \ell_n/\text{h}$ Ar. For other gases the conversion factor K must be taken into account (see section 7.1.3). Looking at the turn-down ratio of 1:50 the minimal flow is $0.02 \ell_n/\text{h}$. The minimal setpoint of the counter is at the order of 0.01ℓ . The minimal fraction of an admixture, which can be added with this method is given by

$$\eta_i = \frac{0.01 \ell \cdot 1 \text{ bar}}{50 \ell \cdot 3 \text{ bar}} = 67 \text{ ppm} \quad (3.14)$$

Whether the mixture contains the right amount of admixture can be checked for O₂ and H₂O, because inside the UGMA special measurement devices are build in.

During the commissioning and test of the UGMA only mixtures with several percent of admixtures have been created. For these mixtures it is sufficient to use the partial pressure and the direct flow method. Hence this mixing mode is foreseen and the basics are implemented, but since this algorithm has not been used, it is untested.

Direct flow

The methods described above are suitable for filling a buffer, because the gases are filled sequentially. The direct flow method is able to provide a continuous gas mixing. The correct mixture is ready at the end of the mixer. This method is able to operate the chamber or exchange continuously part of the gas. The required flows are given by

$$\dot{V}_i = \eta_i \cdot \dot{V}_{\text{total}} \quad (3.15)$$

Each MFC has some uncertainty of flow and hence, the described method is only suitable for quick mixtures test and is not very accurate. But on the other hand, this method can supply a flow of up to $100 \ell_n/\text{h}$ not heavily depending on the composition.

3.3. Mechanical constraints

This system does not supply a defined detector, but rather many possible detectors, with different specifications. Hence, it should match their requirements, which have been described before. Also, for the mechanical part, many compromises have to be made. One example is the choice of the material. Even if stainless steel would be the best material in every place, at some places brass and aluminium are used, because the parts are cheaper or are much easier to produce since stainless steel is hard to machine.

Another challenge is mobility. The system is designed for mobile use. The detectors, which need to be supplied with gas do not come to the UGMA. Instead the UGMA comes to the detectors. For example, this allows measurements at first in the laboratory and at a second stage at a test-beam facility. Due to the same gas-supply this allows comparable results of both measurement campaigns. In general often the gas systems used at a test-beam and inside a laboratory are totally different or at least, they vary a lot. Therefore, the physical results gained at these different positions may vary.

The quest for mobility, limits the size of the UGMA. The system should be able to be moved through „normal“ doors and rooms. To pass through normal doors, the width should not exceed the opening of the door box. This values for Germany are given by DIN 1811-1 [83, Tabelle 1]. For common doors the limit is 811 mm or at maximum 936 mm. The main module should not be higher than 1983 mm. But if a larger height is required, the system can consist of modules, which are stacked after positioning is done. The maximal height for this stack is given by the minimal room height of habitable rooms. The value is given as 240 cm by [84, p. 48]. It is important to meet this limit. Otherwise it is not possible to assemble the system in a „normal“ office. Because the facilities where the system should be operated are not fixed during planning phase, it is rather difficult to set limits. The limits are not going to be exploit, because almost certainly most of the experimental halls or laboratories have larger sizes. But if the system is build as small as possible, the number of possible operational facilities is maximised.

3.4. Electrical requirements

The whole electronic and electromechanical part was built with respect to the guidance given by the Verband der Elektrotechnik Elektronik Informationstechnik e.V. (VDE). Although they are not part of the current law, every electrical part must be constructed and built according to the state of technology. For the lower voltage part the precautions are not too severe, due to the fact, that no humans get hurt. In the section which uses 230 V, safety for the human operator plays an important role.

Special requirements are given by the sensors, valves and other equipment used in the system.

3.5. Usability

The usage of the system should be as simple as possible. Untrained experimentalists should connect their prototype detector and start the delivery of the gas. They should be able to use full functionality without knowledge about the principal functioning of the UGMA, which is described in the flow chart [74].

Before starting, the user just has to select the gas mixture, the mixing and operation mode and the parameters of the chamber such as supply flow and pressure. If the chamber should not be operated in open mode, the gas return ratio (recycling ratio) which proportional to the exhaust flow needs to be selected. All these settings can be done either at the local interface or remote via a device with a browser installed. The interface for local and remote access is exactly the same. Hence the user only needs training for one interface and can operate the UGMA from everywhere. Remote access is needed, when the UGMA cannot be operated locally due to access restrictions.

Before the system can be used, the gases, which should be mixed, must be connected. As a second point gas for the gas chromatograph (GC) (see section 8.3) and the purifier (see 4.2.4) regeneration can be connected, if these features should be usable.

3.5.1. Connections

All connections to the chamber and gas bottles are equipped with 6 mm Swagelok[®] tube fittings. The exhaust vent is a 200 mm folded spiral-seam pipe, which can be extended using a flexible tubing of same diameter. The gas can be supplied with a pressure up to 8 bara. If a lower pressure is used, the user should check, if the mixtures can be created when using the partial pressure method. Typically, it is sufficient to connect a single step pressure reducer which supplies a line pressure of at maximum 5 bara. Higher pressures are not necessary since the safety valves (see section 4.2.1) limit the pressure inside all parts of the UGMA to 4 bara.

To be operational the system needs a compressed air supply with a supply pressure of at least 5 bar, preferable free of water and oil.

Further the UGMA needs one three phase 16 A CEE power connection to power up all subsystems. If the user wants to operate the UGMA not only in local mode, a network connection is needed.

4. Mechanics

4.1. Concept

The UGMA consists of various hardware parts, which are described in detail in [37]. In this chapter the basic concept will be explained. The requirements that the system should meet have been described before.

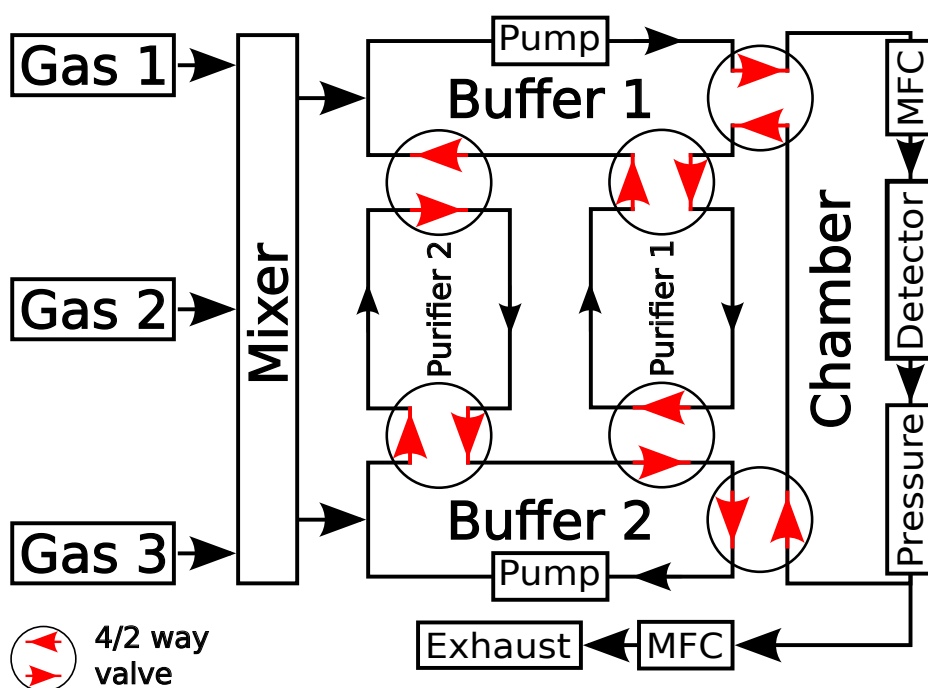


Figure 4.1.: Basic sketch of the UGMA. For clarity the analysis loop is missing and only two purifiers are drawn. Buffer 1 supplies the chamber and is connected to purifier 1. The second buffer is connected to purifier 2 and is either filled with gas or in standby. The return gas can be exhausted or recycled. The two red arrows inside the circle mark 4/2-way valves, which are used to connect the loops with each other.

Each functional block of the UGMA is build as a closed loop with a circular gas flow. There are two exceptions from this circular design, the mixer as the gas source and the exhaust gas the gas dump.

A very simple sketch of the UGMA is shown in figure 4.1. For clarity the analysis loop (section 4.2.2) is not drawn. It can be connected to any other loop of the UGMA. At first

the right gas mixture is created using the mixer (section 4.2.1). Then the gas can be stored inside one of the two buffers (section 4.2.3), where it can be cleaned by the purifier (section 4.2.4) from H₂O and O₂ contaminations. From the buffer the gas flows to the connected chambers (section 4.2.5). The gas flow through the chambers is regulated in flow rate and pressure. After the gas is flown through the chamber it can be exhausted or recycled.

To provide operation as long as possible, all important systems such as buffer and purifier exist twice. If one system is in use, the other can be regenerated or filled. This allows continuous operation.

Both buffer loops are equipped with a pump, which can create a active gas flow inside. All other loops are passive ones, which can only be switched into an active gas flow.

The gaseous particle detector is not part of the UGMA, but when it is connected, it is included into the chamber loop and hence it becomes a temporary part of the system. The chamber loop is a very special loop, because it can be used both in a loop mode but also in a straight mode. If the detector is operated in half-open or closed mode the gas is recycled and hence the chamber is used in loop mode. Otherwise if the detector is operated in open mode the chamber-loop is used as a straight device dumping the gas to the exhaust.

For quick measurements the buffers and purifiers can be bypassed , so that the mixer output is directly connected to the chamber input. This mode is used for direct flow mixing (section 3.2.2). At the same time the output of the chamber is directly connected to the exhaust. Hence the gas cannot be recycled. Due to the fact, that the purifier modules can only be connected to the buffers, also no purification can be applied. The gas can be fully analysed, because the analysis loop can be switched to both the chamber supply and chamber return flow. By measuring at both positions it is possible to estimate the contaminations which are introduced by the chamber itself.

4.1.1. Valve concept

The insertion of the purification module into the buffer loop is treated as an example, how to include loop modules into the system. It is described in detail in the following.

Using normal 2/2-way¹ valves, three valves are needed to insert the purification module into the buffer loop. In the setup shown in figure 4.2 in total six pipe-valve connections are needed. Another six connections have to be done at the two T-pieces. In total this results in 12 connections from which each can be a source of leakage. One further problem might occur, if one valve shows a failure. Then the whole setup cannot be used. Both disadvantages can be solved by using one 4/2-way valve instead of three 2/2-way valves. Using one valve reduces the number of connections to four connections (see figure 4.3) and the probability of valve malfunction.

¹A/B-way means that the valve has A connections and B switch positions. For example: A 2/2-way valve is a valve, which has two connections (typically one input and one output) and two switching positions (on/off). This valve can switch the gas flow on and off.

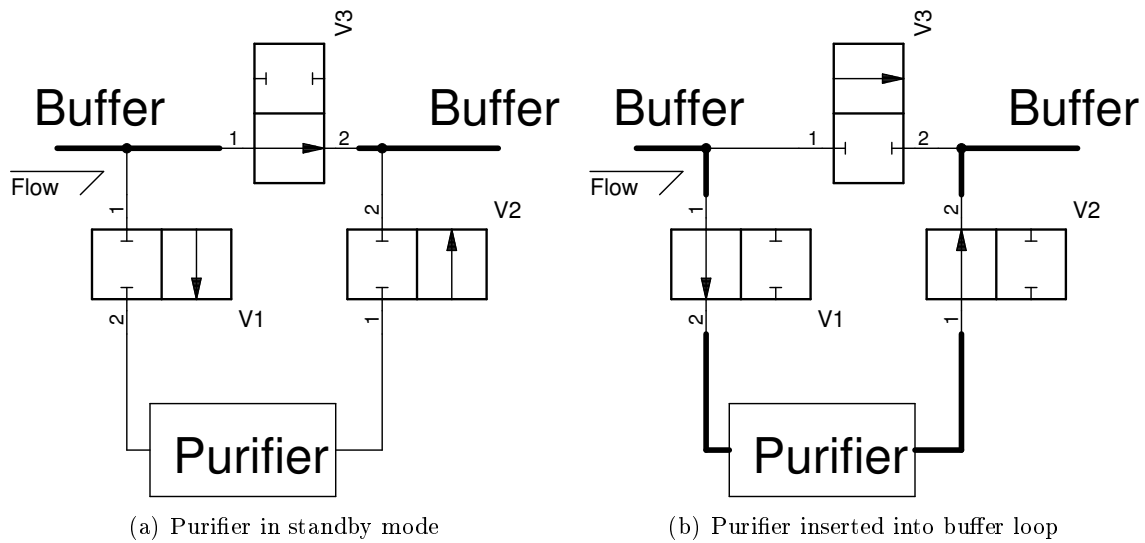


Figure 4.2.: Insertion of the purifier module into the buffer module. Valves V1 and V2 are normal close (NC) valves whereas V3 is a normal open (NO) valve. The flow is directed from left to right and is shown in thick lines.

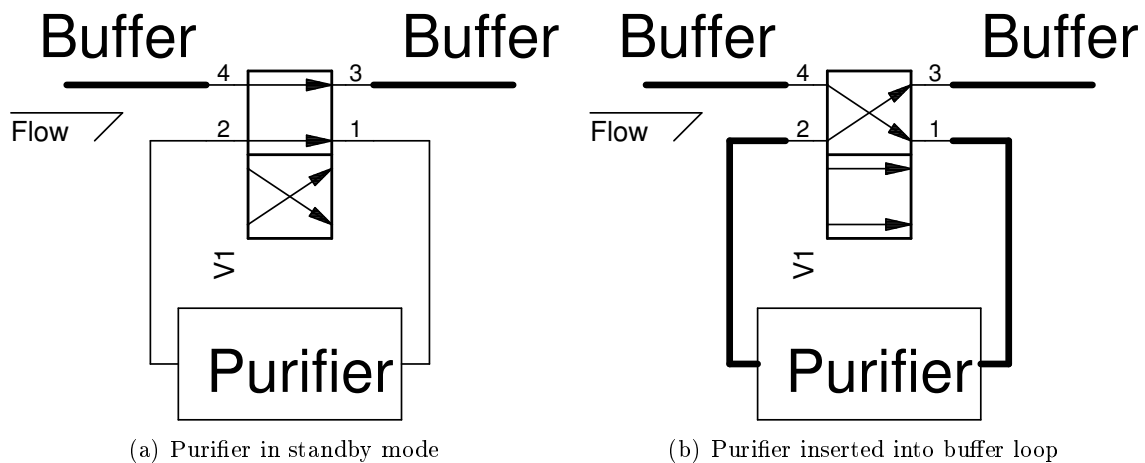


Figure 4.3.: Insertion of the purifier module using one 4/2-way valve. The number of connections is reduced compared to the solution using three 2/2-way valves.

4.1.2. Piping concept

Before starting piping, a concept for this major step has been developed. This was done during the design phase before building anything. During the design phase different approaches have been developed. Two of them are described in detail in the following section.

Fully modular approach

One approach was to build one dedicated module per function block. This means, the functionality is encapsulated in a box, which has a well defined interface at the backside. These modules can be stacked in a 19"-Rack for example and interconnected at the backside. The connection at the back-panel is done using bulkhead connectors. In total, the number of connections per module is given by the internal number of connections and additional two connections per external link.

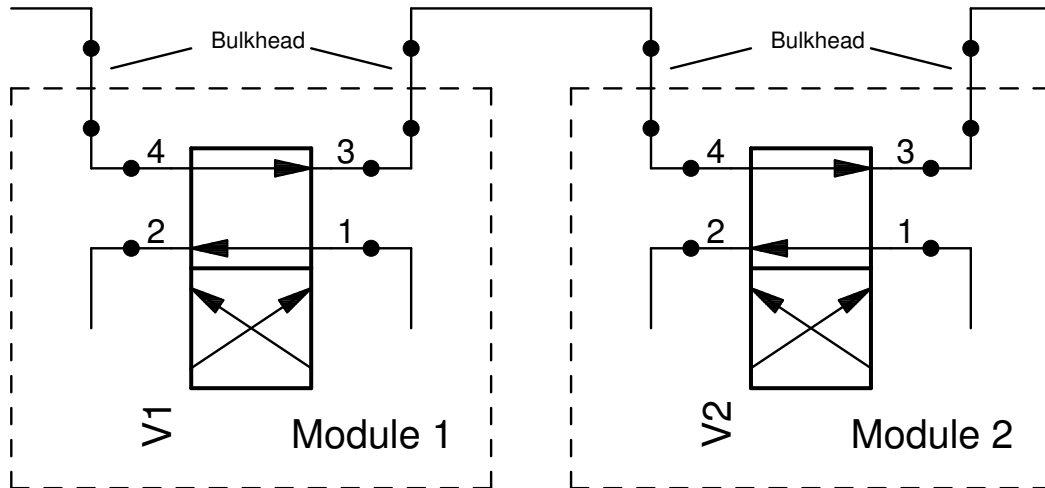


Figure 4.4.: Fully modular piping approach between two 4/2 way valves V1 and V2. The interconnections are displayed as dots.

One advantage of this solution is the interchangeability and the reusability of the module. On the other hand, more than about one hundred connections have to be done in addition compared to the assembly group approach and their tightness has to be checked.

Assembly groups

Another approach was to build assembly groups without a well defined interface at the backside. The interconnection between the modules is done by connecting the valves directly. For the mechanical construction more flexibility is gained. There is no well defined interface for each module and thus each interface can be designed very flexibly according to the present situation. Hence less piping is required. One further advantage of this solution is that there is no need for bulkhead connectors. One disadvantage points out, when looking at the reusability. The building groups are not reusable for future projects. If the design should be reused, this might cause a change in design due to different piping interface locations.

Decision

It was decided to use assembly groups instead of the fully modular approach. This decision is based on the fact that the number of gas connections and through this, the number of

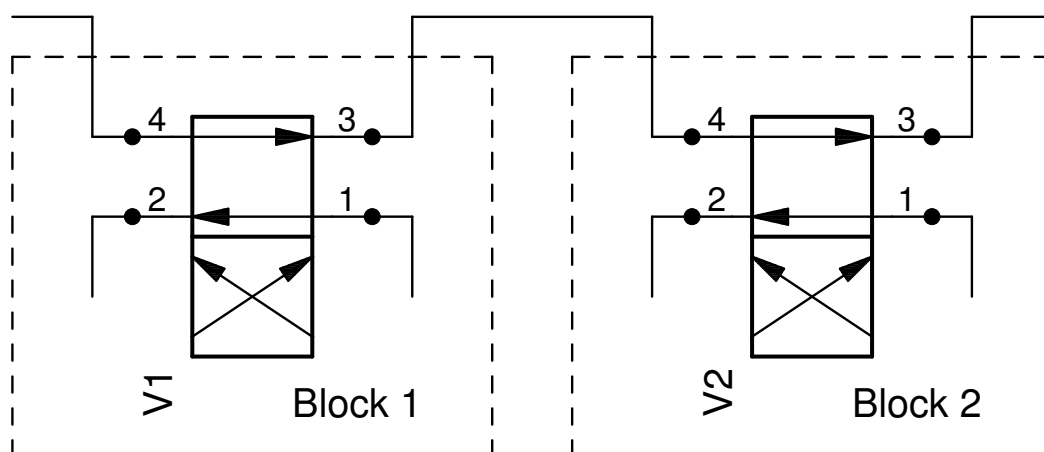


Figure 4.5.: Assembly group piping approach between two 4/2 way valves V1 and V2. The interconnections are displayed as dots.

possible leaks should be kept minimal as the purity of the created gas mixtures is of great importance. Small amounts of contaminations can cause problems to the signal inside the particle detectors. Hence, the number of connections was minimised to allow mixing gas with a high purity.

4.2. System Overview

In this chapter, all assembly groups and their corresponding piping are shown. All described parts are mounted inside the gas handling volume, which is shown in figure 4.6. The mechanical part of the UGMA consists of

Valves:

- 22 pneumatic driven 4/2-way valves
- 56 electrical controlled solenoid-valves

Piping:

- approx. 120 m 6 mm stainless steel pipes
- approx. 20 m 10 mm stainless steel pipes
- approx. 65 m 6 mm flexible tubing

Sensors:

- 18 pressure sensors
- 18 temperature sensors
- 2 other sensors (O_2 and H_2O contamination)

The shown list just gives an overview of the most important parts, small things like adapters mountings etc. are not listed. All items are mounted in the parts of the UGMA, which are described in the following sections. Starting with a full overview shown in figure 4.7. In all figures pipes might have been cropped. These lines are either unimportant pipes, like



Figure 4.6.: View inside the gas handling section of the UGMA. On the right side one of the two buffer is shown. Directly in front of the buffer the pumps of the buffer loops are mounted. In the upper part one can see the valve island.

exhaust etc. or they are connections to other modules, which are not shown in the current detail. All figures are derived from [74].

Each assembly group is protected against overpressure by a combination of a spring loaded overpressure valve and a 2/2 solenoid valve. Each spring loaded valve has been adjusted to 3 barg [37] The solenoid valve can be used to reduce the pressure inside the loop controlled by the pressure sensor.

4.2.1. Mixer

The way of the gas inside the mixer module is shown in figure 4.8. Starting from the bottles, the gas flows through a combination of non-return valve (M102NR) and a 15 μm filter. The non-return valve protects the supply line from gas flowing backwards and contaminating the line. The filter prevents the system from particles, which might get stuck in the flow controller or valves and cause malfunctions in these parts. After this the gas flows through a 3/2-way manual valve (M103YH). This valve allows flushing the connection line to the UGMA, when changing a bottle to another gas. Right after this the gas is sent to the MFCs

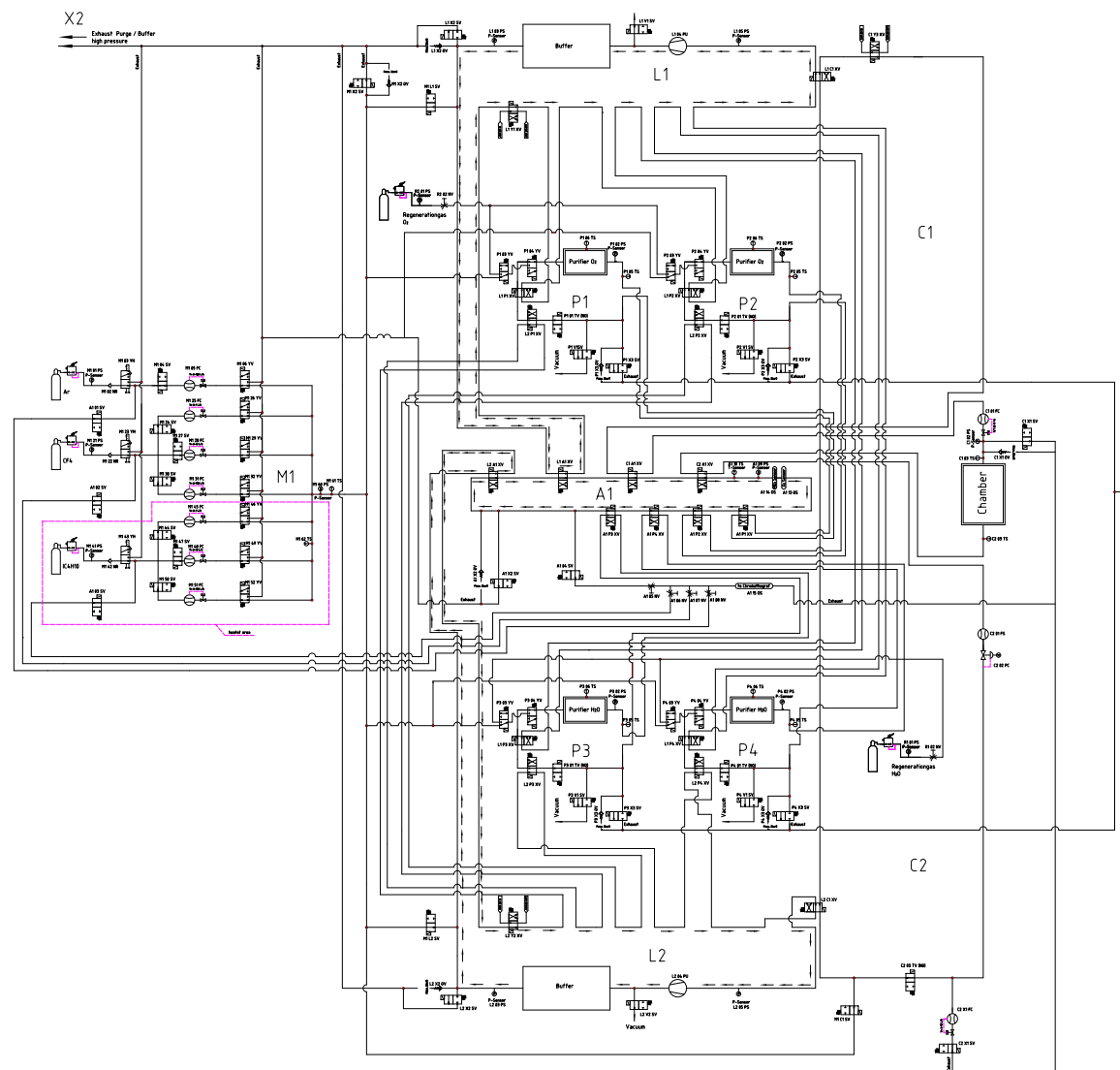


Figure 4.7.: Overview of the piping of the whole system. [74]

(M105FC). Because the MFCs might be not completely gas tight, each MFC can be switched off by a 2/2 solenoid valve (M104SV). Right after the MFC a 3/2 way valve (M106YV) is mounted, to switch the gas flow to the exhaust. This mode can be used to test single MFC without influencing the rest of the system.

The input pressure of each line can be up to 10 bara. Since the maximal pressure inside the rest of the UGMA is limited for safety reasons to 4 bara, it is sufficient to supply the mixer with a slightly higher pressure.

One group consisting of three MFCs (M145FC, M148FC, M151FC) can be equipped with a heater. This possibility might be installed, when the system is operated in areas, which have a lower temperature. Hence some gases might condensate and this unwanted effect should be avoided by increasing the temperature.

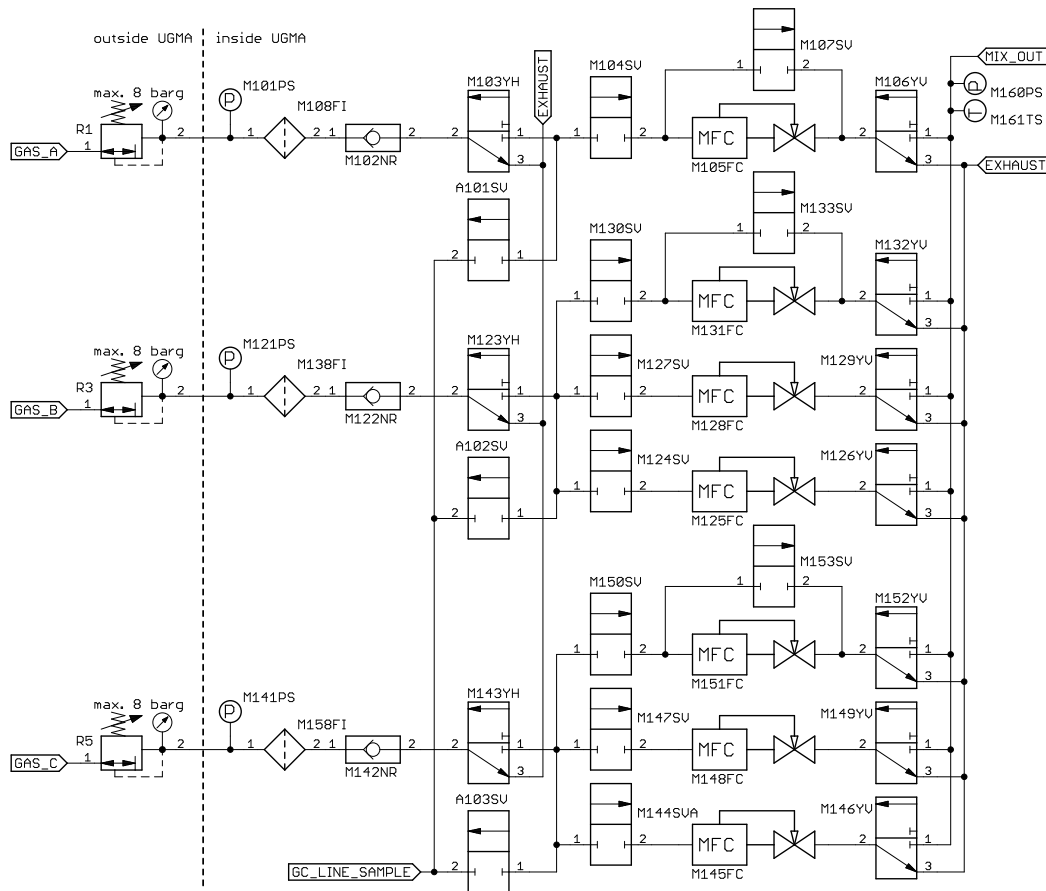


Figure 4.8.: Mixer section of the UGMA. (Based on [74])

4.2.2. Analysis Loop

The analysis loop (shown in figure 4.9) is the central assembly group inside the UGMA. Each other loop can be connected to it. Connection to the other loops is done by pneumatic 4/2 way valves, e.g. L1A1XV, which connects buffer one to the analysis loop. For this loop, the flow direction is drawn. Following the arrows the gas is flowing through different sensors. First the temperature (A110TS) is measured and right after the pressure inside the loop is measured (A109PS). After all this is known, the gas is sent through special sensors for oxygen (A114OS) and water (A113OS). By opening the solenoid valve (A104SV) parts of the gas can be sent to the gas chromatograph (GC) to perform a full analysis of the gas. The GC can also be sourced from each input line. This is needed for calibration purpose.

4.2.3. Buffer

When the UGMA is operated either in half-open or closed mode, a buffer volume is needed. The buffer volume is shown in figure 4.10. The same volume is used when the gas mixture is created by partial pressure mixing. If the buffer should be filled with a mixture it can be connected via a 2/2 way valve (M1L1SV) to the mixing module described before. Inside this

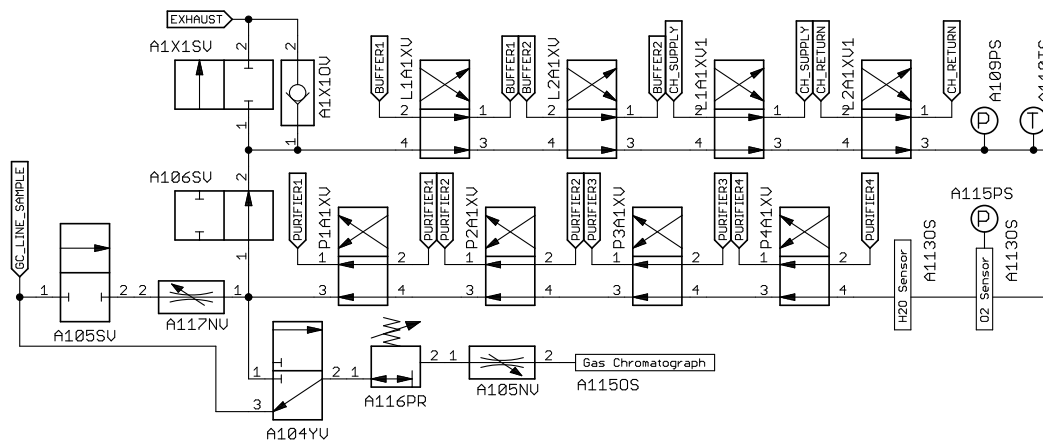


Figure 4.9.: Analysis loop, with direction of inner flow marked by arrows. (Based on [74])

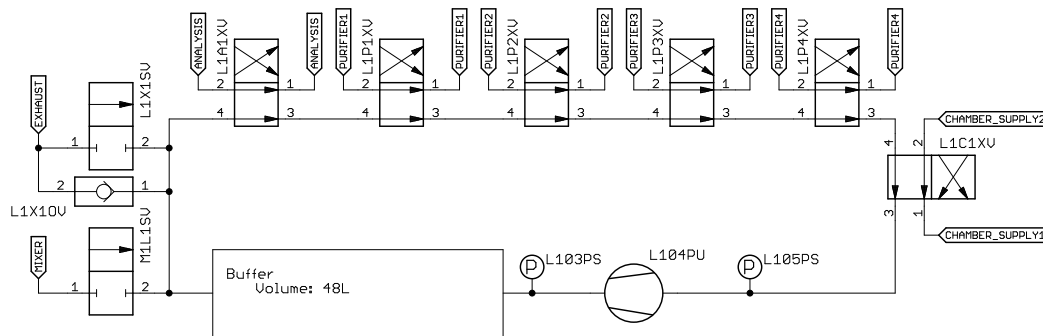


Figure 4.10.: One of the two buffers, which can be used for partial pressure mixing. (Based on [74])

loop, a pump (L104PU) is mounted to create a certain pressure and to stir the gas, when the buffer is in standby. The pressure before and after the pump can be monitored by two pressure sensors (L103PS and L105PS). Via a solenoid valve (L1V1PSV) the buffer can be connected to the vacuum pump and thus be evacuated. When the buffer should be used in combination with the chamber circuit, the 4/2 way valve (L1C1YV) switches the gas flow to the chamber.

In total two of the buffers exists, so that one can always supply the chamber and the other one can be filled.

4.2.4. Purifier

If the gas gets contaminated by O_2 or H_2O , it can be fed through the purification modules, which are shown in figure 4.11.

In total, there are two purifiers of one kind. This allows regeneration of one, while the other one is in use. The purifiers are not combined ones, like it is often done in other experiments.

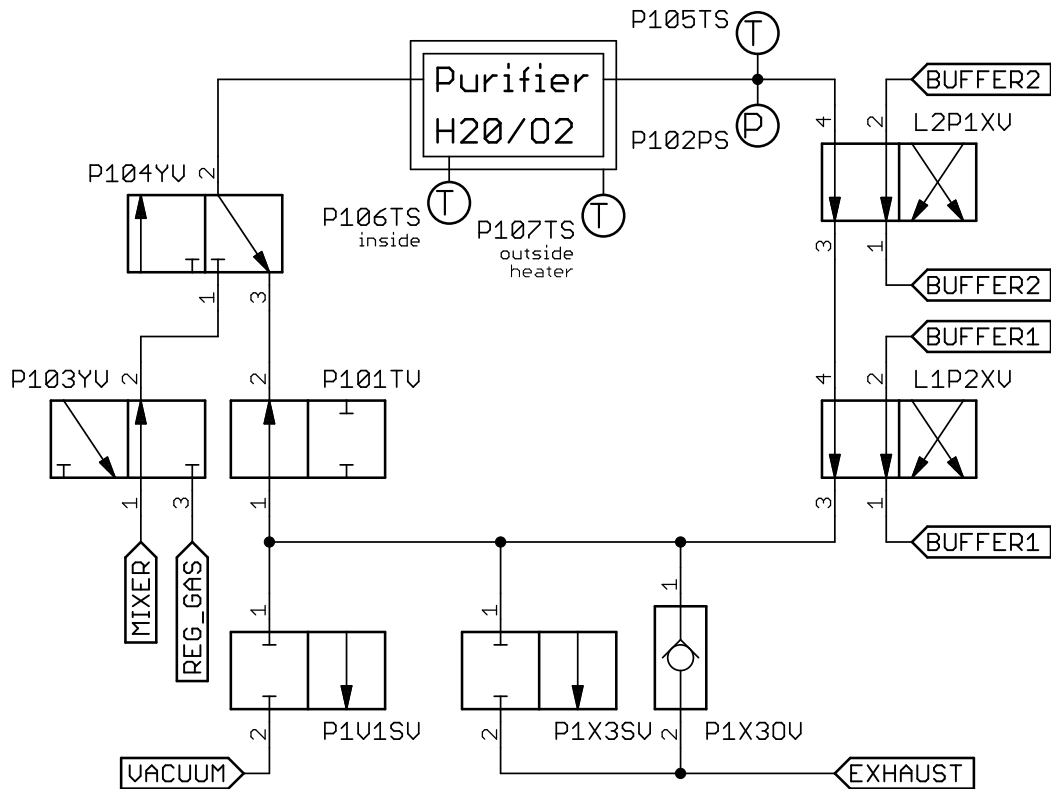


Figure 4.11.: One purifier module of the UGMA. (Based on [74])

Hence it is possible to measure the response of a detector to contaminations of e.g. H_2O , while O_2 is removed.

The purifiers used for the removal of H_2O are filled with a molecular sieve with a size of 3 \AA . This material should only filter H_2O and leave all other constituents of the gas intact. Regeneration of this purifier can be done by evacuation to vacuum and/or flushing with dry gas. [37]

The other purifiers are filled with activated copper and can remove O_2 from the gas. This is done by controlled oxidation of the copper, which binds the oxygen. Regeneration is done by flushing the purifier vessel with a mixture of Argon and about 5 % hydrogen. By this, the oxygen bound at the copper reacts with the hydrogen to water, which is exhausted. [37]

4.2.5. Chamber

Flow and pressure regulation of the connected detector (chamber) is done in two different stages as shown in figure 4.12. Hence both the pressure and flow inside the chamber can be controlled independently. Upstream of the chamber, the flow is regulated by a MFC (C101FC). To know the parameters inside the chamber, the pressure (C102PS) and the temperature (C103TS) is recorded at this point. At this point, an over pressure combination protects the chamber from too much pressure. The spring loaded valve (C1X3OV) is set to the maximal pressure of 3 barg.

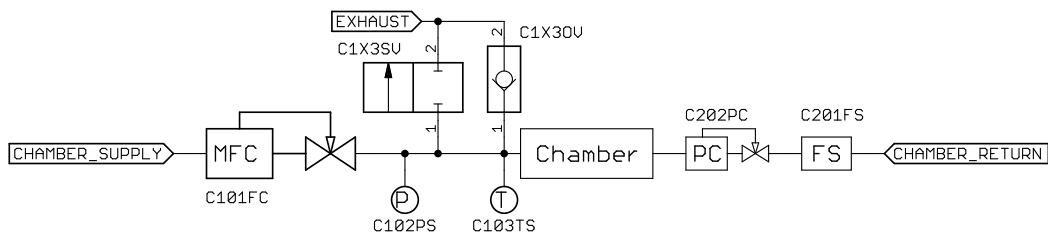


Figure 4.12.: Pressure and flow control of the chamber. The gas is flowing from the left to the right. Adapted from [74].

Behind the chamber, the flow is measured by a flow sensor (C201FS) and the pressure gets regulated by a special pressure controller (C202PC). The pressure of the chamber can be set independent of the flow in a range of 0-4000 mbara. If a pressure below ambient pressure should be applied, the pump of the buffer must be used to create underpressure behind the pressure controller to allow proper operation.

The analysis loop can be switched also before and behind the chamber to estimate which contaminations are caused by the chamber itself and which are caused by the mixed gas. The exhaust section of the chamber is shown in figure 4.13.

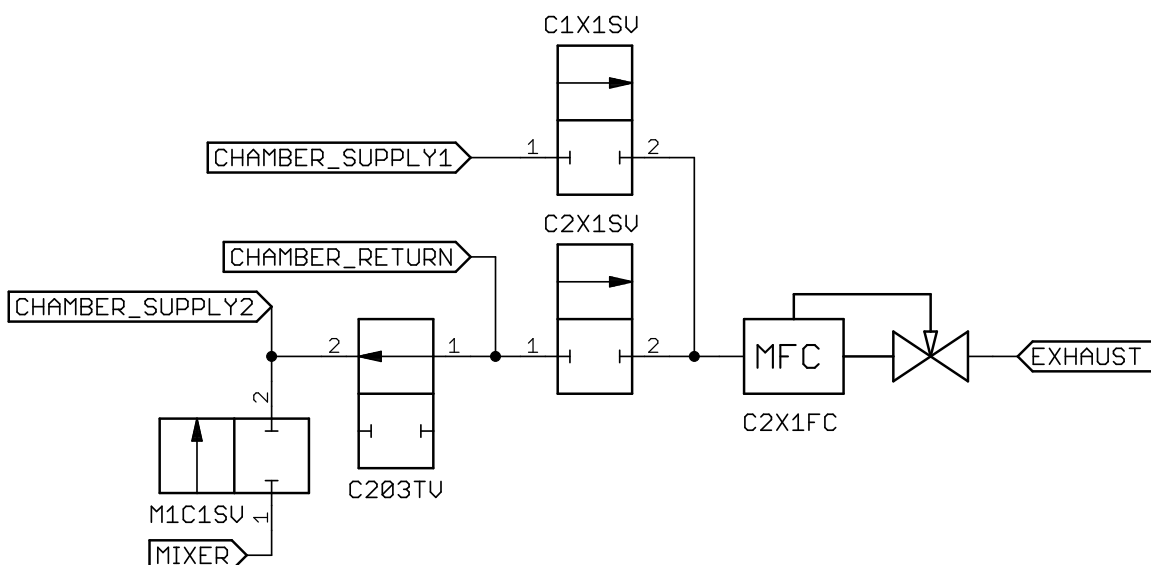


Figure 4.13.: Exhaust section of the chamber loop and the mixer supply line. Adapted from [74].

If the chamber is operated in open mode, the MFC C2X1FC is set to fully open and the 2/2 way valve C203TV is closed to prevent the gas from flowing back into the sourcing loop. By opening the 2/2 way valve M1C1SV the chambers can be sourced by the mixer directly.

If the MFC are fully opened, they act only as a flow sensor and no longer as a controller. In normal operation C2X1SV is opened and C1X1SV is closed. Now the MFC is fully opened and acts as a flow sensor.

If the chamber should be operated in half-open mode, C2X1SV is closed and C1X1SV is opened. Now the gas exchange rate can be adjusted by the setpoint of the MFC. For proper operation of the MFC a certain pressure difference between input and output of the MFC is needed. Hence the MFC is connected to the chamber supply pressure.

When operating in half open mode, we have to distinguish between two scenarios. One scenario is a chamber, which is operated almost at ambient pressure. If the gas flows through C2X1FC it causes a pressure drop, which increases the pressure inside the chamber. This might destroy the chamber. Hence the controller is switched to the chamber supply line and via its setpoint the rate of the gas, which is exhausted can be regulated. The other scenario is a chamber which can be operated at higher pressures. Now the primary pressure is high enough to supply C2X1FC in the exhaust position. This is the more optimal configuration, because the gas from the chamber, which might be contaminated is partially exhausted. For low pressure chambers the return gas first gets diluted and afterwards exhausted. Hence the amount of contaminations inside the gas loop for high pressure chambers can be reduced compared to low pressure chambers.

4.3. Explosion Safety

When handling flammable gases, explosion safety gets a topic. It is quite difficult and expensive to encapsulate all parts, that they resist a possible explosion or that their stored energy which might cause a spark is lower than the ignition energy.

The easier and realised way is to ensure that the concentration of the flammable gas always stays below the critical limit, which is the lower explosion limit (LEL). For safety reasons this limit is reduced by 50 vol.-%. The LEL depends on the gas and varies from 1.4 vol.-% for C_4H_{10} up to 4.4 vol.-% for CH_4 . In case of the UGMA all calculations have been done assuming C_4H_{10} . If other flammable gases should be used in combination with the UGMA, it must be ensured, that their LEL is greater than 1.4 vol.-%.

To make sure that the gas concentration is always below this limit, the UGMA is split into two parts. One part hosts all equipment, which handles the gas (e.g. valves, MFCs, etc.) and the other hosts all electrical equipment (like power supplies). By this separation many ignition sources have been moved out of the critical volume. To increase the safety the critical volume is vented using a fan. If flammable gas leaks into this volume it gets drawn off and hence no explosive atmosphere can establish. For proper operation the exhaust of this fan must be connected to the outside, otherwise the flammable gas can accumulate and the safety cannot be guaranteed. Every system has some leakage rate, which is reduced to the minimum. To fulfil the requirements the leakage rate \dot{V}_L and the ventilation rate \dot{V}_V must have the right relation.

$$\frac{\dot{V}_L}{\dot{V}_V} \geq 50 \% \text{LEL}_{C_4H_{10}} = 0.7 \text{ vol.-%} \quad (4.1)$$

The critical volume is continuously observed by a gas warning system. In normal operation the fan speed is reduced. If the gas warning system detects flammable gas, it triggers an interlock and the fan speed increases to reduce the amount of flammable gas as fast as

possible. At the same time all valves get switched off to turn the UGMA into a stable state, which prevents the system and its ambient from damage. In addition to ensure that the fan really pushes the air to the outside and is not just turning without conveying air, there is a simple pressure sensor and a very simple Pitot-flow sensor mounted. By measuring the dynamic pressure the amount of conveyed air can be calculated. [37, p. 37 f.]. The ventilation section is shown in figure 4.14. All calculations regarding explosion safety are shown in detail in [37].



Figure 4.14.: Photo of the ventilation part including the fan (right side) and ventilation monitoring (left side). The system is connected on its very left side to the exhaust to the ambient outside the lab.

5. Electronics

5.1. System overview

After the definition of the mechanical part, the electrical part has to meet the requirements and restrictions imposed by the mechanical design. Mainly the number of analogue inputs and digital outputs depend on the mechanical design. Also the communication between the control software and the electronics board is part of this concept.



Figure 5.1.: Photo of the electronics readout. In the upper part the crate with the analogue and digital modules can be seen. Directly below this the CAN2ETH and the three RS232ETH modules are mounted. Above the PC, which is the lowest element the PDU and the internal Ethernet-switch is mounted. The white labels mark the cables which control the valves or are connected to the sensors.

It has been decided to use a commonly used 6 U crate with an 96 pole backplane for power, CAN-Bus [93] and interlock distribution. A photograph of the setup is shown in figure 5.1. The modules are described below.

The electrical concept has been implemented using following devices. The sensors are listed in section 4.2. The modules are shortly described in the following section and in detail in [37].

Modules:

- 3 16-channel analogue input boards
- 4 16-channel digital input and output boards
- 3 RS232ETH (bidirectional RS232 Ethernet bridge)
- 1 CAN2ETH (bidirectional CAN-Bus Ethernet bridge)
- 56 valve driver
- 18 PT100-transmitter

Cabling:

- approx. 180 m $3 \times 0,75 \text{ mm}^2$ H05RR-F
- approx. 4 m $3 \times 2,5 \text{ mm}^2$ H05RR-F
- approx. 40 m $3 \times 1,5 \text{ mm}^2$ H07RN-F
- approx. 250 m $2 \times 0,05 \text{ mm}^2$ V(W) Hf-Y

Here H05RR-F, H07RN-F and V(W) Hf-Y is the concrete cable type, which is irrelevant in the following part and just listed for completeness. Important is just the number of conductors and their cross-section.

5.2. Communication

The CAN-Bus was chosen for the communication between the system devices. This bus offers a flexible high speed communication with multi master capability. Communication is done by using a special CAN-Bus transceiver Integrated Circuit (IC) [88]. This IC handles all communication with the CAN-Bus. Basically the CAN-Bus is a multi-master bus, each node connected to the bus can always send a message. If another client sends a message at the same time, collisions and hence invalid messages may occur. The used transceiver IC has a built in collision detection and the protocol of the CAN-Bus describes how the collisions should be handled. Thus there are no invalid messages. A more detailed description of the communication and the implemented message content can be seen in [37].

To get the data send via the CAN-Bus inside the personal computer (PC) for further analysis, a small device based on a 8 bit micro-controller called CAN2ETH has been developed. This device is a bidirectional bridge between the CAN-Bus and Ethernet (using the `SubSystem`-protocol (see 6.1.1)). [37, 8.5]

To communicate with the MFC devices a RS232 serial interface is needed. Today's PCs does not have many RS232 ports, because they have been replaced by universal serial bus (USB). Hence a RS232ETH module, which is based on the CAN2ETH module has been developed. This module is a bidirectional bridge between the RS232 port needed for the MFCs and the Ethernet connection to the PC. [37, 8.5]

5.3. Analogue inputs

For digitisation of the analogue signals from the 36 sensors, which are mounted inside the UGMA, a special board has been developed. [37, 10.5]. These boards reduced the costs compared to commercial available devices. 16 channels are placed on one ADC-Board. This is caused by the limited space on the front panel. Each channel is equipped with a current to voltage converter, a low-pass filter and amplification. After the signal conditioning, the signals are digitised in a 8 channel digitiser with 12 bit resolution. These boards also supply the sensor voltage of 24 V to the sensors.

5.4. Sensors

Inside the UGMA many physical values have to be measured. Most of them are temperatures and pressures. Additionally, there are few other values which are necessary to determine the status of the system. All sensors are connected via a 4-20 mA interface to the Analogue-Digital-Converter (ADC). If the sensor itself does not support this interface, the signal is converted.

5.4.1. Pressure sensors

For each pressure region inside the system a pressure sensor with a proper range has been selected. At chamber supply and inside the analysis loop the pressure sensors mounted are more precise ones. They were chosen because the pressure inside the connected detector should be known as precise as possible, to compensate pressure effects. Due to the possibility of the analysis loop to be connected to every other loop, all other sensors can be calibrated by comparison with this sensor.

Table 5.1.: Overview of the used pressure sensors

Sensor	Accuracy	non-linearity	temperature	total error band
A-10	1 % span 40 mbar	0.5 % span 20 mbar	1 % span max. 2.5 % span 40 mbar max. 100 mbar	
P-31	0.05 % span 2 mbar	0.04 % span 1.6 mbar	0.05 % span / 10 K 2 mbar / 10 K	0.1 % span 4 mbar

The used precise pressure sensors are WIKA P-31 [92] with a span of 0-4 bara. The other sensors are WIKA A-10 [91] sensors with the same span. The maximal uncertainties of these sensors are listed in table 5.1. To measure the primary pressure, there are three WIKA A-10 sensors with a span of 0-10 bara. Since they are just used to detect whether the primary pressure is high enough or not, their uncertainties are not listed in the table.

The accuracy shown for the A-10 sensor includes uncertainties from non-linearity, hysteresis, zero- and end-point deviation. Both sensor types have a long term stability of less than 0.1 % of their span per year.

5.4.2. Temperature sensors

All temperature sensors are industrial resistive Platinum sensors (Type PT100 [94]). Their resistive signal is converted by a two wire transmitter and sensor conditioner [90] into a 4-20 mA current. The measurement range of each sensor is adapted to the expected temperatures at the position where the sensor is mounted. This allows a good resolution for each sensor. The sensor and converter is described in more detail in [37]. The accuracy of the PT100 sensors of the accuracy class B according to [94, 5.1.3]:

$$\sigma_T \leq 0.30^\circ\text{C} + 0.005 \cdot |T| \quad (5.1)$$

5.5. Digital inputs and outputs

To control all valves, special digital input and output boards have been developed. Development of these special boards reduces the costs as for the analogue inputs, for controlling the 56 electrical driven valves. [37, 10.6] The digital input output modules host each 16 digital outputs and another 16 digital inputs. With one input and output, one valve can be controlled. The output delivers a Transistor-Transistor-Level (TTL) signal, which switches the valve. The digital input can be driven with a open collector output. Thus it is biased with 5 V, which needs to be pulled down to change the logic level.

Furthermore a latched interlock circuit is located at the board. The interlock mechanism is triggered if the voltage on one of the two interlock lines is switched off. This can be done by either the gas warning system or by pressing the emergency button. Once the interlock is triggered, first the voltage on the interlock lines need to be restored. If the voltage is restored, the interlock needs to be reset on each board by sending a special command to the board. This makes the whole system more safe, because it does not start operation after the interlock is closed again. When the interlock is triggered, the outputs are set to a high-impedance modus. A proper level inside the connected device can be created using a pull down resistor at the input.

5.6. Valve-driver

In addition to the 22 pneumatic driven valves, there are 56 electrical solenoid valves. Each valve coil represents an electrical load of 9 W. Most of the electrical power is converted to heat and thus the coil and therefore the valve itself are heated up. The maximal temperature which could be measured at a permanently operated valve without active cooling is more than 70°C on the surface. When the valve is heated, the gas temperature increases, too. This effect can have a negative impact on the physical measurements and thus has to be avoided. For reducing the heat input the power consumption of the valve needs to be reduced. The full supply voltage of 24 V is needed to switch the valve, whereas the valve stays open down to a supply voltage of about 5 V. This gives the possibility to reduce the power consumption of the system.

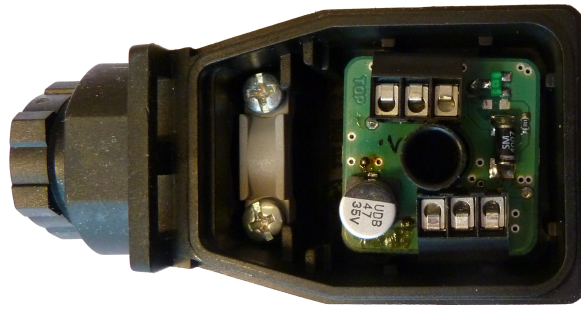


Figure 5.2.: Photograph of the valve driver board mounted inside the connector. For clarity, this picture was taken before the cables are connected.

A special valve driver, which is shown in figure 5.2, has been developed, which supports switching the valve using a TTL signal. The status can be read back by an open collector output. Thus it fits the connections of the digital board described above. When the valve driver is asked to switch the valve it first applies a short 24 V pulse and when the valve has opened, it switches to a pulse width modulation (PWM) with a duty cycle of about 20 %. This reduces the average voltage to 4.8 V and at the same time the average current consumption is reduced. Using this driver the valve coil stays cool and no heat is introduced to the gas.

5.7. Power distribution

Electrical power is distributed in two stages. One stage distributes 230 V and another one 24 V.

The 230 V distribution (shown in figure 5.3) is equipped with a residual-current-operated protective device (RCD) and several breakers to allow selective switching-off of the components connected to this distribution. If parts of the system need to be shut down, this can be done by using the breakers. Otherwise, if any device fails, the breaker triggers and only the circuit with the faulty device is without power. All other devices can operate and observe the status of the system. Inside the manifold, one hardware interlock is build in. If the interlock is triggered, the fan is switched to the fast mode and carries more air through the system to prevent a flammable atmosphere. Additionally all valves are switched off to put the UGMA in a well defined state, which is designed to be safe. [37]

The 24 V manifold consists only of screw clamps, to which the various loads are connected. Each valve inside the system is connected to this manifold. Few other loads, as for example proportional valves are connected, too. If a failure occurs in one valve, the over current protection from the power supply will switch off the power. When the failure disappears, the power is restored and operation resumes automatically.

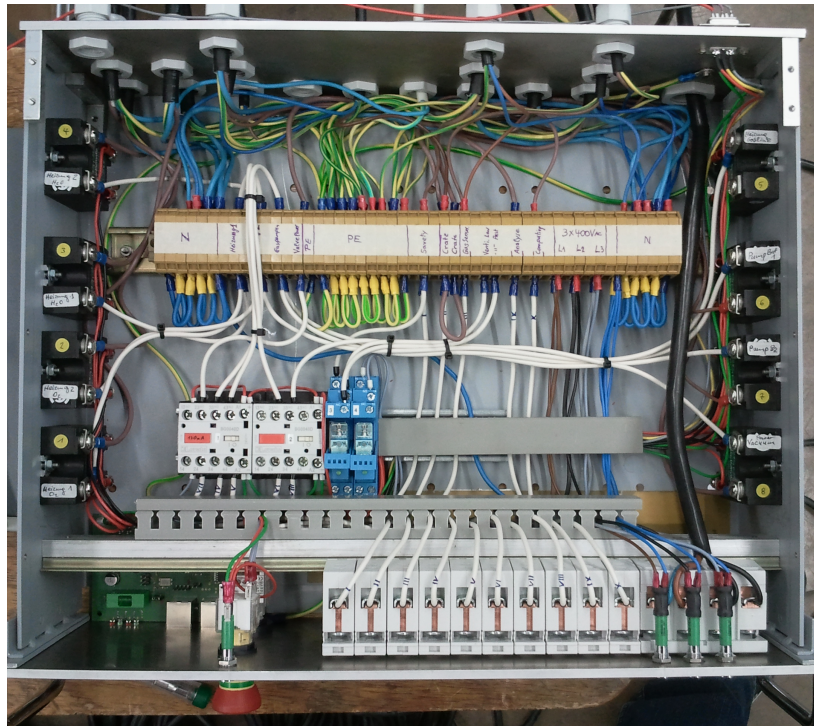


Figure 5.3.: The inside of the 230 V distribution after its final assembly. Right after this picture, the case has been closed and mounted into the rack. On the left and right side, solid state relays to switch various loads are mounted. All cables enter the rack from the backside. On the front side the breakers and the Interlock controller are mounted. [37]

5.8. Valve island

For controlling the pneumatic driven 4/2-way valves, a valve island with 24 5/2-way valves (type Ventilinsel MPA-S) has been installed [87]. In principle a valve island is a Programmable Logic Controller (PLC) with pneumatic valves as outputs. Sometimes, they can also be equipped with electrical inputs and outputs. But inside the UGMA, only pneumatic actuators need to be controlled via this valve island. Hence a configuration with only pneumatic valves was chosen.

The connection of each single valve to the cylinder of the pneumatic driven 4/2-way valves is shown in figure 5.4.

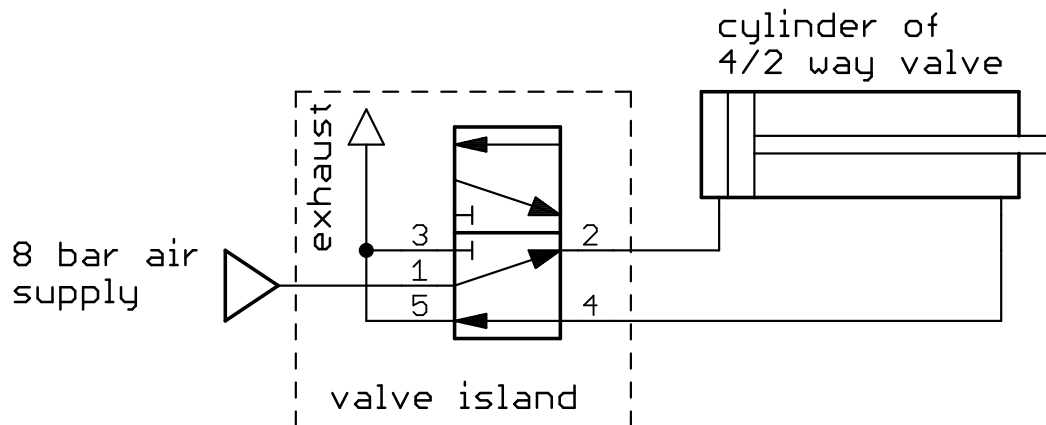


Figure 5.4.: Connection of the valve island to the cylinder of the 4/2-way valve. The air supply and the exhaust lines are common for all valves of the valve island.

The valves of the valve island are controlled by the internal controller (type FESTO CPSX) [86] (see figure 5.5). For interaction the controller is equipped with an Ethernet connection. All configuration and communication can be done using this interface. For the use in the UGMA, the communication is set to Modbus/TCP.

The implementation on the PC side is done using the open source library `libmodbus`. All communication to Modbus is done via this library. With help of this library, the valve island could be integrated into the existing software concept.



Figure 5.5.: Picture of the mounted valve island. On the bottom, the flexible tubing for the connection of the valve cylinders can be seen. The controller can be seen on the left side. The orange LEDs on the top indicate, which valves are currently switched on (valve 4 & 9).

6. Software

All software, which is needed to control the UGMA is running on a normal PC, which is build around a server mainboard. The computer is equipped with one hard disk (500 GB) for the system and one 1 TB Redundant Array of Independent Disks (RAID) system consisting of two hard disks to store the logged data. By using a simple RAID, the data gets automatically mirrored to the second disk. If one disk breaks, all data can be restored. For the system this is not needed, since the source code of all programs is organised in SVN-repositories which are stored externally. Because the PC has to handle the data from all sensors and valve, it is equipped with a Intel quadcore processor, which provides eight cores via hyper threading. Furthermore it is equipped with 16 GB random access memory (RAM). The operational system of the PC is Debian Linux [108] (Kernel 3.2). The PC can be interfaced at the UGMA via a touch-screen. The user interface can be seen in figure 6.1.

For controlling the gas chromatograph, there is a VirtualBox [110] running Windows 7 and the proprietary GC-control-software „PeakSimple“. All other software inside the UGMA has been written using open-source software.



Figure 6.1.: Photo of the user interface of the UGMA. The touchscreen and the special readout modules for the H_2O and O_2 sensor are shown on the right. On the left side the supply lines and the chamber are connected.

6.1. Frameworks

The control and analysis software uses libraries, which encapsulate functionality and allow easy access. Moreover the control software uses libraries, which already exist and have not been programmed for the special purposes of the UGMA. These frameworks are described in the following.

6.1.1. SubSystem

The `SubSystem` framework is a C++ library, which supports data exchange between different programs and computers. The development of this library has been initiated by Dennis Terhorst [105].

The communication inside this library is done by User Datagram Protocol (UDP)-packets. These are sent and received by network sockets. Hence, the protocol can easily be adapted and ported to other programming languages and platforms like microcontrollers.

One central element of the communication via the `SubSystem` is called `server`. This controls the dataflow and is responsible for the forwarding of the packets sent by one client to the others.

Communication is done via a subscription model. Each client can send data to a virtual destination called `abo`. The data is physically send to the server. If data is requested to be send to other clients, they need to subscribe the `abo`. There are no limits on the amount of clients sending or receiving data of one `abo`. Also the amount of `abos` is not limited in general. For the purpose of debugging or logging all data of one `abo` can also be logged into a file.

Each packet sent to the server contains a field, which represents the type. For subscription and other administrative purposes special packet types exist. Some of the most important packet types are shown below.

SUPPLY signalises that the client plans sending data via this `abo`. The server recognises this as a data source and assigns the supply flag to the client. On the other hand, if a client sends data to the server, it is assigned as a data source by the server.

SUBSCRIBE This is the packet which tells the server, that the client would like to receive the data sent to this `abo`. Without this packet no data are sent to the client.

UNSUBSCRIBE Via this command the client is able to unsubscribe the `abo`. Accordingly no data from the `abo` can be received.

SETID The name shown inside the `SubSystem server` is set via this command. This is helpful to distinguish various `abos` and clients.

SETDATA This is a special command. The data sent are just send to the clients supplying data. All listening clients do not receive the packets. This mode is partially used for sending commands.

The user data of the UDP-packet used for transmitting the `SubSystem` data are defined in a struct called `packet_t`. This is defined as

type inside this field, the packet type described above is stored.

namelength this field represents the length of the aboname. To split the following character array between aboname and user data.

alldata All data are stored inside one character array. Aboname and userdata are separated in this array by the C++ string termination character `\0`. The position of this character must be identical to the position given by the `namelength`.

For use in embedded devices (like the CAN2ETH and RS232ETH modules) the basics has been ported. Due to less computational power, it has been abstained from implementing full functionality. Only parts, which are needed to ensure communication have been ported. With the reduced functionality, the embedded devices can subscribe an abo and send / receive data.

6.1.2. LibLab

For control of various devices used in the laboratory a collection of various software modules, which act as an interface between the hardware drivers and the user application exists at the III. Physikalisches Institut B. This collection provides easy access to the hardware connected to a computer. All modules are encapsulated in a C++-framework called **LibLab**.

The user can use functions of the device instead of taking care of programming the hardware. The access to the hardware is encapsulated in functions. By this, the user can concentrate on using the hardware and not programming the read and write functions. All devices used by the UGMA were implemented using the structure of the **LibLab**-library. [109]

6.2. Software concept

The software concept is adapted to the data flow.

Basically the software concept consists of many different small programs. Each is responsible for one task. The great advantage of this concept is that parts of the system can be changed without influencing the others. Each software can be stopped and started again with a different configuration.

It is possible to categorise all programs into layers. Between the programs communication is done via UDP using **SubSystem**-protocol. The protocol is described in detail in section 6.1.1.

There are two main layers

local_control This layer is directly connected to the hardware. Each program controls small parts of the hardware like a group of MFC connected to a gas line.

global_control This layer connects different programs of the `local_control` layer. All gas lines are connected via the mixing program such that the gas conditions always behave like expected. For instance, if a larger chamber flow is needed, this request is passed to the `mixer` program, which computes the new setpoints and sends them to the gas line.

During programming attention has been given to flexibility and reusability of the software. It is possible to start the same program with different configurations. This makes it easy to change the programs controlling the gas lines. Each line should behave like the others but they control different MFC. The configuration for each line is stored in a file and parsed by the program during start.

Parts, which are needed more often were transferred into libraries. Some libraries can be used with a complete different software, not necessarily in scope of the UGMA.

6.3. Data flow inside UGMA

The data flow inside the UGMA is shown in figure 6.2. Here the path of the data from sensor A110PS, which is the pressure inside the analysis loop is shown as an example.

First the current signal from the sensor gets digitised and is sent via the CAN-Bus to the CAN2ETH converter. There it is converted into **SubSystem** packets and send via Ethernet to the central control PC. Now the data from the CAN-Bus are splitted into digital and analogue parts. Each part is fed into the corresponding software.

Both programs have in common, that first the identification is changed from the board and channel number to the six-character name, which is described in detail in A.1. After this mapping, the data are processed individually. The programs are described in section 6.4

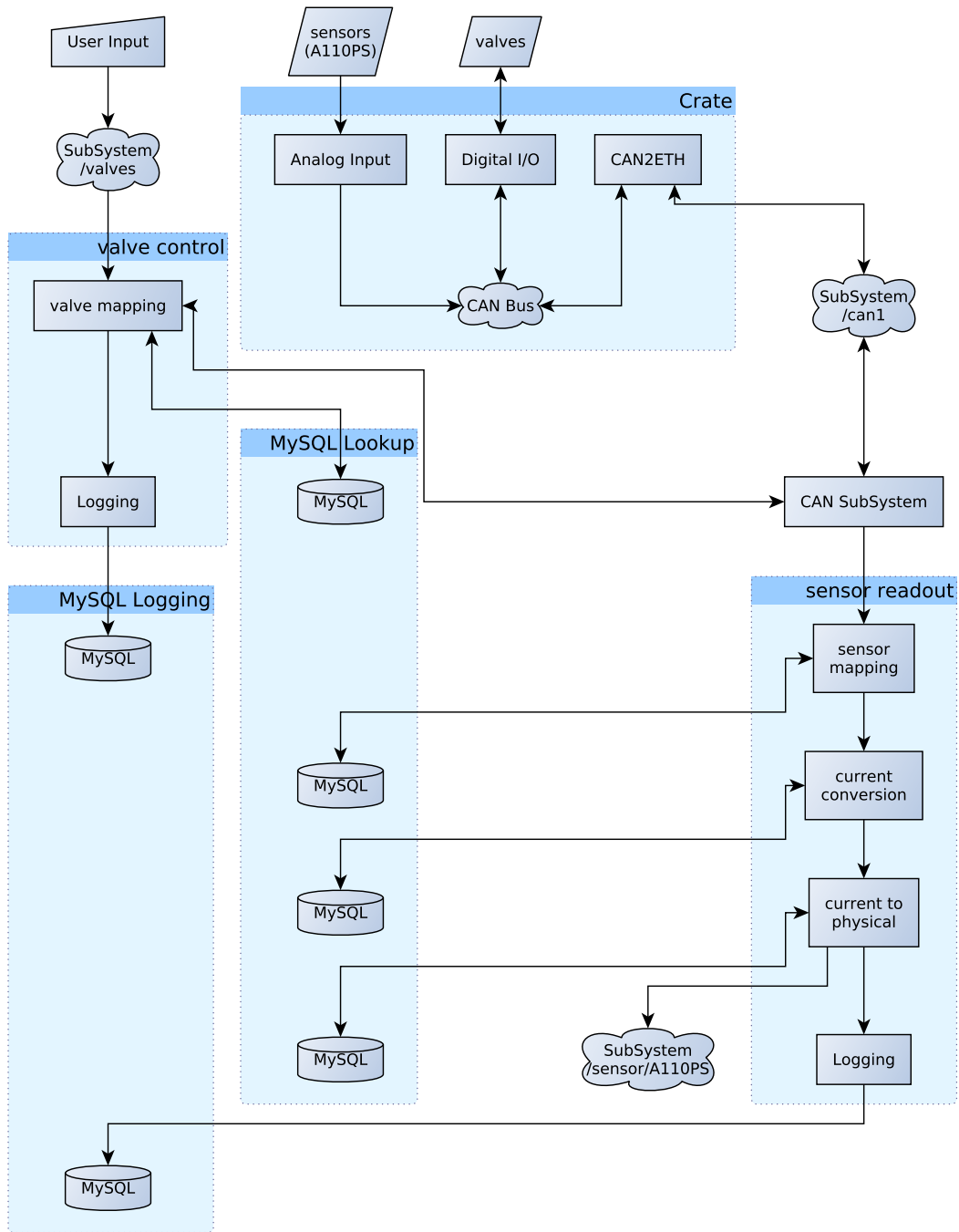


Figure 6.2.: Overview of the internal data flow.

6.4. Programs

All programs are running on the PC inside the UGMA. All of them are hidden from the user. The user can only interact with the user interface „webcontrol“ described in section 6.4. Via the „webcontrol“ commands are send to the other programs to trigger various actions. Communication between different programs is done via sending `SubSystem-Packets`. If an action is triggered via the user interface this is also done via sending such packets.

In the following a very short overview of the different programs running is given. This description does not go into detail.

Sensor Readout The data received from the analogue inputs is given in arbitrary ADC counts. This value is converted into a current using a calibration formula, which is stored in one `MySQL`-table. Now the conversion into the physical value measured by the sensor can be done using the conversion, which can be derived from the data-sheet or optional calibrations. As a final step these values are stored in `MySQL`-tables for later analysis. To trigger further action, the data is sent to other programs, which need the data of special sensors. This is done using the `SubSystem`-protocol.

Valve Control This program is rather simple. It converts the incoming switching requests into the commands, which are needed by the digital board to perform the action and as a second step it logs the switching times of the valves into one `MySQL`-table. If something inside the system is going wrong the status of all valves can be reconstructed from the logged data.

Mixer The mixer is the central part of the UGMA, because it defines the quality of the mixture. The mixture is fed with the gases connected and the requested output mixture and it calculates the needed setpoints. If the chamber is operated in direct flow mode, the setpoints are directly send to the corresponding „line control“ programs. If partial pressure mode is used, the partial pressured are computed on demand if a new mixture is going to be created. When the mixing is done, the measured partial pressures are send to the mixer and it computed the filled mixture.

Implementation of the mixing algorithm The implementation of the algorithm described in equation 3.3 is encapsulated in a `C++`-library. It has been taken into account, that either mixture or pure gases can be chosen as a starting point.

To create the matrix a vector is assigned to each gas. The concentration of the gas is saved at the appropriate position. As an index for the gas, the unique identifier from the internal `MySQL`-database is taken.

Handling matrices and vectors is done by the `ROOT`-toolkit [100]. The class `TMatrixD` supplies all functions, which are needed for solving of such set of linear equations. Due to the fact, that the matrix is not square, only few algorithms can be used. For this implementation Singular Value Decomposition (SVD) from `TMatrixDecompSVG` is used.

This algorithm factorises the matrix \mathbf{M} , which consists of n columns and m rows, into [101]

$$\mathbf{M} = \mathbf{U} \mathbf{S} \mathbf{V}^{\top} \quad (6.1)$$

where \mathbf{U} is a unitary $m \times m$ matrix, \mathbf{V}^{\top} is the conjugate matrix to the unitary $n \times n$ matrix \mathbf{V} and \mathbf{S} is a real $m \times n$ diagonal matrix. With this help the pseudo-inverse matrix \mathbf{M}^{\dagger} can be derived.

$$\mathbf{M}^{\dagger} = \mathbf{V} \mathbf{S}^{\dagger} \mathbf{U}^{\top} \quad (6.2)$$

The matrix \mathbf{S}^{\dagger} is given by

$$\mathbf{S}^{\dagger} = \left(s_{ij}^{\dagger} \right) \quad \text{with} \quad s_{ij}^{\dagger} = \begin{cases} \frac{1}{s_{ij}} & \text{if } s_{ij} \neq 0 \\ 0 & \text{else} \end{cases} \quad (6.3)$$

\mathbf{M}^{\dagger} is now the pseudo-inverse matrix, which solves the equation.

$$\mathbf{M} \vec{x} = \vec{b} \quad (6.4)$$

All transformations are handled inside of `ROOT`. This allows a clear programming of the whole calculation.

Line Control If there are more than one MFC per line mounted, this program selects that MFC which produces the smallest flow error. Furthermore the data of the MFCs are read back and logged into the corresponding MySQL-tables. The program sets the conversion factor and reference gas received from the „mixer“.

Chamber Flow For the chamber there are some parameters to control. At first the gas source, here the user can select between using one of the buffers or the mixer. Depending on the gas source the chamber supply MFC is configured. If the flow is already regulated by the „mixer“ it is set to fully open to avoid strange scenarios, which might occur, when the flow is regulated twice.

As a second step the operation mode of the chamber is selected. This can be changed continuously by the recycle ratio between open and close mode. Depending on this the MFC in the chamber return path must be opened.

At least this program sets the pressure inside the chamber by sending the right setpoint to the pressure regulator.

The program does not care about the order how to set the parameters of the chamber. So every parameter can be changed separately. To avoid situations which are not allowed and might probable damage the system or the connected experiment, the program filters the commands and accepts only valid ones.

Partial Pressure This program controls the process of the partial pressure mixing. The partial pressures are calculated by the „mixer“. Hence this program opens and closes the valves at the right pressure. At first the buffer is evacuated. After this the mixture is filled and at the end the pump inside the buffer is activated to stir the gas.

Sampling Source Manager The analysis loop can be switched to various positions and additionally it can be opened to ambient pressure. It must be ensured that the analysis loop is only connected to one loop at the same time. Otherwise the gas flow gets mixed up and the system might get into an unstable state.

If a sampling source is selected the program reads the corresponding action (e.g. open valve) from the database. Before opening the next valve it first closes the already open valves. This ensures that the analysis loop is only connected to one loop.

PDU Control Inside the PDU, there is a small board, which can be controlled via CAN-Bus. This board switches eight solid-state relays, which are connected to the heaters of the purifiers and the pumps. Five of the relays can be used to regulate the temperature in the purifiers, since they can be operated in a wave-packet-modulation. This means, they are only switched on for a very short $\mathcal{O}(100\text{ ms})$ time. The average voltage applied to the heater get reduced.

Further there is one relay which switches the global interlock. So the user can always deactivate the whole system when he can see the user interface and detects strange behaviour.

Purifier Temperature The temperatures inside the purifier should be kept constant, because the absorption of the material is temperature dependent. This program is able to control the temperatures by sending the right setpoints to the PDU.

Vacuum Manager The vacuum manager is just a bookkeeper, which switches on the vacuum pump when the first valve to the vacuum line is opened. When the last valve is closed, it switches off the pump.

Webcontrol In some cases the user will not be able to control the UGMA at the device itself. This might be caused by positioning the UGMA inside an restricted area related to radiation for example. Sometimes access to the whole experimental hall is prohibited during the measurement period. Hence, operating the system should be possible from remote. In order to have the same layout, one interface has been developed which can be used locally and remotely. Since there is absolute no difference between both interfaces the user needs only one training instead of two for the local and remote control. One view to the user interface is shown in figure 6.3.

The whole user interface is written using HTML, PHP and JavaScript and it is displayed locally using a normal browser. Via the user interface all necessary parameters and measured values can be accessed. For easy and uncomplicated usage, the names of each sensor are extended by their mounting position. The user switches for example the exhaust valve of buffer 2 and not valve L2X2SV. By this also untrained people are able to operate the system without having a look at the flow schema shown in figure 4.7.



Figure 6.3.: Screenshot of the webcontrol application showing the analysis page. At the lower left the history of the H₂O contamination is shown. In the lower right the pressure and temperature history of the analysis loop is shown. In the upper part the latest measurements are shown.

7. Mixing gas

Mixing a gas mixture can be done by various methods. The methods used and tested by the UGMA are described in the following. To reach the highest possible precision and accuracy it is mandatory to know the mechanisms behind the mixing processes.

For detailed analysis regarding the accuracy of the mixing methods please have a look at section 11.2.

7.1. Parallel flow mixing

7.1.1. Function of a Mass Flow Controller

Inside the whole UGMA nine MFC of various types are mounted. Even if they have different configurations regarding the maximal and hence minimal flow or the pressure drop across the device, they all use the same principle to measure the gas flow. One additional device, the mass flow sensor of the chamber return line uses this operation principle too. In principle this device is a MFC without the valve, which controls the flow.

The flow gets measured via its heat capacity. A schematic view of the inside of a MFC is shown in figure 7.1. First the gas flow gets filtered by a turbulence filter, which should ensure laminar gas flow through the device. Then a constant fraction of the flow is separated and send through the sensor tube. This fraction is set via the laminar flow element. The flow resistance of both devices sets the fraction. The laminar flow element consists of multiple discs with precision-etched flow channels which are only a few microns in size. [50]

The gas flowing through the sensor tube gets heated by the first heating element. Afterwards it passes a second heating and measurement point, which just measures the gas temperature. If the first heating element is at constant temperature, the temperature at the second element depends on the gas flow. If flow is applied, the first element gets cooled and the second one heated. This results in a temperature difference to the temperatures at these points without flow ΔT . This temperature difference is proportional to the flow. Due to the flow-split by the laminar flow element, this signal is also proportional to the total mass flow rate. [50]

The flow is regulated by a proportional valve, which is controlled by a proportional plus integral plus derivative element (PID) control. This regulation algorithm ensures with the right parameters, that the valve opens in a stable way.

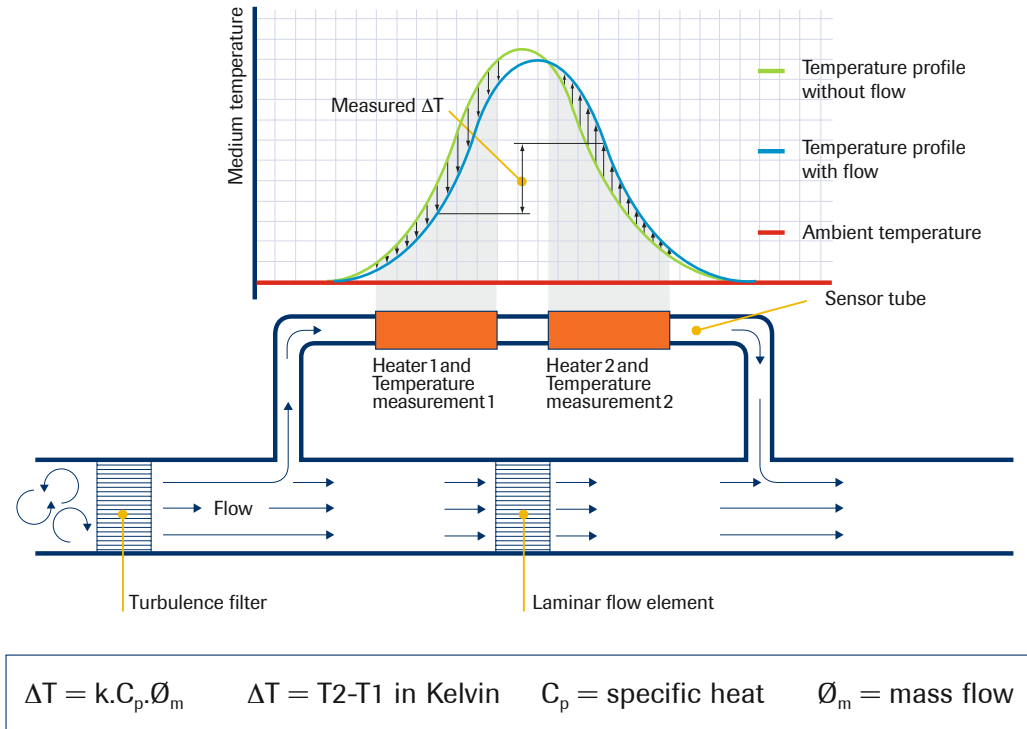


Figure 7.1.: Schematic view of the inside of a MFC. Figure taken from [50].

7.1.2. Uncertainty of the mixture

Two of the three gas lines are equipped with three MFC. Their maximal gas fluxes are designed as a logarithmic scale and can support $0.01\dot{V}_{\max}$, $0.1\dot{V}_{\max}$ and \dot{V}_{\max} . For pure Argon \dot{V}_{\max} is $100 \ell_n/h$. For other gases \dot{V}_{\max} is reduced by the correction factor. This grade allows a wide range of $0.002 - 100 \ell_n/h$ of flow. The lower limit of each MFC is given by the datasheet [48] as

$$\dot{V}_{\min} = \frac{1}{50} \cdot \dot{V}_{\max} \quad (7.1)$$

This means, that some of the MFC overlap in range. The uncertainty of the flow of a MFC is given by [48]

$$\sigma_{\dot{V}} = 0,8\% \dot{V} + 0,2\% \dot{V}_{\max} \quad (7.2)$$

Over the whole flow range, which can be covered by these two lines, the relative error varies. In figure 7.1.2 the relative error of the three flow ranges is shown. In the region, where the flow ranges of two MFC overlap, the uncertainty can be calculated either for the MFC with the lower and upper maximal flow.

$$\text{lower range } \dot{V} = \dot{V}_{\max} \quad \Rightarrow \quad \frac{\sigma_{\dot{V}}}{\dot{V}} = 0.8\% + 0.2\% = 1\% \quad (7.3)$$

$$\text{upper range } \dot{V} = 0.1\dot{V}_{\max} \quad \Rightarrow \quad \frac{\sigma_{\dot{V}}}{\dot{V}} = 0.8\% + 0.2\% \cdot 10 = 2.8\% \quad (7.4)$$

When selecting the MFC, it should be chosen such that the relative error is minimal. If there is no MFC available for the selected flow, the mixing process must be stopped. Otherwise the quality of the mixture cannot be guaranteed.

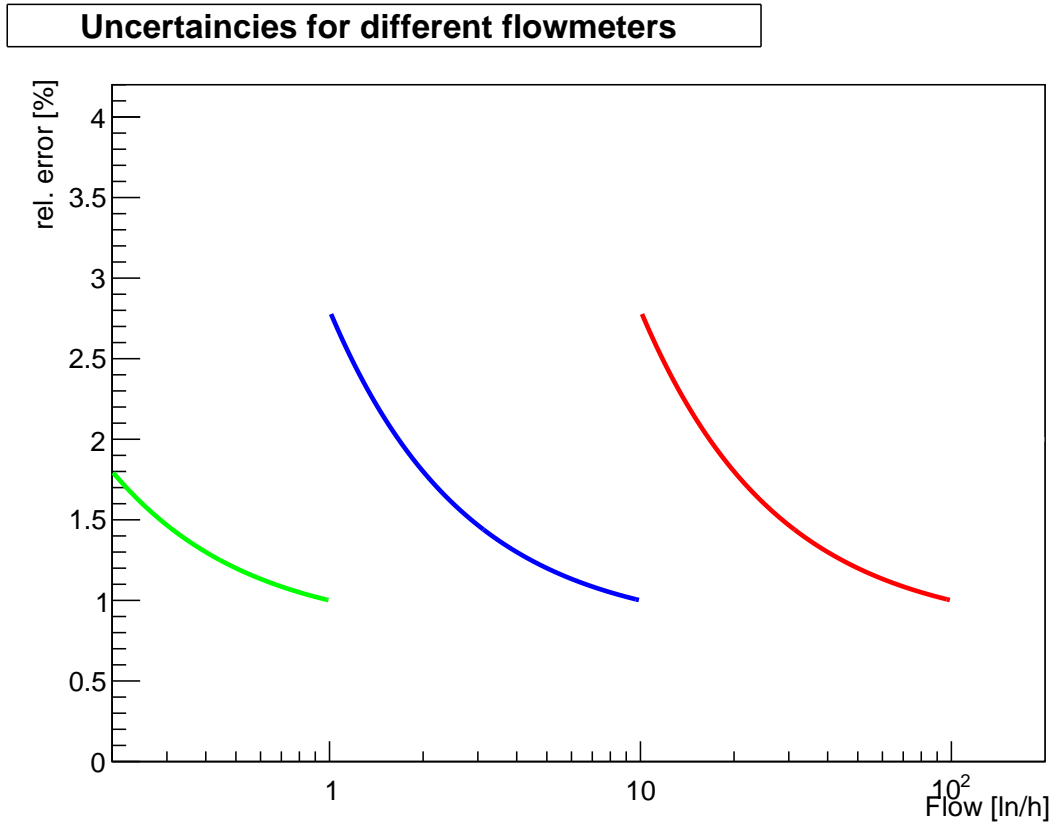


Figure 7.2.: Theoretical relative error of MFC over the entire flow range. The error of each MFC is only shown in the region, this MFC is used.

To get the uncertainty of the final mixture, the errors of all three lines have to be propagated. If one is interested in the error on the fraction σ_{η_i} , the error propagation also needs the input flow of every line \dot{V}_i . With the knowledge of the specific MFC which is used inside the line, the uncertainty of the flow can be computed using equation 7.2. The equation depends on the maximal flow, which can be fed through the MFC.

The total flow \dot{V}_G is given by

$$\dot{V}_G = \sum_i \dot{V}_i \quad (7.5)$$

and its uncertainty is given by

$$\sigma_{\dot{V}_G}^2 = \sum_i \left(\frac{\partial \dot{V}_G}{\partial \dot{V}_i} \right)^2 \sigma_{\dot{V}_i}^2 \quad (7.6)$$

The partial differentiation of 7.5 with respect to \dot{V}_i results in

$$\frac{\partial \dot{V}_G}{\partial \dot{V}_i} = \frac{\partial(\dot{V}_1 + \dot{V}_2 + \dot{V}_3)}{\partial \dot{V}_i} = 1 \quad (7.7)$$

By combining this equation with 7.6 gives the simplified solution for the error on the total flow of a given mixture.

$$\sigma_{\dot{V}_G}^2 = \sum_i \sigma_{\dot{V}_i}^2 \quad (7.8)$$

Starting from a given flow in each MFC, the fractions of the mixture can also be calculated.

$$\eta_i = \frac{\dot{V}_i}{\sum_n \dot{V}_n} = \frac{\dot{V}_i}{\dot{V}_G} \quad (7.9)$$

The error on each fraction is given by

$$\sigma_{\eta_i}^2 = \left(\frac{\partial \eta_i}{\partial \dot{V}_i} \right)^2 \sigma_{\dot{V}_i}^2 + \left(\frac{\partial \eta_i}{\partial \dot{V}_G} \right)^2 \sigma_{\dot{V}_G}^2 + \text{correlation terms} \quad (7.10)$$

To avoid the correlation between $\sigma_{\dot{V}_i}$ and $\sigma_{\dot{V}_G}$ in the formula above, equation 7.9 can be written as

$$\eta_i = \frac{\dot{V}_i}{\dot{V}_1 + \dot{V}_2 + \dot{V}_3} \quad (7.11)$$

Now the errors are no longer correlated, since they are derived directly from the MFC. Hence the error on the fraction can be calculated by

$$\sigma_{\eta_i}^2 = \sum_k \left(\frac{\partial \eta_i}{\partial \dot{V}_k} \right)^2 \sigma_{\dot{V}_k}^2 = \sum_k \left(\frac{\partial}{\partial \dot{V}_k} \frac{\dot{V}_i}{\sum_n \dot{V}_n} \right)^2 \sigma_{\dot{V}_k}^2 \quad (7.12)$$

The differentiation can be expressed by

$$\frac{\partial}{\partial \dot{V}_k} \left(\frac{\dot{V}_i}{\sum_n \dot{V}_n} \right) = \frac{(\sum_n \dot{V}_n) \delta_{ik} - \dot{V}_i}{(\sum_n \dot{V}_n)^2} \quad (7.13)$$

After further mathematical transformations, the error on the fraction can finally be expressed by the following equation

$$\sigma_{\eta_i}^2 = \frac{1}{\dot{V}_G^4} \cdot \sum_k \left(\delta_{ik} \dot{V}_G - \dot{V}_i \right)^2 \sigma_{\dot{V}_k}^2 \quad (7.14)$$

This equation can be split into two parts, one is the gas line whose fraction is going to be calculated and the other gas lines.

$$\sigma_{\eta_i}^2 = \frac{1}{\dot{V}_G^4} \left[\left(\dot{V}_G - \dot{V}_i \right)^2 \sigma_{\dot{V}_i}^2 + \dot{V}_i^2 \sum_{k \neq i} \sigma_{\dot{V}_k}^2 \right] \quad (7.15)$$

By using $\dot{V}_i = \eta_i \dot{V}_G$ this equation can be simplified.

$$\sigma_{\eta_i}^2 = \frac{1}{\dot{V}_G^2} \left[(1 - \eta_i)^2 \sigma_{\dot{V}_i}^2 + \eta_i^2 \sum_{k \neq i} \sigma_{\dot{V}_k}^2 \right] \quad (7.16)$$

7.1.3. Conversion factor used inside a Mass Flow Controller

If the gas sent through the Mass Flow Controller (MFC) is not the gas the MFC has been calibrated with, a conversion factor has to be used. Either this factor is already integrated in the MFC as a polynomial function. Otherwise the factor has to be calculated. If the conversion is already done inside the MFC it is more precise, because not only a single factor is stored.

Connection to Fluidat-On-The-Net Taking a closer look at the webpage of Fluidat-On-The-Net (FDN) [95] it is pointed out, that it is possible to integrate the calculations into the UGMA. The manufacturer of the MFC points out, that the accuracy of the conversion factors from this page is much better than those listed in the datasheet [96]. The values of the datasheet have been copied to the MySQL-database of the UGMA to do further calculations. One possible explanation might be, that the calculations respect the special characteristics of the MFC. But all calculations are hidden, so the difference between the factors of the datasheet and FDN can not be pointed out.

A small program has been created which is able to get the conversion factors from FDN. But the resulting values should be verified before they are used for mixing the gas.

Calculation One important tool for calculating the conversion factors is the webpage Fluidat-On-The-Net (FDN) [95] from Bronkhorst High-Tech GmbH. On this page a lot of conversion factors for different MFC and flow conditions are provided. But this page is not that helpful, when the UGMA is operated without internet connection. There is no version of the webpage, which can be used offline. This is one of the reasons, why an alternative conversion was developed and the calculation has been reconstructed.

Inside the MFC calibrations for some gases are already stored. But if a gas is fed through the MFC, which is not part of the calibration table, the measured values need to be converted. If the conversion is not done, the displayed value differ from the real gas flow. The conversion must be done the other way around, when applying a new setpoint. This correction is done by multiplying the measured flow inside the MFC \dot{V}_2 by the conversion factor $K_{1,2}$. The result is the converted measured flow.

$$\dot{V}_1 = K_{1,2} \cdot \dot{V}_2 \quad (7.17)$$

A table with many conversion factors is given in [96]. Inside this table, the conversion factors have been calculated using N_2 as reference. Hence, the conversion factor for pure nitrogen is $K = 1$.

If the MFC is configured for Ar, and Propane C_3H_8 is sent through it, all values need to be converted by $K_{C_3H_8,Ar}$, which is the conversion factor from Ar to C_3H_8 .

$$\dot{V}_{C_3H_8} = K_{C_3H_8,Ar} \cdot \dot{V}_{Ar} = \frac{K_{C_3H_8,N_2}}{K_{Ar,N_2}} \cdot \dot{V}_{Ar} = \frac{0.34}{1.4} \cdot \dot{V}_{Ar} = 0.243 \cdot \dot{V}_{Ar} \quad (7.18)$$

The conversion factor K is defined according to [97, S. 15]. Where c_p represents the specific heat capacity and ρ the density of the gas.

$$K = \frac{c_{p,1} \cdot \rho_1}{c_{p,2} \cdot \rho_2} \quad (7.19)$$

If the conversion factor is to be calculated for a given gas or mixture, at first, the heat capacity needs to be determined. The molar heat capacity of a single gas is given by the Shomate-equation [104]

$$C_{p,\text{mol}}(\tau) = A + B\tau + C\tau^2 + D\tau^3 + E\tau^{-2} \quad (7.20)$$

Here the temperature τ is scaled such that it can be derived from the ambient temperature via $\tau = T/1000$. Together with the molar mass, the specific heat capacity can be derived.

$$c_p(T) = \frac{C_{p,\text{mol}}(T)}{M_{\text{mol}}} \quad (7.21)$$

These equations can be extended to be used with mixtures of gases. The manufacturer uses a oversimple equation. [97, p. 16]

$$\frac{1}{K_{\text{mix}}} = \sum_i \frac{\eta_{V,i}}{K_i} \quad (7.22)$$

In this equation $\eta_{V,i}$ is the volumetric part of gas i inside the mixture. But on the other hand the approach via the Shomate-equation can also be extended for use with mixtures. The specific heat capacity of a mixture is given by

$$c_p = \sum_i \eta_i c_{p,i} \quad (7.23)$$

This equation can be extended for usage with the Shomate-equation. Each coefficient ($A-E$) needs to be weighted with the fraction of the gas (η_i).

$$A = \sum_i \eta_i A_i \quad (7.24)$$

The same is valid for the other coefficients. The density of the gas mixture is given by

$$\rho_{\text{mix}} = \sum_i \eta_i \rho_i \quad (7.25)$$

The MFC use temperature differences for measuring the mass flow and by this the volume flow. Hence this must be taken into account. The Shomate equation (7.20) describes an approximation for the temperature dependence of the heat capacity. In the datasheet [97, S. 15] a temperature of 50 °C is mentioned. Using this temperature for calculating the conversion factor gives results, which can be compared with the tabulated values. Nevertheless the density should be used at norm conditions (1013 mbara and 0 °C)

Using the equations above, the conversion faktor can be calculated.

$$K_{\text{computed},i} = \frac{c_{p,i}(50^\circ\text{C}) \cdot \rho_i}{c_{p,\text{N}_2}(50^\circ\text{C}) \cdot \rho_{\text{N}_2}} \quad (7.26)$$

By using equations 7.23 and 7.25, this equation can be extended to be used with gas mixtures.

Comparison with tabulated values If nitrogen is chosen for the basic conversion, the values given in the table of the datasheet [96, Appendix 2] can be derived directly. For the calculation gas specific parameters, like density, heat capacity and molar mass, are needed. Most of them can be found on the webpages of National Institute of Standards and Technology (NIST) [104]. To solve the problem of restricted internet access, a local database has been developed. All these values can be downloaded and stored in the database. Normally the values stored locally are used. If the gas is not known from previous runs, the informations need to be aggregated. This can be done either manually or automatically by the program.

In table 7.1 a comparison between the computed factors using equation 7.26 (K_{computed}), those which are given in the datasheet [96] K_{BHT} and those which are calculated by FDN (K_{FDN}) are shown. The values for K_{BHT} and K_{FDN} were looked up manually and also saved in the database.

For the mixtures (data source „MIXTURE“) K_{BHT} has been calculated using equation 7.22. K_{computed} was computed using equation 7.26 and the values from the Shomate-equation for mixtures.

Table 7.1.: Conversion factors for different gases.

Gas	ρ [kg/m ³]	M_{mol} [g/mol]	K_{computed}	K_{BHT}	K_{FDN}	data source
Ar	1.7835	39.948	1.4013	1.40	1.4000	MySQL
O ₂	1.4287	31.9988	0.9865	0.98	0.9814	MySQL
CH ₄	0.7173	16.0425	0.7945	0.76	0.7639	MySQL
CF ₄	3.9455	88.0043	0.4520	0.44	0.4381	MySQL
CO ₂	1.9770	44.0095	0.7563	0.74	0.7358	MySQL
C ₄ H ₁₀	2.7030	58.1222	0.2654	0.25	0.2494	MySQL
iC ₄ H ₁₀	2.6880	58.1222	0.2713	0.25	0.2510	MySQL
He	0.1784	4.0026	1.4033	1.41	1.4060	MySQL
Xe	5.8965	131.2930	1.3930	1.38	1.3750	MySQL
N ₂	1.2501	28.0134	1.0000	1.00	1.0000	MySQL
CO	1.2502	28.0101	1.0003	-	-	MySQL
T2K-Gas	1.8665	41.7532	1.2251	1.3482	-	MIXTURE
SynAir	1.2928	28.9659	0.9997	0.9994	-	MIXTURE
P10	1.6769	37.5575	1.3021	1.3360	-	MIXTURE

For now the flow is corrected using K_{BHT} . If we are able to analyse the mixture at a level, that the effect of different corrections can be seen, one should consider doing a comparison of the different calculation methods. The uncertainties introduced by the additional correction factor become only visible, when a gas is send through the MFC, which is not part of the internal calibration table. Up to now, all mixtures, which have been created using the MFCs only, used the internal calibration. Very few gases (e.g. C₃H₈), which are not part of the internal conversion table, have also been mixed. But mixtures using those gases were created using the partial pressure mixing mode. In this mode the uncertainty of the gas flow can be neglected.

The main difference between the values which are calculated by equation 7.26 and the values given by the manufacturer in [96] and [95] is that K_{computed} does not take the viscosity of the

gas into account. The calculations behind K_{BHT} and K_{FDN} are hidden by the manufacturer. During development of equation 7.26 it was not possible to implement the influence of the gas viscosity, because the bore diameter and the internal geometry of the MFC are not known. The approach using the Shomate-equation should be understood as the last solution, if no other is available.

The additional uncertainty introduced by the conversion factor can be taken as a systematic error, because the flow is either over- or underestimated constantly. Since the values of K_{BHT} are only given at a precision of 0.01, this can be assumed for a very conservative error estimation. The converted flow \dot{V}_{to} can be calculated by

$$\dot{V}_{\text{to}} = \frac{K_{\text{BHT, to}}}{K_{\text{BHT, from}}} \dot{V}_{\text{from}} \quad (7.27)$$

If we assume an error on both conversion factors of $\sigma_{K_{\text{BHT}}} = 0.01$ the resulting uncertainty can be calculated as

$$\sigma_{\dot{V}_{\text{to}}}^2 = \frac{\dot{V}_{\text{from}}^2}{K_{\text{BHT, from}}^2} \left[\sigma_{K_{\text{BHT, to}}}^2 + \frac{K_{\text{BHT, to}}^2}{K_{\text{BHT, from}}^2} \sigma_{K_{\text{BHT, from}}}^2 + \frac{K_{\text{BHT, to}}^2}{\dot{V}_{\text{from}}^2} \sigma_{\dot{V}_{\text{from}}}^2 \right] \quad (7.28)$$

This equation can be simplified to

$$\sigma_{\dot{V}_{\text{to}}}^2 = \frac{\dot{V}_{\text{from}}^2}{K_{\text{BHT, from}}^2} \left[\left(1 + \frac{K_{\text{BHT, to}}^2}{K_{\text{BHT, from}}^2} \right) \sigma_{K_{\text{BHT}}}^2 + \frac{K_{\text{BHT, to}}^2}{\dot{V}_{\text{from}}^2} \sigma_{\dot{V}_{\text{from}}}^2 \right] \quad (7.29)$$

To compare the resulting error, the following scenario is assumed: CH_4 is send ($K_{\text{BHT, to}} = 0.76$) through a MFC, which is set to Ar ($K_{\text{BHT, from}} = 1.40$). If the flow controller is set to the internal calibration, the error on the flow can be calculated as

$$\sigma_{\dot{V}_{\text{to, int}}} = \frac{K_{\text{BHT, to}}}{K_{\text{BHT, from}}} \sigma_{\dot{V}_{\text{from, int}}} \quad (7.30)$$

because it is adequate to assume, that the measured and maximal flow just scale with the conversion factor. Using this we can calculate the additional error for the scenario above.

$$\sigma_{\dot{V}_{\text{to}}}^2 = \dot{V}_{\text{from}}^2 \underbrace{\left[1 + \left(\frac{0.76}{1.4} \right)^2 \right]}_{66.06 \cdot 10^{-6}} \frac{0.01^2}{1.4^2} + \sigma_{\dot{V}_{\text{to, int}}}^2 \quad (7.31)$$

If we further assume that the used MFC is rated for $\dot{V}_{\text{max}} = 100 \ell_{\text{n}}/\text{h}$ Ar and is set to $\dot{V} = 50 \ell_{\text{n}}/\text{h}$ we can calculate the flow uncertainty using 7.2.

$$\sigma_{\dot{V}_{\text{to, int}}} = \frac{0.76}{1.4} (0.8 \% \cdot 50 \ell_{\text{n}}/\text{h} + 0.2 \% \cdot 100 \ell_{\text{n}}/\text{h}) = 0.326 \ell_{\text{n}}/\text{h} \quad (7.32)$$

$$\sigma_{\dot{V}_{\text{to}}} = \sqrt{(50 \ell_{\text{n}}/\text{h})^2 \cdot 66.06 \cdot 10^{-6} + (0.326 \ell_{\text{n}}/\text{h})^2} = 0.331 \ell_{\text{n}}/\text{h} \quad (7.33)$$

Using an external conversion factor increases the flow uncertainty in the scenario above by about 1.6 %.

7.2. Partial pressure mixing

The uncertainty of the mixture created by the partial pressure method is not easy to compute. This is caused by the mixing algorithm itself. The mixture depends on the timing inside the software, because the software closes the valve and stops the flow. Further delay might be introduced between sending the command and receiving the command inside the digital output unit. On the other hand it also depends on the ambient temperature. If the gas expands, it cools down and the pressure decreases. The software itself tries to correct for effects which are caused by cooling or heating the gas. For this purpose between each filling step a break of two minutes is inserted. After this break, experience has shown that the pressure is stable and does not influence the mixture. If the ambient temperature and

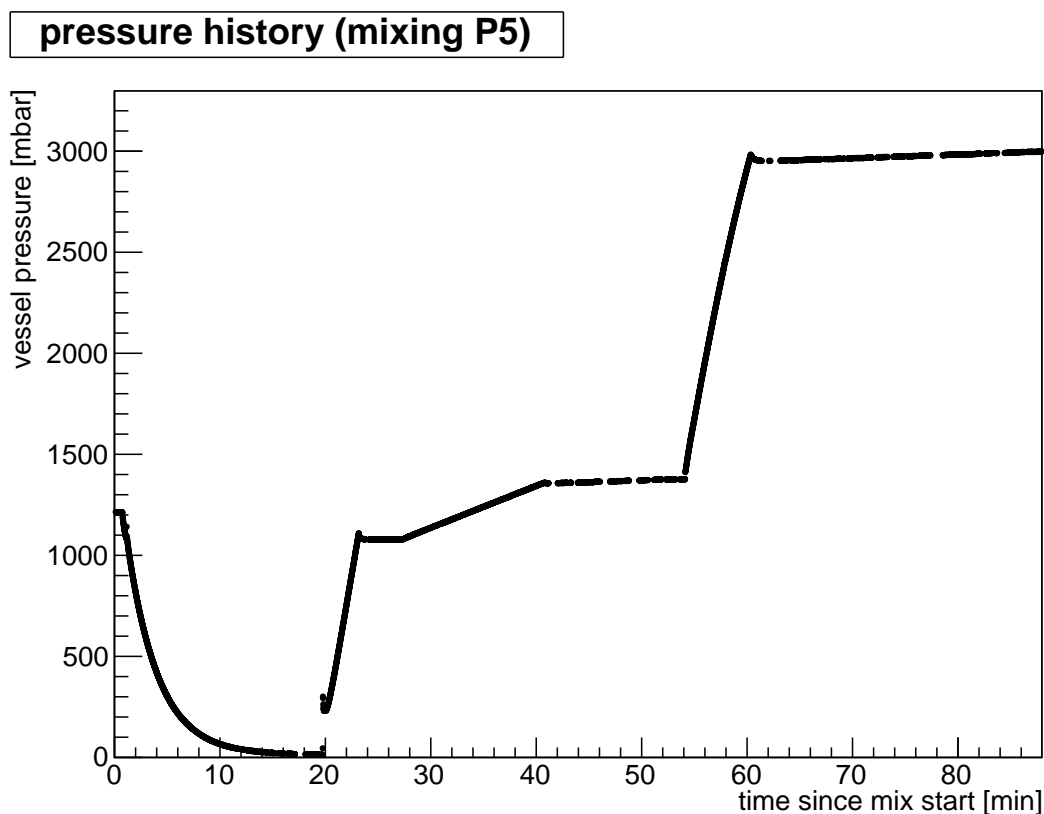


Figure 7.3.: Pressure history during partial pressure mixing of P5 (Ar 95 %, CH₄ 5 %). All four phases of this process can be clearly seen. At first the buffer is evacuated. Right after this after about 20 min filling of Ar is started up to 1100 mbara. Then after 28 min filling of CH₄ is started. After about 42 min the flow is reduced. After 54 min Ar is filled again to finish the requested mixture. The reduction of the flow and the breaks between filling of both gases can be seen.

accordingly the temperature of the vessel varies, the pressure inside the vessel varies, too. This can cause further uncertainties.

For all pressure calculation methods, the mixing software, which opens and closes the valves behave the same. The mixing algorithm consists of six major steps, which are always done. The gas lines are sorted by their primary pressure.

1. Evacuation of the buffer. To save pumping time, the buffer is just evacuated to about 15 mbara.
2. Fill inert gas like Ar to 100 mbarg. Further this line is supposed to have the highest primary pressure.
 - a) Open valve and close when fill pressure is reached.
 - b) After delay of two minutes measure final pressure, which is used for mixture calculation.
3. Fill first gas line up to its partial pressure.
 - a) Open valve, if this gas needs to be filled, and close when fill pressure is reached.
 - b) After delay of two minutes measure final pressure, which is used for mixture calculation.
4. Fill second gas line up to its partial pressure.
 - a) Open valve, if this gas needs to be filled, and close when fill pressure is reached.
 - b) After delay of two minutes measure final pressure, which is used for mixture calculation.
5. Fill rest of inert gas to match its partial pressure.
 - a) Open valve and close when fill pressure is reached.
 - b) After delay of two minutes measure final pressure, which is used for mixture calculation.
6. Calculate mixture filled in the buffer based on the measured filled partial pressures.

7.2.1. Using ideal gas

Computation of the mixture is done by adding the partial pressures Δp_i filled into the vessel.

$$p_G = \sum_i \Delta p_i \quad (7.34)$$

The fraction of the gas is simply given by dividing the partial pressure by the end-pressure p_G .

$$\eta_i = \frac{\Delta p_i}{p_G} \quad (7.35)$$

The uncertainty of the fraction can be calculated as well

$$\sigma_{\eta_i}^2 = \sum_j \left(\frac{\partial \eta_i}{\partial \Delta p_j} \right)^2 \cdot \sigma_{\Delta p_j}^2 \quad (7.36)$$

$$= \sum_j \frac{1}{p_G^4} \left(\delta_{ij} \underbrace{\sum_n \Delta p_n}_{=p_G} - \Delta p_i \right)^2 \sigma_{\Delta p_i}^2 \quad (7.37)$$

Since this mixing algorithm uses the pressure sensor inside the buffer. Under the assumption, that $\sigma_{\Delta p_i}$ does not depend on the pressure, it is the same for all gases. Hence the equation can be simplified, n_{gas} represents the number of gases in the mixture.

$$\sigma_{\eta_i}^2 = \frac{1}{p_G^4} [p_G^2 - 2p_G \Delta p_i + n_{\text{gas}} \Delta p_i^2] \sigma_{\Delta p}^2 \quad (7.38)$$

The mixing program also measures the pressure for all three possible gas lines, even if they are not filled into the buffer. This is done due to programming issues and just causes a longer break for the gas, which has been already filled (Ar) to expand. Hence we have to set $n_{\text{gas}} = 3$ for all mixtures. The uncertainty of the pressure difference $\sigma_{\Delta p}$ can be derived from the error of the pressure sensor.

$$\sigma_{\Delta p} = \sqrt{2} \sigma_p \quad (7.39)$$

The final uncertainty of the gas component can be calculated using equations 7.38 and 7.39.

$$\sigma_{\eta_i}^2 = \frac{1}{p_G^4} [p_G^2 - 2p_G \cdot \Delta p_i + 3\Delta p_i^2] \cdot 2 \sigma_p^2 \quad (7.40)$$

For the mixing process using the ideal gas law, the equation above can be simplified using $\Delta p_i = \eta_i p_G$.

$$\sigma_{\eta_i}^2 = \frac{1}{p_G^2} [1 - 2\eta_i + 3\eta_i^2] \cdot 2 \sigma_p^2 \quad (7.41)$$

This is the theoretical statistical error of the mixture. In addition to this error, one has to look at the systematic uncertainty introduced by the filling algorithm. The filling program switches the gas flow off, when the pressure inside the buffer p_{buffer} is greater or equal to the sum of start pressure p_0 and requested pressure difference Δp_i . Due to expansion of the gas, the pressure needs some time to settle. This causes a pressure difference, which always points to lower concentrations. During the development of the partial pressure mixing software, this effect has been reduced to a minimum.

7.2.2. Using Redlich-Kwong equation

For larger molecules, e.g. $i\text{C}_4\text{H}_{10}$, the ideal gas law reaches its limits and results in larger differences between computed and mixed fractions. For using large molecules in the UGMA, the mixing algorithm (see section 3.2) has been extended. A more real description of gases is given by the Redlich-Kwong-equation [32]

$$p = \frac{RT}{V - b} - \frac{a}{\sqrt{TV}(V + b)} \quad (7.42)$$

This equation can also be written in a form, which is similar to the ideal gas law:

$$pV_{\text{mol}} = ZRT \quad (7.43)$$

The „correction“ factor Z is given by

$$Z = \frac{1}{1 - h} - \frac{\frac{A^2}{B} h}{1 + h} \quad (7.44)$$

A and B can be derived from either the van-der-Waals parameters a and b or from the critical temperature T_C and critical pressure p_C

$$A^2 = \frac{a}{R^2 T^{2.5}} = 0.4278 \frac{T_C^{2.5}}{p_C T^{2.5}} \quad (7.45)$$

$$B = \frac{b}{RT} = 0.0867 \frac{T_C}{p_C T} \quad (7.46)$$

Together with these values the parameter h can be calculated as

$$h = \frac{Bp}{Z} = \frac{b}{V_{\text{mol}}} \quad (7.47)$$

The mixing is done by calculating the volume fractions at 273.15 K and 1013.25 mbar. As a first step the particle number is given by

$$\Delta N = (ZRT)^{-1} \Delta p \cdot V_0 \quad (7.48)$$

Then the volume difference ΔV is calculated by multiplying the particle number ΔN with the molar volume V_{mol} .

$$\Delta V = \Delta N \cdot V_{\text{mol}} \quad (7.49)$$

$$= (ZRT)^{-1} \Delta p \cdot V_0 \cdot V_{\text{mol}} \quad (7.50)$$

With this, the fraction η_i can be calculated

$$\eta_i = \frac{\Delta V_i}{\sum_n \Delta V_n} = \frac{Z_i^{-1} \Delta p_i V_{\text{mol},i}}{\sum_j Z_j^{-1} \Delta p_j V_{\text{mol},j}} \quad (7.51)$$

In each equation, the molar volume is defined via the molar mass M_{mol} and the density ρ .

$$V_{\text{mol}} = \frac{M_{\text{mol}}}{\rho(273.15 \text{ K}, 1013.25 \text{ mbar})} \quad (7.52)$$

The conditions $T = 273.15 \text{ K}$ and $p = 1013.25 \text{ mbar}$ have been chosen to create gas mixtures which are comparable to those from commercial gas suppliers. The conditions are normal conditions according to DIN 1343 [85]. These conditions are also used to compare the measured results with the simulations.

To calculate the partial pressures equation 7.51 has to be solved. This is not possible analytically. Hence, the solution is obtained using a numerical minimisation of the variable m , which is defined by the squared deviations.

$$m = \sum_i (\eta_i - \eta_{i,\text{set}})^2 \quad (7.53)$$

The pressures given by this minimisation are used for mixing the gas.

To compare the pressures calculated by Redlich-Kwong to the values calculated by the ideal gas law the differences of a binary gas mixture is shown in figure 7.4. For this test, the gas of interest is mixed with Argon. The differences depend on the gas used and is proportional to the size of the molecules.

A similar behaviour can be observed looking at the buffer end pressure. For a fixed mixture, the pressure difference between both methods increase with increasing end pressure. This is related to the increasing partial pressure and through this the effect of gas corrections becomes more important.

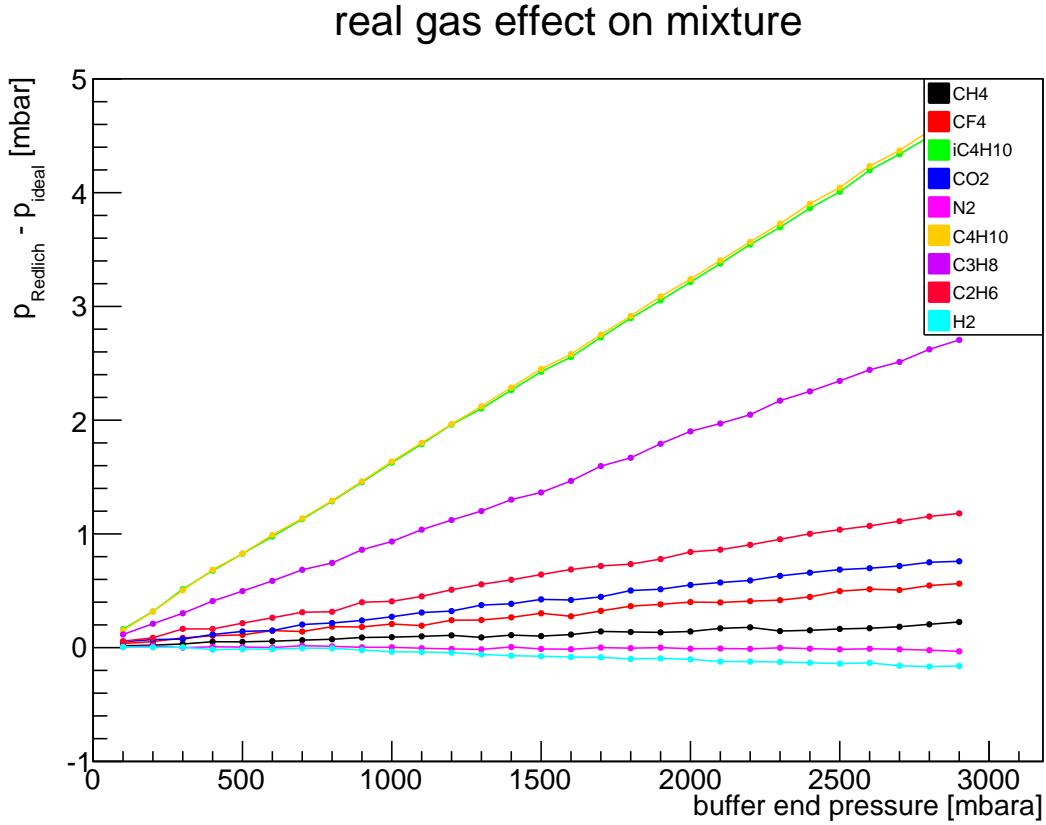


Figure 7.4.: Deviation of the partial pressure calculated by the ideal gas law and the Redlich-Kwong equation. The fraction of the gas which is tested is always at 5 vol.-%, balance is Argon. The buffer end pressure is varied.

7.2.3. Contamination caused by old mixtures

We now want to consider, that the vessel is not evacuated to 0 mbara. To limit the evacuation time the minimal pressure is set to 15 mbara. If the buffer is filled up to 3 bara only 0.5 vol.-% of the gas used before stays inside the buffer. This value is low enough for continuous running. If only single buffers are used, for special short measurements, the option of repeating the procedure to reduce the contamination should be considered. By evacuating the buffer to 15 mbara, the fraction of each gas is given by

$$\eta'_i = \frac{p_i + \eta_{i,\text{old}} \cdot 15 \text{ mbar}}{p_{\text{max}}} \quad (7.54)$$

where p_i represents the partial pressure of the gas i . But even if the gas is no longer present in the mixture, there might be contaminations left. The maximal pressure p_{max} is the pressure of the vessel at the end of the mixing process. The pressure p_P , which is used for calculation of the partial pressures is given by the difference of p_{max} and $p_{\text{offset}} \approx 15 \text{ mbara}$.

$$p_P = p_{\text{max}} - p_{\text{offset}} \quad (7.55)$$

With this filling pressure, the pressure difference of each gas is calculated $\Delta p_i = \eta_i \cdot p_P$. If the previous mixture has been done using the same pressure $p_{\max} = 3000 \text{ mbara}$ and same pressure offset, equation 7.54 can be simplified to

$$\eta'_i = \eta_i + 0.5\% \cdot \eta_{i,\text{old}} \quad (7.56)$$

The contamination from the old gas can be reduced by a higher maximal pressure or a lower offset pressure. A higher maximal pressure can only be achieved if the input pressure is high enough to allow a reasonable flow. The lower offset pressure results in a longer pumping time and hence a longer time until the mixture is produced.

7.2.4. Time needed to create a gas mixture

The time for the production of a mixture strongly depends on the number and type of gases. A mixture from two gases is more rapidly created than a mixture from three gases. The type of gas becomes relevant, when opening the bypass-valve which is only allowed for non-flammable gases. Flammable gases must be fed through one MFC and hence the maximal flow is limited to about $50 \ell_n/\text{h}$ for CH_4 . When the gas has to be sent through an MFC, the amount of gas to be filled is also important for the estimation of the mixing time. A distribution of the mixing times can be seen in figure 7.5.

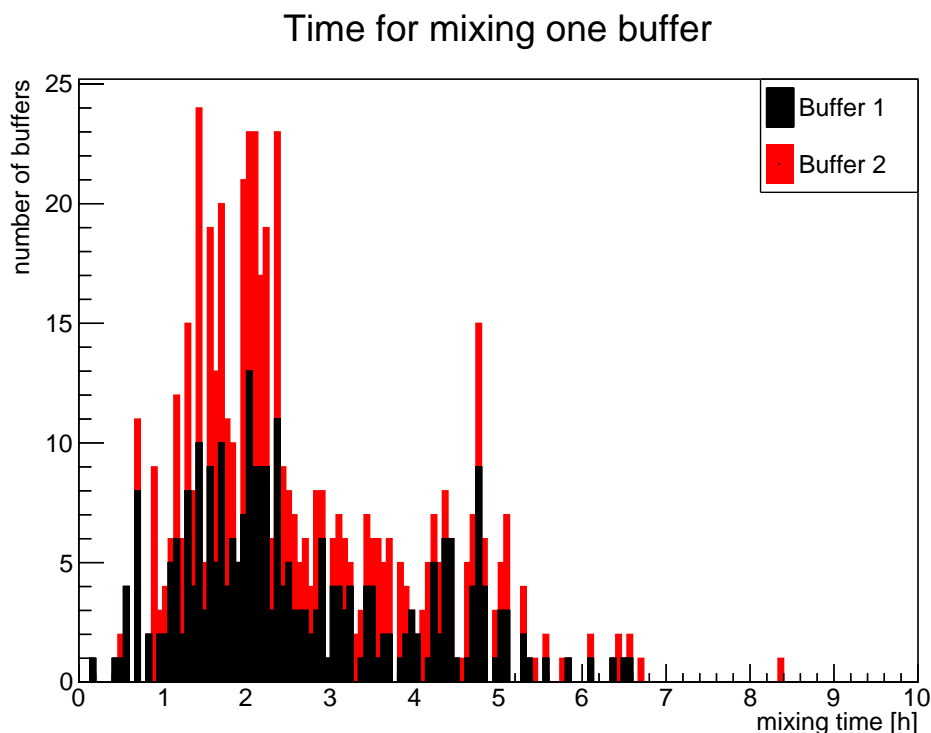


Figure 7.5.: Distribution of the mixing time for one buffer for various gas mixtures. Large times result from filling large amounts of iC_4H_{10} . The distributions for buffer 1 and buffer 2 are stacked.

8. Analysis of mixed gas

The regulation is well tested and works reliably. In addition it is possible to analyse the mixed gas and look for contaminations or admixtures caused by impurities.

For this purpose an analysis loop is built in. This loop can be switched into different positions of the system. Additionally all three inputs can be fed through the loop for calibration purpose. Normal operation position of this loop is at the chamber return line. In this position it determines the contaminations accumulated inside the chamber.

For the determination of the general composition of the gas mixture it can be fed through a gas chromatograph. This device is able to measure the individual gas components with a precision of 0.5 vol.-%. The resolution strongly depends on its calibration.

Gas-based particle detectors are very sensitive to contaminations caused by oxygen or water. For measuring these gases special devices are built in, one dedicated sensor for oxygen and one for water.

8.1. Water-sensor

For the determination of the contamination caused by water vapour a „Shawmeter SuperDew“ [55] is built-in. The device is located inside the analysis loop and can be placed at different sample positions. The device measures the dewpoint of the gas flowing by.

8.1.1. Operation principle

The fact that the dielectric constant of water ($\epsilon_r(20^\circ\text{C}) = 80.20$ [102, 6-4]) is much higher than that of air or other dry gases ($\epsilon_r \approx 1$) [102, 6-170]) can be used for the determination of the water content. A hygroscopic material is placed as a dielectric between the electrodes of a capacitor. This material absorbs water from the gas. If the fraction of water inside the dielectric increases, the capacity changes and this can be interpreted as the water content. If the partial pressure of water outside the capacitor decreases the water diffuses from the capacitor into the gas. Hence the water content inside the dielectric of the capacitor and the capacity also decreases until the content is balanced.

8.1.2. Integration into the UGMA

The temperature of a surface at which water starts condensing is called the dewpoint. If this temperature is lower than 0°C it is also called icepoint.

The dew meter displays the measured dewpoint in degree Celsius on a LC-display and at the same time provides the value via a 4–20 mA current source. This current is digitised in one of the analogue input boards. The current is linear with respect to the dewpoint [55] and can easily be converted.

$$T_{\text{dew}} = \frac{T_{\text{wet}} - T_{\text{dry}}}{20 \text{ mA} - 4 \text{ mA}} \cdot (I - 4 \text{ mA}) + T_{\text{dry}} \quad (8.1)$$

T_{wet} is the maximal and T_{dry} the minimal measurable dewpoint of the device. In the setup a „Gray Spot“ sensor is build in. This can measure dewpoints in the range between -80 °C and 0 °C. If these values are inserted into 8.1 the equation can be simplified to

$$T_{\text{dew}} = \frac{80 \text{ °C}}{16 \text{ mA}} \cdot I - 100 \text{ °C} \quad (8.2)$$

This equation converts the measured current into a dewpoint. But the dewpoint does not directly represent the contamination with water, which is more interesting for the user. Hence the value needs to be converted into the relative content of water.

The content of water depends on both dewpoint and pressure. A conversion is given by the equation of Clausius-Clapeyron used for saturation vapour pressure E_s over water, respectively ice. R_W is the water vapour gas constant.

$$\frac{dE_s}{dT} = \frac{q_v \cdot E_s}{R_W \cdot T^2} \quad (8.3)$$

Solving this equation is difficult because of the temperature dependence of the evaporation heat q_v . In fact a simplified approach is used, for example the Magnus equations.

$$E_{w,i}(T_{\text{dew}}) = \begin{cases} 611.2 \text{ Pa} \cdot \exp\left(\frac{17.62 T_{\text{dew}}}{243.12 \text{ °C} + T_{\text{dew}}}\right) & \text{for } T_{\text{dew}} > 0 \text{ °C} \\ 611.2 \text{ Pa} \cdot \exp\left(\frac{22.46 T_{\text{dew}}}{272.62 \text{ °C} + T_{\text{dew}}}\right) & \text{for } T_{\text{dew}} < 0 \text{ °C} \end{cases} \quad (8.4)$$

The saturation vapour pressure E is given for dewpoints below 0°C as vapour pressure measured over ice E_i . For temperatures above it is measured over water E_w .

A more precise approach is given by the equations developed by Wexler [7] in 1976.

$$E_w(T_{\text{dew}}) = \exp \left[-2991.2729 T_{\text{dew}}^{-2} - 6017.0128 T_{\text{dew}}^{-1} + 18.87643854 - 0.028354721 T_{\text{dew}} + 0.17838301 \cdot 10^{-4} T_{\text{dew}}^2 - 0.84150417 \cdot 10^{-9} T_{\text{dew}}^3 + 0.44412543 \cdot 10^{-12} T_{\text{dew}}^4 + 2.858487 \ln T_{\text{dew}} \right] \quad (8.5)$$

$$E_i(T_{\text{dew}}) = \exp \left[-5865.3696 T_{\text{dew}}^{-1} + 22.241033 + 0.013749042 T_{\text{dew}} - 0.34031775 \cdot 10^{-4} T_{\text{dew}}^2 + 0.26967687 \cdot 10^{-7} T_{\text{dew}}^3 + 0.6918651 \ln T_{\text{dew}} \right] \quad (8.6)$$

With these equations, the saturation vapour pressure can be calculated for the whole temperature range. The transition between dewpoint and icepoint is continuous (see figure 8.1).

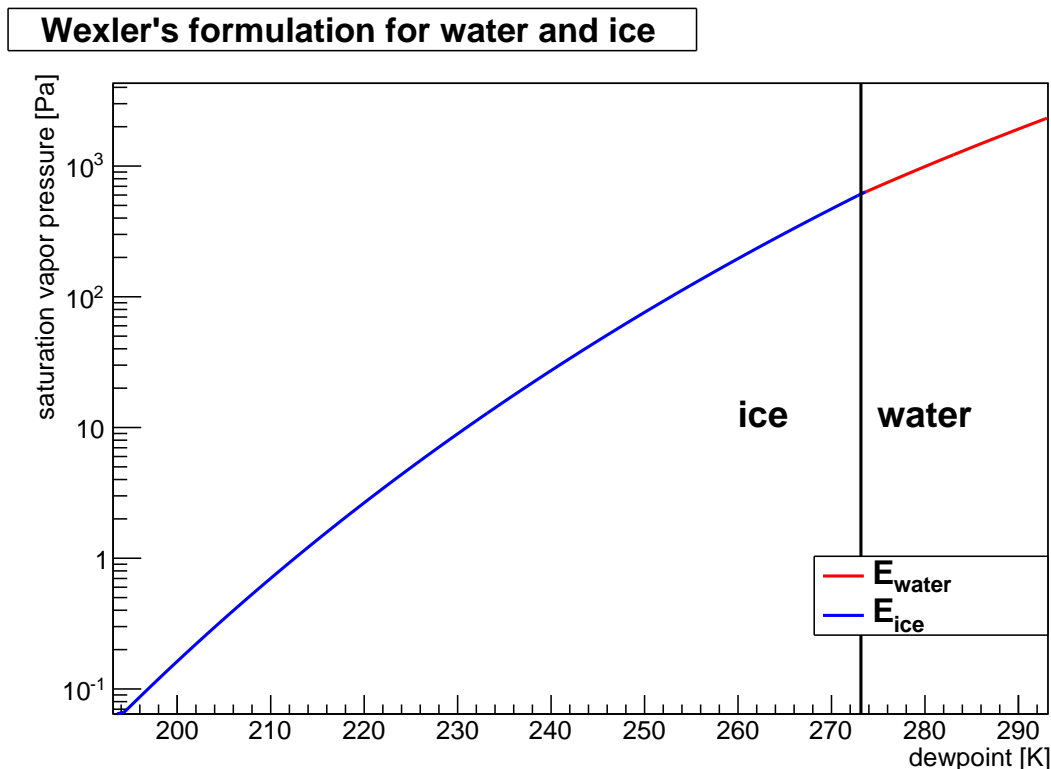


Figure 8.1.: Saturation vapour pressure calculated using the Wexler equation.

Because the values used in the system, express contamination of the gas with water, a correction factor [7] is introduced. This factor takes into account, that the saturation vapour pressure itself depends on the pressure.

$$f_w(T_{\text{dew}}, p) = 4.1 \cdot 10^{-4} + p \cdot \left(3.48 \cdot 10^{-6} + 7.4 \cdot 10^{-10} (T_{\text{dew}} + 30.6 - 3.8 \cdot 10^{-2} p)^2 \right) \quad (8.7)$$

$$f_i(T_{\text{dew}}, p) = 4.8 \cdot 10^{-4} + p \cdot \left(3.47 \cdot 10^{-6} + 5.9 \cdot 10^{-10} (T_{\text{dew}} + 23.8 - 3.1 \cdot 10^{-2} p)^2 \right) \quad (8.8)$$

In equation 8.8 and 8.7 the dewpoint T_{dew} has to be inserted in degrees Celsius and the pressure p in Millibar. Finally, the contamination of water is given by the corrected saturation vapour pressure

$$x_{\text{water}} = \frac{E'}{p - E'} \cdot 10^6 \text{ ppmv} \quad \text{mit } E' = E \cdot (1 + f) \quad (8.9)$$

The pressure dependence of the dewpoint is corrected by equations 8.7 and 8.8. But, on the other hand, measurements have shown that there is still a pressure dependence of the sensors reading.

The H₂O content was measured for various pressures. For having stable gas conditions, to neglect effects caused by the gas mixture, the gas from one filled buffer was used. The water

contamination was measured before the chamber, directly behind the buffer. Hence possible changes in the water contamination are only caused by the buffer itself. It can be assumed, that the contamination should be stable as long as this buffer can supply the experiment. Because the gas is send through the connected chambers, the pressure inside the buffer lowers and causes the pressure variations. Effects like desorption inside the buffer are neglected. The measured dependence is about 0.5 ppm over a pressure range of 2000 mbar according to figure 8.2.

Since there is no possibility to check the measured values, the correction presented in equation 8.10 should be handled with care. Values at ambient pressure are assumed to be correct, because the sensor was calibrated there. The sensor seems to measure systematic less H₂O contamination at higher pressures.

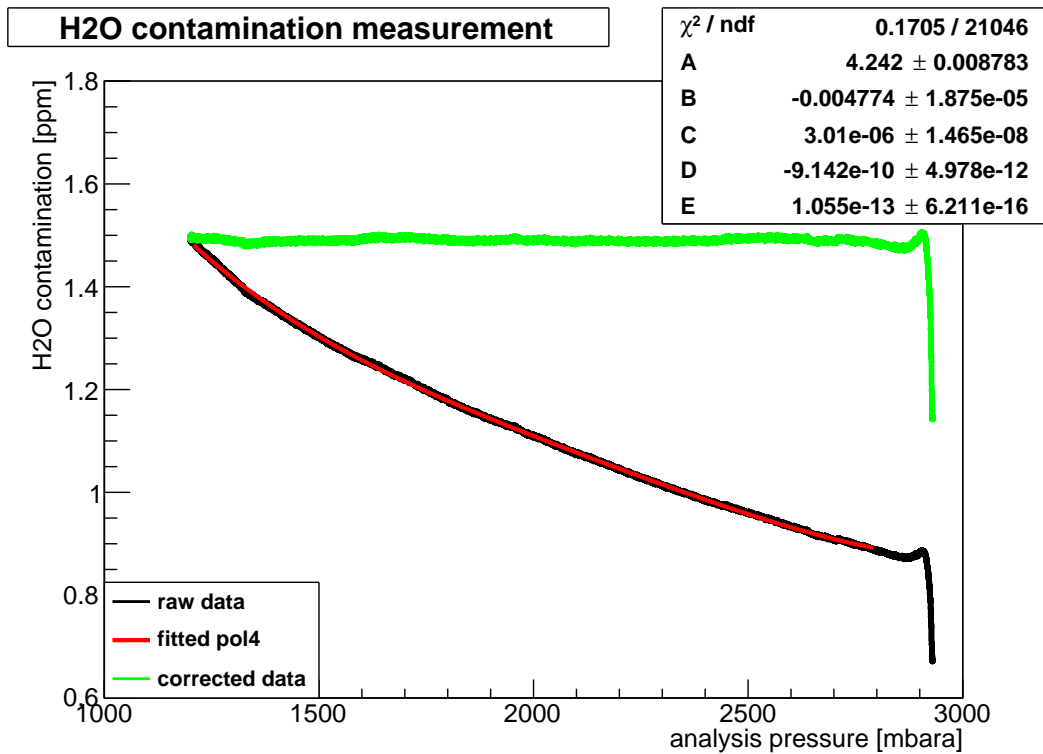


Figure 8.2.: Pressure dependence of the H₂O contamination measurement. The measurement was done using the pressure sensor A109PS inside the analysis loop.

This effect can be corrected using a quartic polynomial ($\text{pol4}(p)$). This function has no further physical motivation, but describes the data quite well as can be seen in 8.2. The large amount of data points results in an underestimation of the deviation from the fit. Hence the χ^2 per degree of freedom is too small.

The data are corrected to the measurement $\eta_{\text{H}_2\text{O},\text{norm}}$ taken at the lowest pressure of this data sample, because the sensor is build and calibrated in this pressure regime. The corrected water contamination is given by

$$\eta_{\text{H}_2\text{O},\text{corr}(p)} = \frac{\eta_{\text{H}_2\text{O}}}{\text{pol4}(p)} \cdot \eta_{\text{H}_2\text{O},\text{norm}} \quad (8.10)$$

Another observation is the correlation between the H_2O measurement and the temperature. This relation is caused by the so called Diurnal Effect and does only appear if one is sampling from a system, which can absorb water.

Assume a stable dry nitrogen system. Every piping material is porous. This allows very small molecules (like water) to stick to the pipe wall. In a stable system the water vapour in the nitrogen and the piping walls is an equilibrium. If the system is heated up, a certain amount of energy is transferred to the pipes and to the diffused water. If the energy reaches the molecules, they start oscillating, the Brownian motion increases and the pressure inside the walls rises. The additional energy has changed the equilibrium and the water leaves the walls entering the dry gas. Hence the water reading increases [54]. This effect can be observed looking at the correlation between temperature and H_2O reading, which is shown in figure 8.3. When sampling from chamber supply, the H_2O reading is not correlated to

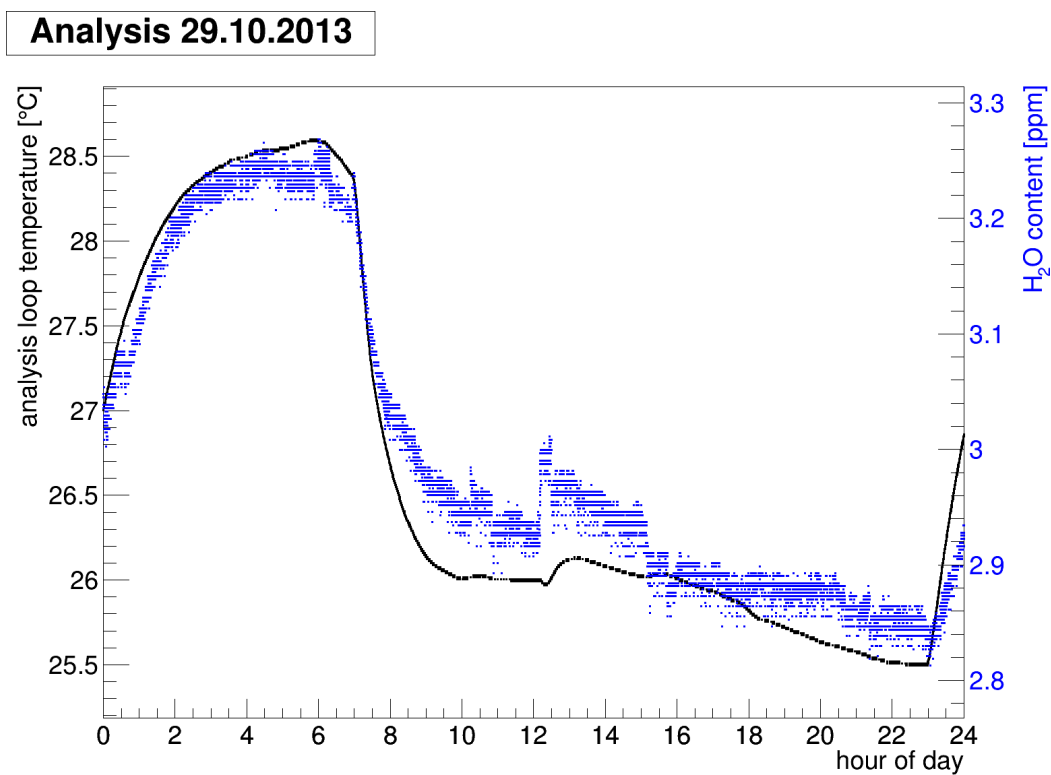


Figure 8.3.: One day of measurements of the H_2O content and the analysis loop temperature (A110TS). The correlation between temperature and H_2O content caused by the Diurnal Effect is clearly visible.

the temperature. On the other hand when sampling from the chamber return line both measurements seem to be correlated. Hence, the influence of the temperature on the H_2O reading is caused by the chambers connected to the UGMA.

Measurements at the chamber supply position have shown a pressure dependency, but these readings are independent of the temperature. This allows drawing the conclusion, that the temperature effect is caused by the chambers and not by the sensor itself. But on the other hand there is still some systematic effect of the pressure correction left. For these variations,

it was not possible to determine the cause of the variations. Either they are caused by the gas mixture or by there is an effect left which is not corrected.

If it is possible to cross-check the measurements of the water sensor with a second measurement device, it should be calibrated again. Also the presented study should be repeated using different gas mixtures to avoid influence of the gas itself.

8.2. Oxygen-sensor

Due to contamination with oxygen, the gas amplification suffers. For monitoring the O₂ contamination a special sensor is included in the analysis loop. This sensor is able to measure the oxygen contamination continuously. The sensor is a „Orbisphere M1100“ connected to a „Orbisphere 410“ evaluation unit. Both are produced by the company „Hach Lange GmbH“. [52,53]

8.2.1. Principle of operation

Common oxygen sensors are based on chemical reactions. An electrolyte inside the sensor gets oxidised. Due to the oxidisation a small current across the sensor cell can be measured. This current is proportional to the oxygen content of the gas. After a certain period of time, the electrolyte is fully oxidised and needs to be replaced. The length of this period depends on the sensor itself but also on the measured contaminations. If there is no oxygen inside, the electrolyte lasts longer than with high contaminations. Moreover, these sensors are not tolerant against ambient air. If these sensors accidentally get exposed to air or pure oxygen, the electrolyte and hence the sensor might become unusable.

Meanwhile sensors have been developed, which are based on optical principles. A luminescence spot is excited by the light of a blue LED. The point responds by emission of red light. The presence of oxygen influences the luminescence lifetime. This lifetime is connected to the partial pressure of oxygen in the medium on the other side of the luminescence spot. The durability of the luminescence spot just depends on the number of measurements and not on the integrated O₂ concentration [51].

The sensor is connected to an evaluation unit. The unit controls the sensor and does the conversion into the selected units of measurement. The sensor was originally developed for use in power plants. Here the oxygen diluted in the cooling or feed water is observed. Monitoring the oxygen content is necessary to avoid corrosion caused by oxidation. Further the same sensor is used in beverage industry to monitor the diluted oxygen inside beer. A short test has shown, that the sensor can reliably be used for measuring the contamination of oxygen in gases.

8.2.2. Pressure dependence

The luminescence signal is proportional to the number of O₂ molecules present in the measurement chamber. Hence a pressure dependence is given by the density of the gas inside

the chamber. The measured value should be converted such, that it represents the oxygen concentration at norm conditions. Inside the sensor a temperature measurement is done, the measurements are already corrected for it.

The parameter, which is not automatically corrected for, is pressure. Therefore we apply a correction using the gas pressure p_{gas} and the reference pressure $p_{\text{ext}} = 1000$ mbara stored in the device. The gas pressure is measured by sensor A115PS. [53]

Using the ideal gas law, the number of molecules n inside the measurement chamber depends on the pressure p and temperature T . Both pressure and temperature are taken inside the chamber. The luminescence signal and through this, the fraction of O_2 , η_{O_2} , is assumed to be proportional to the number of molecules.

$$\eta_{\text{O}_2} \propto n = \frac{p}{T} \quad (8.11)$$

The corrected O_2 concentration can be derived using

$$\eta_{\text{O}_2, \text{norm}} = \eta_{\text{O}_2, \text{sensor}} \cdot \frac{p_{\text{gas}}}{p_{\text{ext}}} \quad (8.12)$$

A measurement done using a test gas which consists of 100 vol.-ppm O_2 dissolved in Argon, has shown that further corrections are necessary. Without additional corrections, the relative deviation of the measurement from given concentration gas is up to 20 %. The deviation $\Delta\eta_{\text{O}_2}$ is shown in figure 8.4 and a pressure dependence is observed. A correction is introduced which is not physically motivated, but just describes $\Delta\eta_{\text{O}_2}$. The correction is derived from a fit to the measured data.

$$\Delta\eta_{\text{O}_2}(p) = A \cdot \log(B \cdot p + C) \quad (8.13)$$

All measurements were done at pressure values between 1000 mbara and 4000 mbara. Hence, the correction is only valid in this region.

8.2.3. Error of measurement

According to the information brochure [52,53,51] of the oxygen sensor a relative measurement error can be assumed. This error is composed of the following parts.

Repeatability 1%. This value is the standard deviation of various measurements done by one operator in one measurement situation.

Reproducibility 2%. The difference to the value stated above is the expansion to multiple operators and different measurement situations.

Accuracy 2%. The deviations to test conditions are stated as accuracy.

8.3. Gas chromatograph

For the basic analysis of the gas composition a gas chromatograph (GC) (see figure 8.5) is installed. With this device the main components of the mixture can be detected and their relative fraction can be measured. The GC needs to be trained before it can detect a component. For this purpose each input line for supply gas can be selected as a sample

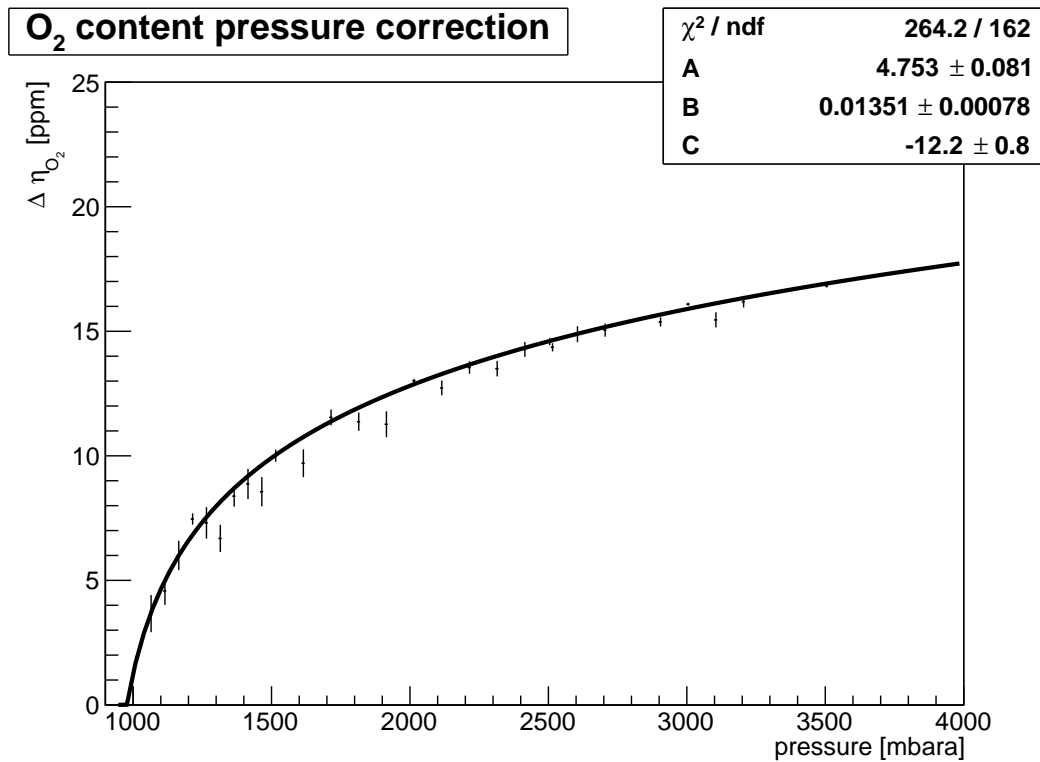


Figure 8.4.: Deviation between measured and given O₂ concentration of a test gas and resulting second pressure correction of the values measured by the oxygen sensor.

source for the GC. Also the analysis loop can be selected which can be switched into many other loops. With this mechanism, each loop can be sampled.

First inside the GC the gas mixture is sampled. This is done via a 10/2 valve. During the load position (figure 8.6(a)) the gas is only flowing through the two sample loops. When the valve is switched to the inject position (figure 8.6(b)), the gas can flow into the columns, depending on the status of the other solenoid valves. The columns separate the gas. At the end of the columns, the gas flow is merged together by a "TEE" (figure 8.6(a)) and fed into the detectors.

The GC mounted inside the UGMA is produced by SRI Instruments [56]. The GC is very modular, so that it can be equipped with various detectors and columns. The installed GC hosts two columns, one Molesiev-13X and one HayeSep-D [58] column.

Sampling inside the GC is done for each column separately. Hence two sample loops each a volume of 1 $\mu\ell$. During the sampling process, they are placed inside the sampling gas flow. When the analysis is triggered, they are switched inside the analysis part of the GC. Depending on the analysis program, the gas from these volumes is sent through the columns. The exact volume of the sample loop is not needed for our purpose, because the GC should determine the composition of the gas in percent, the volume itself cancels out. Thus, the volume can be chosen in order to tune the signal inside the detector. The carrier gas, which is He in this setup, is also called mobile phase.



Figure 8.5.: Photo of the gas chromatograph.

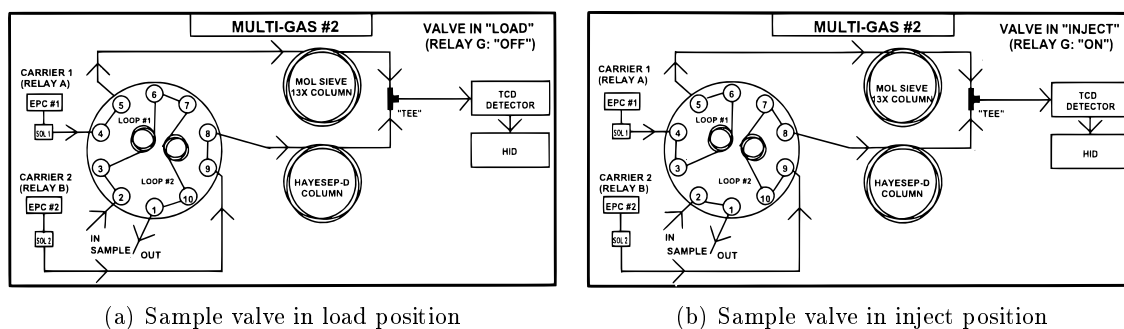


Figure 8.6.: Gas flow inside the GC sampling section.

Inside the columns, the gas mixture is separated. Both used columns are packed columns, which consist of a stainless steel pipe, which is filled with the appropriate material. This material is also called stationary phase. The interaction of the analyt with the mobile and stationary phase defines the time, which the analyt needs to travel trough the column. This time is also called retention time.

Each gas has a specific retention time, which is based on the interaction of the analyt with the stationary phase, the boiling point and the diffusion properties of the substance. The interaction and diffusion properties change with the temperature of the column. At the end of the column, where the detector is mounted, most of the gases are separated in time and can be detected. Some gases can not be separated, because they interact similarly and thus, their retention times are too close together so that they appear in the detector as one peak. The separation power is only influenced by the power of the columns. It can be enhanced by choosing the right temperature program. One example chromatogram is shown in figure 8.7.

The used GC is equipped with a thermal conductivity detector (TCD) module. A helium ionisation detector (HID) module is mounted behind the TCD. The sample gas is first

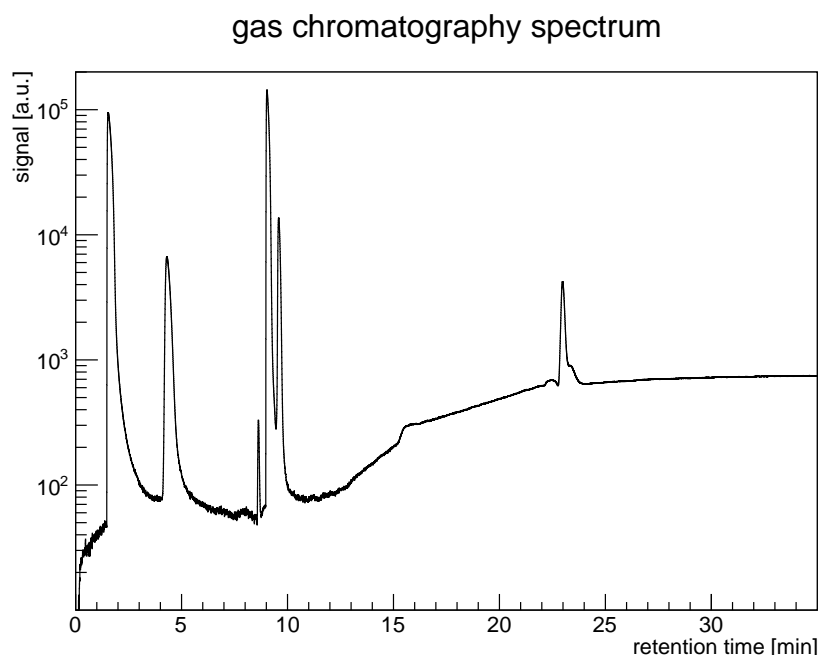


Figure 8.7.: Example chromatogram of a Argon Methane 90:10 mixture detected with the TCD. After integration and calibration the analysis gives a result of 89.07 vol.-% Ar and 10.16 vol.-% CH_4 for the first peaks and 10.30 vol.-% CH_4 for the second peak. Due to switching the columns, it is not possible to integrate the second Ar peak, because the signal and switching peak overlap.

detected inside the TCD. After this detector it is diluted with pure helium and fed through the HID, where it gets ionised. At the output of the HID no further analysis can be done, because inside the detector the gas gets ionised and so its molecular structure may have changed.

The TCD compares the heat capability of the sample gas with a predefined reference gas. In the UGMA helium is selected as reference gas. By this selection, the detection limit is set. This sensor is totally blind to helium. All gases, which have a greater heat capacity produce a positive signal. Those with a smaller heat capacity give a negative signal. With helium reference, hydrogen will cause negative signatures.

The HID measures the ionisation current between two electrodes, one is connected to high voltage and ionises the sample gas. If the energy needed to ionise the sample gas passing by is lower in comparison to helium, the current increases.

In general, the HID is more sensitive than the TCD. On the other hand, the integrated peak signal from the TCD is proportional to the fraction of the gas present in the sample. Comparing the integral of one peak to the sum of all detected peaks one can get a quick estimation of the content inside the sample gas. To get a more precise result a dedicated calibration is needed. Because the HID saturates at lower fractions than the TCD, it is only used for gas identification. In general, the TCD can detect pure gases without saturation. A GC measures the absolute volume of a gas. Because the sample loop has a defined volume, the signal can be converted into a fraction.

The results obtained with the GC strongly depend on the special temperature ramp. The combination of both installed columns helps to distinguish nearly all gases, which might be used inside the UGMA. But on the other hand, the temperature ramp has to be carefully chosen.

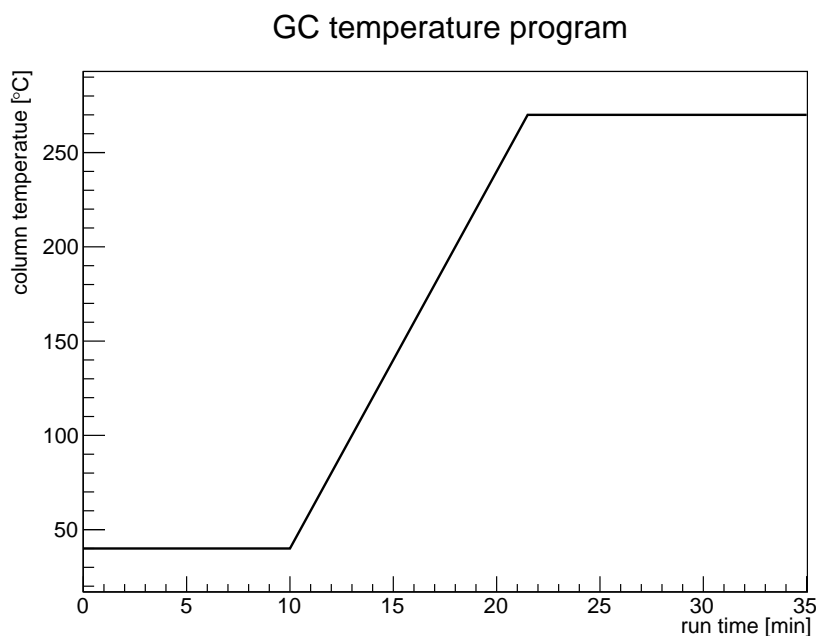


Figure 8.8.: GC temperature program, which is used to analyse the mixed gas. This program was optimised for usage in combination with common drift gases.

One reasonable temperature ramp is shown in figure 8.8. The associated events are shown in table 8.1. Both have been developed by testing. There is no specific reason for the exact positions of the times and temperatures. While creating the temperature and event file the retention times of the gases have to be considered. If a gas of the mixture has a very high retention time (e. g. iC_4H_{10}) the program should last as long as this gas needs for retention. Otherwise it gets stuck inside the columns, they saturate from this components and cannot detect this gas component furthermore. Hence also the detection capability of the other gases decreases. The performance suffers until all columns are baked out again.

Table 8.1.: Event-table used in GC setup

time [min]	command	comment
0.00	ZERO	Adjust signal to zero
0.05	B ON	Stop Flow - Column B
0.50	G ON	Rotate valve in inject position
8.50	B OFF	Start Flow - Column B
8.52	A ON	Stop Flow - Column A
22.00	A OFF	Start Flow - Column A
22.02	B ON	Stop Flow - Column B

8.3.1. Analysis

There are two possible ways of analysing a measured spectrum. When looking at the spectrum and searching peaks, one can identify if a gas is present in the sample or not. Each gas is identified by its retention time. The retention time can be calibrated using a reference source. Sometimes one can guess the gas, which fits to a retention time. Here a lot of experience is necessary and it should be checked, that the peak is identified correctly.

If gases should only be identified the precision of the reference mixture can be neglected. On the other hand, if one is interested in the fraction of gas solved in the sample, a high precision reference gas is needed. Here the area below the retention peak needs to be calibrated.

Since the software, supplied with the GC, does not allow reintegration and scripting, it is just used for sampling and storing the data. The analysis is done by a small program, which supports all needed features and which is connected to a MySQL-database where all calibration constants and functions can be stored.

For calibration purposes, a very precise reference is needed. The normal gas mixtures delivered are not usable, because they have a relative error of 10 % in the gas fractions. On the other hand, it is not recommended to use pure gases for volume calibration. Experience from the past has shown, that for some gases, like CH₄, CF₄, etc. the peak broadens up and its width lasts over half the spectrum when used as pure gas. Furthermore, the peak position changes, because the slow rate seems to be limited. Both effects result in a wrong calibration. In connection with Argon, both effects have not been observed. Therefore it is recommended to use a mixture of argon with e.g. only 5 % of the gas, which should be calibrated. The precision of the mixture should have reference gas quality. Such a mixture will prevent the sensors from saturation and will give reliable results.

8.3.2. Off-line analysis

Due to heating and different pressure levels while switching between the columns a background level and additional fake peaks appear. The background can be subtracted using a measurement without sample gas. The switching times are known from the event file (see table 8.1). After a short delay, the fake peaks appear and can be masked for further analysis. The general data flow inside the analysis framework is shown in figure 8.9. For detection of the integration area, the spectrum is differentiated. The slope between two points is calculated. At the beginning of a peak the slope suddenly rises and at the end of a peak, it is getting back to the normal. With a threshold, the integration area can be determined. Integration is done by adding up bin by bin. At the end, the value is feed into the calibration function to receive the content of the measured gas.

8.3.3. Resolution

The performance of the GC always depend on the calibration. Hence a proper calibration is needed to ensure the best results from the GC. During a first calibration and commissioning test the results shown in table 8.2 have been gained. The results are split into the two

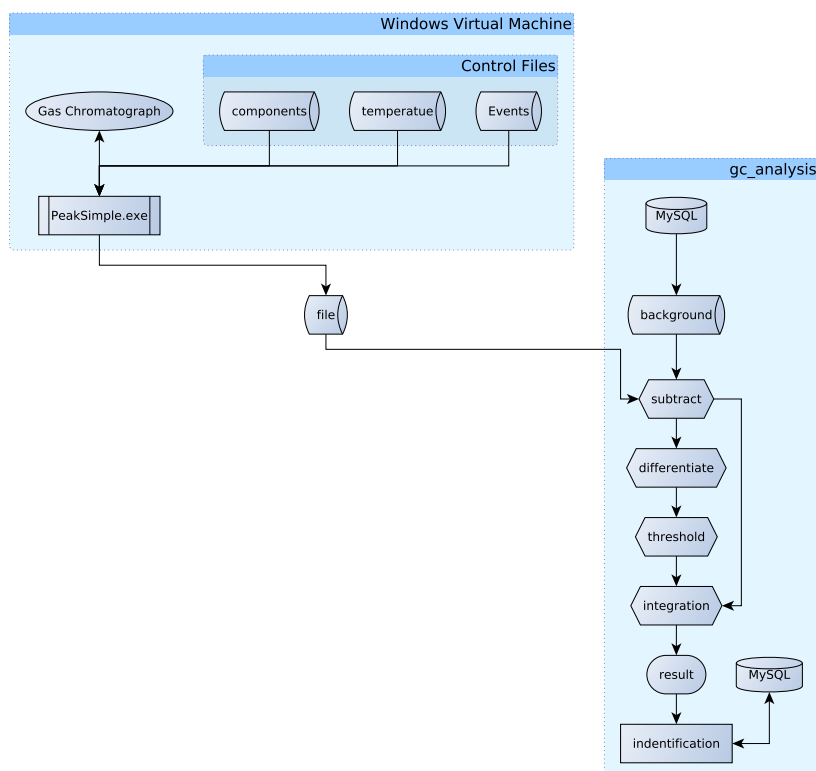


Figure 8.9.: Data flow of the GC offline analysis. Additionally the GC online program is shown.

different columns. All results have been measured using the TCD detector. The points, which have been used to measure the accuracy are not part of the calibration.

The precision is the maximal statistical error using various measurements and concentrations. The accuracy is the maximal absolute deviation from either setpoint or fitted mixture (see section 11.2). CO_2 is only detectable on the HayeSep column.

Table 8.2.: Precision and accuracy of the GC. All results are given in vol.-%. The accuracy has been tested once with respect to the setpoint and once with respect to the values gained from the v_d -fit method (see section 11.2) [15]

Gasname	Column	Precision	Accuracy (Setpoint)	Accuracy (Fitting)
CH_4	Molesiev	0.057	0.112	0.11
CH_4	HayeSep	0.046	0.091	0.16
$i\text{C}_4\text{H}_{10}$	HayeSep	0.21	0.16	not tested
$i\text{C}_4\text{H}_{10}$	Molesiev	0.27	0.19	not tested
CO_2	HayeSep	0.076	0.22	0.21

8.4. Cavity Enhanced Differential Optical Absorption Spectroscopy

In atmospheric physics an optical method called Cavity Enhanced Differential Optical Absorption Spectroscopy (CEDOAS) is used [31,39,16,30]. This method is used to detect trace gases like NO_x in the atmosphere. For development purpose, the setup can also be used in laboratories to analyse gas samples.

The measurement principle is based on optical absorption. When light is sent through a medium, it is partially absorbed. Due to the cross-section of the molecules dissolved in the gas, it is not absorbed uniformly over all wavelengths. There exist absorption peaks, which are typical for each molecule. These absorption peaks can be measured using a spectrometer illuminated by a light source with a broad spectrum. The absorption follows the law of Lambert-Beer. The power $P(d)$ transmitted through a medium of thickness d is given by equation 8.14.

$$P(d) = P_0 \cdot e^{-\epsilon' d} \quad (8.14)$$

$\epsilon'(\lambda)$ describes the absorption-coefficient and depends on the material and wavelength λ . The incoming power is represented by P_0 . To achieve a large effect, i.e. a high absorption, a long lightpath is needed. For building an instrument, which fits into a laboratory one can use optical cavities. A cavity extends the light path through the gas up to several kilometres by reflection. The cavity only needs space of a length of the order of 1 m.

The resolution of this measurement principle strongly depends on the resolution of the spectrometer. To distinguish two gases, whose peaks are quite near to each other, it should be able to resolve them. On the other hand, it is important to measure smallest differences in intensity. This means, that the spectrometer should have a high dynamic range and sensitivity.

For cancelling out peaks introduced by the main component, which for drift gases is Ar and for atmospheric measurements is air, differential spectra are taken. This means, at first the background introduced by the main component is measured. It has to be made sure that the gas taken during this measurement is free of the gases, which should be detected in a later stage. In a second run at the same settings a spectrum is taken from the sample gas. The background measured earlier is subtracted from this measurement and the spectrum should only contain peaks from contaminations to the main components.

For identifying the peaks, data tables like high-resolution transmission molecular absorption database (HITRAN) [33], Gestion et Etude des Informations Spectroscopiques Atmosphériques: Management and Study of Atmospheric Spectroscopic Information (GEISA) [11] and Carbon Dioxide Spectroscopic Database (CDSD) [38] exist to identify absorption peaks caused by different molecules. For atoms NIST provides a database. All databases have in common, that their data start in the visible spectrum and they provide a lot of data for infrared light.

Using CEDOAS for analysis of drift gases is new and has not yet been tested. There are a lot of studies done for atmospheric measurements, but none for the detection of drift gases. This analysis method has been evaluated for use together with drift gases during a feasibility study to determine the necessary resolution of the spectrometer and the length of the light

path. Furthermore during these studies the absorption wavelength of the typical gases used in gaseous detectors and their coverage by a possible light source has been calculated.

8.5. Gas Monitoring Chambers

8.5.1. ND280 TPC Gas Monitoring Chambers

For the first tests a setup of two Gas Monitoring Chamber was used. Both chambers are quite similar to the ones, which were produced for use at the ND280-detector in the T2K-experiment in Tokai, Japan (see section 2.1.3). One chamber is the predecessor and the other one the successor of the monitoring chambers mounted in Japan. A small sketch of the chamber is shown in figure 8.10. These small chambers are readout by a segmented plane.

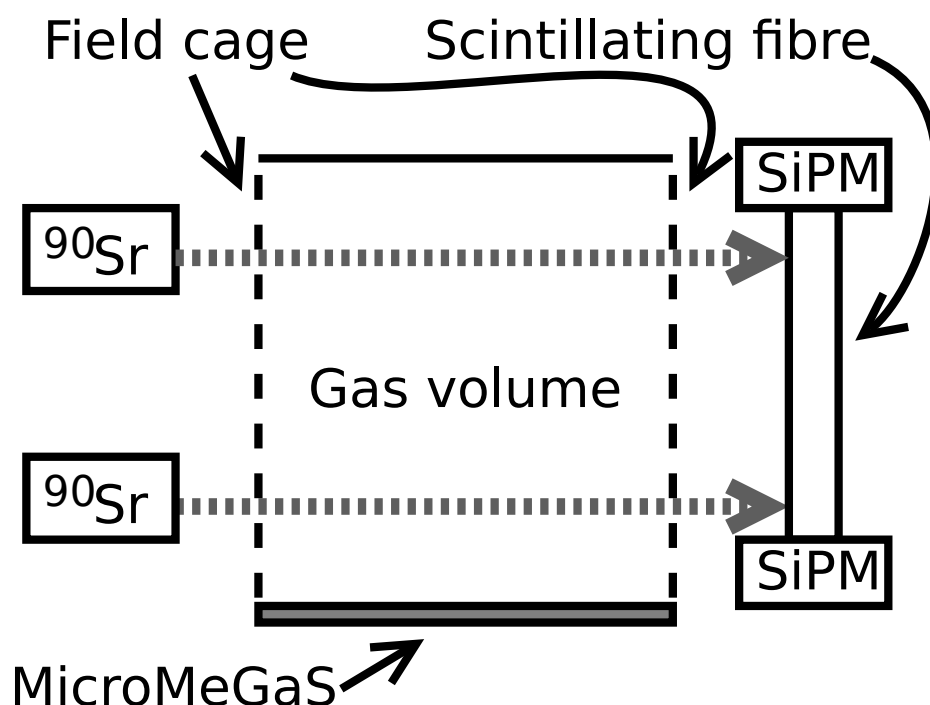


Figure 8.10.: Sketch of the general prinziple of the ND280 GMC. [25]

For amplification of the incoming electrons, a MicroMegas is placed. In this setup the mesh of the MicroMegas is typically supplied with 350–480 V depending on the gas composition. Mixtures based on $i\text{C}_4\text{H}_{10}$ typically need a lower voltage to achieve the same amplification. Higher voltages need to be used for mixtures based on Ar-CH_4 . The mesh is positioned $128\ \mu\text{m}$ above the pads. This results in a quite homogeneous electrical field at the magnitude of 2.73–3.75 MV/m.

For getting the electrons towards the amplification region, a drift field can be applied. The monitoring chambers consist of a 14.8 cm long field cage. There are strips on the inside and on the outside of the Kapton-foil forming the field cage. The combination of overlapping strips on the inside and outside forms a very homogeneous field. Along all strips a voltage

divider made from standard Surface-mounted device (SMD) resistors is soldered. Within their tolerances, they provide a constant voltage difference between two parallel strips.

One end of the cage is connected to the cathode and on the opposite side, the last strip is connected to the mesh. The cathode can be supplied with a maximal voltage of -6 kV. This results in a dependence of the drift field on the mesh voltage of

$$E_{\text{drift}} = \frac{U_{\text{cathode}} - U_{\text{mesh}}}{14.8 \text{ cm}} \quad (8.15)$$

The maximal drift field can be achieved with maximal cathode voltage $U_{\text{cathode}} = 6 \text{ kV}$ and minimal mesh voltage $U_{\text{mesh}} = 350 \text{ V}$. Hence the maximal possible drift field is about 380 V/cm .

For measurements of the drift velocity the chambers are equipped with two Sr^{90} sources at a fixed distance of 12.1 cm. The sources create two electron beams, both parallel to the readout plane. The beams cross four rows of readout pads. After crossing the chamber, they hit a scintillating fibre. The fibre is instrumented by two Multi Pixel Photon Counter (MPPC). When both MPPC register a signal at the same time, the Flash Analogue Digital Converter (FADC) is triggered and the signal of one readout pad is recorded. After registration of the electrons coming from the triggered event, the relative arrival time is recorded in a histogram (see figure 8.5.1). When enough measurements are done, the histogram is analysed. The

Drift Signal

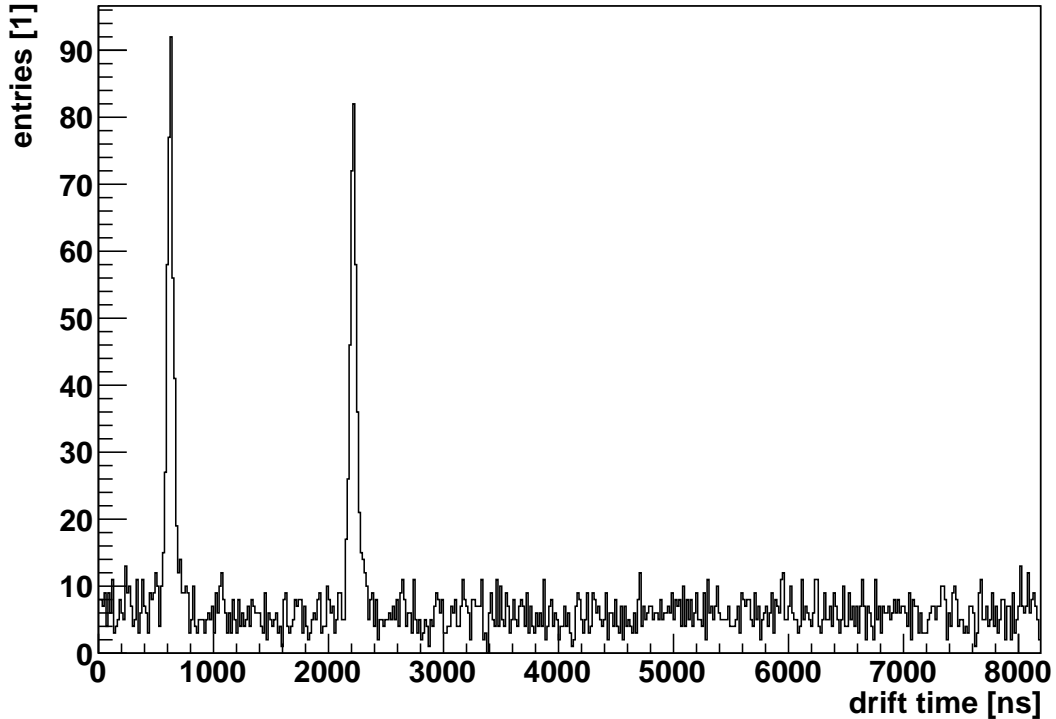


Figure 8.11.: Drift time distribution

time difference between both peaks, one resulting from the „near“ and the other from the

„far“ source, is used in combination with the distance between the sources to compute the drift velocity.

$$v_{\text{drift}} = \frac{12.1 \text{ cm}}{\Delta t} \quad (8.16)$$

Additionally, both chambers can be used to monitor changes in gas amplification and absolute gain, when applying a correct calibration of the whole data acquisition chain. The calibration has to start at the pre-amplifier and ends inside the computer after integrating the signal. Hence this chain is quite difficult to calibrate and the results of the simulations are not usable to specify the gas inside the chambers, only the drift velocity is used in the following. Here the data fit quite well to the simulations.

The systematic errors of this chamber have been estimated by Lukas Koch [26, p. 26 ff.] to be

$$\left(\frac{\sigma_{v_d}}{v_d} \right)_{\text{sys}} \lesssim 4 \text{‰} \quad (8.17)$$

and

$$\left(\frac{\sigma_{ET/p}}{ET/p} \right)_{\text{sys}} \lesssim 4 \text{‰} \quad (8.18)$$

8.5.2. L3 TEC Velocity Drift Chamber

The L3-detector which has been used at the Large Electron-Positron Collider (LEP), the predecessor of the LHC, at European Organization for Nuclear Research (CERN) from 1989 until 2000. Inside this detector, the central track detector consists of a Time Expansion Chamber (TEC), which is operated using a gas mixture of 80 % CO_2 and 20 % $i\text{C}_4\text{H}_{10}$ at a pressure of 1.2 bara. The drift velocity of this mixture is $6 \mu\text{m/ns}$. [29] This value is quite low compared to the drift velocities used in TPCs. For monitoring the drift velocity inside the TEC, a monitoring chamber is placed inside the gas flow (Figure 8.12).

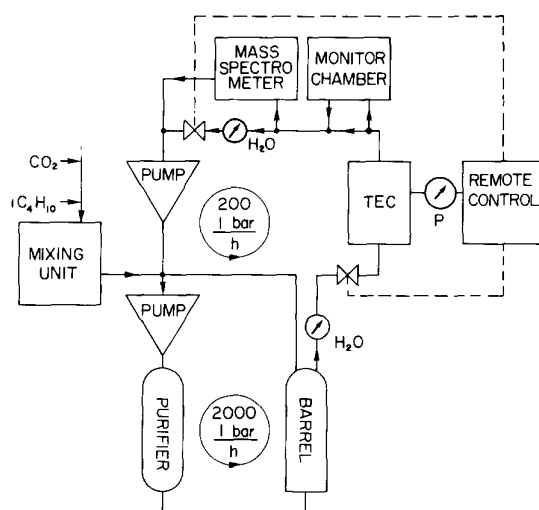


Figure 8.12.: TEC gassystem with the monitoring chamber. Figure taken from [4, p. 37]

In figure 8.13 it can be seen, that the chamber is separated into two parts. In the drift volume, a homogeneous field is created by the field forming wires, which are connected to a voltage divider. Hence the electrons can drift with a constant velocity towards the detection volume. In this volume, the gas amplification takes place. The anode wire is supplied by a voltage of about 1.6 kV. Both volumes are separated by grounded metallic plates. In the middle of the plates a small slit connects both volumes. This slit is large enough for the transfer of the drifting electrons but on the other hand, it decouples the electrical fields. [45] Before this chamber has been used for systematic studies in combination with the UGMA, the

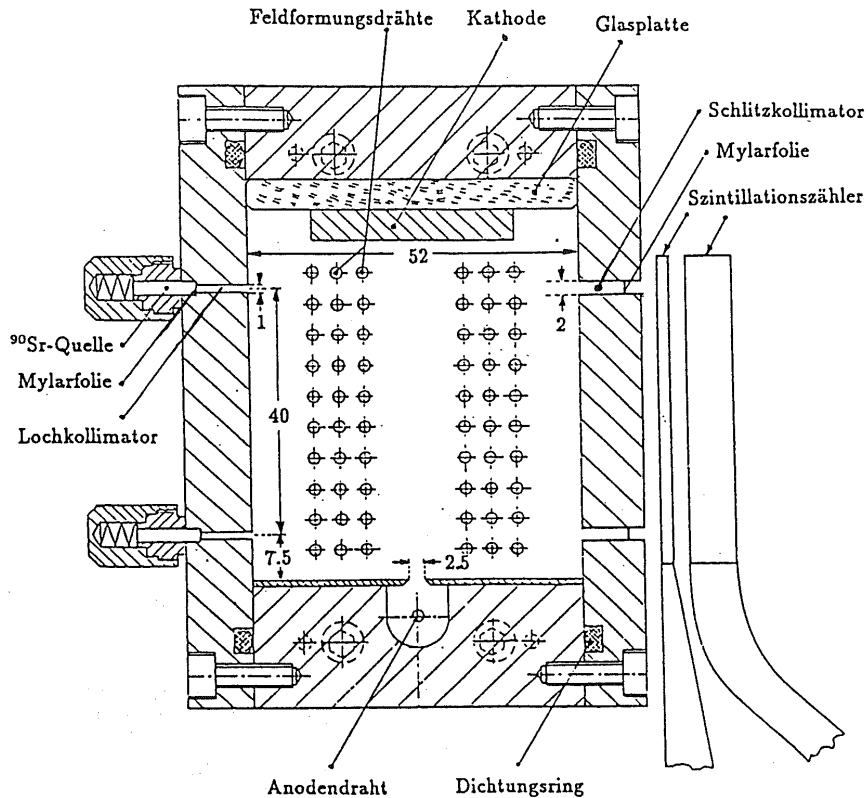


Figure 8.13.: Technical drawing of the L3 VDC. In the current setup both scintillators shown on the right side have been replaced by one thick one, which is readout by one PMT on each end. Drawing taken from [19].

distance between both Sr^{90} sources Δz and the distance between ground and cathode l_f have been measured.

$$\Delta z = 39.97 \pm 0.29 \text{ mm} \quad \text{design value: 40 mm} \quad (8.19)$$

$$l_f = 54.91 \pm 0.03 \text{ mm} \quad \text{design value: 55 mm} \quad (8.20)$$

The chamber has been connected in series to the ND280 GMC. The trigger setup for this chamber has been slightly modified from the version shown in figure 8.13. The original setup consists out of two scintillators, one very thin and one thick. This setup has been replaced

by one thick scintillator, which is readout on both ends with one PMT. The coincidence of the PMT signals triggers the FADC.

The L3 chamber uses the same temperature and pressure sensors, digitizer, and also a similar high voltage supply. Hence the estimation of the systematic errors can be calculated according to [26, p. 27]. To estimate the systematic uncertainty of the drift length Δz the Sr^{90} is assumed to be punctual and the scintillator behind the chamber.

$$\frac{\sigma_{\Delta z}}{\Delta z} = \frac{0.5 \text{ mm}/\sqrt{12}}{39.966 \text{ mm}} \lesssim 4 \text{ ‰} \quad (8.21)$$

The systematic error of the field distance l_f is given by the digitisation error of the used calliper $\sigma_{l_f} = 0.01 \text{ mm}$.

$$\frac{\sigma_{l_f}}{l_f} = \frac{0.029 \text{ mm}}{54.906 \text{ mm}} \lesssim 0.6 \text{ ‰} \quad (8.22)$$

Combining these new calculated values with the ones described in [26] yields to the systematic uncertainties

$$\left(\frac{\sigma_{v_d}}{v_d}\right)_{\text{sys}} = \sqrt{\left(\frac{\sigma_{\Delta z}}{\Delta z}\right)^2 + \left(\frac{\sigma_{\Delta t}}{\Delta t}\right)^2} \lesssim 4.5 \text{ ‰} \quad (8.23)$$

and

$$\left(\frac{\sigma_{ET/p}}{ET/p}\right)_{\text{sys}} = \sqrt{\left(\frac{\sigma_{U_f}}{U_f}\right)^2 + \left(\frac{\sigma_{l_f}}{l_f}\right)^2 + \left(\frac{\sigma_T}{T}\right)^2 + \left(\frac{\sigma_p}{p}\right)^2} \lesssim 2.5 \text{ ‰} \quad (8.24)$$

The signal from the anode wire is amplified and discriminated and then fed to the FADC. Amplification is done by using the anode amplifier of the VDCs used at the CMS muon system [21]. Discrimination of the signal is not necessary but during the re-commissioning phase of the L3 VDC in the current setup, the signal was also fed to a oscilloscope, by using a fan-out. Unfortunately only a digital version was available, and thus the discrimination was introduced and after this it has not been removed.

The signal from the PMTs is fed into a discriminator and after this into a mean-timer, which gives the mean time between both signals. If the time difference between both signals exceeds the maximal accepted time, no trigger is generated. Thus it acts like an coincidence. The output of the mean-timer triggers the FADC and the signal from the wire is recorded and afterwards analysed.

9. Commissioning of assembly groups

All assembly groups have been commissioned and tested one by one. During testing some improvements have already been introduced. In the following part, the experience and results from these early tests are described.

9.1. Power supply

Before all other groups could be commissioned, the power supply had to be connected and commissioned. This group distributes the three-phase input to all other sub-groups. The load is equally distributed to all phases, in order to get the current on the neutral conductor as low as possible. This is done inside the PDU. If the load is very asymmetric, the current on the neutral conductor increases. This does not harm the operation but is frowned upon by the electricity supplier. Furthermore each output is connected to a circuit breaker for safety issues. The input is fused by an RCD with a residual current of 30 mA. This device is the crosspoint for every 230 V power line.

9.2. PowerBar

After connection of all cables to the sub-distribution of the PowerBar, each block was tested separately. For this purpose each block is supplied by a current-limited power supply. Consecutively every valve has been switched. At the same time, the current was monitored. That means, that the current consumption of each valve was measured. The mean current consumption is

$$\Delta I = I_{\text{on}} - I_{\text{off}} \approx 60 \text{ mA} \quad (9.1)$$

If the current is much higher, the valve connection and the valve driver must be checked again. The complete PowerBar is fed by one 24 V power supply, which can supply a maximal power of 480 W. Each of the three sub-distributions consists of 22×3 clamps. The connection between power supply and sub-distribution is done using a cable with a cross-section of 2.5 mm^2 .

The valves are connected to the PowerBar by cables with a cross-section of 0.75 mm^2 . Each valve is connected with three wires to the power bar. For control another cable is used.

1. 24 V
2. 0 V or commonly called ground
3. Protective earth. Inside the solenoid, this wire is connected to the metallic surface and when the valve is mounted together, it is connected to the piping as well.

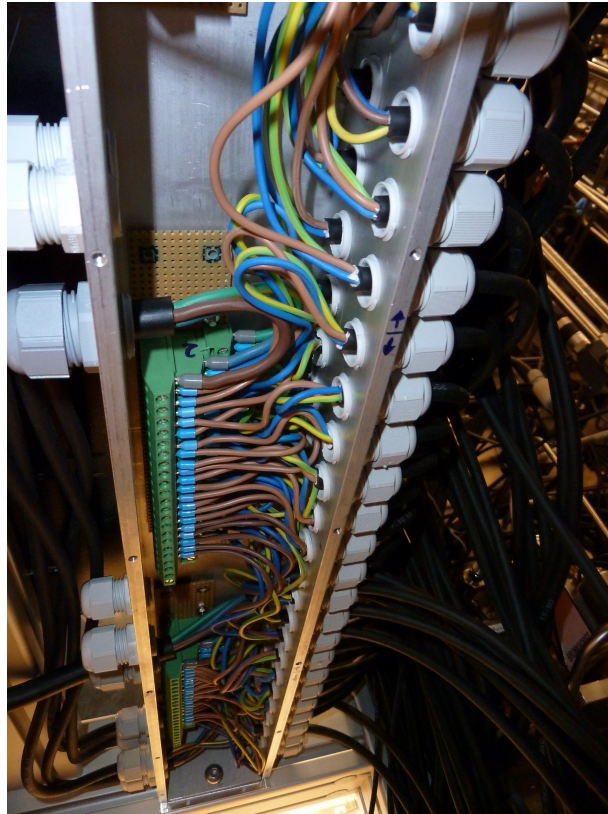


Figure 9.1.: View inside the PowerBar. Two of three connections blocks are visible. The valves are connected via the cables on the right side. On the left side the power supply and further special devices are connected.

In total the PowerBar is capable of distribution of the full power (480 W) delivered by the power supply. If no special valve driver is used, the maximal number of valves, which can be connected is given by

$$N_{\text{valves}} = \frac{I_{\text{max, power supply}}}{I_{\text{valve}}} \quad (9.2)$$

$$= \frac{20 \text{ A}}{375 \text{ mA}} \quad (9.3)$$

$$= 53 \quad (9.4)$$

The power supply is able to supply 53 valves in continuous mode. Due to the large inductance of the solenoid, during switch large current peaks might appear. Inside the valve driver, the voltage of the valve is switched and due to this, the average current is reduced to about 20 %. With the reduced current, the power supply can supply 260 valves:

$$N'_{\text{valves}} = \frac{N_{\text{valves}}}{20\%} > 260 \quad (9.5)$$

9.3. Valve-driver

Before mounting, each valve driver has been tested and specified. This test was done while mounting the valve-driver inside the plug. The qualification was done by analysing the voltage across the solenoid by an oscilloscope.

There are three parameters, which characterise a valve-driver. All values given are the mean values of the distribution. In total 56 valve driver have been qualified.

1. Frequency f . This is the frequency of the rectangular output signal. It has been determined by the internal measurement function of the oscilloscope.

$$f = (92.95 \pm 2.06) \text{ kHz} \quad (9.6)$$

The internal oscillator frequency is given by the relation [89, figure 4]

$$R_{\text{freq}} = \frac{6808417}{f^{1.0288}} \quad (9.7)$$

Using this equation, the frequency can be calculated from the design value of the resistor R_{freq} .

$$f = 96.27 \text{ kHz} \quad (9.8)$$

2. Duty-Cycle D is the ratio between the time τ , during which the valve is switched on, and the whole cycle time T .

$$D = \frac{\tau}{T} \quad (9.9)$$

$$= 1 - (79.35 \pm 0.48) \% \quad (9.10)$$

$$= (20.65 \pm 0.48) \% \quad (9.11)$$

The duty cycle can be estimated using [89, table III]. But there is no equation to calculate this value because the duty-cycle depends on the oscillator frequency used.

3. Startup-delay-time T_{delay} . To ensure switching the valve, a large pulse is applied when the switching command is received. The small current later is large enough to keep the valve open (see section 5.6), but it is not large enough to switch it.

$$T_{\text{delay}} = (26.88 \pm 1.10) \text{ ms} \quad (9.12)$$

The design value is given by [89, p. 8]

$$T_{\text{delay}} = C_D \cdot 10^6 \text{ s/F} \quad (9.13)$$

$$= 22 \text{ nF} \cdot 10^6 \text{ s/F} \quad (9.14)$$

$$= 22 \text{ ms} \quad (9.15)$$

The difference between the measured and calculated value might be caused by part tolerances and influences of the printed circuit board (PCB).

After mounting the valve-driver on the solenoid a second functional test was performed. This time, the switching performance in combination with the valve was tested. Faulty valve-drivers were checked again and if possible, the source of the error was removed. Only drivers, which passed both tests remained inside the system.

9.4. Tightness & leakage

Each loop has been tested for potential leakages. Due to the huge amount of screw joints, a test of every single connection is not feasible. To determine the tightness of a loop, the whole loop has been pressurised up to the maximum permitted pressure. After this step, the valve has been closed and the pressure was monitored.

The mounted sensors are so sensitive, that even smallest changes in temperature result in pressure changes. For compensation of this effect, the quotient of pressure and temperature is plotted. This coefficient is proportional to particle density n . The relation is motivated by the ideal gas law.

$$p \cdot V = NRT \quad (9.16)$$

$$\frac{p}{T} = \frac{N}{V}R \stackrel{!}{=} \text{const} \quad (9.17)$$

It is not possible to build a completely tight system. Hence, minimal leaks remain and the particle density decreases. For getting a simple discrimination variable, the measured particle density is plotted versus time. In order to draw a conclusion a linear fit is done, where the slope is taken as the discriminator. For larger volumes a maximum leakage rate of $5 \cdot 10^{-6} \text{ mbar K}^{-1} \text{ s}^{-1}$ is used. For volumes, which mainly consist of piping, this value can not be used. Those lines have such a very small volume that even tiny holes can cause a measurable drop. But on the other hand, these small holes cannot be detected. Hence the threshold is varied according to the rather small volume of the device under test.

If the pressure does only depend on the temperature, the system can be marked as sufficiently tight. Not every loop has its own temperature sensor, therefore the temperature sensors of other loops have to be used. Further huge temperature inhomogeneities across the device under test itself might appear. Related to both issues it has been observed, that the particle density increases although no extra gas has been added.

9.4.1. Determination of vacuum-leakage-rate in the buffer & purifier

For both, buffer- and purifier-vessels, the leakage-rate has been measured at vacuum. At lower pressure, the influence of the temperature on the pressure can be neglected. It is sufficient to plot just the pressure versus time. The volume of the purifiers is derived from the calculations to $V_P = 1.25 \ell$. According to the manual, the buffer-vessel has a volume of $V_B = 48 \text{ L}$. For the pipes a specific volume v of

$$v = \pi r^2 \cdot l = \pi \cdot (2 \text{ mm})^2 \cdot 1 \text{ m} = 12.6 \text{ ml} \quad (9.18)$$

can be assumed. The approximated length in both loops of 6 m each results in an additional volume of 100 ml. Using this volume the leakage-rate can be calculated. The quotient of Δp and Δt is derived using the slope of a straight line, which has been fitted to the measured values (see figure 9.2).

A increasing pressure is expected. The values from the measurement after a appropriate time are shown in table 9.1. As a comparison, the leakage rate gained from the pressure difference between start- and endpoint is shown as well.

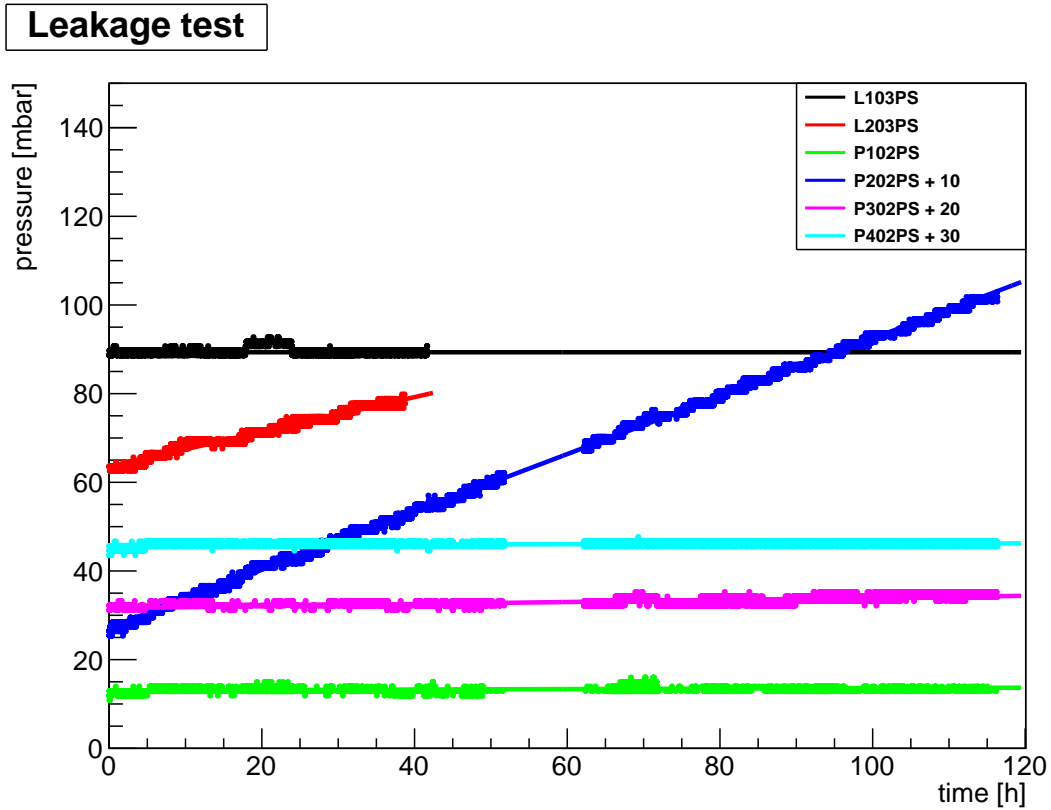


Figure 9.2.: Determination of the leakage-rate at vacuum before filling the vessels with purification material.

It has to be said, that the measurement is limited by the resolution of the digitised pressure sensor ($\Delta p \leq 1$ mbar). The needed resolution can only be achieved by quite a long measurement time.

For determination of the tightness, the pressure of the vessel has been chosen to be higher than the pressure where the sensors start behaving strange. Measurements in connection with the vacuum-sensor have shown, that the normal pressure sensors, which cover a pressure range of 0–4 bara, show a strange behaviour below 11 mbara (see figure 10.6). Below this pressure, they reach kind of a plateau and do not react immediately on pressure changes. Hence it has been abdicated to evacuate the vessels to the lowest possible pressure. It is

Table 9.1.: Comparison of leakage-rates buffer and purifier vessels

loop	Fit [mbar ℓ/s]	endpoint [mbar ℓ/s]
Buffer 1	$(0.00 \pm 0.19) \cdot 10^{-6}$	$3.24 \cdot 10^{-4}$
Buffer 2	$(52.4 \pm 0.04) \cdot 10^{-4}$	$4.90 \cdot 10^{-3}$
Purifier 1	$(2.08 \pm 0.03) \cdot 10^{-6}$	$3.27 \cdot 10^{-6}$
Purifier 2	$2.45 \cdot 10^{-4}$	$2.43 \cdot 10^{-4}$
Purifier 3	$(8.90 \pm 0.04) \cdot 10^{-6}$	$9.82 \cdot 10^{-6}$
Purifier 4	$(1.17 \pm 0.02) \cdot 10^{-6}$	$9.81 \cdot 10^{-6}$

already known, that both buffer 2 and purifier 2 have a higher leakage rate than the other loops. A lot of time has been spent on reduction of the leakage rate in these loops. The error of the value for purifier 2 is not shown, because it is so small, that it can be neglected. The pressure differences between start and end of the measurement should be just used as a quick reference, because they take statistical fluctuations into account.

9.5. Analysis-loop

The analysis-loop is the most flexible and most frequently used circuit inside the system. Beside the connection of the GC, it allows measurements of the oxygen and water contamination. On the other hand, this loop hosts most connections of the whole system. Due to this, it is difficult to determine the leakage rate. The leakage rate Q_l itself is determined by the sum of the specific leakage rates Q_i of each device. Thus the leakage rate of the loop increases with the number of connections.

$$Q_l = \sum_i Q_i \quad (9.19)$$

Hence the analysis loop has the highest leakage rate.

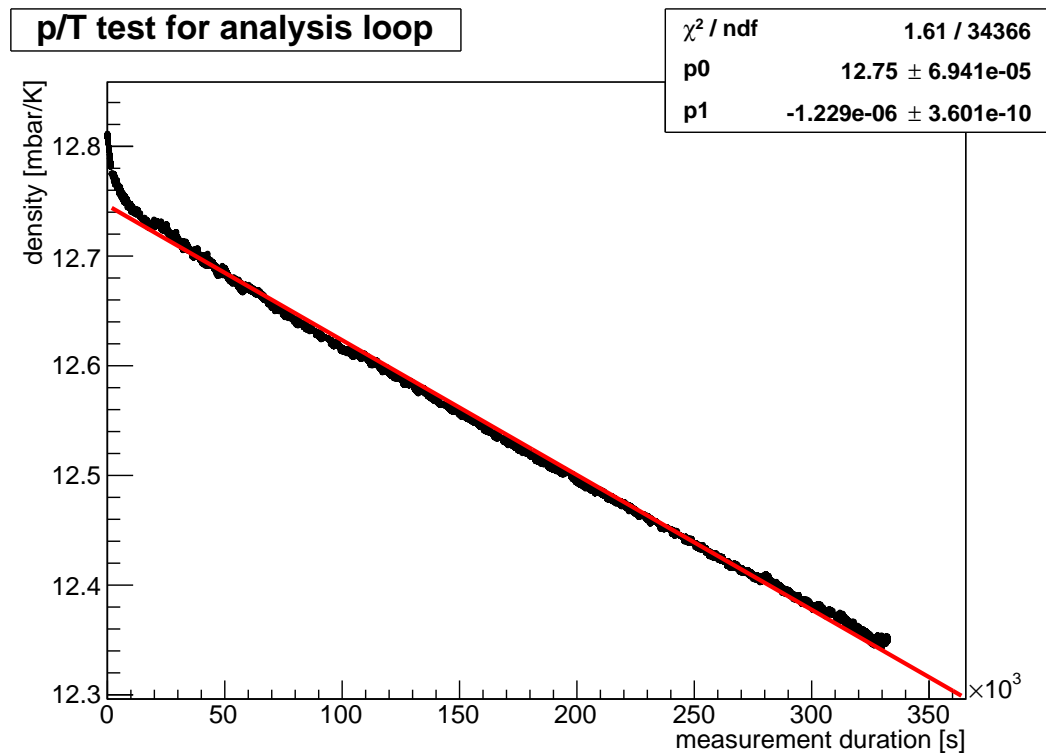


Figure 9.3.: Determination of the leakage rate of the analysis loop.

The leakage rate has been determined for the analysis loop by measuring the difference in gas density p/T . The measurement is shown in figure 9.3. According to this measurement the leakage rate can be determined to be

$$Q'_l = \frac{\Delta \left(\frac{p}{T} \right)}{\Delta t} = 1.23 \cdot 10^{-6} \text{ mbar/K/s} \quad (9.20)$$

Related to the measurement process, the unit of the result does not match the common one. This is caused by the fact, that usual measurements are done in vacuum and thus the influence of the gas temperature is far less. Hence in vacuum technology the leakage rate is defined by the volume of the vessel V , the pressure drop Δp and the measurement duration Δt . [59, p. 48]

$$Q_l = V \frac{\Delta p}{\Delta t} \quad (9.21)$$

To convert the measured value Q'_l into the leakage rate, the temperature has to be cancelled out. This can be done by assuming one standard temperature, e.g. $T = 293.15 \text{ K}$. Hence, the resulting leakage rate is only valid for the assumed temperature. Further the volume of the test device must be taken into account. For a well known device, this is quite easy, because the volume should be known from preceding design and construction processes. In case of the UGMA, the volume of many loops is not well known, but this does not limit the function of the system, since it does not depend on the exact volumes. To estimate the volume of the analysis loop, the sum of the inner volumes over all parts can be computed. Early measurements have shown, that one 4/2 way valve has a volume of $1.62 \pm 0.17 \text{ m}\ell$. Inside the analysis loop, eight of them are mounted. If the volume of the other (2/2 and 3/2) valves is almost the same, the volume of the analysis loop caused by the valves can be assumed to be about $20 \text{ m}\ell$. The piping will add about $60 \text{ m}\ell$ to the volume. Finally it can be assumed to be about $100 \text{ m}\ell$.

Using the assumptions from above, the correct leakage rate can be calculated:

$$Q_l = Q'_l \cdot T_{\text{ref}} \cdot V \quad (9.22)$$

$$= 1.23 \cdot 10^{-6} \text{ mbar/K/s} \cdot 293.15 \text{ K} \cdot 100 \text{ m}\ell \quad (9.23)$$

$$= 3.61 \cdot 10^{-5} \text{ mbar } \ell/\text{s} \quad \text{at } 20^\circ\text{C} \quad (9.24)$$

The resulting leakage rate is not proportional to the temperature, because the flow through the leak depends on the viscosity and kind of flow, which are not linear in T .

9.6. Vacuum

9.6.1. Minimal pressure

The minimal reachable pressure is given by the throughput of the vacuum-pump S and the leak-rate Q_l . Further it is influenced by the permeation Q_{perm} . This describes the ability of single molecules to travel through the walls of the vacuum vessel. But on the other hand, this effect starts at pressures lower than $1 \cdot 10^{-8} \text{ mbara}$. The gas molecules, which are attached to the inside walls, desorb gradually and another time dependent effect Q_{des} is

created. At a pressure of about $1 \cdot 10^{-6}$ mbara plastics start desorption and diffusion Q_{diff} of molecules [59, p. 48].

$$p(t) \cdot S = Q_{\text{des}}(t) + Q_{\text{diff}}(t) + Q_{\text{perm}} + Q_l \quad (9.25)$$

Because the minimum reachable pressure is about 10^{-3} mbar, the leakage-rate dominates. If the vessel is pumped at the throughput S , after a while the equilibrium pressure p_{eq} is reached. At this point, the throughput is equal to the leak-rate.

$$p_{\text{eq}} = \frac{Q_l}{S} \quad (9.26)$$

The leak-rate of the vacuum buffer itself can be determined using the minimum pressure p_{eq} and the throughput of the pump S . It should be further noted, that the throughput itself depends on the pressure. Inside the vacuum-tank without any other vessel connected a minimal pressure of $p_{\text{eq}} = 2.9 \cdot 10^{-3}$ mbara can be reached.

9.6.2. Effective throughput

The maximal throughput is one point, which needs to be considered, when choosing a vacuum pump [37]. Due to the connected pipes and valves and other orifices, the throughput is reduced. The computation of the effective throughput is not trivial. Many parameters can only be assumed. Hence, the throughput inside the buffer vessels has to be measured.

The throughput S is given by the pressure at the beginning p_0 and the current pressure p . Further the volume V_0 , which should be evacuated, and the time t needs to be considered [59, p. 164].

$$S = \frac{V_0}{t} \cdot \log\left(\frac{p_0}{p}\right) \quad (9.27)$$

All measurements were done using the vacuum sensor V101TS. This sensor has a better resolution at lower pressures compared to the normal pressure sensors. Hence this makes a more precise measurement of the throughput possible.

The result of the measurement is shown in figure 9.4. One can clearly see the reduction from the curve derived from the datasheet of the pump „Varian PT300“ [57]. Both buffers have almost the same throughput. The value of buffer two is slightly reduced, which is related to a longer piping from the vacuum pump to the vessel.

9.7. Mixing

As a reference for all mixing processes, the precision of a pre-mixed gas is taken. According to the informations given by the manufacturer [41] all these mixtures are created with a relative uncertainty of 10 %. This value is valid for mixtures without an analysis certificate. If a mixture is certified, the precision can be much better.

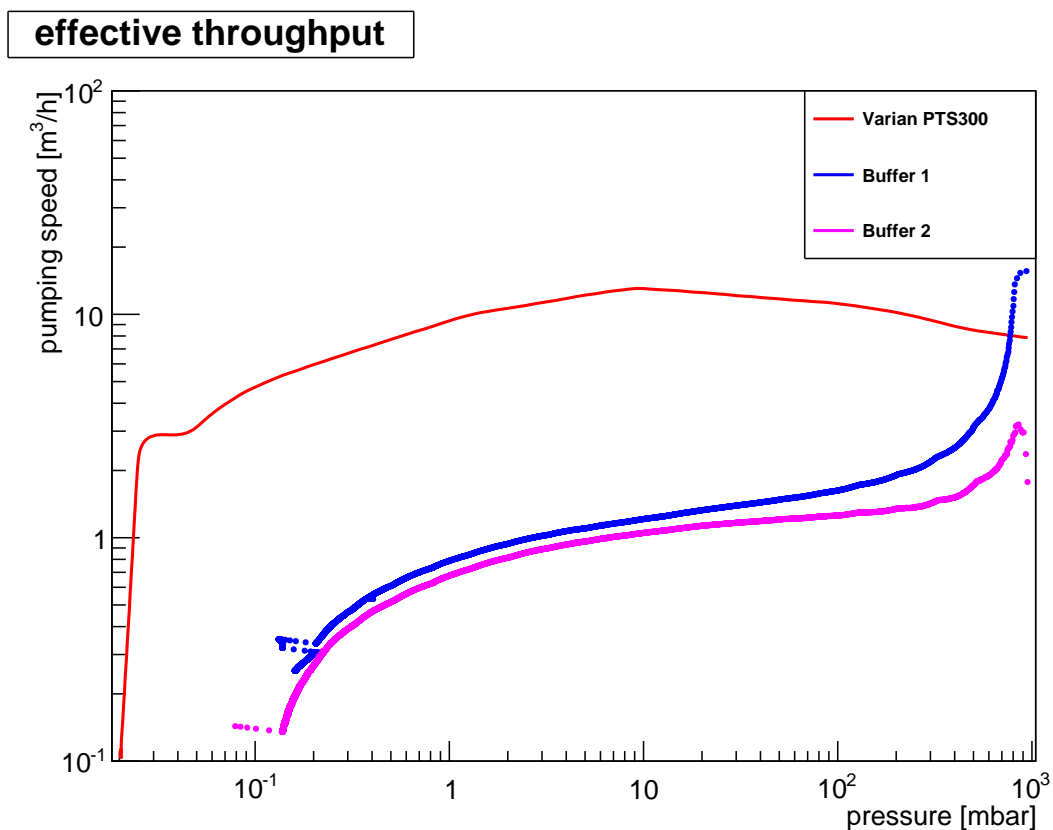


Figure 9.4.: Measurement of the effective throughput

Parallel mixing

The setpoints of the flow are set according to the calculations which are presented in section 7.1. If the MFC is set to the correct type of gas, the uncertainty of the mixture is dominated by fluctuations of the MFC itself. Otherwise the uncertainty is increased by the conversion factor (see section 7.1.3).

In figure 9.5 it can be seen, that the MFCs operate at stable conditions. They produce a gas mixture with stable fractions. Each fraction is calculated from the measured values using equation 7.9.

All deviations are fully correlated to each other. If one MFC delivers less gas, the concentrations of the other gases increase. At the same time, the total flow decreases. All deviations are less than 0.02 vol.-%. This measurement just shows the stability of the mixture created by the MFC. There the analysis of the output gas is shown (see section 11.2).

Partial pressure mixing

For partial pressure mixing the deviation from the requested mixture $\eta_{i,\text{requested}}$ is given by

$$\Delta\eta_i = \eta_{i,\text{requested}} - \eta_{i,\text{measured}} \quad (9.28)$$

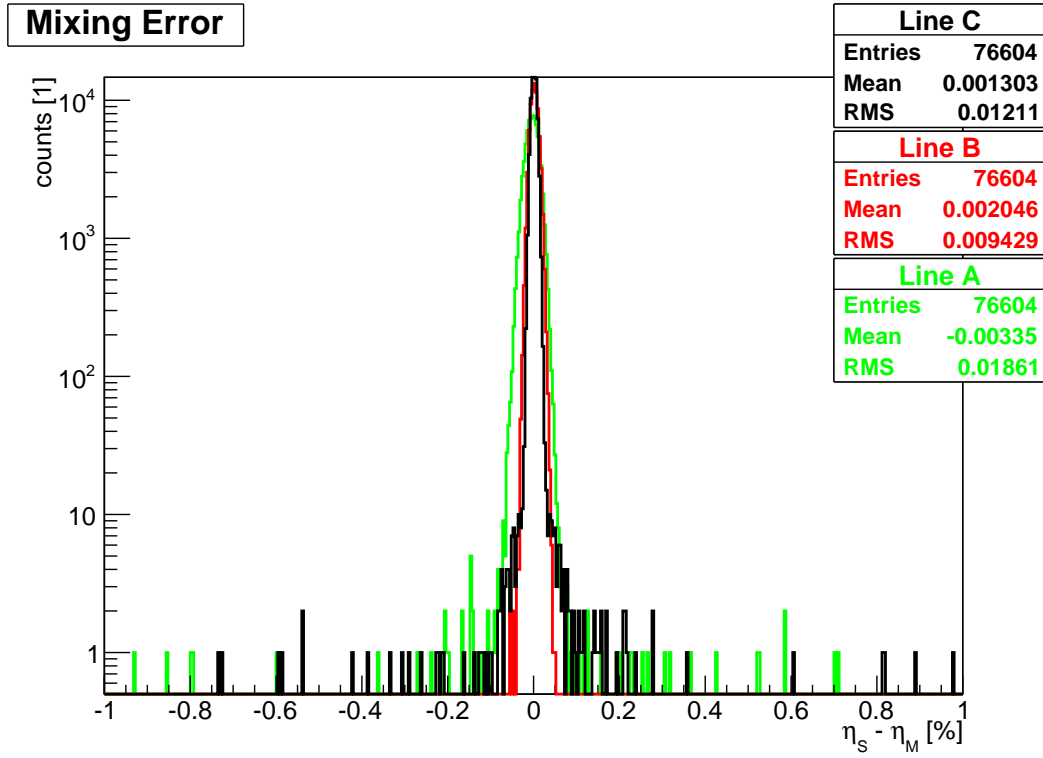


Figure 9.5.: Deviation of each line from the setpoint of a requested T2K-mixture at a total flow of $\dot{V}_{\text{tot}} = 5 \text{ Ln/h}$. For a better comparison, the measured value η_S is subtracted from the setpoint η_M .

where $\eta_{i,\text{measured}}$ is the mixture, which is calculated based on the measured pressure values using the Redlich-Kwong equation (equation 7.51). Before the algorithm has been switched to the Redlich-Kwong equation, the ideal gas law has been used for the calculations. Related to the other measurement campaign most of the tests were done using ternary mixtures with various compositions and gases. Among these tests a few tests were done using binary mixtures. In figure 9.6 the deviation between the requested mixture and the calculated mixture is shown. During the measurement period, the fractions of the gas components have been varied. The lower limit shown is derived by the minimal pressure step of the sensors using the ideal gas law.

$$\Delta\eta_{\text{limit}} = \frac{\Delta p}{p_{\text{max}}} = \frac{1 \text{ mbar}}{3000 \text{ mbar}} = 0.033 \text{ vol.-%} \quad (9.29)$$

The blue line shows the time, when the mixing algorithm was changed from using the ideal gas law to the Redlich-Kwong equation.

The distribution of the maximal absolute deviation is shown in figure 9.7. By taken a closer look at this histogram, there are two peaks inside the histogram. Both seem to be related to the quantisation of the pressure sensor. The vertical line marks the interval, which separates the 68 % of the area of the histogram. Here only the admixtures are taken into account, because the third deviation is also influenced by the deviation of both admixtures. This behaviour is related to the mixing algorithm itself.

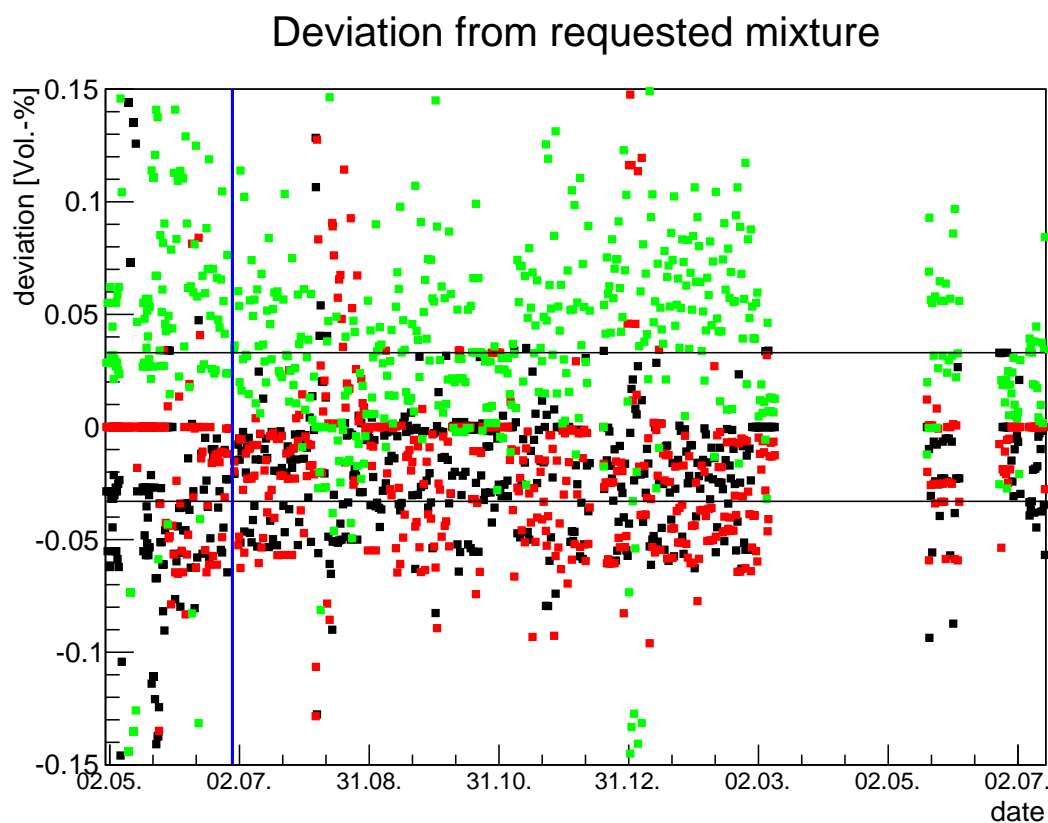


Figure 9.6.: Deviations of each gas line plotted over time. In the first mixing period, the ideal gas law has been used. All other periods are based on the Redlich-Kwong equation. The black lines indicate the deviation, which can be resolved by the pressure sensors. The periods where no points are drawn are periods, where the UGMA has been used in direct flow mode.

Looking at the maximal relative uncertainty of the partial pressure method (shown in figure 9.8), it can be confirmed, that this method has a maximal relative error per gas component of less than

$$\sigma_{\eta_i, \text{rel}} \leq 1.83 \% \quad (9.30)$$

The relative uncertainty was derived looking at the one-sigma (68.3%) interval. Commercial gas supplier only present an upper limit. To compare both values, the three-sigma interval (99.7%) should be taken into account. Hence there is only a probability of 0.3% to get a gas mixture, which has an relative uncertainty of larger than 9.05% in both admixtures. If all components are taken into account, the maximal relative deviation is underestimated.

If heavier gases are mixed it might happen, that the mixture decomposes or is not created homogeneous. This effect has been observed in drift velocity measurements of a mixture containing $i\text{C}_4\text{H}_{10}$ and CF_4 with each 4 vol.-% in Argon. During the measurement, the drift field is cycled. One cycle consists of 11 different driftfields and lasts about four hours. The time, one buffer can supply the experiment with $5 \ell_n/\text{h}$ is about 16 hours. Because the chambers have to be flushed with the new mixture, the first two hours are skipped. Hence the

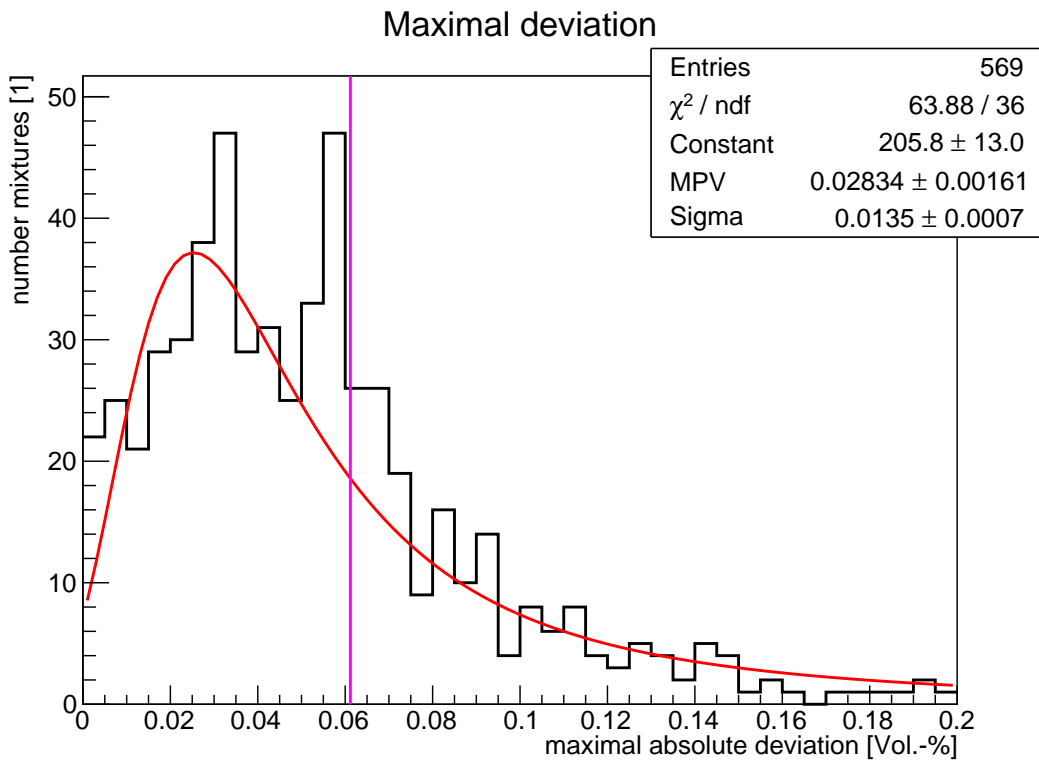


Figure 9.7.: Distribution of the maximal absolute deviation per mixture. To guide the eye, a Landau-distribution was fitted to the data. There is no physical motivation, why the data follow this distribution. The vertical line (magenta) marks the 68 % quantile.

measurement time is about 14 hours. Thus, each driftfield step is measured multiple times. If the gas mixture is stable over time, each cycle should result in comparable results.

The measurement shown in figure 9.9(a), shows a non stable mixture. Here the repetitions of one single driftfield are not compatible with the others. The observed structure is caused by small deviations in the gas mixture. All other possible causes for this deviation have been already excluded.

Small deviations in the gas mixture may be caused by either a decomposition or some layering inside the buffer. Layering may be caused by filling the gas into the buffer from the top. It seems, that the internal flow is too low to stir the mixture.

Hence one possible solution for creating a homogeneous gas mixture is adding external stirring. Each buffer is equipped with one pump which can pump the gas through the buffer. This pump is used to stir the mixture inside the buffer. Due to the internal structure, the mixture can only be pumped, when the buffer loop is not connected to the chamber. Otherwise the solenoid valve, which switches the chamber to the open mode closes the pump inlet. One other restriction is the differential pressure across the pump. Hence the two pressure sensors, which are located at the pump inlet and outlet measure different values. This can result in further uncertainties of the mixing algorithm. Hence the pump is only switched on during the time, when mixing is done and the buffer is not connected to the chamber.

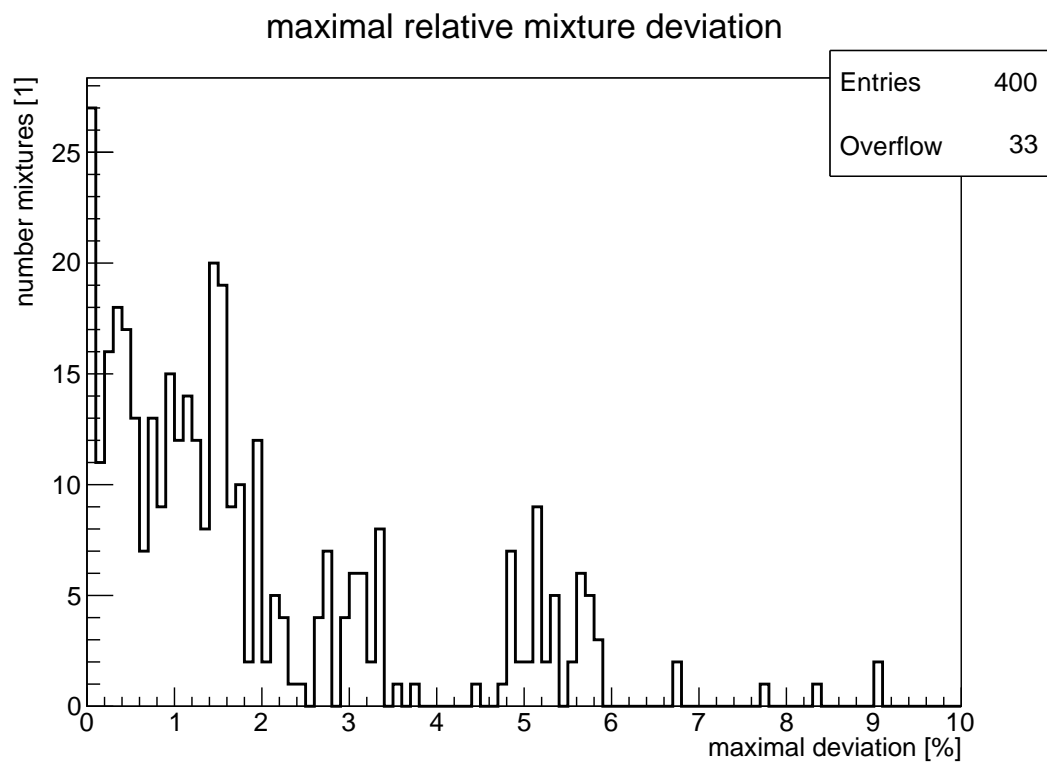


Figure 9.8.: Distribution of the maximal relative deviation per mixture.

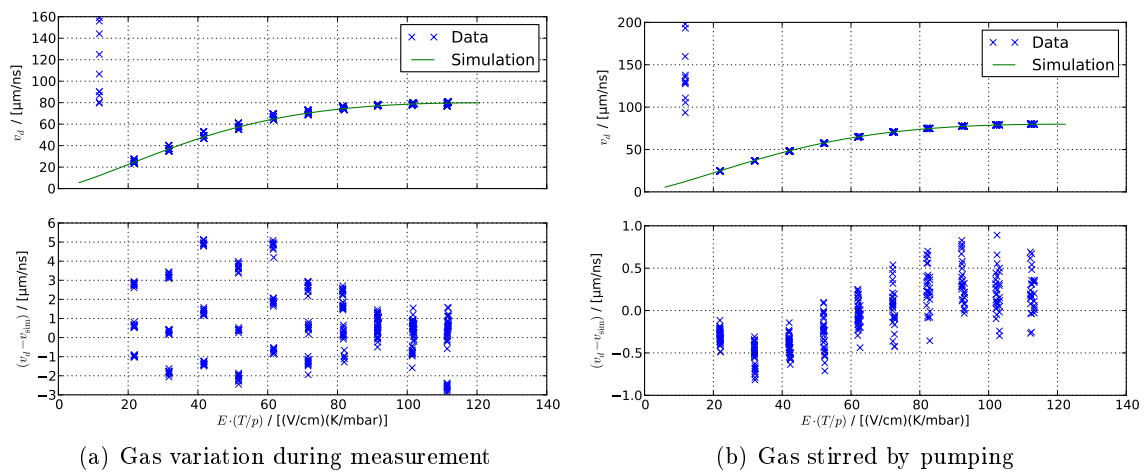


Figure 9.9.: Variation of the gas mixture during one measurement cycle of about 14 h. [26]

The results measured with this modification show an improvement of the stability of the measurement points. As it is shown in figure 9.9(b) the timing of the pumping seems to be sufficient.

9.8. Pressure drop

Pressure drops have to be considered for the proper functioning of the working system. For example, the position of the analysis loop can change the pressure inside the connected chambers. It is important to control this effect and if needed to correct for it.

For a characteristic curve, the pressure drop is plotted versus flow. According to the characteristic curve, which is described in [37] this dependence is quadratic.

9.8.1. Characteristic curve of the analysis loop

Due to the fact, that this loop can be switched at different positions in the whole system, its characteristics are very important. With the knowledge of the pressure drop, it is possible to correct this effect, if it is unwanted.

The analysis loop can sample gas from various positions. Depending on the position relative to the chamber, the internal flow resistance of the piping and valves can increase the pressure inside the connected detector. The pressure inside the detector increases, when the analysis loop is switched between the return output of the chamber and the pressure regulator. This position is called „chamber return“. Hence this is the most interesting pressure drop, the following study was done using this sampling position.

In addition to the pressure drop, the pressure inside the detector depends on the tightness of the chambers itself. If the chambers are not tight enough, a certain fraction of the flow is lost before returning to the UGMA. The reduced flow causes less pressure drop. In figure 9.10 the pressure distribution inside the system is shown for a mixer flow of $5 \ell_n/h$. The pressure distribution has been measured for various flow setpoints. The characteristic curve of the analysis loop can be derived by plotting the mean pressure against the flow value. This curve is shown in 9.11. Each pressure sensor shows the characteristic parabolic behaviour. This can be described by the following function

$$p(\dot{V}) = a \cdot \dot{V}^2 + b \quad \text{with} \quad a = \frac{\Delta p_{\text{nom}}}{\dot{V}_{\text{nom}}^2} \quad (9.31)$$

The parameter a represents the defined pressure drop per given volume flow [37, p.34]. The parameter b was introduced for taking the absolute pressure into account. Although all curves show this parabolic behaviour, they do not cross the same point at a flow $\dot{V} = 0 \ell_n/h$. This can be caused by different pressure offsets, which were not removed completely at the time, this measurement has been performed. The sensors used for this study are placed along the gas flow. The position and the fit result of each sensor is described in table 9.2.

For this measurement the current experimental setup was still connected. Hence the pressure drop for the setup is included in the measurements. Together with the results in table 9.2 it is possible to calculate the pressure drop inside the used parts of the UGMA and correct for it. For example if the analysis loop is placed in the „chamber return“ position, it increases the pressure inside the chamber. If this effect is unwanted, it can be corrected for by using equation 9.31. Due to the fact, that these results depend on the density and viscosity of the

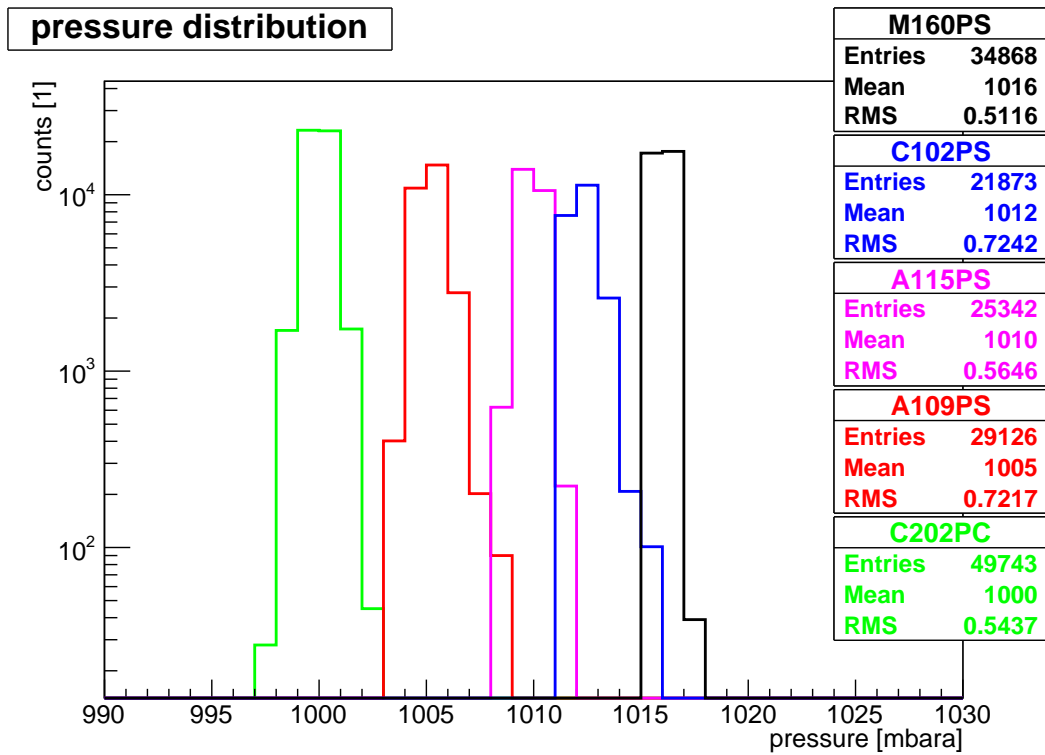


Figure 9.10.: Pressures at a flow of $5 \ell_n/h$ at the output of the mixing block. The analysis loop is connected to the return line of the chambers.

Table 9.2.: Sensors used to determine the characteristic curve of the analysis loop. The gas is flowing from top to bottom.

	sensor position	name	$a[\text{mbara}/(\ell_N/h)^2]$	$b[\text{mbara}]$
1	mixing output	M160PS	0.204 ± 0.022	1009.91 ± 0.97
2	chamber supply pressure	C102PS	0.086 ± 0.018	1007.95 ± 0.77
3	analysis loop oxygen sensor pressure	A115PS	0.110 ± 0.022	1009.02 ± 1.00
4	analysis loop pressure	A109PS	0.083 ± 0.025	1002.99 ± 1.10
5	chamber return pressure	C202PC	-	-

gas, it is recommended to repeat these measurements for the used mixture if a correction is needed. The presented measurement has been done using a mixture of Ar- CF_4 - $i\text{C}_4\text{H}_{10}$ 95:3:2.

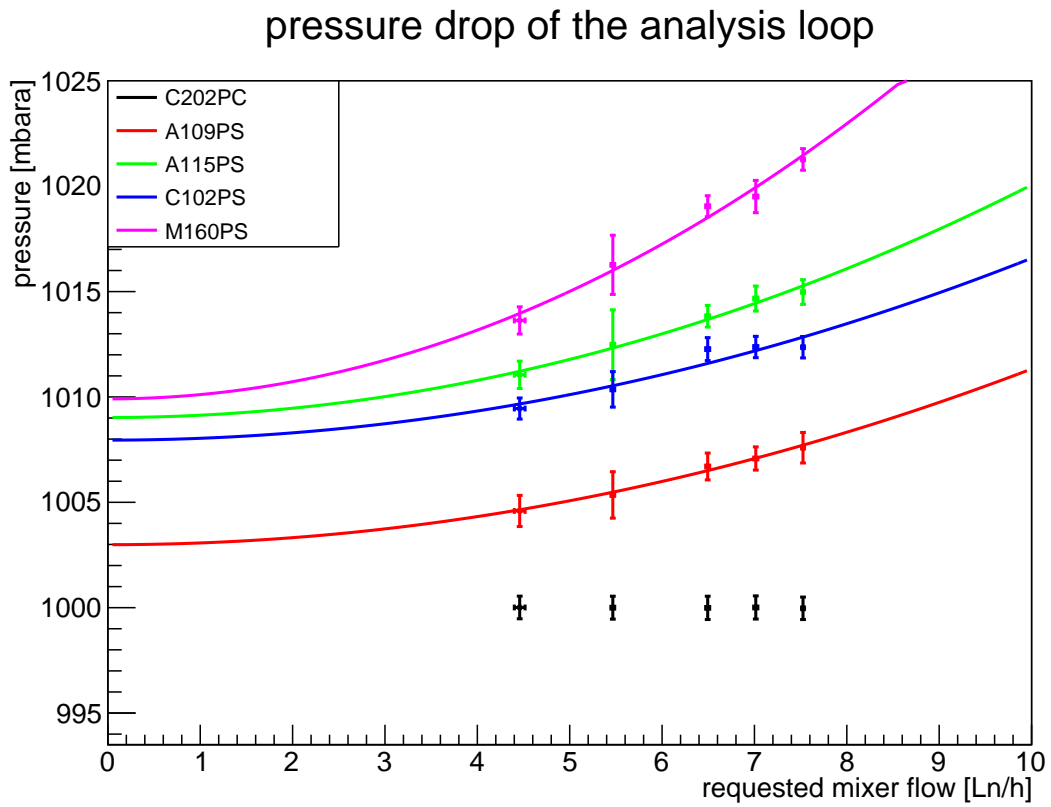


Figure 9.11.: Characteristic curve of the analysis loop while operating in the chamber return mode. The curve fitted is described in equation 9.31. The locations of the sensors are listed in table 9.2

10. Systematic studies

10.1. Sensors

The function of the UGMA depends on the measurements of several sensors. To estimate the effect of uncertainties introduced by the sensors, as a first step they need to be determined. Hence, some special data analyses have been done.

10.1.1. Temperature sensors

Once the temperature sensor is mounted, only the statistical error can be determined. Because even in an air conditioned room a temperature gradient between all temperature sensors occurs, no systematic study can be done, when they are in place. Hence, all sensors must be removed from their positions and placed all together in a liquid bath with a well defined stable temperature. Due to the mounting positions, they cannot be removed easily. If they are broken, it is hard but possible to replace them. Hence the effort for dismounting them for calibration is not feasible. Thus it has been decided to believe in the characteristics of a PT100 [94] and the calculations of the XTR101 [90].

Nevertheless studies were done to estimate the statistical error on the temperature measurement itself. This study was done by looking at the difference of two successive measurements. This reduces the influence of changes in room temperature, which are at the order of 5°C within one day. Because the measurement rate of the temperature sensors is about 0.5 Hz the influence of external temperature changes can be neglected.

$$\Delta T = T_n - T_{n-1} \quad (10.1)$$

Both temperature measurements are effected by the statistical error σ_T . By plotting the difference, the width of the resulting distribution (RMS) is the combined error.

$$\text{RMS} = \sqrt{2}\sigma_T \Rightarrow \sigma_T = \frac{\text{RMS}}{\sqrt{2}} \quad (10.2)$$

By doing the study on the temperature differences, it is only possible to determine the precision of the sensor. The accuracy needs to be checked in further studies. For the purpose the temperature sensors are used inside the UGMA, it is sufficient to believe the characteristics and calculations [37].

One example for the distribution of the temperature differences is shown in figure 10.1. Since the data logged to the database is compressed, less points are having a difference equal to zero. These points are suppressed by the data compression algorithm. This effect can also be observed in the histogram. Further, the statistical error suffers from the resolution of the

analogue input. The presented values represent the statistical error after all digitisation and conversion steps.

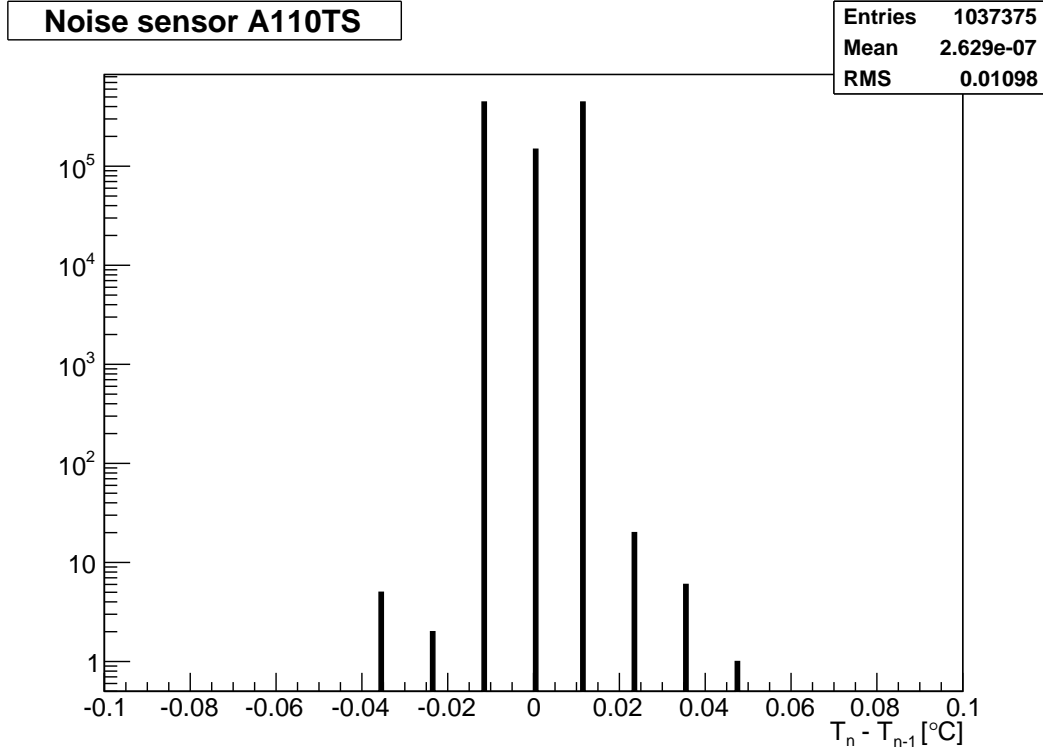


Figure 10.1.: Estimation of the statistical error of the temperature sensor A110TS located inside the analysis loop.

Due to different temperature ranges, and hence different resolution, the statistical error varies, too. This is shown in table 10.1.

Table 10.1.: Statistical error of temperature sensors

sensor		temperature range	statistical error
analysis loop	A110TS	0.87 – 47.47 °C	8 mK
chamber supply	C103TS	-0.19 – 46.41 °C	8 mK
chamber return	C203TS	0.42 – 47.03 °C	8 mK
purifier 1 inner	P107TS	0.73 – 268.25 °C	41 mK
purifier 2 inner	P207TS	0.57 – 268.58 °C	42 mK
purifier 3 inner	P307TS	0.85 – 268.91 °C	42 mK
purifier 4 inner	P407TS	0.58 – 268.64 °C	41 mK

The expected statistical error for the temperature sensors should be less than

$$\sigma_T \leq \sigma_{T,\text{limit}} = \frac{T_{\text{high}} - T_{\text{low}}}{N_{\text{ADC}}} \quad (10.3)$$

where T_{high} and T_{low} are the upper and lower boundary of the temperature range and N_{ADC} is the number of usable ADC-bins. For a conservative approximation N_{ADC} can be set to 4000. For the purifier temperature sensors we get an upper limit of $\sigma_{T,\text{limit}} \approx 68$ mK and for the other sensors $\sigma_{T,\text{limit}} \approx 12$ mK.

10.1.2. Pressure sensors

Like in the case of the temperature sensors a similar measurement has been performed. The calibration for all sensors was taken from the calibration measurement of the manufacturer, which is attached to each sensor. Again the statistical error is determined. At the same

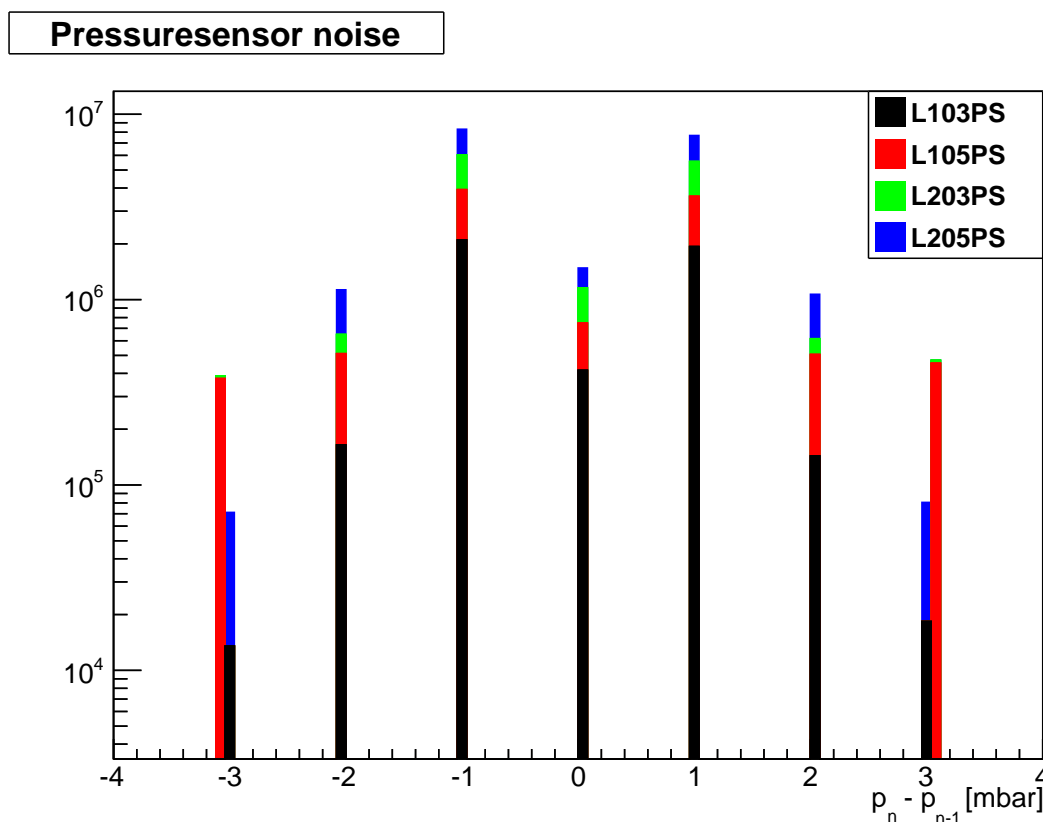


Figure 10.2.: Determination of the statistical error for the four pressure sensors mounted inside the buffer loops.

time a rough estimation of the pressure difference per bit was done by dividing the maximal pressure of 4000 mbar by the maximal value of the ADC (4096). According to [37] processing the offset of 4 mA reduces the resolution by a few bits. Hence this results in a limit for the resolution of about 1 mbar/bit. This fits quite well to the plotted result, which can be seen in figure 10.2.

The measurements were done during operation and so special times were selected. Hence the distribution gets a bit broadened due to fluctuating pressures. This must be taken into account, when estimating the statistical uncertainty of the pressure sensors.

The result for the pressure sensors is shown in table 10.2. The pressure range for all shown sensors is 0 – 4 bara.

Table 10.2.: Statistical error of pressure sensors

sensor		statistical error
loop 1 before pump	L105PS	0.73 mbar
loop 1 behind pump	L103PS	0.71 mbar
loop 2 before pump	L205PS	0.76 mbar
loop 2 behind pump	L203PS	0.77 mbar

10.2. Purifier

10.2.1. Heater

For the purifier section mainly the temperature regulation was tested. The components involved in the heater are shown in figure 10.3. The heater is embedded in the isolation, as well as the temperature sensor. For clarity only one heating loop is shown. The real heater consists of one heater for the mantle and one for each cap. All heating modules are connected internally to one supply cable. Together the heating power is 500 W. The embedded temperature sensor is also a PT100, which is readout by the normal readout chain. The regulation has to be reliable to avoid damage of the purification material due

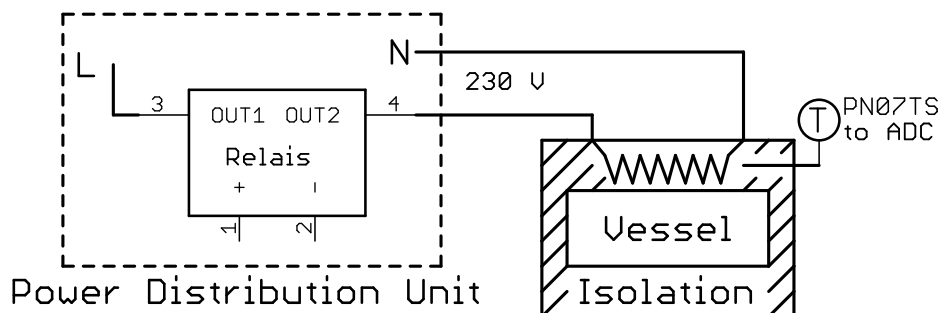


Figure 10.3.: Schematic view of the purifier heater. Only the tested components are drawn.

to overheating. At high temperatures, which are normally used for the gas regeneration, the precision of the regulation can be ignored, but it must be ensured, that no overheating happens. Overheat measured at the outside temperature sensor can be ignored if they are short enough to have no influence on the inner volume.

At lower temperatures, which are close to ambient temperature, a good stability is required, because the absorption performance strongly depends on the temperature of the material. To allow regulation, the temperature of the purifier is normally set to 30 °C. This is well above the ambient temperature and useful to allow a stable regulation.

Though the purifiers are filled with copper or zeolite, the internal temperature rises much slower than the temperature of the heater, which is used for regulation. Hence for achieving

the adjusted temperature inside it takes some time. A small temperature gradient prevents the system from mechanical stress. Looking at figure 10.4 it can be observed, that the

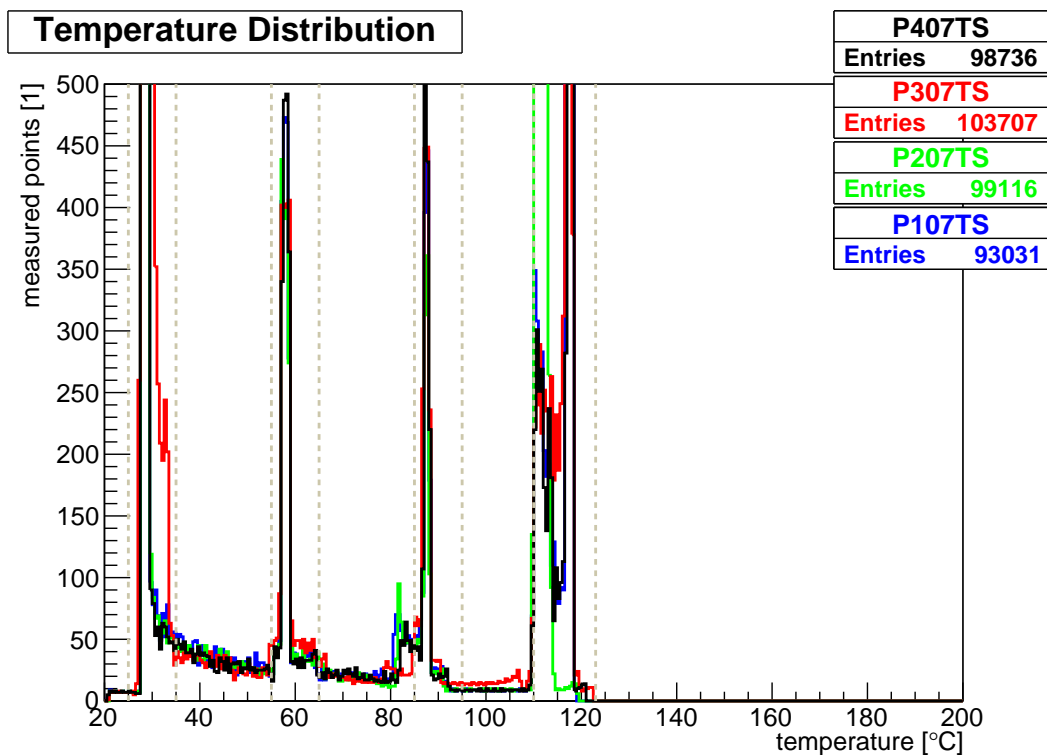


Figure 10.4.: Temperature distribution for different setpoints (30, 60, 100, 120°C). For guiding the eye dotted lines are plotted at $\pm 3^\circ\text{C}$ respectively $-5, +3^\circ\text{C}$.

regulation works at 30°C within $\pm 3^\circ\text{C}$ whereas the regulation range broadens up to -10°C and $+3^\circ\text{C}$ for higher temperatures with a strong tendency to lower temperatures. This behaviour is volitional and prevents damage to the inner material.

10.2.2. Regeneration

Regeneration of the H_2O -purifier has been performed by evacuating the vessel. This method is also called pressure swing regeneration. Due to the lower gas pressure, the equilibrium between the water attached to the zeolite and the gas gets disturbed. Hence there is less water in the residual gas, the water diffuses into the vacuum and a pressure increase can be observed, if the vacuum pump is disconnected. This procedure is done several times until the pressure increase stays below a certain acceptable value. The process can be speeded up by increasing the temperature. After the regeneration is done, the vessel is pressurised with dry Argon and sealed. After cooling down, a small overpressure stays to protect the purifier from water diffusing from the outside.

10.3. Buffer

For operation of the UGMA using the buffer, many parameters have been determined at a very early development phase. These values have been re-checked during commissioning.

10.3.1. Volume

It is mandatory to know the volume of the buffer and the pipes connected. Determination of the volume must be done by using gases, because contamination with water must be avoided. For this method, the ideal gas law is used

$$p_0 V_{\text{buffer}} = p_{\text{buffer}} V_0 \quad (10.4)$$

where $V_0 \approx 50 \ell$ is the volume of the buffer and $p_0 = 1013 \text{ mbar}$ is the ambient pressure. V_{buffer} is the volume of the gas at ambient pressure, which is stored inside the buffer at buffer pressure p_{buffer} . If this equation is differentiated with respect to time t .

$$p_0 \frac{dV_{\text{buffer}}}{dt} = \frac{dp_{\text{buffer}}}{dt} V_0 \quad (10.5)$$

This can also be written as

$$p_0 \dot{V}_{\text{buffer}} = \dot{p}_{\text{buffer}} V_0 \quad (10.6)$$

With this equation the V_0 can be calculated

$$V_0 = \frac{p_0 \dot{V}_{\text{buffer}}}{\dot{p}_{\text{buffer}}} \quad (10.7)$$

The flow taken from the buffer \dot{V}_{buffer} is measured by the chamber supply MFC C101FC while the slope of the pressure \dot{p}_{buffer} is given by a linear fit on the data of each pressure sensor. Because the buffer is equipped with two pressure sensors, the measurement was done for both sensors. The distribution of the measurements can be seen in figure 10.5.

The statistical error of each measurement is given by Gaussian error propagation.

$$\sigma_{V_0} = \sqrt{\left(\frac{p_0 \dot{V}_{\text{buffer}}}{\dot{p}_{\text{buffer}}^2} \sigma_{\dot{p}_{\text{buffer}}} \right)^2 + \left(\frac{p_0}{\dot{p}_{\text{buffer}}} \sigma_{\dot{V}_{\text{buffer}}} \right)^2} \quad (10.8)$$

The error for $\sigma_{\dot{V}_{\text{buffer}}}$ is gained from the distribution of the flow and $\sigma_{\dot{p}_{\text{buffer}}}$ is the error gained from the fit. The measurement was repeated for some fills and at the end, all results for one sensor were combined using a weighted mean. The results of this method are shown below.

Buffer 1

$$V_{L103PS} = 43.995 \pm 0.002 \ell \quad (10.9)$$

$$V_{L105PS} = 43.891 \pm 0.002 \ell \quad (10.10)$$

Buffer 2

$$V_{L203PS} = 43.369 \pm 0.002 \ell \quad (10.11)$$

$$V_{L205PS} = 43.364 \pm 0.002 \ell \quad (10.12)$$

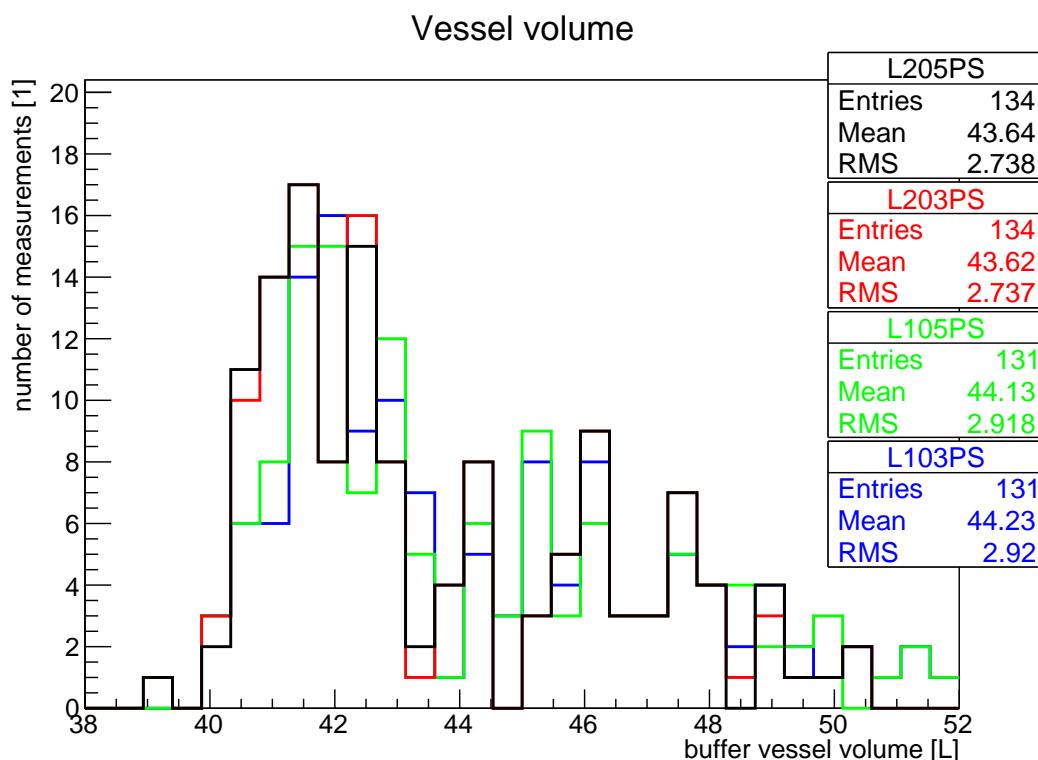


Figure 10.5.: Measurements of the buffer vessel volume.

It seems, that the statistical error derived from the weighted mean underestimate the statistical fluctuations seen in figure 10.5. Also the values for the mean are not consistent within the calculated error.

According to the producer company the volume of the buffer has a design value of $V_{\text{Buffer}} = 48 \ell$ [49]. Compared with this value a large systematic deviation of about 5ℓ can be observed. So if the volume of the vessel is needed for calculations, the design value should be used unless a more accurate measurement is done.

Caused by the additional volume from the piping and pump, the measured buffer volume should be slightly larger than the design value. But the other behaviour has been observed. One explanation for this difference might be, that these measurements have been done during normal measurement time, when the UGMA is operated with various mixtures. Hence, there is a systematic error on the flow measured by the MFC, which dominates the measurements. During these measurements various mixtures have been fed to the chamber. This causes the used MFC to use a conversion constant, which increases the uncertainty of the flow.

At the end, it turned out, that this method seems to be quite precise, but not very accurate. This might be related to the uncertainty of the measured flow and pressure. If the measurements are going to be repeated the pressure sensors should be recalibrated and the measurement should be repeated using pure Ar, because this is the gas the MFC is calibrated for.

10.3.2. Evacuation-time

Before filling the buffer with a new mixture, it can be evacuated. To measure the speed of evacuation, the buffer has been evacuated from ambient pressure to minimal pressure (shown in figure 10.6). During this time, the pressure has been measured by the special vacuum sensor V101PS and both pressure sensors mounted at the buffer. The drop in

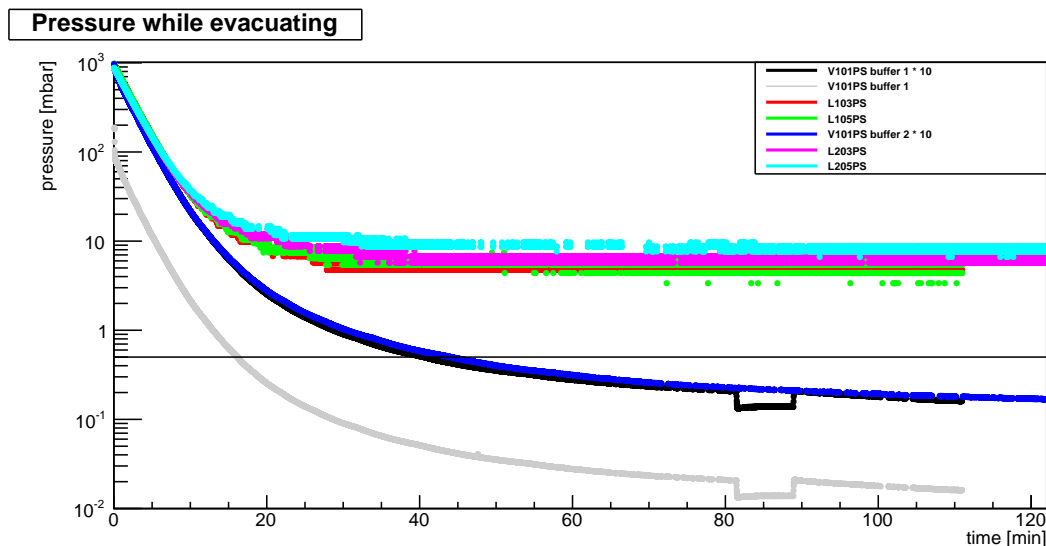


Figure 10.6.: Evacuation of the buffer vessels

V101PS during evacuation of buffer 1 is caused by a malfunction of the control software. The valve between the vacuum line and the vessel was closed during this time.

To match the special vacuum sensor and all other pressure sensors in the region between 1000 mbar and 100 mbar it is necessary to multiply the value of the vacuum sensor by a factor of ten. The reason for this extra factor is not yet understood. In figure 10.6 it is observable, that the normal pressure sensors (L103PS - L205PS) saturate at about 10 mbar. At this value the sensor reaches its lower endpoint, which is labelled by the manufacturer as 0 bara.

To evacuate the vessel to the requested pressure of 0.5 mbara takes about 40 min. This value is larger than the value assumed in [37]. But the throughput is reduced due to the piping and valves, hence only a small fraction of the pump capacity can be used.

10.3.3. Maximal blow-off rate

The blow-off rate, which is the maximal flow rate into the exhaust, has been already determined in [37]. The calculations are based on the assumption, that before and after the valve no piping exists. This cannot be realised. The blow-off rate has been measured by pressurising the vessel up to 3840.32 mbara Argon. The exhaust valve has been opened and the pressure has been recorded as function of time. During the measurement, the circulation pump was switched off and the proportional valve was closed. This measurement is shown

in figure 10.7. This measurement has shown, that a maximum flow of $\dot{V}_{\max} = 6.37 \text{ m}^3/\text{h}$ can

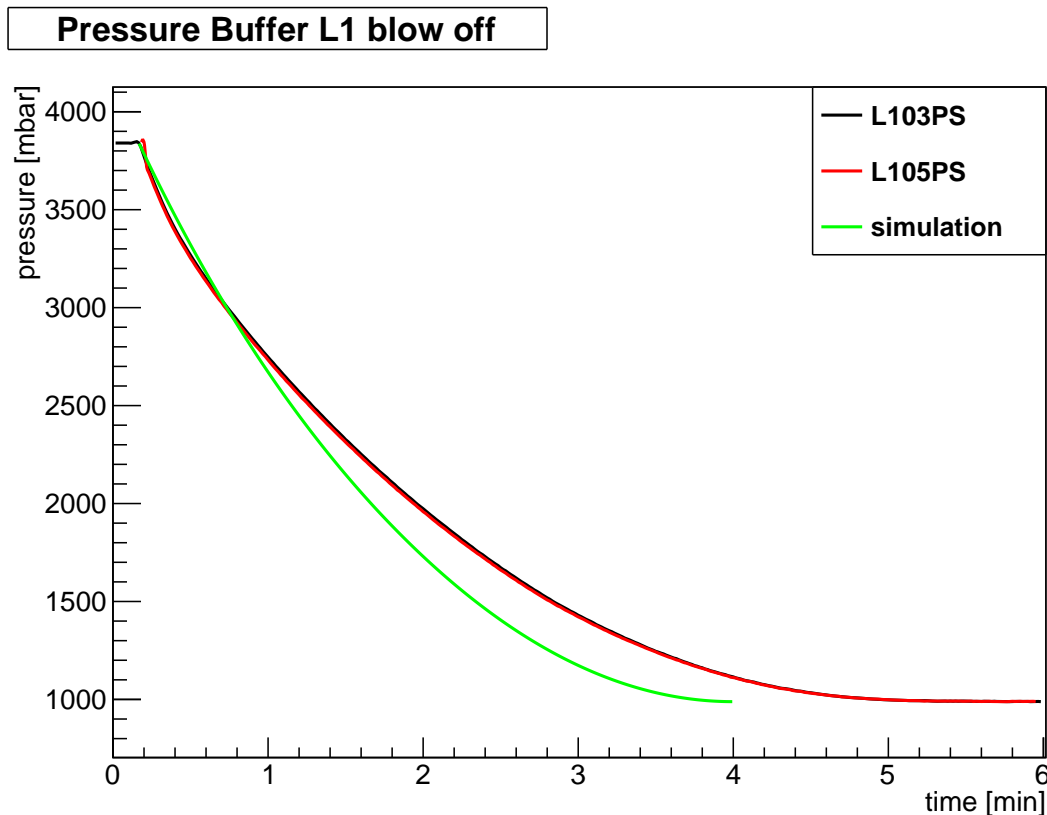


Figure 10.7.: Blow-off of an Argon filled buffer vessel with $p_0 = 3840.32 \text{ mbar}$

be achieved. The time to blow off the complete buffer lasts about six minutes. This value depends on the filled mixture and ambient pressure. Different mixtures result in different densities and viscosities, which influence the flow resistance of the valves and pipes.

10.3.4. Maximum filling rate

Along with the blow-off rate, the filling rate is important for operation. This rate describes the minimal time, which is needed to fill the buffer. The maximum filling rate has been measured in the pressure range from vacuum to maximum line pressure. The pressure history of one measurement is shown in figure 10.8.

This measurement has been done using pure Argon. It is important, that the measurement is done using gases, which do not condensate when they flow into the buffer. Condensation can distort the measurements and result into a danger, which can not be neglected. Possible danger can result from a higher amount of flammable gas inside the buffer. If the buffer gets filled with liquid gas, the pressure rises after closing the inlet. Hence, the pressure might rise above the maximal pressure, which is set by the pressure-relief-valve and gets blown-off to the environment. Here it gets diluted with oxygen and a possible flammable gas mixture can be created.

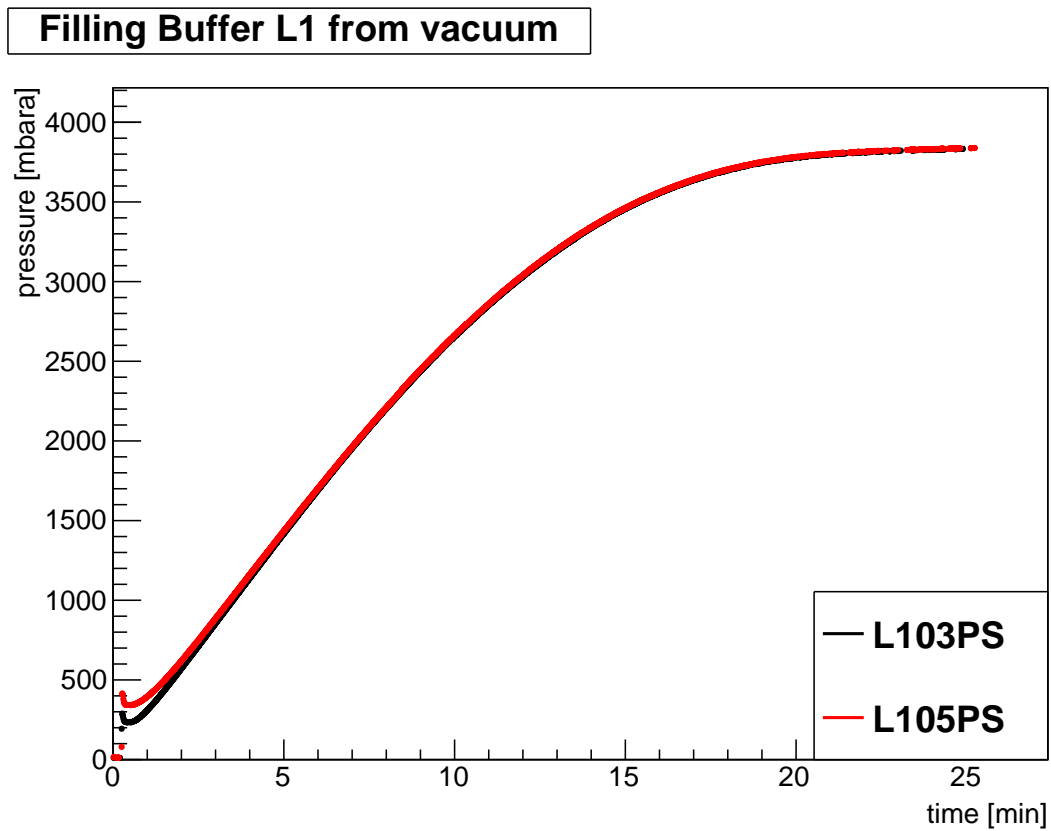


Figure 10.8.: Filling the buffer with Argon starting from vacuum.

11. Drift velocity

The quality of the mixture can also be determined using physical parameters. Due to the fact, that the drift velocity can be simulated and measured with a adequate precision, the drift velocity is a good indicator for the quality of the gas. The comparison between simulation and measurement even allows determination of the mixture composition (see section 11.2).

To ensure proper gas quality the contaminations of the gas are continuously measured by dedicated sensors. As a further reference a bottle with premixed gas is used. To ensure the same conditions for the gas in the chambers, when gas from the premixed bottles is used, the chamber return flow is sent through the UGMA for using the pressure regulation and contamination monitoring.

During all measurements no oxygen contamination was measurable. The water contamination was always below 5 ppmv and decreasing until it stabilises at about 2 ppmv. The continuous reduction of the water contamination is related to the system getting more and more dry. The Gas Monitoring Chamber (GMC) are covered on their inside with Kapton¹. Kapton is a hygroscopic material. If the flow is switched on, the water diffuses into the gas and the water content of the gas falls slowly. Furthermore the connections from the UGMA to the GMC are made from copper. Copper also absorbs water at the inside surface. This water is also released over a long time. If the system is tight, no water is introduced and the water content of the gas falls down to a minimum.

11.1. Systematic studies

During final commissioning of the partial pressure method, several systematic studies with different gas mixtures have been performed. During this phase, the gas is characterised by the drift velocity. These studies have been done using ternary mixtures, but for completeness, also their binary parts have been measured. [26] One example for a binary measurement is shown in figure 11.1.

The working point is defined as the maximum of the drift velocity. At this point, the dependence from small variations in $E^* = ET/p$ is minimal. From the data the maximum is derived by fitting a function, which describes the shape of the curves. This function is defined as [26]

$$f(E^*) = (a + bE^*) \exp(-dE^*) + c \quad (11.1)$$

The maximum can be derived by analytical transformations. For visualisation the width of the maximum, which can be defined as the range of E^* , where $v_{d,\max} - v_d < 1\% v_{d,\max}$ is shown. In the following plots, the horizontal bars visualise the width of the maximum.

¹Brand name of DuPont, also known as Polyimid

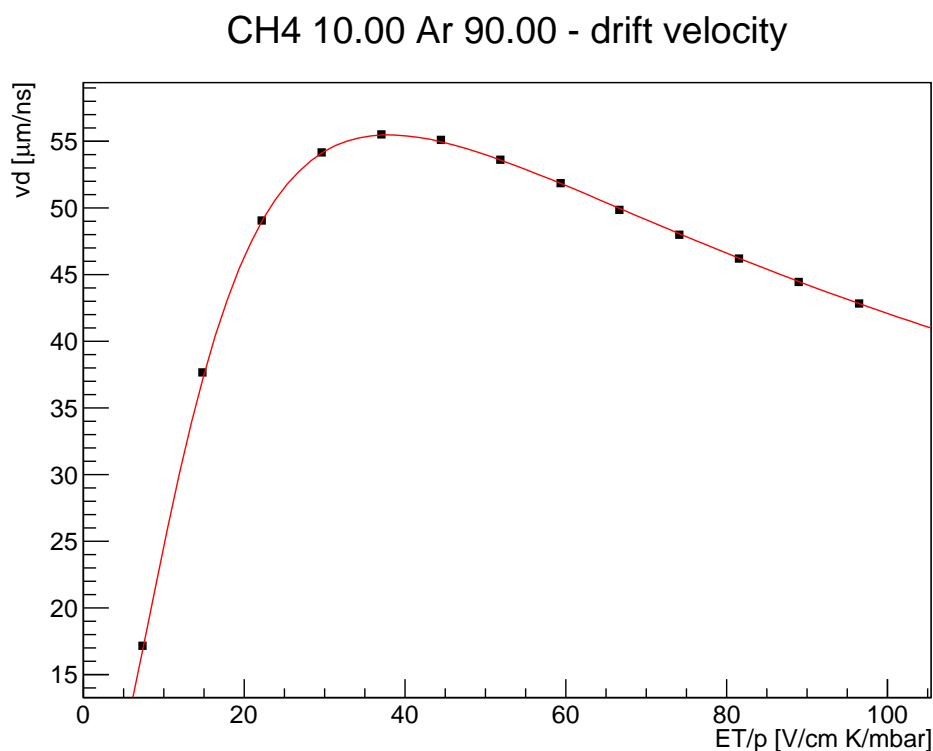


Figure 11.1.: Example of one v_d curve measurement. The error bars of each point are hidden by the marker. In red the matching simulation is shown.

Due to limitations of the experimental setup, it is possible to do measurements of v_d with a maximal reduced field of 110 V/cm K/mbar. With these datasets, it is possible to determine the maximum up to 100 V/cm K/mbar

Some of the studies presented below are part of the work of Lukas Koch [26]. Some were measured later using the same analysis framework. All measurements and simulations are available online at <http://web.physik.rwth-aachen.de/gasDB/>. In the following spider-plots, the vertices of the grid mark the simulated points. All measurements are marked by coloured points.

Additional to the purpose of these studies to have a systematic overview of the behaviour of v_d depending on the gas mixture, the following studies give a nice opportunity to check the performance of the UGMA over a wide range of mixtures.

The data in the following plots has been measured using the ND280 GMC. Although the values match quite well to the simulation, there is still some tension visible. This tension is dependent on the used gas mixture. In [26] only the systematics of the chamber and the readout are handled. Systematic effects which might be caused by the gas have not been estimated up to now. The comparison of the data measured with the ND280 GMC and the L3 VDC has shown, that there is a systematic difference of about 4% observable. This might be caused by the different response of the chamber's readout electronics to the longitudinal diffusion.

The following measurements show the flexibility and the possibilities of the UGMA. In the „spider-plots“ the intersections of the solid lines were determined from simulated data. The coloured marks show measured data. For the simulated data only the position of the working point is shown.

11.1.1. Argon-Methane-Carbondioxide

The classical drift gases, which have been used in the past, are mixtures containing Ar and CH₄. Despite the risk of flammability the success of these mixtures continues in many gas based detectors.

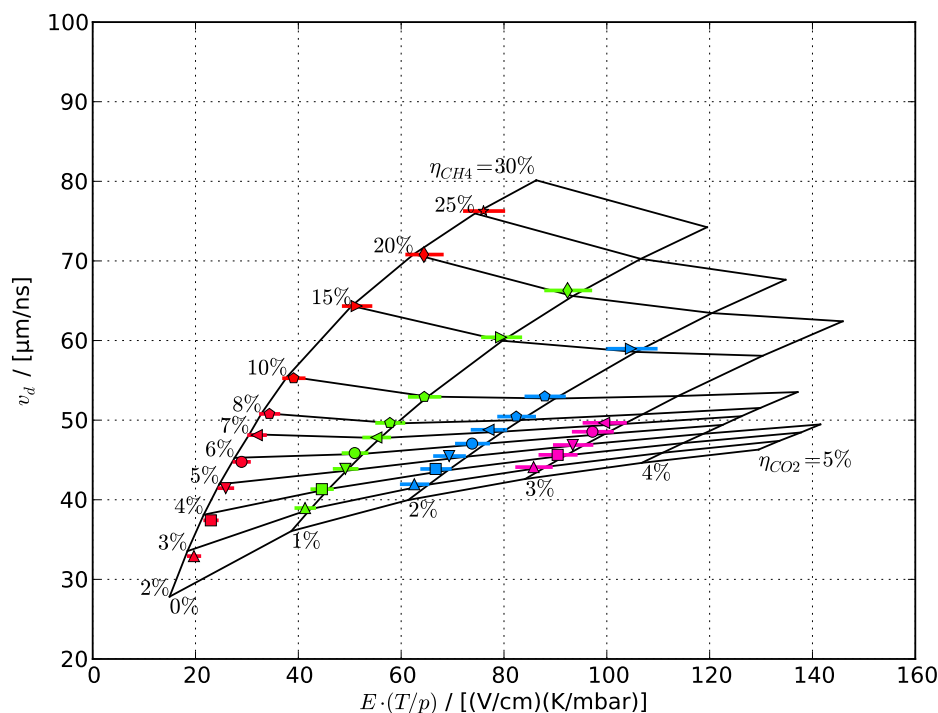


Figure 11.2.: Working points in mixtures containing Ar, CH₄ and CO₂. Plot taken from [26].

The proposed gas for the TPC at the ILD is a mixture consisting of 93 vol.-% Ar, 5 vol.-% CH₄ and 2 vol.-% CO₂. To determine the effect of variations of the gas mixture on the drift velocity a grid around this mixture has been measured.

The results of Ar-CH₄ mixtures and Ar-CH₄-CO₂ are shown in figure 11.2. Measurements with pure Ar-CO₂ have been made in addition, but they have no maximum within the field-range of the GMC. Hence, they do not appear in the plot.

11.1.2. Argon-Methane-Isobutane

Methane is a well known and often used quencher gas. Although its usage is these days disfavoured, due to its flammability. By adding iC₄H₁₀ to the Ar CH₄ mixture, the drift

velocity is pulled to a kind of plateau of about $55 \mu\text{m}/\text{ns}$. If the drift velocity of the pure Ar- CH_4 mixture is above this value, it is lowered by adding iC_4H_{10} to the value of this plateau. If the drift velocity is below this value, it is increased by adding more iC_4H_{10} . Both effects can be seen in figure 11.3.

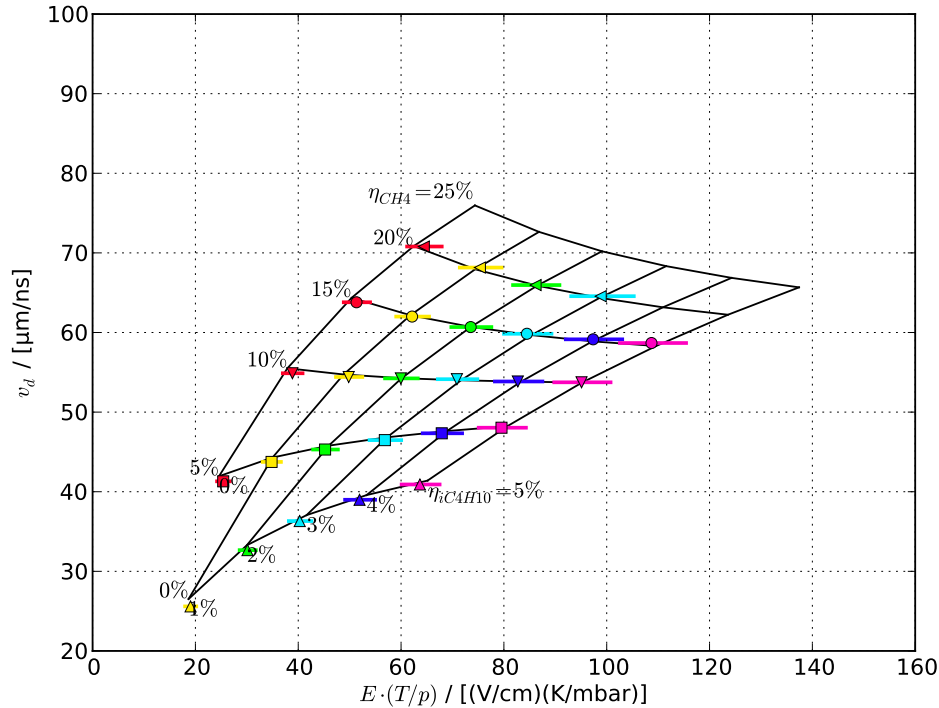


Figure 11.3.: Working points in mixtures containing Ar, CH_4 and iC_4H_{10} .

11.1.3. Argon-Methane-Hydrogen

Adding a small amount of H_2 to Ar- CH_4 mixtures flattens the maximum. This effect can be seen in figure 11.4. Some of the mixtures, which do not have a defined maximum below $E^* = 100 \text{ V/cmK/mbar}$ have an observable plateau. This effect makes these mixtures interesting for applications with very inhomogeneous fields. If the fraction of H_2 is tuned the plateau is stable up to 1400 V/cm K/mbar . [26, p. 40] For security reasons, a premixed gas of Ar 90 vol.-% and H_2 10 vol.-% was used. For this mixture, the gas distributor guarantees a mix within the relative accuracy of 10 % [82]. Hence this uncertainty dominates for mixtures with more than one percent hydrogen.

11.1.4. Argon-Isobutane-Tetrafluoromethane

The mixture containing 95 vol.-% Ar, 3 vol.-% CF_4 and 2 vol.-% iC_4H_{10} is also known as T2K-gas, because it is used at the TPC located at the ND280 detector of the T2K-experiment. Measurements of variations of T2K-gas are shown in figure 11.5. Due to the production

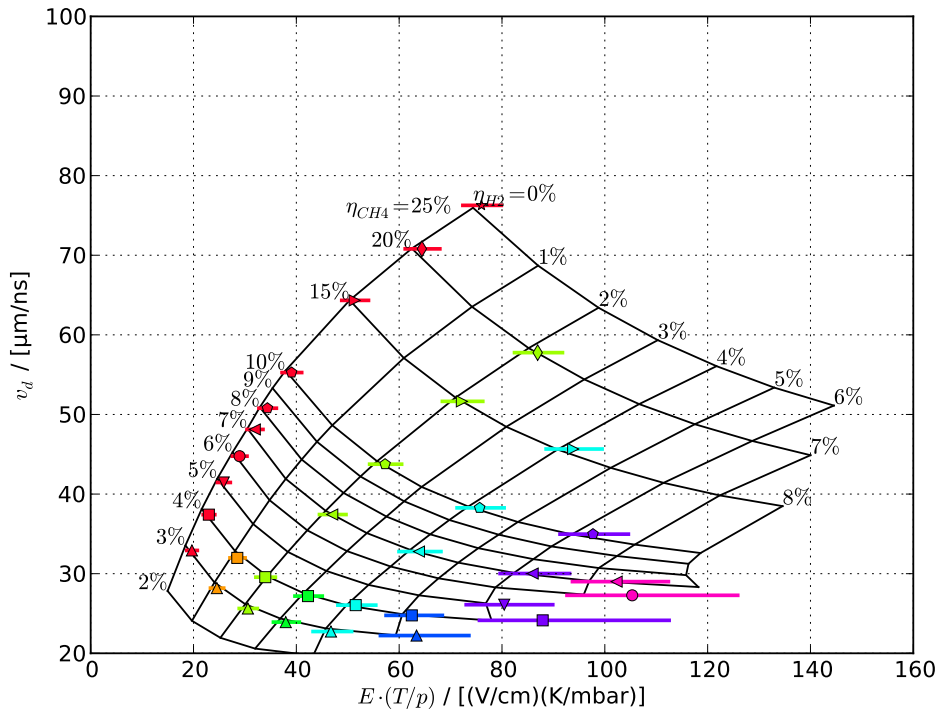


Figure 11.4.: Working points in mixtures containing Ar, CH₄ and H₂. Plot taken from [26].

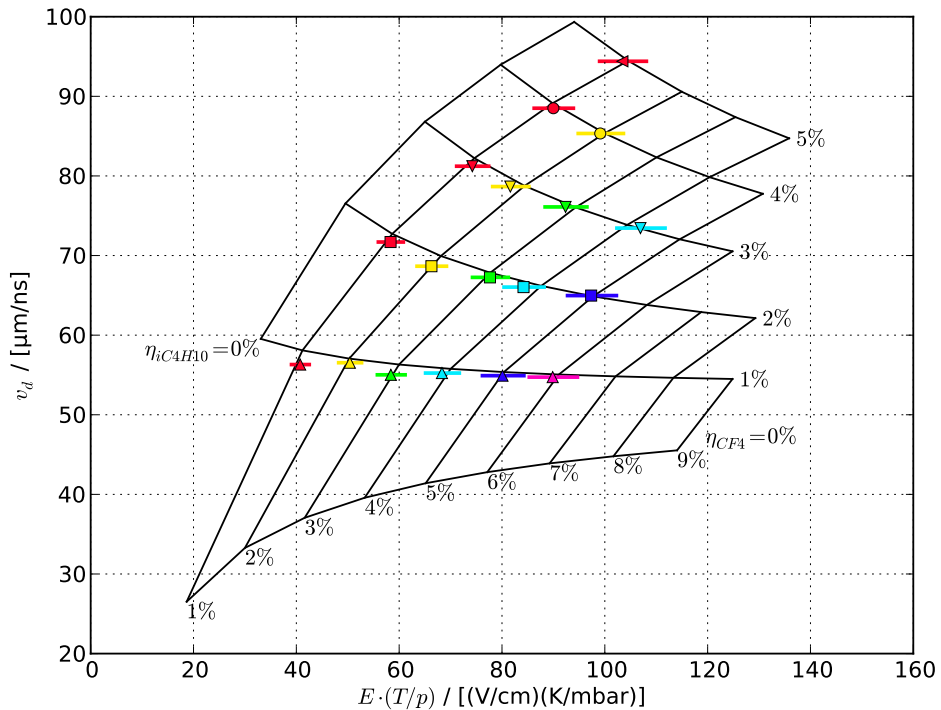


Figure 11.5.: Working points in mixtures containing Ar, CF₄ and iC₄H₁₀. Plot taken from [26].

method of iC_4H_{10} it is difficult to reach high purities. Hence, some other gases may remain. One of the highest contaminations in iC_4H_{10} gas beside C_4H_{10} results from C_3H_8 .

11.1.5. Argon-Propane-Tetrafluoromethane

These mixtures are the same as shown in figure 11.5 with iC_4H_{10} replaced by C_3H_8 . Propane (C_3H_8) is the next smaller alkane starting from butane. Hence we expect a similar effect on the drift velocity. Measurements done with this mixture are shown in figure 11.6.

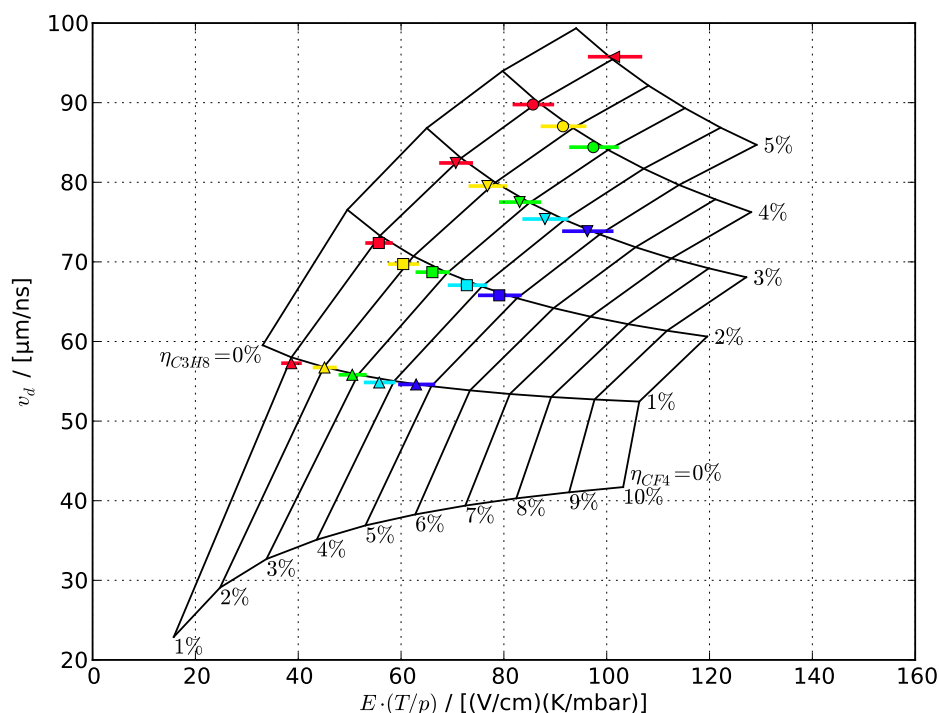


Figure 11.6.: Working points in mixtures containing Ar, C_3H_8 and CF_4 .

11.1.6. Conclusion

The measured working-points and the simulated ones agree quite well. If the maximum is very broad, the algorithm cannot determine the exact positions and thus, differences appear. This effect can be observed in figure 11.4. The observable mismatch between the simulation and measurement can be caused by:

- uncertainties of the mixture. The quality of the mixture is evaluated in 11.2.
- contamination of the pure gases. The quality of the base gas Ar is 5.0 (= 99.999 %). The admixtures have a purity of at least 3.5 (= 99.95 %) except propane which has only 2.5 (= 99.5 %). Assuming 10 % of admixture, e.g. CH_4 results in a possible contamination of 50 ppm. This concentration is below our current detection limit of the build in GC.

- contaminations with oxygen and/or water. With the internal sensors it has been ensured, that these contaminations are below 2 ppm.
- systematic effect caused by longitudinal diffusion.

11.2. Fitting of the mixture

The GMC can be used to determine the gas composition under study, by comparing the drift velocity measurements with an appropriate simulation. In the following mixtures ± 1 vol.-% around the setpoint are simulated with a step size of 0.01 vol.-%. One example for the simulation spread are shown in figure 11.7.

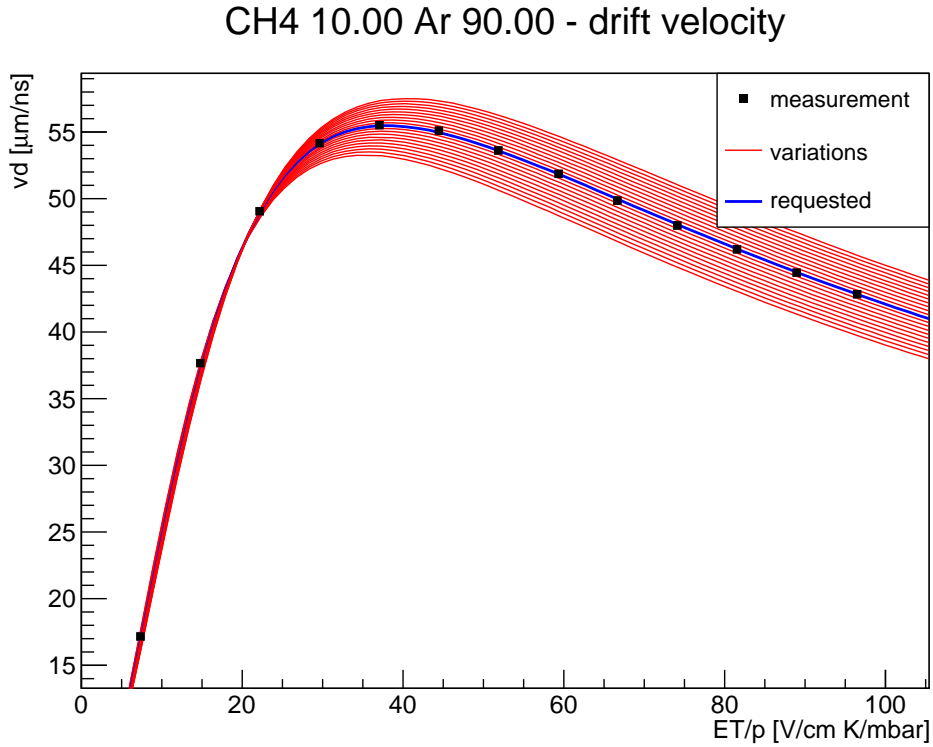


Figure 11.7.: Drift velocity measurement and simulation steps. In blue the requested simulation is shown. The variations are shown in red. For clarity only every tenth simulation is drawn.

This analysis method uses the χ^2 -test to determine the fraction of the gases inside the mixture. Here χ^2 is defined as

$$\chi^2 = \sum_n \frac{(v_{d,\text{meas}}(E_n) - v_{d,\text{sim}}(E_n))^2}{\sigma_{v_d,\text{meas}}^2(E_n) + (v'_d(E_n) \sigma_{ET/p,\text{meas}}(E_n))^2} \quad (11.2)$$

where $\sigma_{ET/p,\text{meas}}$ and $\sigma_{v_d,\text{meas}}$ are the statistical error gained from the fluctuations of measurements. The statistical error of ET/p is taken into account by transformation using the slope v'_d of the simulated data. The best match mixture is at the lowest χ^2 value (see figure 11.8). The statistical errors are calculated by a linear interpolation between the point of the minimal χ^2 and the point, which is larger than $\chi^2_{\text{min}} + 1$ (only for binary mixtures). This calculation is done in both directions and results in an asymmetric error. In figure 11.8 the maximum of both errors is printed. A closer view to the minimum of the distribution shown in figure 11.8 is shown in figure 11.9.

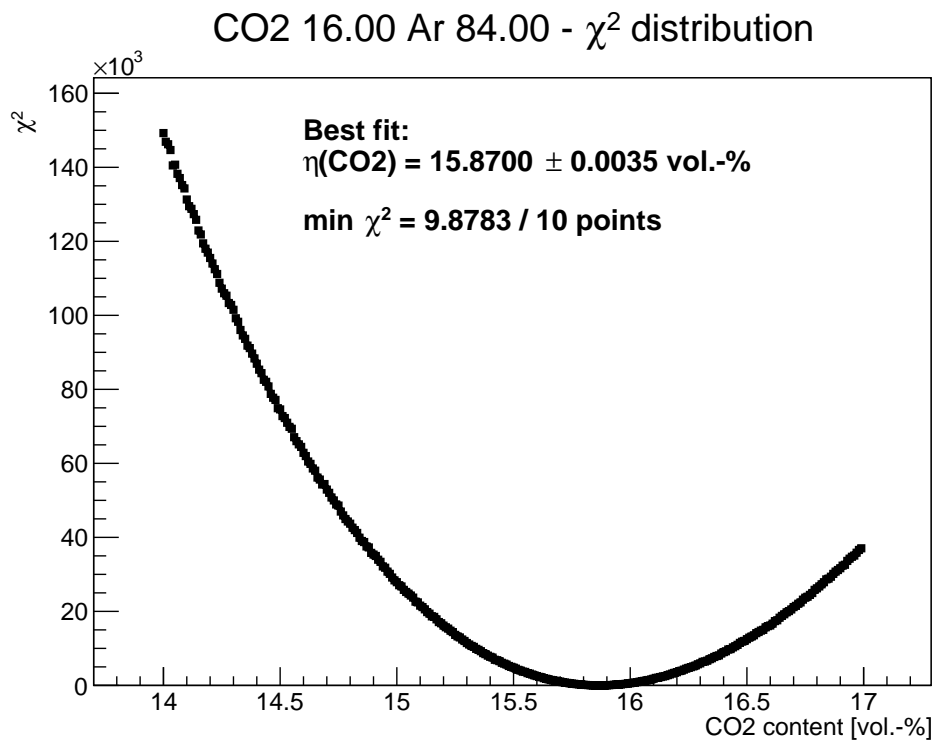


Figure 11.8.: Example for a χ^2 distribution. The data was measured during partial pressure mixing of ArCO₂ 84:16.

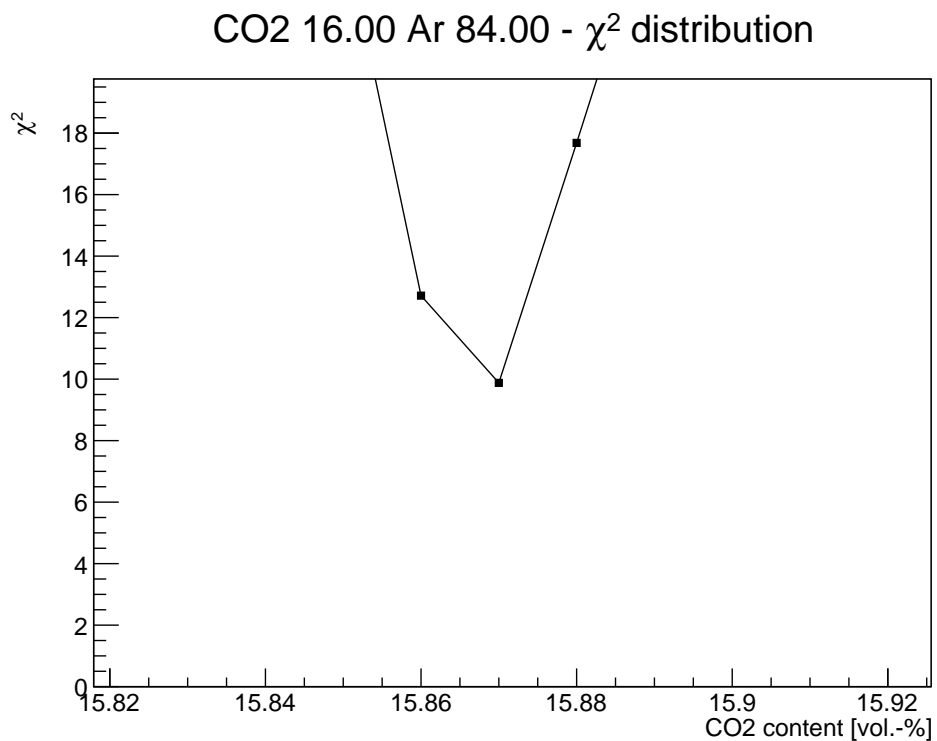


Figure 11.9.: Zoom of the region with low χ^2 .

11.2.1. Binary mixtures

To determine the performance of the UGMA several binary gas mixtures have been fitted. This has been done for the direct flow mixing and the partial pressure mixing mode. Both measurements have been done using the L3 VDC. All gases, which have been used for determination of the mixture composition are rated within **Magboltz** with five of five stars. Hence we assume that this rating ensures accurate simulations.

In every mode the first two hours after a change of the mixture are ignored. This ensures stable gas in all chambers.

For the mixture η the statistical error $\sigma_{\eta, \text{stat}}$ is derived from a χ^2 -fit of the measured data to the reference simulations (see figure 11.8).

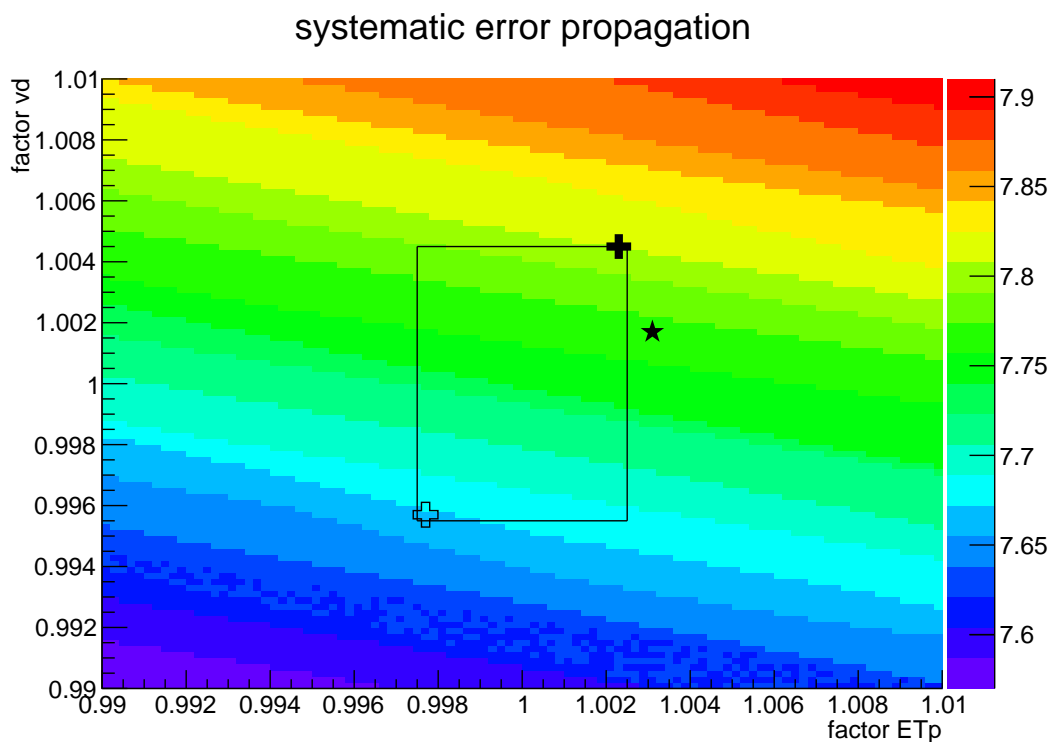


Figure 11.10.: Propagation of the systematic uncertainties of the chambers. The black star marks the position of the overall minimal χ^2 value. The solid cross marks the maximal, the hollow cross the minimal mixture. The rectangle shows the range of the estimated systematic errors of the L3 VDC (see equations 8.23 and 8.24). The z-axis represents the admixture, here CH_4 with a setpoint of 8 vol.-%.

After this the systematic errors of the chamber are propagated in the following way: All data point are shifted in x and y direction by multiplying with factors within a grid of 1 ± 0.01 in each direction. (see figure 11.10) After each shift a χ^2 minimisation is done and the best fit mixture is saved. Inside the rectangle, which is spread by the relative systematic errors

(see section 8.5.2) the maximal η_H and minimal η_L concentration is noted. The propagated systematic error is now calculated to be

$$\sigma_{\text{sys},+} = \eta_H - \eta \quad \sigma_{\text{sys},-} = \eta - \eta_L \quad (11.3)$$

For mixtures based on Ar and CH₄, the first data points at low electrical field have not been used for this study, because it seems that they show influence of the longitudinal diffusion. For mixtures of Ar and CO₂ some points could not be measured, because their drift velocity is too low and hence only one peak of the drift time spectrum can be digitised. The peak from the far source moves out of the acquisition window. All measurements where $v_D \geq 4 \mu\text{m/ns}$ are used for the analysis.

Direct Flow Mixing

Testing the performance of this mixing mode has been done using a mixture of Ar and CH₄ with various concentrations. Because the error of the MFCs is flow dependent, for some points, the total mixer flow has been increased to test this effect. The measurement can be seen in figure 11.11. All gases used in this test have been already calibrated inside the MFC, thus no additional correction factor is introduced. The statistical error bars are mostly hidden by the marker symbol. If they are visible they are drawn as thick lines. The vertical lines show the limit ($\pm 0.1 \text{ vol.-%}$) from the partial pressure mixing.

It is clearly visible, that there is some systematic effect, which reduces the content of the admixture at higher requested fractions. This effect is also visible for higher flow rates ($10 \ell_n/h$). It seems that the observable deviation is introduced by the flow controllers, because the regulation seems to work well but the measured values seem to differ from the real value. Related to this systematic effect further studies should be done, to evaluate whether this effect can be corrected for.

The uncertainty of the computed mixture is dominated by the statistical fluctuations of the flow measurements. Hence the error of the device itself can be neglected. The maximal deviation of the mean supplied mixture is less than 10 ppm_V to the setpoint.

Finally it can be said, that the direct flow mixing method is able to produce mixtures of Ar and CH₄ or CO₂ with an accuracy better than 7% of the requested concentration over a wide range of concentrations (3-18 vol.-%).

Partial Pressure Mixing

To test the performance of the partial pressure mixing mode, the same method like for the direct flow mixing has been used. The results are shown in figure 11.12. For the partial pressure mixing, we set a limit of 0.1 vol.-% within all mixtures should be mixed.

As it can be seen in figure 11.12 all mixtures are compatible with this limit. Only very few mixtures are slightly outside this limit, but compatible within their systematic uncertainties.

UGMA performance (direct flow mixing)

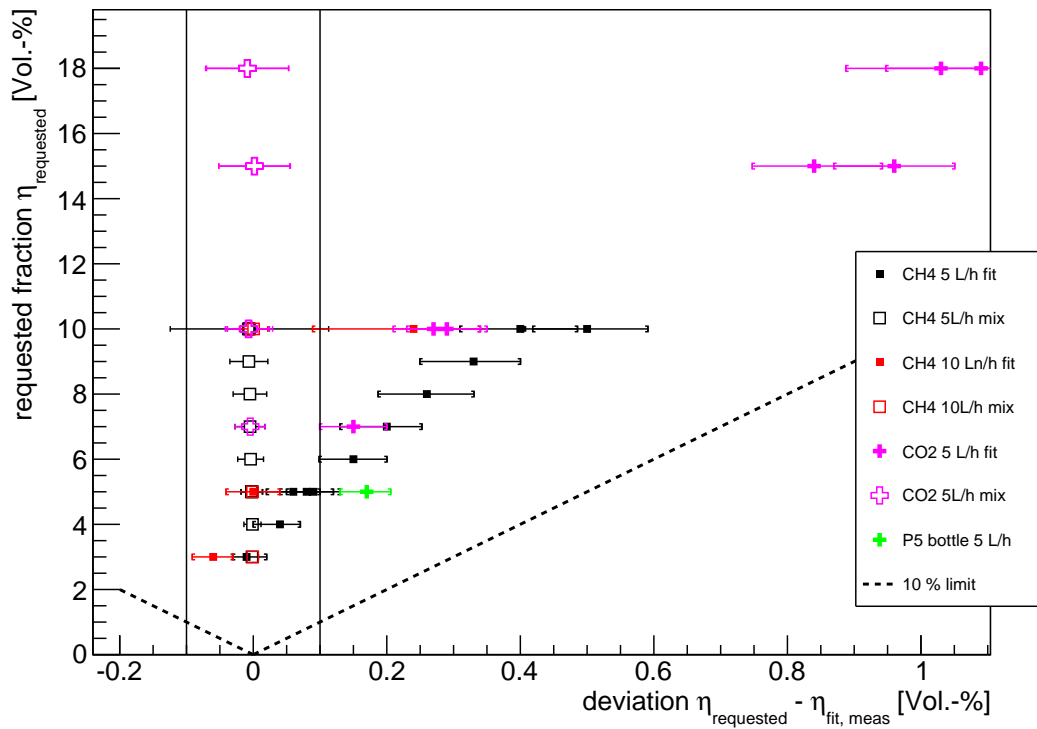


Figure 11.11.: Performance of the UGMA for Ar-CH₄ and Ar-CO₂ mixtures in the direct flow mixing mode. As reference the analysis for a premix Ar-CH₄ 95:5 mixture is shown. The filled symbols show the result of the fit of the v_D measurements to the simulation. The brackets indicate the uncertainty of the fitted mixture introduced by the systematic errors of the chamber. For comparison reasons also the limit from commercial gas suppliers ($\pm 10\%$) is shown. The hollow symbols mark the computation of the mixture given by the measured values of the MFCs.

Even if iC_4H_{10} is only rated with three of five stars inside **Magboltz**, the performance regarding this gas has been tested. The result can be seen in 11.13. But one has to keep in mind that it is not clear whether the simulation can be trusted or not. For this analysis all measured points have been used. The maximal observable absolute deviation among the tested mixtures is 0.22 vol.-% at a iC_4H_{10} concentration of 3 vol.-%. This results in an relative error of less than 7.5 %, which is better than the commercial supplier guarantee.

Compared with the direct flow mixing method, the partial pressure mixing method can produce mixtures without any dependency of the requested fraction. This can be ensured over the whole tested range 3-18 vol.-%. Hence this method is more accurate and the set limits are fulfilled.

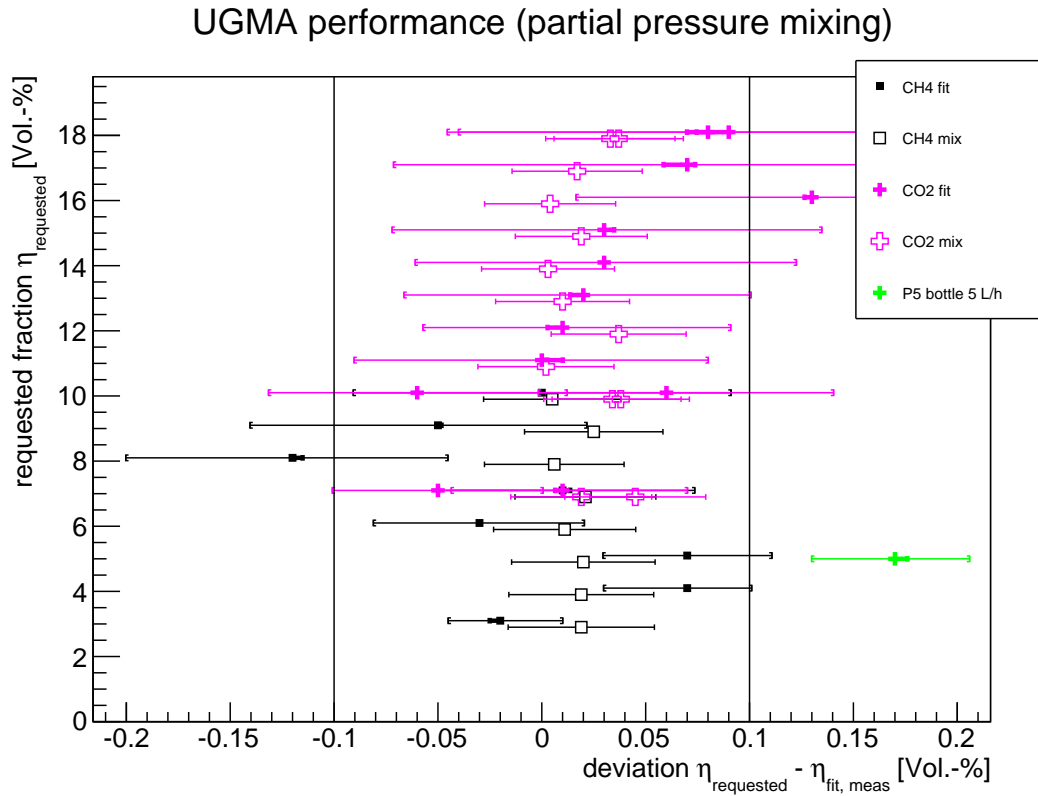


Figure 11.12.: Performance of the UGMA for Ar-CH₄ and Ar-iC₄H₁₀ mixtures in the partial pressure mixing mode. As reference the analysis for a premix Ar-CH₄ 95:5 mixture is shown. The brackets indicate the uncertainty of the fitted mixture introduced by the systematic errors of the chamber. The points labelled with „L3“ indicate that these points result from a v_d -fit analysis, whereas points labelled with „mixing“ result from the calculation of the mixture from measured and hence filled partial pressures. For optical reasons, the computed points have been moved by -0.1 vol.-% in y-direction and the measured points by +0.1 vol.-%.

Conclusion

At the moment „fitting the fractions“ is the only gas analysis method, which can be used without previous calibration. But this method suffers from systematic effects and uncertainties, which need to be well understood to gain reliable results. All known systematic effects are corrected and calibrated inside the readout of the GMC.

Due to lack of analysis devices the quality of the pure gases cannot be checked during runtime. We have to trust the analysis certificate delivered with the gas cylinder or if an analysis certificate is not ordered, we have to trust the numbers given for the purity of the gas. Small contaminations by other gases are not included in the simulations and hence, their effect on the drift velocity is not known.

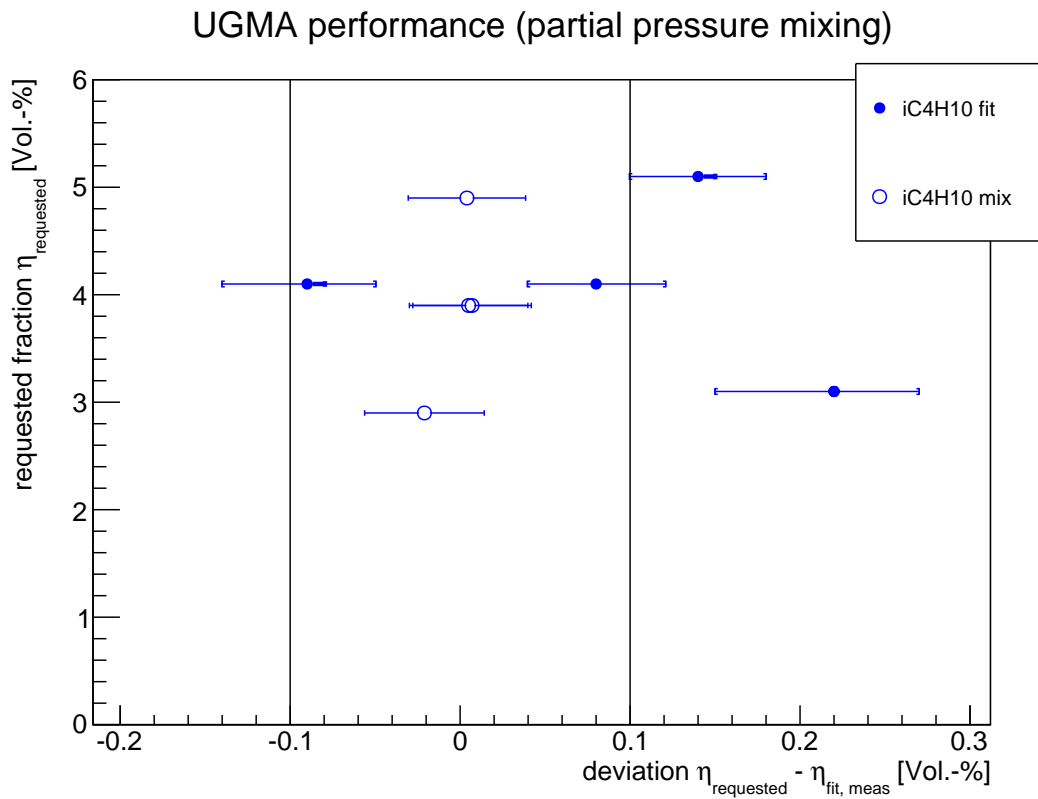


Figure 11.13.: Performance of partial pressure mixing using Ar- $i\text{C}_4\text{H}_{10}$ mixtures.

Finally using this analysis method it could be demonstrated that the direct flow mixing method is able to create mixtures with an relative accuracy better than 7% (i.e. better than 0.7 vol.-% for a 10 vol.-% mixture) for the admixture of CH_4 and CO_2 . The partial pressure mixing method is able to create mixtures within ± 0.1 vol.-% around the requested mixture. This has been tested for CH_4 and CO_2 diluted in Ar.

The results shown using $i\text{C}_4\text{H}_{10}$ must be handled with care, because it is unknown whether we can trust the simulation or not. In case we can trust the simulation the limits for this gas are slightly larger. For $i\text{C}_4\text{H}_{10}$ the mixture can be created within 0.2 vol.-% accuracy.

12. Conclusion

During the work on this thesis, the Universal Gas Mixing Apparatus system has been planned, designed, built and commissioned. At the end, the system is able to mix gases with a precision better than 0.1 vol.-% using partial pressure mixing. This limit has been verified using various gases and mixtures. At the same time, the system is able to control the pressure and flow through a connected particle detector.

For future research and development of gaseous particle detectors, this system is able to provide free selectable precise gas mixtures independent of the type of the connected detector. Thus the system can be used to supply gas for gas ionisation detectors of different kinds, like TPCs, drift tubes etc. Also any other kind of detector using a special gas mixture can be supplied. One important feature is the quick changeability of the gas mixture. With the UGMA it is possible to change the gas mixture sent through the detector within a few seconds in parallel flow mixing mode. When using partial pressure mixing, the time to change the gas mixture takes as long as it lasts to mix a new buffer filled with the new mixture.

For tests regarding the response of a detector to changes in the gas mixture, the system can be used as well as for searches for new gas mixtures, which may improve the performance of a detector.

One great feature of the system is mobility. By disconnecting the supply lines, ventilation and the connected particle detector the system is put into transportation mode. Due to the small size of the system, it can be transported with small effort. Hence the system can be used to operate a particle detector inside the laboratory and with the same configuration at a test beam facility. The UGMA is equipped with all necessary safety devices. Together with the ventilation a safe operation can be guaranteed. If flammable gases are used, the operation conditions may be adjusted to meet potential restrictions given by local administration.

A. Convention

A.1. Naming

Each component is named with six characters, which follow the rules described in the following. Most of the components connect two loops. Thus the naming has been optimised for this purpose.

$$\underbrace{AA}_{\text{loop from}} \quad \underbrace{BB}_{\text{loop to}} \quad \underbrace{CC}_{\text{device type}} \quad (\text{A.1})$$

If a component is an internal one, BB is replaced by a increasing number. The device type is an abbreviation which can be looked up in table A.1.

Table A.1.: Device type used for naming inside the UGMA

device type	description
FC	flow controller
FI	Filter
FS	flow sensor
NR	non return valve
NV	needle valve
OS	other sensor
OV	overpressure safety valve
PC	pressure controller
PR	pressure regulator
PS	pressure sensor
PT	PT100 flow controller
PU	pump
PV	proportional valve
SH	2/2 way hand valve
SV	2/2 way solenoid valve normal close
TS	temperature sensor
TV	2/2 way solenoid valve normal open
XV	4/2 way valve pneumatic operation
YV	3/2 way solenoid valve

Each loop is represented by one letter and one number (1-4). The identification code for each loop is shown in table A.2.

Table A.2.: Loop identification code

identification code	description
A	analysis loop
C	chamber
L	loop
M	mixing
P	purifier
V	vacuum
X	exhaust
Y	auxiliary

A.2. Units

There are a lot of different units, which are used to describe the state of gases or devices, which use gases. In this section, the units and general definitions are described.

A.2.1. Pressure

The pressure is given as an absolute pressure (bara) or as a differential pressure (bar). A conversion, which takes the height above the sea level into account is not applied. The differential pressure is based on the current ambient pressure or in calculations on normal pressure 1013 mbara.

A.2.2. Volume

The volume is given in litres (ℓ). Because of the compressibility, the volume is given in norm-litres (ℓ_n). One norm litre is the amount of gas, which fills a volume of one litre at a pressure of 1013.25 mbara and a temperature of 273.15 K (0°C). The given pressure and temperature are norm conditions compatible with DIN 1343 [85].

Due to the fact, that the UGMA is not placed in a laboratory, which can be set to norm conditions, for the necessary data, conditions were chosen, which can be met. The standard conditions for the gas monitoring chambers consist of a pressure of 1013 mbara and a temperature of 25°C.

A.2.3. Volume-flow

Unless otherwise noted, the flow is based on Argon. The flow is given in norm-litres per hour. [97]

A.3. Commonly used gas mixtures

There are few mixtures, where a special focus has been put on. In the meanwhile they are commonly known by their own names.

T2K 95 %Ar, 3 %CF₄, 2 %iC₄H₁₀ gas used in the TPC at the near detector (ND280) of the T2K-experiment located in Tokai, Japan.

P5 95 %Ar, 5 %CH₄

P10 90 %Ar, 10 %CH₄

ILD 93 %Ar, 5 %CH₄, 2 %CO₂ gas which is foreseen for the TPC inside the ILD at ILC

A.4. Norms, law and provisions

Some parts of the system had to be designed in compatibility with the legal norms and provisions. Most of the time, the system will be located in Aachen or Germany. For this reason, the German norms, law and provisions had been respected. Some of them are the states implementation of European ones. But for other ones, no European pendants exist. Norms, laws and provisions exists at different levels.

Starting at the top level, there are international norms, which are created by International Organisation for Standardization (ISO). These norms can either be adopted by the norming organisation of the country itself (DIN ISO) or by the European norming association (DIN EN ISO).

The next level are European norms. For this norms to be valid in each country they need to be adopted by the norming organisation of the country (DIN EN). If these norms are adopted, every country, who is member of European Committee for Standardization (CEN) or European Committee for Electrotechnical Standardization (CENELEC), has to adopt them without changing.

Every norm is published by the local norming institutes (DIN), for Germany this is Deutsches Institut für Normung e. V. (DIN). The DIN also publishes all local norms, which are only valid inside Germany.

Due to the fact that each level has its own numbering schema, some norms have the same number but a total different topic. These can be distinguished using the prefix (DIN, DIN EN, etc.).

For laws and provisions a comparable mechanism exists.

List of abbreviations

ADC	Analogue-Digital-Converter
ALICE	A Large Ion Collider Experiment
CDS	Carbon Dioxide Spectroscopic Database
CEDOAS	Cavity Enhanced Differential Optical Absorption Spectroscopy
CENELEC	European Committee for Electrotechnical Standardization
CEN	European Committee for Standardization
CERN	European Organization for Nuclear Research
CMS	Compact Muon Solenoid
DESY	Deutsches Elektronen-Synchrotron
DIN	Deutsches Institut für Normung e. V.
FADC	Flash Analogue Digital Converter
FDN	Fluidat-On-The-Net
GC	gas chromatograph
GEISA	Gestion et Etude des Informations Spectroscopiques Atmosphériques: Management and Study of Atmospheric Spectroscopic Information
GEM	Gas Electron Multiplier
GMC	Gas Monitoring Chamber
HID	helium ionisation detector
HITRAN	high-resolution transmission molecular absorption database
IC	Integrated Circuit
ILC	International Linear Collider
ILD	International Large Detector
IP	Interaction Point
ISO	International Organisation for Standardization
ITS	Inner Tracking System
LED	light-emitting diode
LEL	lower explosion limit
LEP	Large Electron-Positron Collider
LHC	Large Hadron Collider
LPTPC	Large Prototype TPC
MAG	metal active gas
MDT	Muon Drift Tubes
MFC	Mass Flow Controller
MicroMegas	Micro-Mesh-Gaseous-Structure
MPGD	Micro Pattern Gas Detector
MPPC	Multi Pixel Photon Counter
MWPC	Multi-Wire-Proportional-Chamber
NIST	National Institute of Standards and Technology
PCB	printed circuit board

PC	personal computer
PDU	Power Distribution Unit
PID	proportional plus integral plus derivative element
PLC	Programmable Logic Controller
PMT	Photomultiplier Tube
PWM	pulse width modulation
RAID	Redundant Array of Independent Disks
RAM	random access memory
RCD	residual-current-operated protective device
RMS	Root Mean Square
SMD	Surface-mounted device
STP	Standard temperature and pressure
SVD	Singular Value Decomposition
TCD	thermal conductivity detector
TEC	Time Expansion Chamber
TPC	Time Projection Chamber
TTL	Transistor-Transistor-Level
UDP	User Datagram Protocol
UGMA	Universal Gas Mixing Apparatus
USB	universal serial bus
VDC	Velocity Drift Chamber
VDE	Verband der Elektrotechnik Elektronik Informationstechnik e.V.

List of Figures

2.1	Principle of how a MWPC functions	14
2.2	Working principle of a TPC	15
2.3	Simulation result to determine the W-value	19
2.4	Detected charge in dependency of the operation voltage. Plot taken from [46]	21
2.5	Computed electric field in one multiplying channel of a GEM	23
2.6	Gain and discharge probability of various GEM configurations	24
2.7	All v_d measurements of GMC A during RUN3	32
2.8	Relative gain versus relative density change	33
2.9	Correction of the data sample containing the first week of RUN4.	33
2.10	Determined slope of one week data	34
2.11	Average gain over one week data	35
2.12	Overview of the improvement gained by the correction	35
4.1	Basic sketch of the UGMA	45
4.2	Insertion of the purifier module into the buffer module	47
4.3	Insertion of the purifier module using one 4/2-way valve	47
4.4	Fully modular piping approach between two 4/2 way valves V1 and V2	48
4.5	Assembly group piping approach between two 4/2 way valves V1 and V2	49
4.6	View inside the gas handling section of the UGMA.	50
4.7	Overview of the piping of the whole system	51
4.8	Mixer section of the UGMA	52
4.9	Analysis loop, with direction of inner flow marked by arrows	53
4.10	One of the two buffers, which can be used for partial pressure mixing	53
4.11	One purifier module of the UGMA	54
4.12	Pressure and flow control of the chamber	55
4.13	Exhaust section of the chamber loop and the mixer supply line	55
4.14	Photo of the ventilation part	57
5.1	Photo of the electronics readout.	59
5.2	Photograph of the valve driver board mounted inside the connector.	63
5.3	The 230 V distribution after its final assembly	64
5.4	Connection of the valve island to the cylinder of the 4/2-way valve	65
5.5	Picture of the mounted valve island	66
6.1	Photo of the user interface of the UGMA.	68
6.2	Overview of the internal data flow.	72
6.3	Screenshot of the webcontrol application showing the analysis page	76
7.1	Schematic view of the inside of a MFC.	78

7.2	Theoretical relative error of MFC over the entire flow range.	79
7.3	Pressure history during partial pressure mixing of P5	85
7.4	Deviation of the partial pressure	89
7.5	Distribution of the mixing times	90
8.1	Saturation vapour pressure calculated using the Wexler equation.	93
8.2	Pressure dependence of the H ₂ O contamination measurement	94
8.3	One day H ₂ O and temperature measurements	95
8.4	Pressure dependence of the O ₂ measurement	98
8.5	Photo of the gas chromatograph.	99
8.6	Gas flow inside the GC sampling section.	99
8.7	Example chromatogram of a Argon Methane 90:10 mixture	100
8.8	GC temperature program	101
8.9	Data flow of the GC offline analysis	103
8.10	Sketch of the general prinziple of the ND280 GMC. [25]	105
8.11	Drift time distribution	106
8.12	TEC gassystem with the monitoring chamber.	107
8.13	Technical drawing of the L3 VDC	108
9.1	View inside the PowerBar	112
9.2	Determiation of the leakage-rate	115
9.3	Determiation of the leakage rate of the analysis loop.	116
9.4	Measurement of the effective throughput	119
9.5	Deviation of each line from the setpoint	120
9.6	Deviations of each gas line plotted over time	121
9.7	Distribution of the maximal absolute deviation per mixture	122
9.8	Distribution of the maximal relative deviation per mixture.	123
9.9	Variation of the gas mixture during one measurement cycle	123
9.10	Pressures at a flow of 5 ℓ _n /h	125
9.11	Characteristic curve of the analysis loop	126
10.1	Estimation of the statistical error of A110TS	128
10.2	Determiation of the statistical error of four pressure sensors	129
10.3	Schematic view of the purifier heater. Only the tested components are drawn.	130
10.4	Temperature distribution for different setpoints	131
10.5	Measurements of the buffer vessel volume.	133
10.6	Evacuation of the buffer vessels	134
10.7	Blow-off of an Argon filled buffer vessel with $p_0 = 3840.32$ mbara	135
10.8	Filling the buffer with Argon starting from vacuum.	136
11.1	Example of one v_d curve measurement	138
11.2	Working points in mixtures containing Ar, CH ₄ and CO ₂	139
11.3	Working points in mixtures containing Ar, CH ₄ and iC ₄ H ₁₀	140
11.4	Working points in mixtures containing Ar, CH ₄ and H ₂	141
11.5	Working points in mixtures containing Ar, CF ₄ and iC ₄ H ₁₀	141
11.6	Working points in mixtures containing Ar, C ₃ H ₈ and CF ₄	142
11.7	Drift velocity measurement and simulation steps.	144
11.8	Example for a χ^2 distribution.	145

11.9	Zoom of the region with low χ^2	145
11.10	Propagation of the systematic uncertainties	146
11.11	Performance of the UGMA in direct flow mode	148
11.12	Performance of the UGMA in partial pressure mixing mode	149
11.13	Performance of partial pressure mixing using Ar- i C ₄ H ₁₀ mixtures.	150

List of Tables

2.1	Comparison of different values of W_β from different references and simulations.	20
2.2	Run periods of the ND280 experiment.	31
5.1	Overview of the used pressure sensors	61
7.1	Conversion factors for different gases.	83
8.1	Event-table used in GC setup	101
8.2	Precision and accuracy of the GC	103
9.1	Comparison of leakage-rates buffer and purifier vessels	115
9.2	Sensors used to determine the characteristic curve of the analysis loop	125
10.1	Statistical error of temperature sensors	128
10.2	Statistical error of pressure sensors	130
A.1	Device type used for naming inside the UGMA	153
A.2	Loop identification code	154

Bibliography

Physics

- [1] F. Bauer et al. Construction and test of MDT chambers for the ATLAS muon spectrometer. *Nuclear Instruments and Methods in Physics Research Section A: Accelerators, Spectrometers, Detectors and Associated Equipment*, 461(1–3):17 – 20, 2001. 8th Pisa Meeting on Advanced Detectors.
- [2] F. Bauer et al. Construction and test of the precision drift chambers for the ATLAS Muon Spectrometer. In *Nuclear Science Symposium Conference Record, 2000 IEEE*, volume 1, pages 5/11 –5/15 vol.1, 2000.
- [3] Ties Behnke, Chris Damerell, John Jaros, and Akiya Miyamoto. International Linear Collider - Reference design report - Volume 4: Detectors. Technical report, International Linear Collider, 2007.
- [4] F. Beissel et al. Construction and Performance of the L3 central tracking detector. *Nuclear Instruments and Methods in Physics Research Section A: Accelerators, Spectrometers, Detectors and Associated Equipment*, 332(1):33–55, 1993.
- [5] W. Blum, W. Riegler, and L. Rolandi. *Particle Detection with Drift Chambers*. Particle Acceleration and Detection. Springer, 2008.
- [6] T. E. Bortner and G. S. Hurst. Ionization of Pure Gases and Mixtures of Gases by 5-Mev Alpha Particles. *Physical Review*, 93:1236–1241, March 1954.
- [7] Arden L. Buck. New Equations for Computing Vapor Pressure and Enhancement Factor. *Journal of applied meteorology*, 20:1527–1532, 1982.
- [8] Campbell, M. et al. Detection of single electrons by means of a Micromegas-covered MediPix2 pixel CMOS readout circuit. *Nuclear Instruments and Methods in Physics Research A*, 540:295–304, March 2005.
- [9] M. Capeans. Aging of Gaseous Detectors: assembly materials and procedures. *ICFA Instrum. Bull.*, 24:85–109, 2002.
- [10] V Blanco Carballo, M Chefdeville, M P Decowski, M Fransen, H van der Graaf, W J C Koppert, and J Schmitz. Applications of gridpix detectors. *Journal of Instrumentation*, 5(02):P02002, 2010.
- [11] Alexei A. Chursin, N. Jacquinet-Husson, G. Lefevre, Noelle A. Scott, and Alain Chedin. GEISA-97 spectroscopic database system related information resources: current status and perspectives. *Proc. SPIE*, 4063:287–291, 2000.

- [12] M. Danilov et al. Aging studies for the muon detector of HERA-B . *Nuclear Instruments and Methods in Physics Research Section A: Accelerators, Spectrometers, Detectors and Associated Equipment*, 515(1–2):202 – 219, 2003. Proceedings of the International Workshop on Aging Phenomena in Gaseous Detectors.
- [13] G. Dellacasa et al. ALICE - Technical Design Report of the Time Projection Chamber. Technical report, CERN, 1999.
- [14] Deutsches Elektronen-Synchrotron DESY. LCTPC - A Time Projection Chamber for a future Linear Collider. electronic resource. <http://www.lctpc.org/>.
- [15] Harshit Dubey. Precision and Accuracy of the gas chromatograph. private communication, July 2014.
- [16] Sven E. Fiedler, Achim Hese, and Albert A. Ruth. Incoherent broad-band cavity-enhanced absorption spectroscopy. *Chemical Physics Letters*, 371:284–294, 2003.
- [17] H. Geiger and W. Müller. Elektronenzählrohr zur Messung schwächster Aktivitäten. *Naturwissenschaften*, 16:617–618, August 1928.
- [18] Y. Giomataris, Ph. Rebourgeard, J.P. Robert, and G. Charpak. MICROMEGAS: a high-granularity position-sensitive gaseous detector for high particle-flux environments. *Nuclear Instruments and Methods in Physics Research Section A: Accelerators, Spectrometers, Detectors and Associated Equipment*, 376:29-35, 1996.
- [19] Peter Göttlicher. *Entwicklung und Bau eines rechnergesteuerten Gassystems für die Spurenkammer des L3-Experiments*. PhD thesis, RWTH Aachen, 1991.
- [20] C. Hearty et al. T2K ND280 TPC Technical Design Report. Technical report, University of British Columbia, January 2007. Version 1.0.
- [21] Carsten Heidemann. Direkte Messung der Driftgeschwindigkeit im Gas der CMS-Myonenkammern mit VDC-Kammern. Diplomarbeit, III. Physikalisches Institut A - RWTH Aachen University, 2010.
- [22] Erik Johansson, Jörgen Dalmau, Erik Johansson, et al. Hands-on-CERN. electronic resource, May 2006. http://hands-on-cern.physto.se/hoc_v21en/index.html.
- [23] D. Karlen et al. Time projection chambers for the T2K near detectors. *Nuclear Instruments and Methods in Physics Research Section A: Accelerators, Spectrometers, Detectors and Associated Equipment*, 637(1):25 – 46, 2011.
- [24] M. Killenberg, S. Lotze, J. Mnich, A. Münnich, S. Roth, and M. Weber. Development of a GEM-based High Resolution TPC for the ILC . *Nuclear Instruments and Methods in Physics Research Section A: Accelerators, Spectrometers, Detectors and Associated Equipment*, 573(1–2):183 – 186, 2007. Proceedings of the 7th International Conference on Position-Sensitive Detectors.
- [25] Lukas Koch. private communication.
- [26] Lukas Koch. Systematic measurement and simulation of drift gas properties. Master's thesis, III. Physikalisches Institut B, RWTH Aachen, 2013.

-
- [27] L. Koch, S. Roth, and J. Steinmann. Temperature and pressure correction of specific ionisation, gain and drift velocity inside the T2K ND280 TPC. Technical report, III. Physikalisches Institut B, RWTH Aachen, 2013. internal document available at III. Physikalisches Institut B, RWTH Aachen.
- [28] Sebastian Korff. Das Geiger-Müller-Zählrohr. *NTM Zeitschrift für Geschichte der Wissenschaften, Technik und Medizin*, 20(4):271–308, 2012.
- [29] L3 Collaboration. Results from the L3 experiments at LEP. *Physics Reports*, 236(1-2):1–146, 1993.
- [30] J. Meinen, J. Thieser, U. Platt, and T. Leisner. Technical Note: Using a high finesse optical resonator to provide a long light path for differential optical absorption spectroscopy: CE-DOAS. *Atmospheric Chemistry and Physics*, 10:3901–3914, 2010.
- [31] U. Platt, J. Meinen, D. Pöhler, and T. Leisner. Broadband Cavity Enhanced Differential Optical Absorption Spectroscopy (CE-DOAS) - applicability and corrections. *Atmospheric Measurement Techniques*, 2:713–723, 2009.
- [32] Otto Redlich and J. N. S. Kwong. On the thermodynamics of solutions. V - An Equation of State. Fugacities of Gaseous Solutions. *Symposium on Thermodynamics and Molecular Structure of Solutions*, September 1948.
- [33] Rothman, L. S. et al. The HITRAN 2008 molecular spectroscopic database. *Journal of Quantitative Spectroscopy and Radiative Transfer*, 110(9-10):533–572, June 2009.
- [34] E. Rutherford, H. Geiger, and J. Harling. An Electrical Method of Counting the Number of α -Particles from Radio-Active Substances. *Royal Society of London Proceedings Series A*, 81:141–161, August 1908.
- [35] F. Sauli. Principles of operation of multiwire proportional and drift chambers. Lectures given in the academic training programme of CERN, 1975-1976.
- [36] F. Sauli. GEM: A new concept for electron amplification in gas detectors. *Nuclear Instruments and Methods in Physics Research Section A: Accelerators, Spectrometers, Detectors and Associated Equipment*, 386:531-534, November 1997.
- [37] Jochen Steinmann. UGMA - Technische Dokumentation. Technical report, III. Physikalisches Institut B - RWTH Aachen, 2013. available at III. Physikalisches Institut B - RWTH Aachen.
- [38] S.A. Tashkun, V.I. Perevalov, and J.-L. Teffo. CDSD-296, The High-Precision Carbon Dioxide Spectroscopic Databank: Version for Atmospheric Applications. In Agnès Perrin, Najate Ben Sari-Zizi, and Jean Demaison, editors, *Remote Sensing of the Atmosphere for Environmental Security*, NATO Security through Science Series, pages 161–169. Springer Netherlands, 2006.
- [39] R. Thalman and R. Volkamer. Inherent calibration of a blue LED-CE-DOAS instrument to measure iodine oxide, glyoxal, methyl glyoxal, nitrogen dioxide, water vapour and aerosol extinction in open cavity mode. *Atmospheric Measurement Techniques*, 3:1797 – 1814, 2010.
- [40] Rob Veenhof. Choosing a gas mixture for the Alice TPC, February 2003.

- [41] Teja Wrobel. Systematische Messungen der Driftgeschwindigkeit und der Gasverstärkung mithilfe einer Gasmonitorkammer für das T2K-Experiment. Diplomarbeit, III. Physikalisches Institut B, RWTH Aachen, Mai 2011.
- [42] J. Beringer et al., editor. *Particle Physics Booklet*. Particle Data Group, 2012.
- [43] Klaus Dehmelt, editor. *A Large TPC Prototype for an ILC Detector*, 2009.
- [44] Gas Detectors Development Group. electronic ressource. <http://gdd.web.cern.ch/GDD/>.
- [45] III. Physikalisches Institut - RWTH Aachen University. *Lab experiment IV - Drift Chamber (VDC) - Lab class particle physics (Master)*, 2013.
- [46] III. Physikalisches Institut - RWTH Aachen University. *Fortgeschrittenenpraktikum für Bachelorstudenten der Physik - Versuch T7 - Gasdetektoren und Statistik*, January 2010.
- [47] *The CMS muon project: Technical Design Report*. Technical Design Report CMS. CERN, Geneva, 1997.

Mechanics

- [48] Bronkhorst High-Tech B.V. *EL-FLOW Thermische Massendurchflussmesser und -regler für Gase*.
- [49] Binder GmbH Apparate- und Behälterbau. *Konformitätserklärung nach Druckgeräterichtlinie 97/23/EG*. Rokfelder Str. 58, 74564 Crailsheim, März 2012.
- [50] Bronkhorst High-Tech B.V. *EL-FLOW Digital Thermal Mass Flow Meters and Controllers for Gases*.
- [51] HACH LANGE GmbH. *Information - Prozess-Messtechnik - Sauerstoffsensoren - Orbisphere M1100*.
- [52] Hach Lange GmbH. *Orbisphere Model K- M1100 Sensor and Model 410 Analyzer - Basic User Manual*, 7 edition, August 2013.
- [53] Hach Lange GmbH. *Orbisphere Model K1100 or M1100 Sensor and Model 410 Analyzer - User Manual*, c edition, January 2010.
- [54] Shaw Moisture Meters. *The Diurnal Effect on Dewpoint*.
- [55] Shaw Moisture Meters. *Super-Dew*. <http://www.shawmeters.com>.
- [56] SRI Instruments. GC, HPLC, Data Systems and Hydrogen Generators. <http://www.srigc.com/>.
- [57] Varian Inc. Vacuum Technologies. *Dry Scroll Pumps*.
- [58] Hayes Separations, Inc. *Analytical Polymers - Porous Polymers*.
- [59] *The Vacuum Technology Book*. Pfeiffer Vacuum GmbH, 2008.

Drawings

- [60] Barthel Philipps. Dachblech UGMA-01-00455-R1-A3, März 2012.
- [61] Barthel Philipps. Grundplatte UGMA-01-00421-R1-A1, Dezember 2012.
- [62] Barthel Philipps. Frontplatte UGMA-01-00425-R1-A1, Januar 2012.
- [63] Barthel Philipps. Gehäuse Drucksensor P31 Leitung UGMA-01-00431-R1-A3, Januar 2012.
- [64] Barthel Philipps. Gehäuse Temperatursensor UGMA-01-00432-R1-A3, Januar 2012.
- [65] Barthel Philipps. Siebklemmring UGMA-01-00442-R1-A4, Januar 2012.
- [66] Barthel Philipps. Trommel Schweißkonstruktion UGMA-01-00446-R1-A3, Februar 2012.
- [67] Barthel Philipps. Blindflansch oben UGMA-01-00447-R1-A2, Februar 2012.
- [68] Barthel Philipps. Blindflansch unten UGMA-01-00448-R1-A2, Februar 2012.
- [69] Barthel Philipps. Zusammenstellung Rekooperation UGMA-01-00449-R1-A1, Februar 2012.
- [70] Barthel Philipps. Siebklemmring II UGMA-01-00456-R1-A4, März 2012.
- [71] Barthel Philipps. Zusammenbau E-Schaltschrank UGMA-01-00457-R1-A0, März 2012.
- [72] Barthel Philipps. E-Frontplatte UGMA-01-00458-R1-A1, März 2012.
- [73] Barthel Philipps. Drucksensoradapter UGMA-01-00459-R1-A4, April 2012.
- [74] Barthel Philipps. Fließschema Universalgasmischanlage UGMA-01-00474-R1-A0, Juni 2012.
- [75] Barthel Philipps. Zusammenstellung 4/2 Wege Ventil, Januar 2011.
- [76] Barthel Philipps. Hebel, November 2011.
- [77] Barthel Philipps. Zusammenbau Rahmen, Dezember 2011.
- [78] Barthel Philipps. Druckbehälterzeichnung UGMA-01-00416-R1-A2, Dezember 2011.
- [79] Barthel Philipps. Tür Hinten Gasrack UGMA-01-00417-R1-A2, Dezember 2011.
- [80] Barthel Philipps. Tür Seite Gasrack UGMA-01-00418-R1-A2, Dezember 2011.

Standards

- [81] DIN EN 60751 - Industrielle Platin-Widerstandsthermometer und Platin-Temperatursensoren, May 2009.
- [82] DIN EN ISO 14175 - Schweißzusätze - Gase und Mischgase für das Lichtbogenschweißen und verwandte Prozesse, June 2008.
- [83] DIN 18111-1 - Türzargen - Stahlzargen - Teil1: Standardzargen für gefälzte Türen in Mauerwerkswänden, August 2004.
- [84] Bauordnung für das Land Nordrhein-Westfalen - Landesbauordnung (BauO NRW), March 2000.
- [85] DIN 1343 - Referenzzustand, Normzustand, Normvolumen, January 1990.

Electronics

- [86] Festo AG & Co. KG. *Beschreibung Elektronik - Systembeschreibung - Installation und Inbetriebnahme von CPX-Terminals*. 73726 Esslingen, 2009.
- [87] Festo AG & Co. KG. *Beschreibung Pneumatik MPA-S - Ventilinsel mit MPA-S Pneumatik*. 73726 Esslingen, 2009.
- [88] Microchip Technology Incorporated. *MCP2515 - Stand-Alone CAN Controller with SPI Interface*, 2007.
- [89] Texas Instruments. *DRV103 - PWM LOW-SIDE DRIVER (1.5A and 3A) for Solenoids, Coils, Valves, Heaters, and Lamps*, 2012.
- [90] Texas Instruments. *XTR101 - Precision, Low Drift 4-20mA TWO-WIRE TRANSMITTER*, 2004.
- [91] WIKA Alexander Wiegand SE & Co. KG. *Druckmessumformer für allgemeine industrielle Anwendungen - Typ A-10*, January 2013.
- [92] WIKA Alexander Wiegand SE & Co. KG. *Druckmessumformer für Präzisionsmessungen - Typ P-30 & Typ P-31*, January 2013.
- [93] CAN in Automation (CiA) e. V., Kontumazgarten 3, 90429 Nürnberg. *CiA 102 - CAN - Physical layer for industrial applications*, 3.0.0 edition, February 2010.
- [94] Industrielle Platin-Widerstandsthermometer und Platin-Temperatursensoren (IEC 60751:2008); Deutsche Fassung EN 60751:2008, May 2009.

Software

- [95] Bronkhorst High-Tech B.V. Fluidat on the net <http://www.fluidat.com/>. [electronic resource].
- [96] Bronkhorst High-Tech B.V. *Gas Conversion Table*, 2004.
- [97] Bronkhorst High-Tech B.V. *General instructions for digital massflow/pressure instruments*, 2004.
- [98] Stephen Biagi. MIP. electronic resource, 10 2012. <http://magboltz.web.cern.ch/magboltz/>.
- [99] Stephen Biagi and Rob Veenhof. Magboltz - transport of electrons in gas mixtures. electronic resource, April 2013. <http://magboltz.web.cern.ch/magboltz/>.
- [100] Rene Brun and Fons Rademakers. ROOT - An Object Oriented Data Analysis Framework. In *AIHENP'96 Workshop, Lausanne*, volume 389, pages 81–86, 1996.
- [101] P. Furlan. *Das gelbe Rechenbuch: Für Ingenieure, Naturwissenschaftler und Mathematiker: Rechenverfahren der Höheren Mathematik in Einzelschritten erklärt*. Furlan, 1995.
- [102] D.R. Lide. *Handbook of chemistry and physics*. CRC HANDBOOK OF CHEMISTRY AND PHYSICS. CRC, 2007.
- [103] Igor Smirnov. Heed - modelling of ionization produced by fast charged particles in gases. electronic resource, February 2009. <http://ismirnov.web.cern.ch/ismirnov/heed>.
- [104] National Institute of Standards and Technology (U.S.). Nist chemistry webbook [electronic resource].
- [105] Dennis Terhorst. NOTE001 - The Subserver Protocol. available at <https://forge.physik.rwth-aachen.de/documents/5>, November 2008.
- [106] Rob Veenhof. Garfield - simulation of gaseous detectors. electronic resource, September 2010. <http://garfield.web.cern.ch/garfield/>.
- [107] Rob Veenhof and Heinrich Schindler. Garfield++. electronic resource. <http://garfieldpp.web.cern.ch/garfieldpp/>.
- [108] Debian - The universal operating system. electronic resource. <https://www.debian.org/>.
- [109] C++ Laboratory Software Framework - LibLab. electronic resource. <https://forge.physik.rwth-aachen.de/projects/liblab>.
- [110] Oracle - Virtual Box. electronic resource. <https://www.virtualbox.org/>.

Acknowledgement

Die Reihenfolge der Danksagungen hat nichts mit irgendeiner Bewertung zu tun, sie ist komplett willkürlich gewählt. Dank an . . .

- Stefan Roth, der sich dieses Projekt ausgedacht hat und mir viel Spielraum bei der Realisierung gelassen hat.
- Oliver Pooth, der sich mit der Rechtschreibung und Struktur auseinander gesetzt hat und Tipps gegeben hat diese zu verbessern.
- Achim Stahl, der zum Ende hin das Projekt mit leichtem Druck beschleunigt hat.
- Lutz Feld, der sich glücklicherweise „spontan“ bereiterklärt hat das Zweitgutachten zu übernehmen.
- Barthel Philipps, der sich (fast) alle mechanischen Teile ausgedacht und geplant/gezeichnet hat.
- Dieter Jahn, der versucht hat den Überblick über die verschiedenen Teile und Arbeitsschritte zu behalten. Es ist ihm auch (fast) immer gelungen.
- Benjamin Walla, der jedes Rohr mit Namen kennt und alle (!) Verschraubungen angezogen hat. Ebenfalls hat er den Rohrverlauf vieler Rohre stark vereinfacht und so geholfen das System übersichtlicher zu machen.
- Carsten Westhofen, der viele Teile mit der CNC-Fräse bearbeitet hat und ansonsten auch immer hilfreich zur Seite stand.
- die Auszubildenen der Mechanischen Werkstatt, die auch das ein oder andere Teil gefertigt haben.
- der mechanischen Werkstatt vom III. Physikalischen Institut A, die einige Teile für dieses Projekt gefertigt haben und an einigen Stellen mit Material ausgeholfen haben.
- Frank Beissel, mit dem ich in der Anfangszeit viel über die Realisierung der Elektronik diskutiert habe und von dem der ein oder andere gute Tipp im Bezug auf Realisierung von Elektronik und Mechanik kam. Leider hat er mir in der Schlussphase nicht mehr zur Seite stehen können, da er am 16. Juni 2012 unerwartet verstorben ist.
- Eric Bock, der alle Platinen bestückt hat und mich gerade in der heißen Phase mit Rat und Tat unterstützt hat.
- Jin Yao, der in den Anfängen des Projektes viele Studien zur Software gemacht hat. Ebenfalls hat er die erste Test-Version des User-Interfaces programmiert und getestet.
- Dennis Terhorst, der als Mit-Büro-Insasse auch lange Zeit das Projekt mit Ratschlägen begleitet hat und immer dann geholfen hat, wenn es besonders klemmte.
- alle anderen Arbeitsgruppen, die während der Bauzeit auf verschiedene Dinge aus der elektrischen und mechanischen Werkstatt warten mussten. Da alle Kapazitäten mit dem Bau des GasSystems ausgelastet waren.
- der Verwaltung Frau Roder und Frau Rosewick, die mit viel Geduld meine Bestellungen ver- und bearbeitet haben. Teilweise waren diese gar nicht so einfach.

-
- allen Bachelorstudenten, die während ihrer Bachelorarbeit auch den Fortschritt des Projektes begleitet haben.
 - Lukas Koch, der bei der finalen Inbetriebnahme geholfen hat und die ersten Testmessungen durchgeführt hat. Er ist auch für die ersten systematischen Messungen mit diesem System verantwortlich.
 - meinen Bruder Thomas Steinmann, der oft für Diskussionen abseits des Projektes und der Physik gesorgt hat und damit eine nette Abwechslung geboten hat.
 - meine Mutter und meinen Vater, die mich während der gesamten Zeit meines Studiums und meiner Promotion unterstützt haben.
 - meinen mittlerweile ehemaligen Mitbewohnern und Mitbewohnerinnen (vor allem Manu, Thomas, Sascha, Kerstin, Raik, Clemens, Andi und Julia) mit denen ich während meiner Promotionszeit viele nette Erfahrungen gemacht habe, und die sich teilweise erbarmt haben die technische Dokumentation nach bestem Wissen zu korrigieren.
 - allen denen, die in der obigen Liste nicht auftauchen, aber meinen ich sei Ihnen zu dank verpflichtet. Vielen Dank.

Besonderer Dank geht auch an die Firma GKD - Gebr. Kufferath AG, die uns für dieses Projekt verschiedene Metallgewebe zur Verfügung gestellt haben. Diese Metallgewebe finden sich jetzt als Filter in den Purifiern.

Die Fertigung der Plexiglastüren wurde von der Firma drei-h-Kunststoffe übernommen.